3 THE MINIMAL SUPERSYMMETRIC STANDARD MODEL WITH CP PHASES

3.1 Introduction

Maarten Boonekamp, Marcela Carena, Seong Youl Choi, Jae Sik Lee and Markus Schumacher

One of the most theoretically appealing realizations of the Higgs mechanism for mass generation is provided by supersymmetry (SUSY). The minimal supersymmetric extension of the standard model (MSSM) has a number of interesting field–theoretic and phenomenological properties, if SUSY is softly broken such that super–particles acquire masses not greatly exceeding 1 TeV. Specifically, within the MSSM, the gauge hierarchy can be made technically natural [1–6]. Unlike the SM, the MSSM exhibits quantitatively reliable gauge-coupling unification at the energy scale of the order of 10^{16} GeV [7–14]. Furthermore, the MSSM provides a successful mechanism for cosmological baryogenesis via a strongly first-order electroweak phase transition [15–29], and provides viable candidates for cold dark matter [30–37].

The MSSM makes a crucial and definite prediction for future high-energy experiments, that can be directly tested at the Tevatron and/or the LHC. It guarantees the existence of (at least) one light neutral Higgs boson with mass bounded from above at $\mathcal{O}(140\ \mathrm{GeV})$ [38–44]. This rather strict upper bound on the lightest Higgs boson mass is in accord with global analyses of the electroweak precision data, which point towards a relatively light SM Higgs boson, with $M_{H_{\rm SM}} \lesssim 186$ GeV at the 95 % confidence level [45]. Furthermore, because of the decoupling properties of heavy superpartners, the MSSM predictions for the electroweak precision observables can easily be made consistent with all the experimental data [46, 47].

An important and interesting phenomenological feature of the MSSM Higgs sector is that loop effects mediated dominantly by third-generation squarks may lead to sizeable violations of the tree-level CP invariance of the MSSM Higgs potential, giving rise to significant Higgs scalar–pseudoscalar transitions [48, 49], in particular. As a consequence, the three neutral Higgs mass eigenstates $H_{1,2,3}$, labeled in order of increasing mass such that $M_{H_1} \leq M_{H_2} \leq M_{H_3}$, have no definite CP parities, but become mixtures of CP-even and CP-odd states. In this case, the conventional CP-odd Higgs mass M_A is no longer a physical parameter. Instead, the charged Higgs mass is still physical and can be used as an input.

Much work has been devoted to studying in greater detail this radiative Higgs–sector CP violation in the framework of the MSSM [50–61]. In the MSSM with explicit CP violation, the upper bound on the lightest Higgs boson mass is almost identical to the one obtained in the CP conserving case [50]. The couplings of the Higgs bosons to the SM gauge bosons and fermions, to their supersymmetric partners and to the Higgs bosons themselves may be considerably modified from those predicted in the CP-conserving case. Consequently, radiative CP violation in the MSSM Higgs sector can significantly affect the production rates and decay branching fractions of the Higgs bosons. In particular, the drastic modification of the couplings of the Z boson to the two lighter Higgs bosons H_1 and H_2 might enable a relatively light Higgs boson with a mass M_{H_1} even less than about 70 GeV to have escaped detection at LEP 2 [62]. The upgraded Tevatron collider and the LHC will be able to cover a large fraction of the MSSM parameter space, including the challenging regions with a light Higgs boson without definite CP parity [62–77]. Furthermore, complementary and accurate explorations of the CP-noninvariant MSSM Higgs sector may be carried out using high-luminosity e^+e^- [78–82] and/or $\gamma\gamma$ colliders [83–93]. In addition, a complete determination of the CP properties of the neutral Higgs bosons is possible at muon colliders by exploiting polarized muon beams [94–102].

This introductory section is devoted to a short description of the key aspects and important experimental implications of the MSSM Higgs sector with radiatively–induced CP violation.

3.1.1 CP phases in the MSSM

Any phenomenologically viable SUSY model requires us to introduce terms which break SUSY *softly*, without spoiling the supersymmetric mechanism solving the hierarchy problem. There are three kinds of soft SUSY breaking terms in the framework of the MSSM:

– The gaugino mass terms:

$$\frac{1}{2}\left(M_3\,\widetilde{g}^a\widetilde{g}^a + M_2\,\widetilde{W}^i\widetilde{W}^i + M_1\,\widetilde{B}\widetilde{B} + \text{h.c.}\right)\,, \tag{3.1}$$

where M_3 is a gluino mass parameter of the gauge group SU(3)$_c$ and M_2 and M_1 are wino and bino mass parameters of the gauge groups SU(2)$_L$ and U(1)$_Y$, respectively.

– The trilinear A terms:

$$\widetilde{u}_R^*\,h_u\,A_u\,\widetilde{Q}H_2 - \widetilde{d}_R^*\,h_d\,A_d\,\widetilde{Q}H_1 - \widetilde{e}_R^*\,h_e\,A_e\,\widetilde{L}H_1 + \text{h.c.}\,, \tag{3.2}$$

where $\widetilde{Q}$ and $\widetilde{L}$ are SU(2)$_L$ doublet squark and slepton fields and $\widetilde{u}_R$, $\widetilde{d}_R$, and $\widetilde{e}_R$ are SU(2)$_L$ singlet fields.

– The scalar mass terms:

$$\begin{aligned}&\widetilde{Q}^\dagger\,M_{\widetilde{Q}}^2\,\widetilde{Q} + \widetilde{L}^\dagger\,M_{\widetilde{L}}^2\,\widetilde{L} + \widetilde{u}_R^*\,M_{\widetilde{u}}^2\,\widetilde{u}_R + \widetilde{d}_R^*\,M_{\widetilde{d}}^2\,\widetilde{d}_R + \widetilde{e}_R^*\,M_{\widetilde{e}}^2\,\widetilde{e}_R\\ &+ m_2^2H_2^*H_2 + m_1^2H_1^*H_1 - (m_{12}^2H_1H_2 + \text{h.c.})\,.\end{aligned} \tag{3.3}$$

One crucial observation is that all the massive parameters appearing in the soft SUSY breaking terms can be complex with non-trivial CP-violating phases. Together with the phase of the Higgsino mass parameter μ of the term $-\mu H_1H_2$ in the superpotential, all the physical observables depend on the CP phases of the combinations $\text{Arg}[M_i\,\mu\,(m_{12}^2)^*]$ and $\text{Arg}[A_f\,\mu\,(m_{12}^2)^*]$ [103, 104]. We have taken the convention of $\text{Arg}(m_{12}^2) = 0$ keeping the explicit dependence of μ. These new CP phases would lead to various interesting phenomena and, moreover, reopen the possibility of explaining the baryon asymmetry of the Universe in the framework of MSSM [16, 18, 20–22, 25–27, 29, 105, 106].

3.1.2 Loop-induced CP violation in the Higgs sector

Through the radiative corrections, the CP-violating mixing among the CP-even $\phi_{1,2}$ and CP-odd a states is induced [48–54]. Due to large Yukawa couplings, the third generation scalar quarks contribute most significantly at one-loop level. The size of the mixing is proportional to

$$\frac{3}{16\pi^2}\,\frac{\text{Im}\,(A_f\mu)}{m_{\tilde{f}_2}^2 - m_{\tilde{f}_1}^2} \tag{3.4}$$

with $f = t, b$. At two-loop level, the gluino mass parameter becomes relevant, for example, through the possibly important threshold corrections to the top- and bottom-quark Yukawa couplings. More CP phases become relevant by including other radiative corrections than those from the stop and sbottom sectors [55–57].

A. Mass spectra and couplings

The most comprehensive calculation of the CP-violating mixing and Higgs-boson mass spectrum in full consideration of the dependence on CP phases can be found in Refs. [53, 58] and [60, 61]. The Higgs-boson pole masses are calculated and all leading two-loop logarithmic corrections are incorporated in the one-loop RG–improved diagrammatic approach.

Due to the loop-induced CP-violating mixing, the neutral Higgs bosons do not have to carry any definite CP parities and the mixing among them is described by 3×3 real orthogonal matrix O instead of 2×2 one with a rotation angle α. The matrix O relates the Electroweak states to the mass eigenstates as:

$$(\phi_1\,,\phi_2\,,a)^T = O\,(H_1\,,H_2\,,H_3)^T\,. \tag{3.5}$$

We find the relation $O = R^T$ in which the rotation matrix R is given by Eq. (2.27) in Section 2.1. The Higgs-boson couplings to the SM and SUSY particles could be modified significantly due to the CP violating mixing. The most eminent example is the Higgs-boson coupling to a pair of vector bosons, g_{H_iVV}, which is responsible for the production of Higgs bosons at e^+e^- colliders:

$$\mathcal{L}_{HVV} = gM_W\left(W^+_\mu W^{-\mu} + \frac{1}{2c_W^2}Z_\mu Z^\mu\right)\sum_{i=1}^{3} g_{H_iVV}H_i\,, \tag{3.6}$$

where $g_{H_iVV} = c_\beta O_{\phi_1 i} + s_\beta O_{\phi_2 i}$ which is normalized to the SM value and given by the weighted sum of the CP-even components of the i-th Higgs mass eigenstate. Compared to the CP-conserving case, it's possible for the lightest Higgs boson to develop significant CP-odd component and its coupling to a pair of vector bosons becomes vanishingly small. The interactions of a pair of Higgs bosons to a vector boson are given by

$$\begin{aligned}
\mathcal{L}_{HHZ} &= \frac{g}{4c_W}\sum_{i,j=1}^{3} g_{H_iH_jZ}\,Z^\mu(H_i\,i\overleftrightarrow{\partial}_\mu\,H_j)\,,\\
\mathcal{L}_{HH^\pm W^\mp} &= -\frac{g}{2}\sum_{i=1}^{3} g_{H_iH^+W^-}\,W^{-\mu}(H_i\,i\overleftrightarrow{\partial}_\mu\,H^+) + \text{h.c.}\,,
\end{aligned} \tag{3.7}$$

where

$$g_{H_iH_jZ} = \text{sign}[\det(O)]\;\varepsilon_{ijk}\,g_{H_kVV} \quad\text{and}\quad g_{H_iH^+W^-} = c_\beta\,O_{\phi_2 i} - s_\beta\,O_{\phi_1 i} - iO_{ai} \tag{3.8}$$

leading to the following sum rules:

$$\sum_{i=1}^{3} g^2_{H_iVV} \;=\; 1 \quad\text{and}\quad g^2_{H_iVV} + |g_{H_iH^+W^-}|^2 \;=\; 1 \quad\text{for each } i\,. \tag{3.9}$$

The effective Lagrangian governing the interactions of the neutral Higgs bosons with quarks and charged leptons is

$$\mathcal{L}_{H_i\bar{f}f} \;=\; -\sum_{f=u,d,l}\frac{gm_f}{2M_W}\sum_{i=1}^{3} H_i\,\bar{f}\left(g^S_{H_i\bar{f}f} + ig^P_{H_i\bar{f}f}\gamma_5\right)f\,. \tag{3.10}$$

At the tree level, $(g^S_{H_i\bar{f}f}, g^P_{H_i\bar{f}f}) = (O_{\phi_1 i}/c_\beta, -O_{ai}\tan\beta)$ and $(g^S_{H_i\bar{f}f}, g^P_{H_i\bar{f}f}) = (O_{\phi_2 i}/s_\beta, -O_{ai}\cot\beta)$ for $f = (l,d)$ and $f = u$, respectively. We observe that all neutral Higgs bosons can couple to both scalar and pseudoscalar fermion bilinear currents simultaneously ($\bar{f}f$ and $\bar{f}\gamma_5 f$, respectively) in the presence of CP-violating mixing. In the case of third-generation quarks, the couplings depend on the threshold corrections induced by the exchanges of gluinos and charginos which modify the relations between quark masses and the corresponding Yukawa couplings as:

$$\begin{aligned}
h_b &= \frac{\sqrt{2}m_b}{v\cos\beta}\,\frac{1}{1+(\delta h_b/h_b)+(\Delta h_b/h_b)\tan\beta}\,,\\
h_t &= \frac{\sqrt{2}m_t}{v\sin\beta}\,\frac{1}{1+(\delta h_t/h_t)+(\Delta h_t/h_t)\cot\beta}\,.
\end{aligned} \tag{3.11}$$

We note that the corrections do not decouple in the limit of large SUSY breaking parameters and the dominant contributions to h_b are $\tan\beta$-enhanced. The relation between m_τ and the Higgs–tau-lepton Yukawa coupling h_τ is also modified, but the corrections are expected to be smaller than those to h_b. The corrections depend on the combinations of μM_3 and μA_t, stop and sbottom masses, etc. We refer to, for example, Ref. [58] for details of them.

The couplings of the charged Higgs bosons to quarks are of the form $\mathcal{L}_{H^\pm t\bar{b}} = \bar{b}\,(g^L_{H^- t\bar{b}} P_L + g^R_{H^- t\bar{b}} P_R)\, t H^- + \text{h.c.}$ with the couplings given by

$$g^L_{H^- t\bar{b}} \simeq \frac{\sqrt{2}\, m_b}{v} \tan\beta - \frac{\Delta h_b}{\cos\beta} \qquad \text{and} \qquad g^R_{H^- t\bar{b}} \simeq \frac{\sqrt{2}\, m_t}{v} \cot\beta - \frac{(\Delta h_t)^*}{\sin\beta}\,. \tag{3.12}$$

An explicit computation of the CP-violating $H^- t\bar{b}$ vertex can be found in Ref. [58].

For large values of the charged Higgs boson mass and for heavy supersymmetric particles, the expressions of the lightest neutral Higgs boson coupling to fermions reduce to those of the (CP-conserving) SM Higgs boson, as expected for the decoupling limit. In contrast, the two heavy neutral Higgs bosons are still admixtures of CP-even and CP-odd eigenstates; hence, CP-violating effects are still present in the heavy neutral Higgs sector. However, due to the high degeneracy in mass of the heavy scalar sector (especially in the decoupling limit [107]), CP–violating effects may be difficult to observe without precision measurements of the heavy neutral Higgs properties.

The so called CPX scenario has been defined as a benchmark point for studying the CP-violating Higgs-mixing phenomena [54]. In this scenario, the parameters have been fixed as follows:

$$\begin{aligned} &M_{\tilde{Q}_3} = M_{\tilde{U}_3} = M_{\tilde{D}_3} = M_{\tilde{L}_3} = M_{\tilde{E}_3} = M_{\rm SUSY}\,, \\ &|\mu| = 4\, M_{\rm SUSY}\,, \;\; |A_{t,b,\tau}| = 2\, M_{\rm SUSY}\,, \;\; |M_3| = 1 \;\; \text{TeV}\,. \end{aligned} \tag{3.13}$$

The parameter $\tan\beta$, the charged Higgs-boson pole mass $M_{H^\pm}$, and the common SUSY scale $M_{\rm SUSY}$ can be varied. For CP phases, taking $\Phi_\mu = 0$ convention and a common phase for A terms $\Phi_A = \Phi_{A_t} = \Phi_{A_b} = \Phi_{A_\tau}$, we have two physical phases to vary: Φ_A and $\Phi_3 = \text{Arg}(M_3)$.

Corrections to the MSSM Higgs boson sector have been evaluated in several approaches. At the one loop level the complete result for radiative corrections to the masses and mixing angles in the MSSM Higgs sector is known [38–44]. Concerning the two-loop effects, their computation is quite advanced and has now reached a stage such that all the presumably dominant contributions are known [108–129] with a remaining theoretical uncertainty on the light CP-even Higgs boson mass which is estimated to be below ~ 3 GeV [47, 130]. The results of the radiative correction calculations have been implemented into public codes.

The code `CPsuperH` [131] is based on the renormalization group (RG) improved effective potential approach [109–111, 132–140] and it implements the results obtained in Refs. [53, 58, 141–143], see Section 3.4. The program `FeynHiggs` [144–148] is based on the results obtained in the Feynman-diagrammatic (FD) approach [113–115, 129, 130], see Section 3.5. For the MSSM with real parameters the two codes can differ by up to ~ 4 GeV for the light CP-even Higgs boson mass, mostly due to subleading two-loop corrections that are included only in `FeynHiggs`. For the MSSM with complex parameters the phase dependence at the two-loop level is included in a more advanced way in `CPsuperH`, but, on the other hand, `CPsuperH` does not contain all the subleading one-loop contributions that are included in `FeynHiggs`. The plots of this Introduction have been obtained by use of `CPsuperH`.

Figure 3.1 shows the Higgs-boson pole masses M_{H_i} and the couplings squared $g^2_{H_i VV}$ as functions of Φ_A for the CPX scenario. When $M_{H^\pm} = 120$ GeV (left frames), around $\Phi_A = 90^\circ$, we observe H_1 becomes light with vanishingly small couplings. In other words, it becomes lighter than 50 GeV and behaves almost like a CP-odd state. In this case, H_1 production rate at LEP is very low and H_2 dominantly decays into a pair of the lightest Higgs bosons which subsequently decays into 4 b quarks.

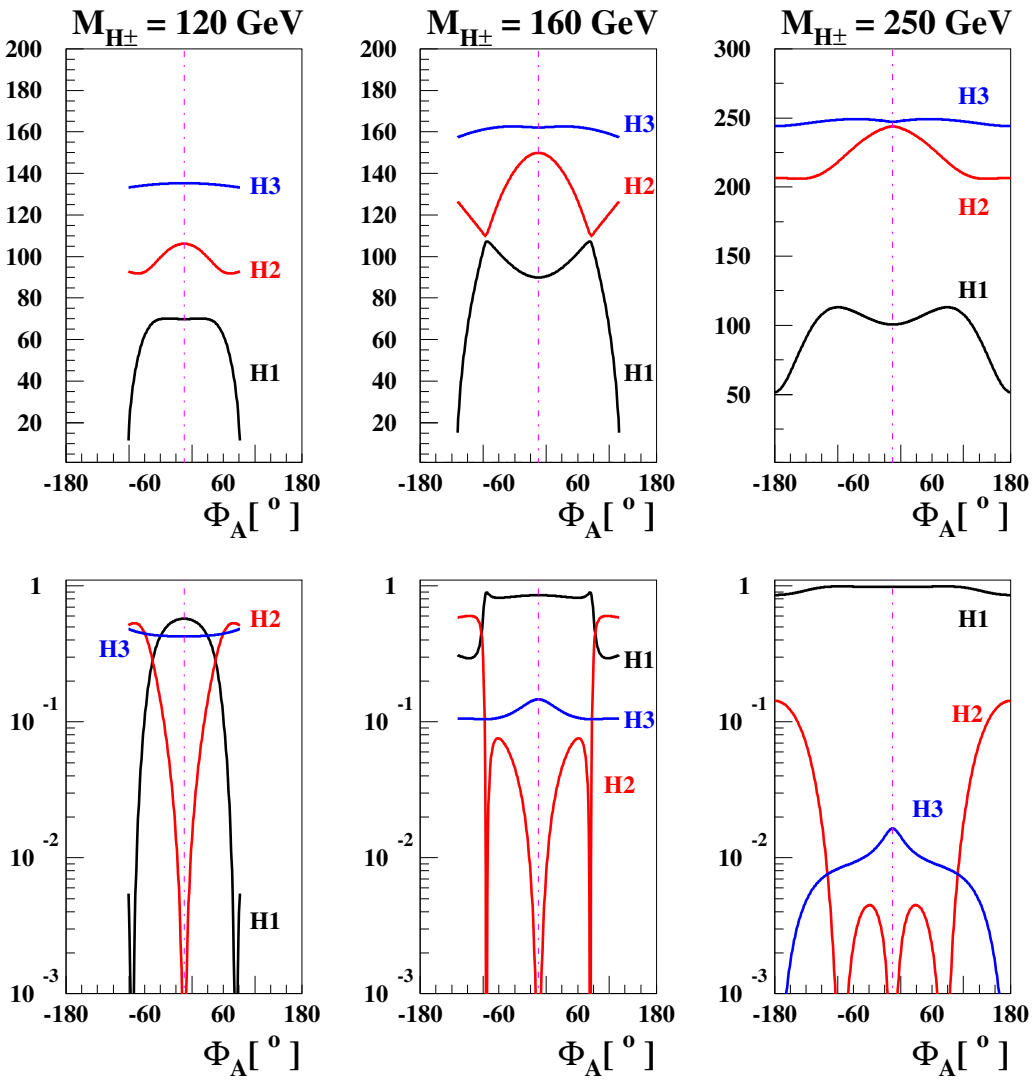

Fig. 3.1: The Higgs-boson masses M_{H_i} (upper frames) in GeV and $g^2_{H_iVV}$ (lower frames) as functions of Φ_A for the CPX scenario when $\tan\beta = 4$, $\Phi_3 = 0°$, and $M_{\rm SUSY} = 0.5$ TeV. Three values of the charged Higgs-boson pole mass have been taken: 120 GeV (left frames), 160 GeV (middle frames), and 250 GeV (right frames).

This makes the Higgs detection at LEP difficult and the region with $M_{H_1} \leq 50$ GeV and $\tan\beta = 4$–8 has not been excluded yet [149, 150]. In the middle frames with $M_{H^\pm} = 160$ GeV, we observe a resonant-mixing behavior between H_1 and H_2 around $\Phi_A = 90°$. The lightest Higgs becomes SM-like Higgs boson and decouples from the 3×3 mixing when the charged Higgs boson becomes heavy, see the right frames of Fig. 3.1. Nevertheless, there still can be significant mixing between the two heavier neutral mass eigenstates due to their highly–degenerate masses.

The Higgs-boson decay patterns strongly depend on the CP-violating mixing. For this we show the branching fractions and decay widths of the MSSM Higgs bosons in Figs. 3.2 and 3.3. In the CP-conserving case (Fig. 3.2), the decay channels $H_2 \to H_1H_1, WW, ZZ$ and $H_3 \to H_1Z$ are forbidden. In the CP-violating case (Fig. 3.3), on the other hand, all the decay channels are open for the heavier Higgs bosons. We note that, in the CP-violating case, both heavier Higgs bosons H_2 and H_3 dominantly decay into the lightest Higgs-boson pairs where the decay widths drastically increase. Also there, the decay width of the charged Higgs boson increases and it mainly decays into $W^\pm H_1$.

The phenomenological implication of the CP-violating couplings of the charged Higgs boson to

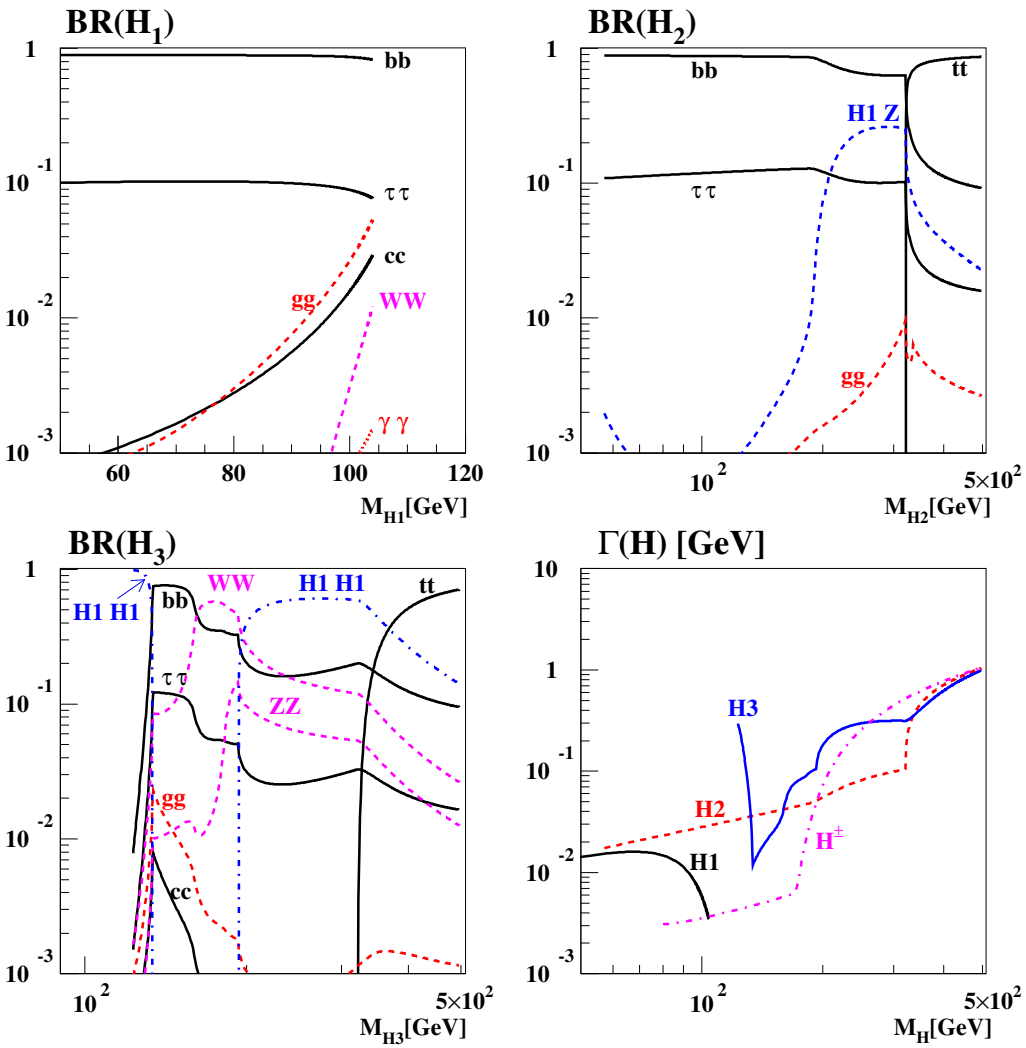

Fig. 3.2: The branching fractions and decay widths of the MSSM Higgs bosons for the CPX scenario with $\tan\beta = 4$ and $M_{\rm SUSY} = 0.5$ TeV as functions of their masses. Here, we are taking the CP-conserving case ($\Phi_A = \Phi_3 = 0°$). See Fig. 3.3 for the CP-violating case.

quarks can be found in Ref. [68].

B. Low–energy constraints

Low-energy observables provide indirect constraints on the soft SUSY breaking parameters. The observables are particularly useful for identifying the favoured range of parameter space when the SM predictions for them are strongly suppressed and/or precise experimental measurements of them have been performed. Such observables include EDMs, $(g-2)_\mu$, BR$(b \to s\gamma)$, $\mathcal{A}_{\rm CP}(b \to s\gamma)$, BR$(B \to Kll)$ and BR$(B_{s,d} \to l^+l^-)$.

Currently, the EDM of the thallium atom provides one of the best constraints on the CP-violating phases, depending on the SUSY scale. The main contributions to the atomic EDM of ^{235}Tl come from two terms. One of them is the electron EDM d_e and the other is the coefficient C_S of a CP-odd electron-nucleon interaction. The coefficient C_S is essentially given by the gluon-gluon-Higgs couplings and the two-loop Higgs-mediated electron EDM [151, 152] is given by the sum of contributions from third-generation quarks and squarks and charginos. As can be seen for example in Ref. [153], the two kinds of dominant contributions could cancel each other allowing narrow region compatible with the EDM

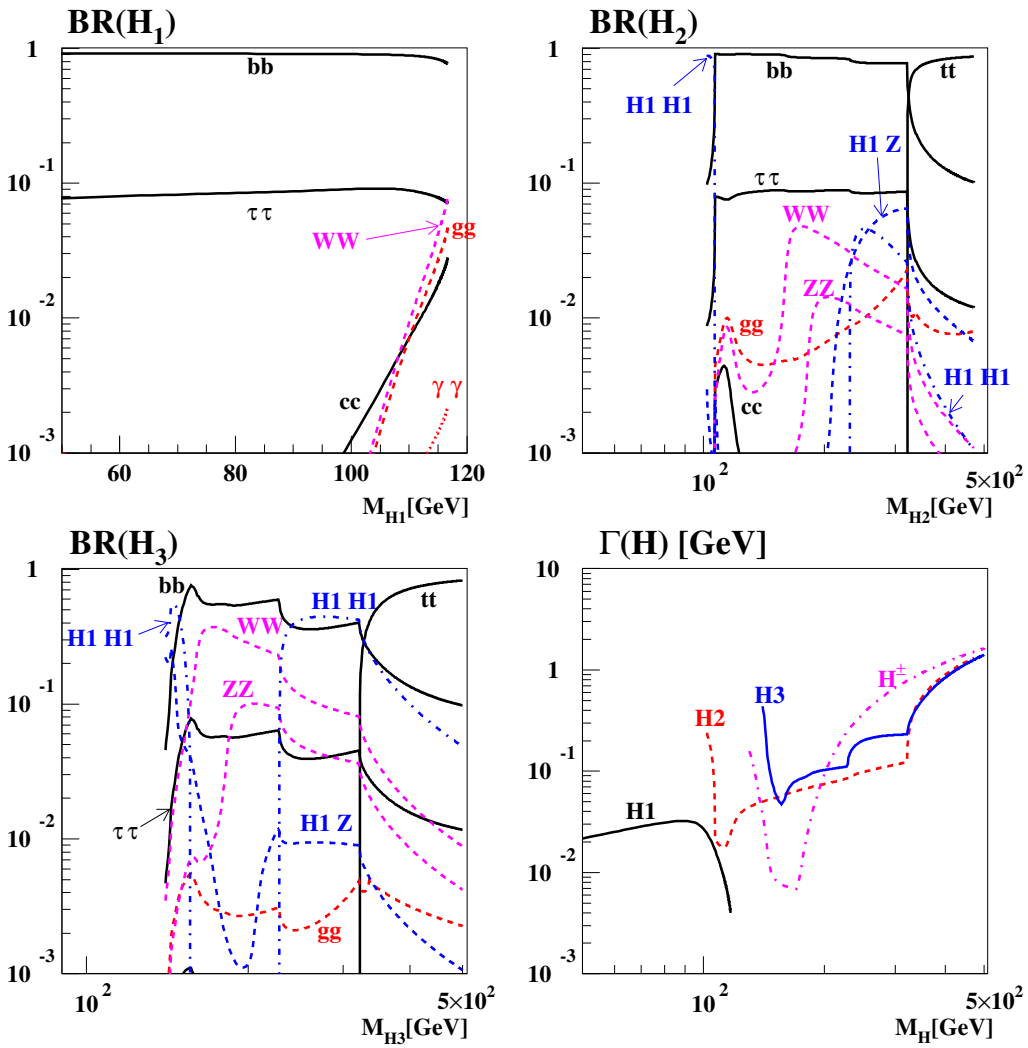

Fig. 3.3: The same as in Fig. 3.2 but with $\Phi_A = \Phi_3 = 90°$.

constraint but with sizable CP phases. If no cancellations take place, the allowed CP-phases are highly constrained, in particular for large values of $\tan\beta$ and small values of the CP-odd Higgs mass. However, they may be large enough to allow for the possibility of electroweak baryogenesis in the MSSM [154–156]. The Thallium EDM constraint can be evaded more easily by assuming cancellations between the two-loop and possible one-loop contributions. This shows that the possibility of large CP phases which can induce significant CP-violating mixing in the Higgs sector cannot be excluded *a priori*.

3.1.3 Coupled channel analysis

In the presence of non-trivial CP violating phases, the MSSM neutral Higgs bosons have a tendency to show strong mixing among them, with small mass differences comparable to their widths. When the charged Higgs boson is heavy, the two heavier Higgs bosons mix significantly. On the other hand, all three neutral Higgs bosons show strong three-way mixing acquiring significant CP-even and CP-odd components when the charged Higgs boson is light and, especially, when the values of $\tan\beta$ is large. In this case, when considering Higgs boson production at colliders, each Higgs boson can not be treated separately and all three neutral Higgs boson should be considered as a coupled system. The characteristic feature of the coupled–channel analysis lies in the off-diagonal absorptive parts in the inverse of the full

3×3 propagator matrix [157–159]. For an explicit example, see Ref. [160] that shows the effects of including the off-diagonal absorptive parts in the Higgs-boson propagators based on a scenario in which all three neutral Higgs bosons are nearly degenerate in mass, around 120 GeV, and with widths of the order of 1–3 GeV.

3.1.4 Experimental signatures

A. The Large Electron-Positron Collider

At LEP, CP violating scenarios are probed *via* a re-interpretation of the usual (CP-conserving) MSSM or 2HDM searches [149, 161, 162]. Compared to the MSSM, the mass and coupling constraints are relaxed, leading to an often richer mixture of final states. The results of Refs. [149, 161, 162] exploit the earlier searches for the $e^+e^- \to hA, hZ$ processes (in CP-conserving nomenclature), now accounting for the possible presence of more than two neutral Higgs bosons in the spectrum, and for generally diluted cross-sections and modified branching fractions.

The considered modes include the familiar $H_i \to bb, \tau\tau$ [163], but also gluonic or photonic decays (so-called flavour-blind and fermiophobic searches, respectively) [164–168]. Details concerning the analyses and the statistical combination procedure are given in Section 3.2.

B. The Large Hadron Collider

At the LHC, via gluon fusion, we probe loop-induced Higgs-boson couplings to two gluons. The diagrams with top and bottom quarks inside loops can induce both scalar S_i^g and pseudoscalar P_i^g form factors simultaneously for a specific H_i when CP is violated. We refer to Sec. 3.4 for specific forms of the form factors. Also, note that the CP-odd component of each Higgs boson can contribute to the scalar form factor in the presence of non-vanishing CP phases.

The s-channel production cross section of a neutral Higgs boson H_i in gg fusion is given by

$$\sigma(pp \to H_i) = K\,\frac{\alpha_s^2}{256\pi v^2}\left(|S_i^g|^2 + |P_i^g|^2\right)\,\tau\frac{d\mathcal{L}^{gg}}{d\tau}\,, \tag{3.14}$$

where the factor $K \approx$ 1.5-1.7 for QCD corrections and the Drell-Yan variable $\tau = M_{H_i}^2/s$ with s being the invariant hadron collider energy squared. The gluon-gluon luminosity $\tau d\mathcal{L}^{gg}/d\tau \sim 500$ when $M_{H_i} \sim 100$ GeV at the LHC and $\alpha_s^2/256\pi v^2 \sim 0.1$ pb.

Even the absolute values of the scalar and pseudoscalar form factors depend strongly on the CP phases [62–74], we need observables which vanish in the CP-conserving limit to establish CP-violating Higgs mixing at the LHC. The product $\mathrm{Re}\,(S_i^g P_i^g)/(|S_i^g|^2 + |P_i^g|^2)$ might be measured by examining the azimuthal angular distribution of the tagged forward protons [75]. On the other hand, when the Higgs bosons decay into τ leptons, one can construct CP-odd observables if the polarizations of the τ leptons can be determined reasonably. Even the production rates are known to be low in general, the exclusive double diffractive process, thanks to a clean environment due to the large rapidity gap and a good Higgs-mass resolution of the order of 1 GeV, may offer unique possibilities for exploring Higgs physics in ways that would be difficult or even impossible in inclusive Higgs production at the LHC [76].

The inclusion of supersymmetric threshold corrections to the b-quark mass [124–126, 128, 169–176] has significant consequences in scenarios with large CP-mixing effects in the Higgs sector. Depending on the size of $\mathrm{Arg}(A_{t,b}\,\mu)$, $\mathrm{Arg}(M_3\,\mu)$, and the details of the spectrum, the lightest sbottom squark becomes tachyonic and, possibly, the b-quark Yukawa coupling nonperturbative for values of $\tan\beta$ ranging from intermediate up to large or very large [77]. In this case, the main production mechanism of Higgs bosons at the LHC is not gluon fusion but b-quark fusion. Inability of distinguishing gluon fusion from b-quark fusion leads us to consider W^+W^- fusion into Higgs bosons and subsequent decays of Higgs bosons into tau leptons [158]. It would be a promising channel for studying signature of Higgs-sector CP violation at the LHC.

Finally, we note that the existing MSSM Higgs CP studies at the LHC are mostly at the parton level and still in need of a detailed experimental validation including detector simulations.

C. The International Linear Collider

At the international linear collider (ILC), the neutral Higgs bosons are produced via Higgs couplings to vector boson pairs, g_{H_iVV}, and vector-boson couplings to Higgs boson pairs, $|g_{H_iH_jZ}| = |\epsilon_{ijk}\, g_{H_kVV}|$. This relation, together with the sum rule Eq. (3.9), leads to the selection rule that only two CP-even Higgs bosons can appear in the Higgs–strahlung process and only two pairs of CP-even and CP-odd Higgs bosons can be produced in CP-invariant MSSM framework. In other words, if one observe three Higgs bosons in Higgs–strahlung and/or all the three pairs of Higgs bosons, H_1H_2, H_2H_3, and H_1H_3, in pair productions, this is a signal of CP violation in the MSSM framework [78,79]. But in the non-minimal supersymmetric extension(s) of the SM, there can be additional Higgs singlet(s) and/or doublets(s) implying the observation made above does not necessarily mean a signal of CP violation.

Higgs-boson production via the Higgs–strahlung process $e^+e^- \to H_i\, Z$, where the Z boson decays into electron or muon pairs, offers a unique environment for determining the masses and widths of the neutral Higgs bosons by the recoil-mass method [80–82]. Thanks to the excellent energy and momentum resolution of electrons and muons coming from the Z-boson decay, the recoil mass against the Z boson, $p^2 = s - 2\cdot\sqrt{s}\cdot E_Z + M_Z^2$, can be reconstructed with a precision as good as 1 GeV. Here s and E_Z are the the collider centre-of-mass energy squared and the energy of the Z boson, respectively. It is shown [153] that the production lineshape of a coupled system of neutral Higgs bosons decaying into $b\bar{b}$ quarks is sensitive to the CP-violating parameters. When the Higgs bosons decay into $\tau^-\tau^+$, two CP asymmetries can be defined using the longitudinal and transverse polarizations of the τ leptons.

D. Photon Linear Collider

By means of Compton back–scattering of laser light, almost the entire energy of electrons/positrons at ILC can be transferred to photons [83] so that $e\gamma$ and $\gamma\gamma$ processes can be studied for energies close to the ILC energy scale [84, 177, 178]. The luminosities are expected to be about one third of the e^+e^- luminosity in the high energy regime. Especially, the photon–photon collision is an ideal option to look for the signatures of neutral Higgs bosons. The $\gamma\gamma$ formation allows us to generate heavy Higgs bosons [179, 180] in a wedge centered around medium $\tan\beta$ values, in which neither the LHC nor the ILC give access to the spectrum of heavy Higgs bosons. Various options of choosing the photon polarization, circular and linear, allow unique experimental analyses of the properties and interactions of Higgs bosons. For example, more than 20 independent observables, half of which are CP-odd, can be constructed by exploiting the controllable photon beam polarization and the possibly measurable final–state fermion polarizations.

In the narrow-width approximation, the s-channel Higgs-boson production $\gamma\gamma \to H_i$ can be expressed in the simple form,

$$\sigma(\gamma\gamma \to H_i) = \frac{\alpha_{\rm em}^2}{32\pi v^2}\left(|S_i^\gamma|^2 + |P_i^\gamma|^2\right)\delta(1 - M_{H_i}^2/s)\,, \tag{3.15}$$

where s is the c. m. energy squared of two colliding photons and $\alpha_{\rm em}^2/32\pi v^2 \sim 4$ fb. For the scalar S_i^γ and pseudoscalar P_i^γ form factors, we again refer to Section 3.4. The s-channel production of neutral Higgs bosons and its decays into several final states have been studied by many authors taking account of possible interference effects with the tree-level t- and u-channel continuum amplitudes [85–92,159]. Recently, a comprehensive study has been done taking into account $\mu^+\mu^-$, $\tau^+\tau^-$, $\bar{b}b$ and $\bar{t}t$ final states [93]. Some signatures of the resonant CP–violating Higgs mixing due to near degeneracy of heavy Higgs bosons in the decoupling limit [107] have been investigated as well [159], cf. Section 3.12.

E. Muon colliders and other experimental probes

The main physics advantage of the muon collider is that the larger Yukawa coupling of muons in many cases admits copious production of Higgs bosons as s-channel resonances. Moreover, with controllable

energy resolution and beam polarizations, the muon collider provides a powerful probe of the Higgs sector CP violation [94–100, 181]. Several detailed studies considering fermion and/or sfermion final states can be found, for example, in Refs. [101, 102].

3.2 Search for CP-violating neutral Higgs bosons in the MSSM at LEP

Philip Bechtle

In this section, the results from the combination of the Higgs boson searches of the four LEP collaborations [149, 182–184] at $\sqrt{s} = 91$–209 GeV in model-independent cross-section limits on various MSSM-Higgs-like topologies and in exclusion of CP-violating MSSM benchmark scenarios are presented. Because of the different Higgs boson production and decay properties outlined in the previous sections, the experimental exclusions published so far for the CP-conserving MSSM scenario are partly invalidated by CP-violating effects.

3.2.1 Higgs boson searches at LEP

In the CP-conserving MSSM, the two dominant production mechanisms Higgsstrahlung ($e^+e^- \to hZ$, $\sigma_{hZ} \propto \sin^2(\beta-\alpha)$) and pair production ($e^+e^- \to hA$, $\sigma_{hA} \propto \cos^2(\beta-\alpha)$) are complementary and ensure the coverage of the whole kinematically accessible plane of Higgs boson masses, because for large $\cos^2(\beta-\alpha)$ the two Higgs bosons h (CP-even) and A are close to each other in mass.

In the CP-violating MSSM, the experimental coverage of the mass plane is lost, since first all three Higgs bosons can be produced in Higgsstrahlung (and hence the direct complementary of two modes is lost), and second, because there can be large mass differences between M_{H_1} and M_{H_2} over the whole parameter space. Additionally, the cascade decay $H_2 \to H_1H_1$ is dominant in large areas of the parameter space. Hence, the coverage of non-diagonal pair production mechanisms and the coverage of cascade decays is crucial for the experimental access to the CP-violating models. This is shown in Fig. 3.4. In (a), the 95 % confidence level (CL) exclusion limits on $\sigma \times BR$ in the process $e^+e^- \to H_2Z \to H_1H_1Z \to b\bar{b}b\bar{b}Z$ relative to the nominal 2HDM cross-section is shown. For M_{H_2} up to 105 GeV and all M_{H_1}, models which predict a $\sigma \times BR$ value of more than 40 % of the SM cross-section can be excluded. In (b), the coverage for the process $e^+e^- \to H_2H_1 \to H_1H_1H_1 \to b\bar{b}b\bar{b}b\bar{b}$ is shown, with limits relative to the nominal pair-production cross-section with $\cos^2(\beta-\alpha) = 1$.

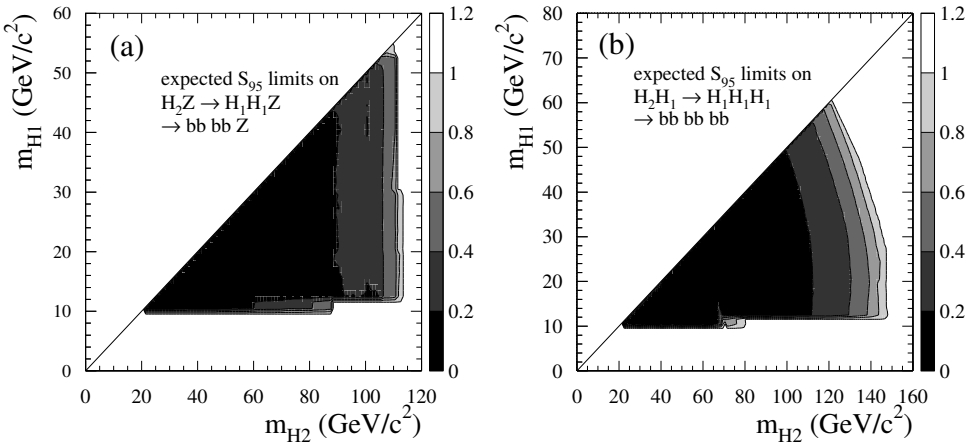

Fig. 3.4: Model independent limits on $\sigma \times BR$ relative to the nominal 2HDM cross-sections for $\sin^2(\beta-\alpha) = 1$ in (a) and $\cos^2(\beta-\alpha) = 1$ in (b). The scale on the right side of the figures shows the fraction of the nominal cross-section which can be excluded at the 90 % CL.

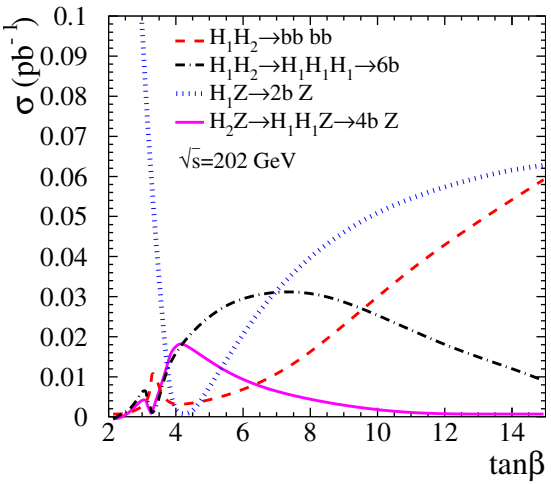

Fig. 3.5: Model predictions for $\sigma \times BR$ values of dominant Higgs boson production mechanisms in the CPX scenario for $30\,\text{GeV} < M_{H_1} < 40\,\text{GeV}$ at the average center-of-mass energy of LEP in the last two years of data-taking.

3.2.2 MSSM models with additional CP violation

The benchmark model used in the combination of the LEP data is the CPX scenario [54]. It is characterized by large mixing between CP-even and CP-odd states in the mass eigenstates. The CP-even/CP-odd mixing $\mathcal{M}^2_{SP}$ is characterized by

$$\mathcal{M}^2_{SP} \propto \frac{m_t^4}{v^2} \frac{\text{Im}\,(A_{t,b}\mu)}{M^2_{SUSY}}. \tag{3.16}$$

Therefore, large values of the top quark mass m_t, the Higgsino mixing parameter μ and the imaginary part of the trilinear couplings in the stop and sbottom sector $A_{t,b}$ ($\arg A_{t,b,\tau} = \Phi_3 = 90°$), coupled with a not too large scale of the squark masses M_{SUSY} is chosen. Effects of the variation of these parameters are studied. Detailed calculations on the two-loop order [60, 144] or on the one-loop renormalization-improved order [54] are used to calculate the model predictions.

The resulting predictions for selected processes in the CPX scenario are shown in Fig. 3.5 for lightest Higgs masses of $30\,\text{GeV} < M_{H_1} < 40\,\text{GeV}$. For low $\tan\beta \sim 2$, the SM-like production mechanism $H_1 Z \to (b\bar{b}, \tau^+\tau^-)Z$ is dominant and has a large production cross-section. For intermediate $\tan\beta \sim 4$, however, all production cross-sections are reduced with respect to the area at $\tan\beta \sim 2$, since the kinematically accessible H_1 decouples from the Z because it becomes entirely CP-odd, hence no Higgsstrahlung occurs, and since $M_{H_2} \approx 110\,\text{GeV}$ is close to the kinematic limit. Additionally, the experimentally more difficult cascade decay $H_2 \to H_1 H_1$ becomes dominant. For large $\tan\beta$ the production cross-sections increase and finally $H_1 H_2 \to b\bar{b}b\bar{b}$ becomes the dominant mode at $\tan\beta > 15$.

3.2.3 Interpretation of the LEP data in the CPV MSSM

The statistical combination of all Higgs boson searches from all four LEP collaborations uses the modified frequentist approach as implemented in [185, 186]. The result of this combination shows no statistically significant excesses of the data over the expected background. Hence, limits on the parameter space are computed [162]. These limits are shown in Fig. 3.6, 3.7 and 3.8 for the CPX scenario. In each case, the full set of MSSM parameters is fixed to the values chosen for the scenario (as given in [54, 162]), apart from $\tan\beta$ and the charged Higgs boson mass $M_{H^\pm}$, which are scanned. The result is then shown in the $\tan\beta, M_{H_1}$ projection.

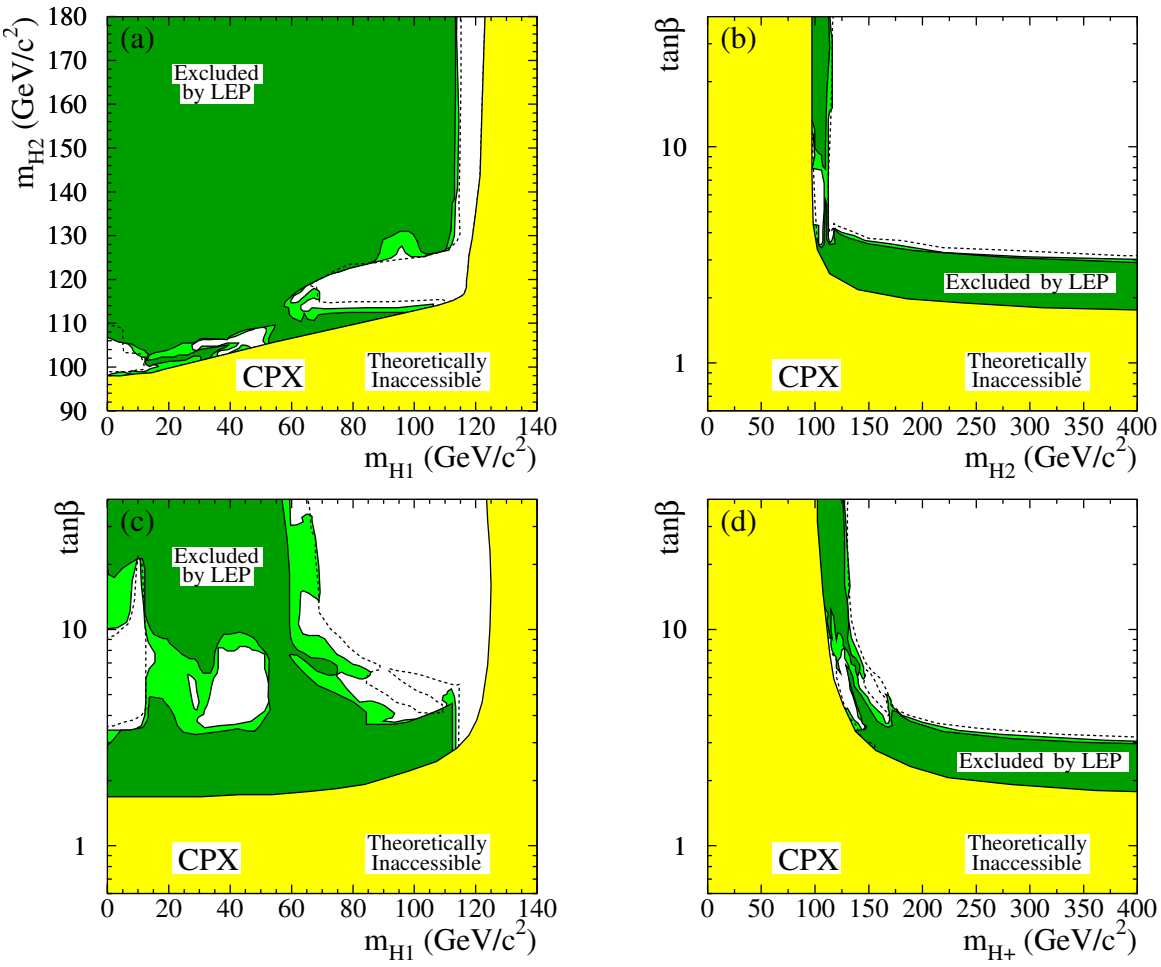

Fig. 3.6: Exclusion areas in the (a) (M_{H_2}, M_{H_1}), (b) $(\tan\beta, M_{H_2})$, (c) $(\tan\beta, M_{H_1})$ and (d) $(\tan\beta, M_{H^\pm})$ planes in the CPX scenario for $m_t = 174.3\,\text{GeV}$. Theoretically inaccessible regions are shown in yellow, experimentally excluded areas in light green ($CL = 95\,\%$) and dark green ($CL = 99.7\,\%$).

Fig. 3.6 shows the excluded region in the CPX scenario for four different projections and $m_t = 174.3\,\text{GeV}$. The reduction of production cross-sections for intermediate $\tan\beta$ described in Section 3.2.2 causes unexcluded regions for low values of the lightest Higgs boson mass M_{H_1}. No absolute limit on M_{H_1} can be set. In Fig. 3.7 the results in the CPX scenario are shown for different top quark masses m_t. The present experimental value of $m_t = 172.7\,\text{GeV}$ [187] lies between the values used for Fig. 3.7 (a) and the nominal CPX scenario shown in Fig. 3.6 (c). For larger values of m_t the unexcluded region increases, since m_t strongly influences the mixing of the mass eigenstates (see (3.16)) and increases the mass splitting between M_{H_1} and M_{H_2}, hence further decreasing the production cross-sections of ZH_2 states for intermediate $\tan\beta$.

The effect of unexcluded regions in the parameter space for low M_{H_1} is clearly connected to the CP-violating imaginary phase of the trilinear couplings $A_{t,b}$. This is shown in Fig. 3.8. Only for large phases (and hence large mixings in (3.16)) the effect of large inaccessible regions is strong.

3.2.4 Conclusions

The results from neutral Higgs bosons searches in the context of the MSSM described in this paper are based on data collected by the four LEP collaborations, ALEPH, DELPHI, L3 and OPAL at $\sqrt{s} =$

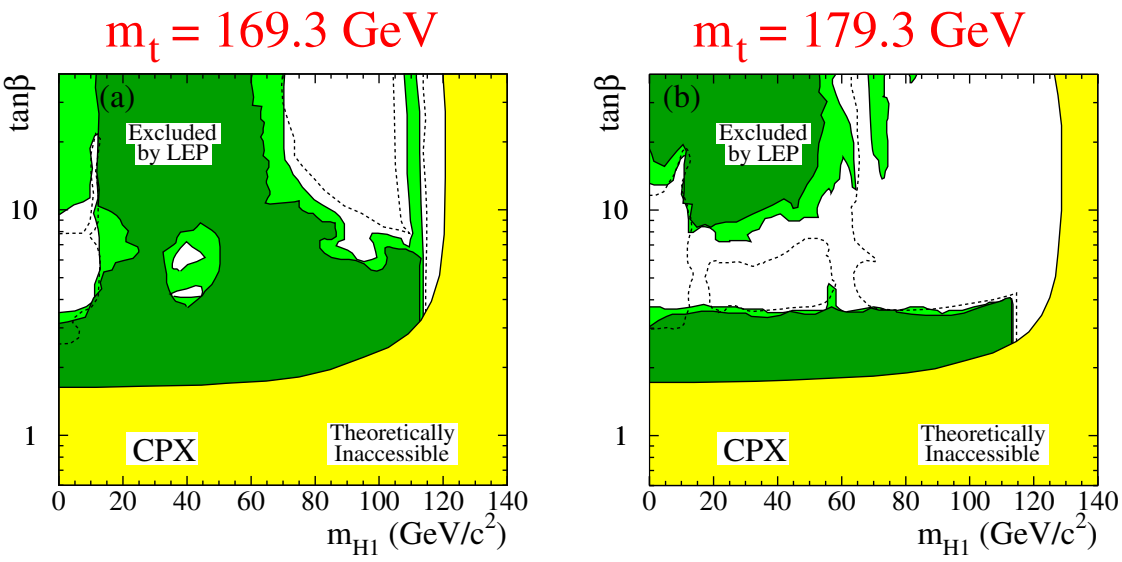

Fig. 3.7: Exclusion areas in the $(\tan\beta, M_{H_1})$ plane in the CPX scenario for $m_t = 169.3\,\text{GeV}$ and $179.3\,\text{GeV}$. For the corresponding exclusion areas for $m_t = 174.3\,\text{GeV}$ please see Fig. 3.6 (c). Theoretically inaccessible regions are shown in yellow, experimentally excluded areas in light green ($CL = 95\,\%$) and dark green ($CL = 99.7\,\%$). The phase is set to $\arg A = \Phi_3 = 90°$.

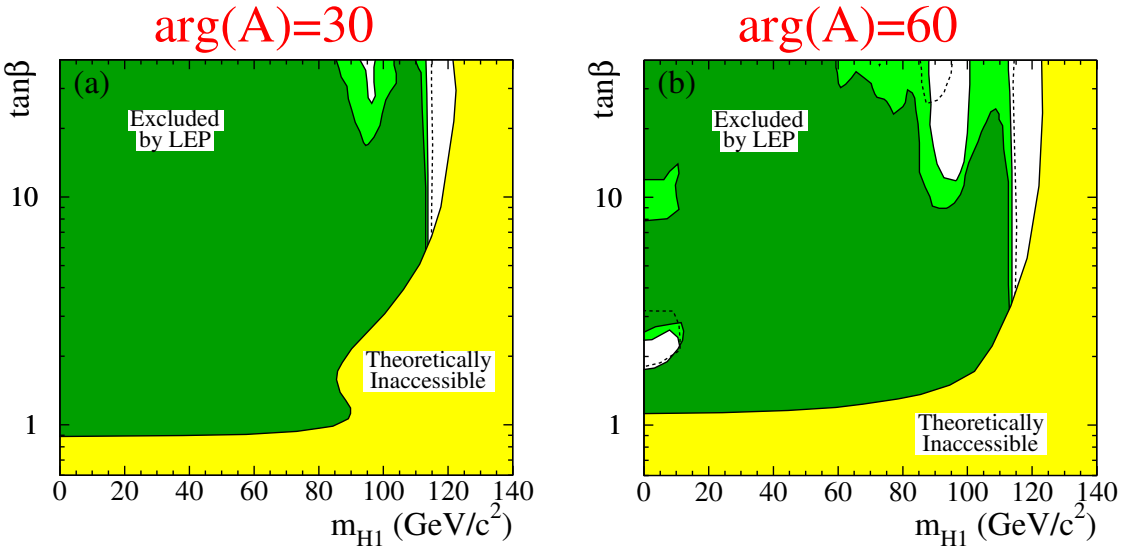

Fig. 3.8: Exclusion areas in the $(\tan\beta, M_{H_1})$ plane for different values of the phase $\arg A = \Phi_3 = 30°, 60°$ of the trilinear coupling parameters in the stop and sbottom sector. a value of $m_t = 174.3\,\text{GeV}$ is chosen and the unvaried parameter values are identical to those of the CPX scenario. For the corresponding plot of the nominal CPX phase of $\arg A = \Phi_3 = 90°$ see Fig. 3.6 (c).

$91 - 209\,\text{GeV}$. No significant excess of data over the expected backgrounds has been found. From these results, upper bounds are derived for the cross sections of a number of Higgs event topologies. These upper bounds cover a wide range of Higgs boson masses and are typically much lower than the largest cross sections predicted within the MSSM framework. In the CP-violating benchmark scenario CPX and the variants which have been studied, the combined LEP data show large unexcluded domains, down to the smallest masses; hence, no absolute limits can be set for the Higgs boson masses. On the other hand,

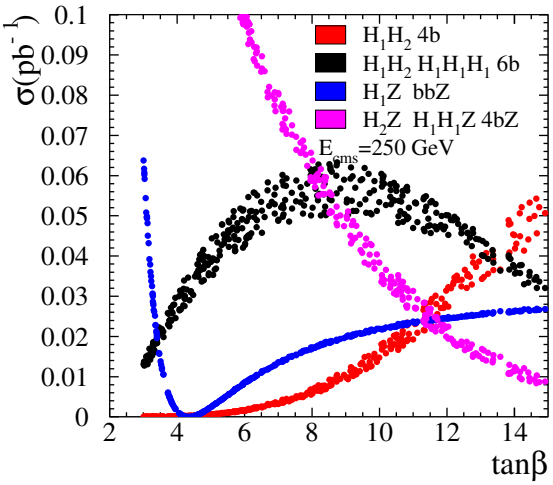

Fig. 3.9: Model predictions for $\sigma \times BR$ values of dominant Higgs boson production mechanisms in the CPX scenario for $30\,\mathrm{GeV} < M_{H_1} < 40\,\mathrm{GeV}$ at $\sqrt{s} = 250\,\mathrm{GeV}$.

$\tan\beta$ can be restricted to values larger than 2.9 for $m_t = 174.3\,\mathrm{GeV}$. While the excluded mass domains vary considerably with m_t, the bound in tan is barely sensitive to the precise choice of the top quark mass.

Fig. 3.9 shows a selection of the same cross-sections as in Fig. 3.5, this time for a center-of-mass energy of 250 GeV instead of 202 GeV. At higher energies, the ZH_2 Higgsstrahlung channel is kinematically open and no suppression of the cross-sections at intermediate $\tan\beta$ can be seen. Therefore it is expected that in this model the ILC will have the same access to the Higgs sector as in a CP conserving MSSM model.

3.3 The ATLAS discovery potential for Higgs bosons in the CPX scenario

Markus Schumacher

The investigation of the discovery potential for Higgs bosons of the MSSM at the LHC has so far concentrated on the CP conserving case with real SUSY breaking parameters. Here we discuss a preliminary investigation of the discovery potential of the ATLAS experiment for Higgs bosons in the CPX scenario [58] of the CP violating MSSM. The soft SUSY breaking parameters have been fixed according to Eq. 3.13 with the common SUSY scale chosen to be M_{SUSY} = 500 GeV, the SU(2) gaugino mass parameter M_2 = 500 GeV and M_1, the U(1) gaugino mass parameter, is derived from M_2 using the GUT relation. The mass of the top quark used in this study is 175 GeV. The two parameters $\tan\beta$ and $M_{H^\pm}$, which determine the Higgs sector at Born level, have been scanned between 1 to 40 and 50 to 1000 GeV, respectively.

3.3.1 Experimental peculiarities

The results of the published ATLAS Monte Carlo (MC) studies, shown in Table 3.1, are used for the investigation of the discovery potential. The key performance figures for e.g. lepton identification and isolation, b-tagging, τ identification, trigger efficiencies and mass resolutions have been obtained from studies using a full simulation of the ATLAS detector. The number of expected signal and background events have been estimated then using a fast simulation of the ATLAS detector.

In order to evaluate the discovery potential of a search channel in a specific $(\tan\beta, M_{H^\pm})$ parame-

ter point, the number of expected signal and background events after all selection cuts need to be derived for this parameter set. This is done in the following way:

3.3.1.1 Masses, coupling and branching ratios

The masses of the Higgs bosons, their coupling strength and branching ratios are calculated with `FeynHiggs 2.1` [145]. Preliminary checks have also been performed using an alternative program `CPsuperH` [131]. The differences in the predictions among the two programs are significant for certain areas of the parameter space e.g. a shift in the mass of H_1 of about 5 GeV can be achieved. This results in a change of the contribution of a particular search channel, however the basic conclusions stay the same. In this report results are only shown which were obtained with `FeynHiggs`.

3.3.1.2 Production cross sections

Leading order cross sections are used for all production processes. All cross sections are calculated using the CTEQ5L parton distribution functions [188]. For the production of neutral Higgs bosons via gluon fusion, weak boson fusion[1] and heavy quarks (ttH_i and bbH_i) the SM like cross sections are calculated using the programs from reference [189][2] and then applying the appropriate correction factors to obtain the MSSM cross section values as detailed below:

$$\text{Gluon fusion}: \quad \sigma^{GGF}_{MSSM} = \frac{\Gamma_{H_i\to\text{gluons}}(MSSM)}{\Gamma_{H\to\text{gluons}}(SM)} \times \sigma^{GGF}_{SM} \tag{3.17}$$

$$\text{Weak Boson Fusion}: \quad \sigma^{WBF}_{MSSM} = \left(\frac{g_{H_iVV}(MSSM)}{g_{HVV}(SM)}\right)^2 \times \sigma^{WBF}_{SM} \tag{3.18}$$

$$\text{ffH}_\text{i}: \quad \sigma^{ffH_i}_{MSSM} = \left(\frac{g^S_{H_iff}(MSSM)}{g^S_{Hff}(SM)}\right)^2 \times \sigma^{Hff}_{SM} + \left(\frac{g^P_{H_iff}(MSSM)}{g^S_{ffH}(SM)}\right)^2 \times \sigma^{ffA}_{2HDM,tan\beta=1} \tag{3.19}$$

Here g_{H_iVV} denote the coupling to weak gauge bosons and $g^P_{H_iff}$ and $g^S_{H_iff}$ the scalar and pseudoscalar coupling to fermions, respectively. The SM values are equal to unity in our convention. For heavy charged Higgs bosons ($M^\pm_H > 180$ GeV) production via the process $gb \to tH^\pm$ is considered. For a light Higgs boson ($M^\pm_H < 170$ GeV) the production in the decay of a top quark in a charged Higgs boson and b quark are investigated. The intermediate mass region is for now excluded from the evaluation of the discovery potential. A discussion of a proper handling of this transition region may be found in [190–192] and is awaiting a detailed experimental MC study.

The cross section $\sigma_{Pseudo-SM}$ for $gb \to H^\pm t$ as a function of the charged Higgs boson mass is calculated with the program of [193]. Here "pseudo" means that the factor $(M_b \tan\beta)^2 + (M_t/\tan\beta)^2$, which enters the cross section, is set to one. The cross section for each parameter point is then scaled according to:

$$\sigma_{MSSM} = [(M_b(\ in\ GeV)\tan\beta)^2 + (M_t(\ in\ GeV)/\tan\beta)^2)]\sigma_{Pseudo-SM} \tag{3.20}$$

Here M_b and M_t denote the running quark masses at the scale $(M_{H^\pm} + M_t)/4$ as recommended in [190, 193].

[1] H_i here and in the following denotes a general neutral Higgs boson mass eigenstate. Only its CP even component couples to W and Z boson. Associated production with weak gauge bosons ($W(Z)H_i$) is not considered as a discovery channel at the LHC.

[2] The codes for `HIGLU`, `VV2H` and `HQQ` are accessible via `http://people.web.psi.ch/spira/proglist.html`.

Table 3.1: Channels contributing to the ATLAS discovery potential. Shown are the production mechanisms, decay channels, mass ranges considered and references for the analysis.

Production process	Decay mode	Mass range (GeV)	Reference
Inclusive	$H_i \to \gamma\gamma$	60 to 400	[196]
Gluon Fusion	$H_i \to ZZ \to 4$ leptons	100 to 450	[196]
Gluon Fusion	$H_i \to WW \to l\nu l\nu$	140 to 200	[196]
Weak Boson Fusion	$H_i \to WW \to l\nu\nu(qql\nu)$	110 (130) to 250	[197]
Weak Boson Fusion	$H_i \to \tau\tau \to ll4\nu, lhad.3\nu$	110 to 180	[197]
ttH_i	$H_i \to bb$	70 to 150	[198]
Gluon Fusion/bbH_i	$H_i \to \mu\mu$	70 to 1000	[199, 200]
Gluon Fusion/bbH_i	$H_i \to \tau\tau \to l\ had.(had.\ had.)$	110(450) to 1000	[201, 202] ([203])
Gluon Fusion	$H_i \to H_jH_k \to \gamma\gamma bb$	100(40) to 360(130)	[196]
Gluon Fusion	$H_i \to H_jZ \to bbll$	100(40) to 360(130)	[196]
Gluon Fusion	$H_i \to tt$	350 to 500	[196]
$tt \to H^\pm bWb$	$H^\pm \to \tau\nu, W \to qq(l\nu)$	70 to 170	[204] ([196])
$gb \to H^\pm t$	$H^\pm \to \tau\nu$	180 to 1000	[192]

The cross section for charged Higgs boson production in top quark decay is calculated in the following way. A leading order top quark pair production cross section of 492 pb is used and multiplied with the $t \to H^\pm b$ branching ratio as obtained from PYTHIA [194, 195] depending on $\tan\beta$ and the charged Higgs boson mass.

3.3.1.3 Signal and background rates

The expected background rates are independent from the MSSM parameter point and their values for a given Higgs boson mass are taken directly from the published ATLAS MC studies. The expected signal rate N_{signal} is calculated according to:

$$N_{signal} = \sigma_{MSSM} \times BR \times \mathcal{L} \times \epsilon \quad , \tag{3.21}$$

where $\mathcal{L}$ denotes the integrated luminosity and $\sigma_{MSSM} \times BR$ the product of cross section times branching ratio for the particular MSSM parameter. The signal efficiency ϵ for a given Higgs boson mass is taken from published detailed ATLAS MC studies. However two type of corrections are applied to the efficiencies as discussed below.

Most experimental MC studies have been performed for a light SM like Higgs boson or for the heavy Higgs bosons for particular choice of the MSSM parameters. These parameter choices include e.g. the following assumptions: (i) the natural total decay width of the Higgs bosons is negligible compared to the mass resolution, (ii) the mass degeneracy between e.g. $\mathcal{H}_2$ and $\mathcal{H}_3$ is perfect i.e. the masses are exactly the same, which means the signal contributions can be simply added. During the scan of the MSSM parameter space these assumption might no be fulfilled for all points. Deviations from the above assumptions have been corrected for in the following way.

The effect of an increased total decay width leading to a broadening of the reconstructed mass peak and therefore to a reduced signal efficiency when using the standard mass window cuts are taken into account by multiplying the signal efficiency with the following correction factor K_{width}:

$$K_{width} = \frac{\int_{M-\Delta M}^{M+\Delta M} BW(\Gamma_{total}^{MSSM}) \otimes G(\sigma_M)}{\int_{M-\Delta M}^{M+\Delta M} BW(\Gamma_{total}^{MC\ study}) \otimes G(\sigma_M)} \tag{3.22}$$

The integration borders $M - \Delta M$ and $M + \Delta M$ are the mass window cuts in the standard MC study. $\Gamma_{total}^{MC\ study}$ denotes the total decay width assumed in the ATLAS MC study, Γ_{total}^{MSSM} the total decay width in the particular MSSM point and σ_M the mass resolution for the signal. $BW(\Gamma_{total})$ is the Breit-Wigner distribution which is folded ($\otimes$) with the Gaussian mass resolution $G(\sigma_M)$. The correction factor is calculated and applied for each individual search channel and each MSSM parameter point separately. In the case that Γ_{total}^{MSSM} is smaller than $\Gamma_{total}^{MCstudy}$ no correction factor, which would be larger than 1, is applied.

Depending on the MSSM parameter point the masses of two of the neutral Higgs bosons might be closer than the expected mass resolution or the mass window cut applied. Then the partially overlapping signal will lead to an increased discovery potential. Examples of such channels are: production via weak boson fusion, associated production with b-quarks and Higgs boson production with decay to a pair of top quarks. In such cases the signal rate of the two contributing mass states are combined in the following way. Consider that the masses of the two bosons are M_1 and M_2. The expected signal and background rate for the Higgs boson with mass M_1 have been evaluated. In addition the signal rate of the boson with mass M_2 leaking into the mass window around M_1 is evaluated and added to the expected signal rate. The same procedure is repeated interchanging the role of the two Higgs bosons. For both cases the significance for observation of a signal excess is evaluated and the one yielding the larger value is retained.

Two luminosity scenarios are distinguished: (i) low luminosity running at $\mathcal{L}$ = 10^{33} cm^{-2}s^{-1} yielding an integrated luminosity of 10 fb^{-1} per year, (ii) high luminosity running at $\mathcal{L}$ = 10^{34} cm^{-2}s^{-1} yielding an integrated luminosity of 100 fb^{-1} per year. At high luminosity running several performance numbers are degraded e.g. b-tagging performance, mass resolutions etc. This change in the detector performance is taken into account when deriving the signal and background rates and from those the discovery potential.

3.3.2 ATLAS discovery potential in the CPX benchmark scenario

The evaluation of the discovery potential is based on Poissonian statistics requiring that the probability of a background fluctuation to the number of expected signal+background events is less than 2.85×10^{-7}. In the case of combining different final states the likelihood ratio method [205] is applied. The results are shown for integrated luminosities of 30 fb^{-1} and 300 fb^{-1}. In the latter case 30 fb^{-1} collected during low luminosity running and 270 fb^{-1} collected at high luminosity running are assumed. The weak boson channels, charged Higgs boson channels for the Higgs boson mass below the top quark mass and the decay $H_i \to \tau\tau$ have only been studied for low luminosity running. Hence all results for these channels are only shown for an integrated luminosity of 30 fb^{-1}.

The discovery potential for the lightest neutral Higgs boson H_1 after collecting an integrated luminosity of 30 and 300 fb^{-1} for the two projections $(M_{H^\pm}, \tan\beta)$ and $(M_{H_1}, \tan\beta)$ is shown in Fig. 3.10. In the $(M_{H^\pm}, \tan\beta)$ projection the discovery potential for 30 fb^{-1} is dominated by the weak boson fusion channels which cover a large area left over by the LEP experiments [206]. Additional small areas of parameter space are covered by associated production with b and top quarks. With 300 fb^{-1} the coverage of the latter two channels is increased and furtheron a large fraction of parameter space is covered also by the decay into a pair of photons and a pair of Z bosons. Masses below 60 GeV have been not studied up to now. In the weak boson fusion channels only masses above 110 GeV have been investigated. Therefore a significant area in the $(M_{H_1}, \tan\beta)$ plane has not been investigated yet.

The discovery potential for the heavier neutral Higgs boson H_2 and H_3 and the charged Higgs bosons in the projection $(M_{H^\pm}, \tan\beta)$ are shown in Fig. 3.11. For the heavy neutral Higgs bosons the area of large $\tan\beta$ is covered by the associated production with b quarks. Areas of low $M_{H^\pm}$ are covered by the production of $H_{2/3}$ in weak boson fusion with subsequent decay into tau leptons and the associated production with top quarks. The area of small $\tan\beta$, which to large extent has already excluded by the LEP searches, is covered by one ore more of several search channels as indicated in the

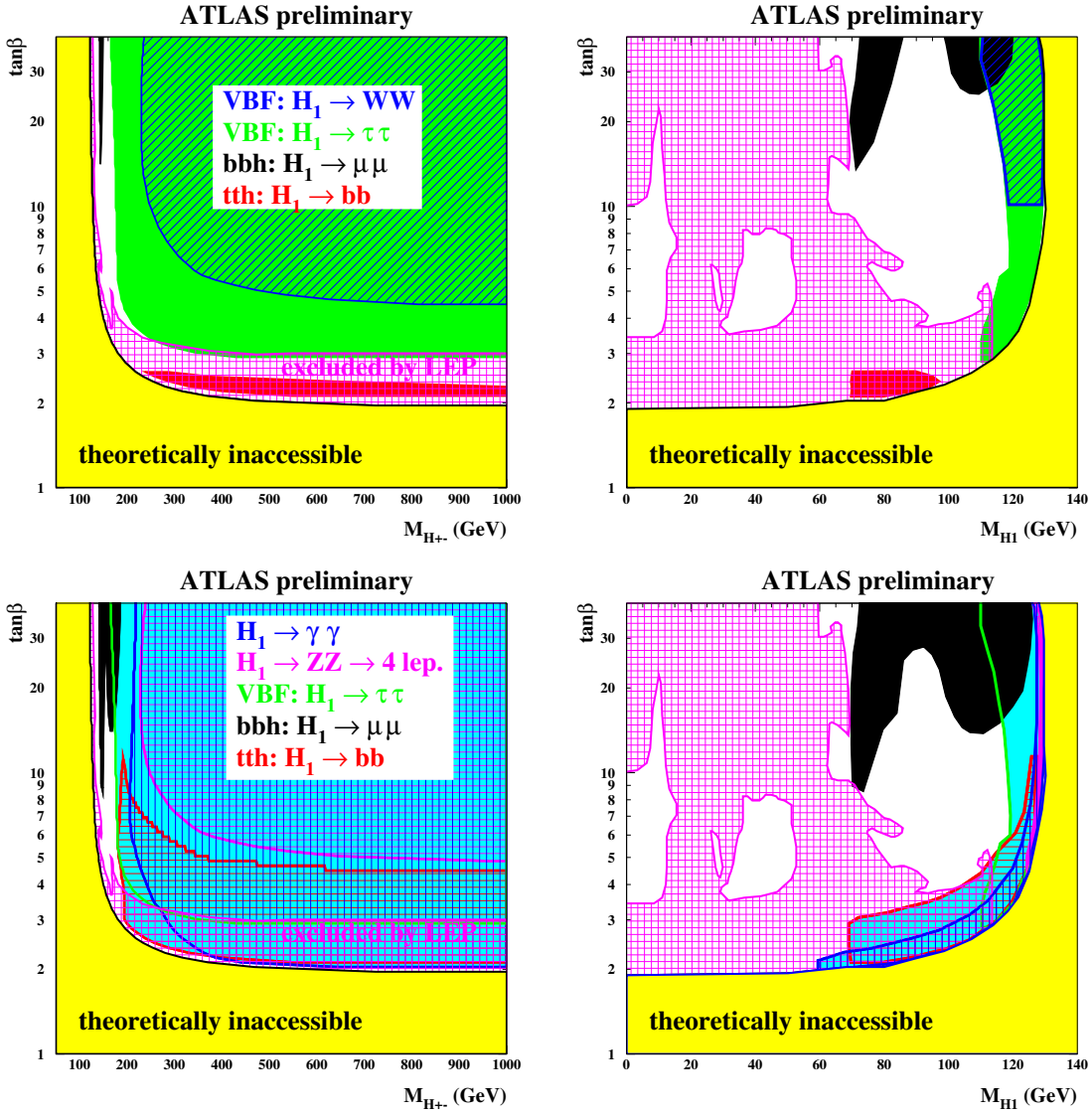

Fig. 3.10: Top row: discovery potential for the lightest neutral Higgs boson H_1 after collecting 30 fb^{-1} In the black area observation via $bbH_1, H_1 \to \mu\mu$ is expected, in the medium grey (green) area via WBF $H_1 \to \tau\tau$, in the single hatched (blue) area via WBF, $H_1 \to WW$ and in dark grey (red) area via $ttH_1, H_1 \to bb$.
Bottom row: discovery potential for the lightest neutral Higgs boson H_1 after collecting 300 fb^{-1}, for the WBF channels only 30 fb^{-1} are used. In the black area observation via $bbH_1, H_1 \to \mu\mu$ is expected, and in the horizontally lined (red) area at low $\tan\beta$ via $ttH_1, H_1 \to bb$, in the horizontally lined (magenta) area at large $\tan\beta$ via $H_1 \to ZZ \to 4$ leptons, in the vertically lined (blue) area via $H_1 \to \gamma\gamma$, and in the remaining solid area surrounded by the green line via WBF, $H_1 \to \tau\tau$.
The light grey (yellow) area is theoretically inaccessible. The cross hatched (magenta) area is excluded by the LEP experiments [206].

figure. At intermediate $\tan\beta$ and charged Higgs boson masses above 700 GeV no discovery potential is found with the current analysis and an integrated luminosity of 300 fb^{-1}. Light charged Higgs bosons below the top quark mass are expected to be observed in the tau lepton decay mode produced in top quark pair productions. Heavy charged Higgs bosons can be discovered via $gb \to tH^{\pm}$ and subsequent decay to $\tau\nu$ for large values of $\tan\beta$.

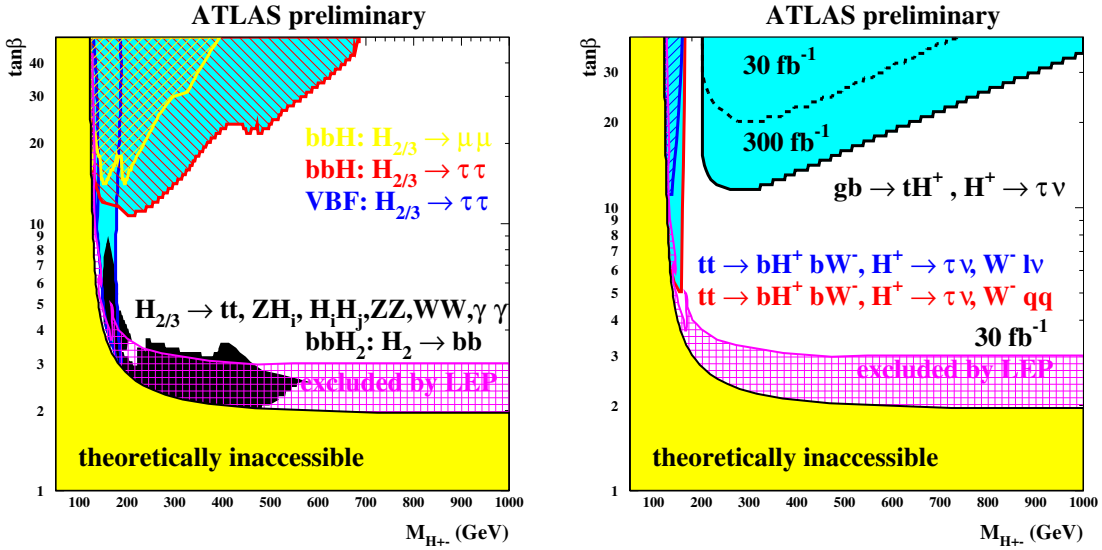

Fig. 3.11: Left: discovery potential for the heavy neutral Higgs bosons. In the black area at small $\tan\beta$ one or both Higgs boson are expected to be observed in the decays $H_{2/3} \to tt, ZH_i, H_iH_j, ZZ, WW, \gamma\gamma$ or in $ttH_{2/3}$ production with $H_{2/3} \to bb$ after collecting 300 fb^{-1}. In the area surrounded by the dark gray (blue) line the WBF channel with $H \to \tau\tau$ contributes, shown for 30 fb^{-1} only. In the left bottom to top right hatched (yellow) area discovery is expected via $bbH_{2/3}, H_{2/3} \to \mu\mu$ after collecting 300 fb^{-1} and in the right bottom to left top hatched (red) area discovery is expected via $bbH_{2/3}, H_{2/3} \to \tau\tau$ after collecting 30 fb^{-1}.
Right: discovery potential for the charged Higgs bosons. In the area at large $\tan\beta$ with $M_{H^\pm}$ >180 GeV discovery is expected via $gb \to tH^\pm, H^\pm \to \tau\nu$. The dashed and solid line show the expected sensitivity after collecting 30 and 300 fb^{-1}, respectively. For $M_{H^\pm}$ <170 GeV observation is expected via charged Higgs bosons produced in top decays with $H^\pm \to \tau\nu$. The expected sensitivity for the leptonic and hadronic decay of the W boson after collecting 30 fb^{-1} is shown in the blue hatched and red solid area, respectively.
The cross hatched (magenta) area is excluded by the LEP experiments [206]. The light grey (yellow) area is theoretically inaccessible.

The overall ATLAS discovery potential after collecting an integrated luminosity of 300 fb^{-1} for the two projections $(M_{H^\pm}, \tan\beta)$ and $(M_{H_1}, \tan\beta)$ are shown in Fig. 3.12. Almost the whole parameter space in the projection $(M_{H^\pm}, \tan\beta)$ is covered by the observation of at least one Higgs boson (see Fig. 3.12 top left). In the intermediate $\tan\beta$ regime only the lightest neutral Higgs boson H_1 is expected to be observable. The zoom in for small charged Higgs boson masses and moderate $\tan\beta$ in the projection $(M_{H^\pm}, \tan\beta)$ shows a small yet uncovered and not yet by LEP excluded region (see Fig. 3.12 top right). The same uncovered region is visible in the $(M_{H_1}, \tan\beta)$ projection (see Fig. 3.12 bottom). Using `FeynHiggs 2.1` for the calculations and assuming a top quark mass of 175 GeV the uncovered region corresponds to the following mass values: $M_{H_1} < 50$ GeV, $105 < M_{H_2} < 115$ GeV, $140 < M_{H_3} < 180$ GeV and $130 < M_{H^\pm} < 170$ GeV. Preliminary studies with `CPsuperH` and a different top quark mass indicate that the size and location of the uncovered region depends on the calculation used, but that this region is existing in all investigations performed. So far the LHC collaborations have not investigated the discovery potential for such a light Higgs boson.

3.3.3 Conclusions

The discovery potential of the ATLAS experiment for Higgs bosons in the CPX scenario of the CP violating MSSM based on current MC studies has been discussed. Almost all of the model parameter space is covered by the observation of at least one Higgs boson. However a "small" corner of the

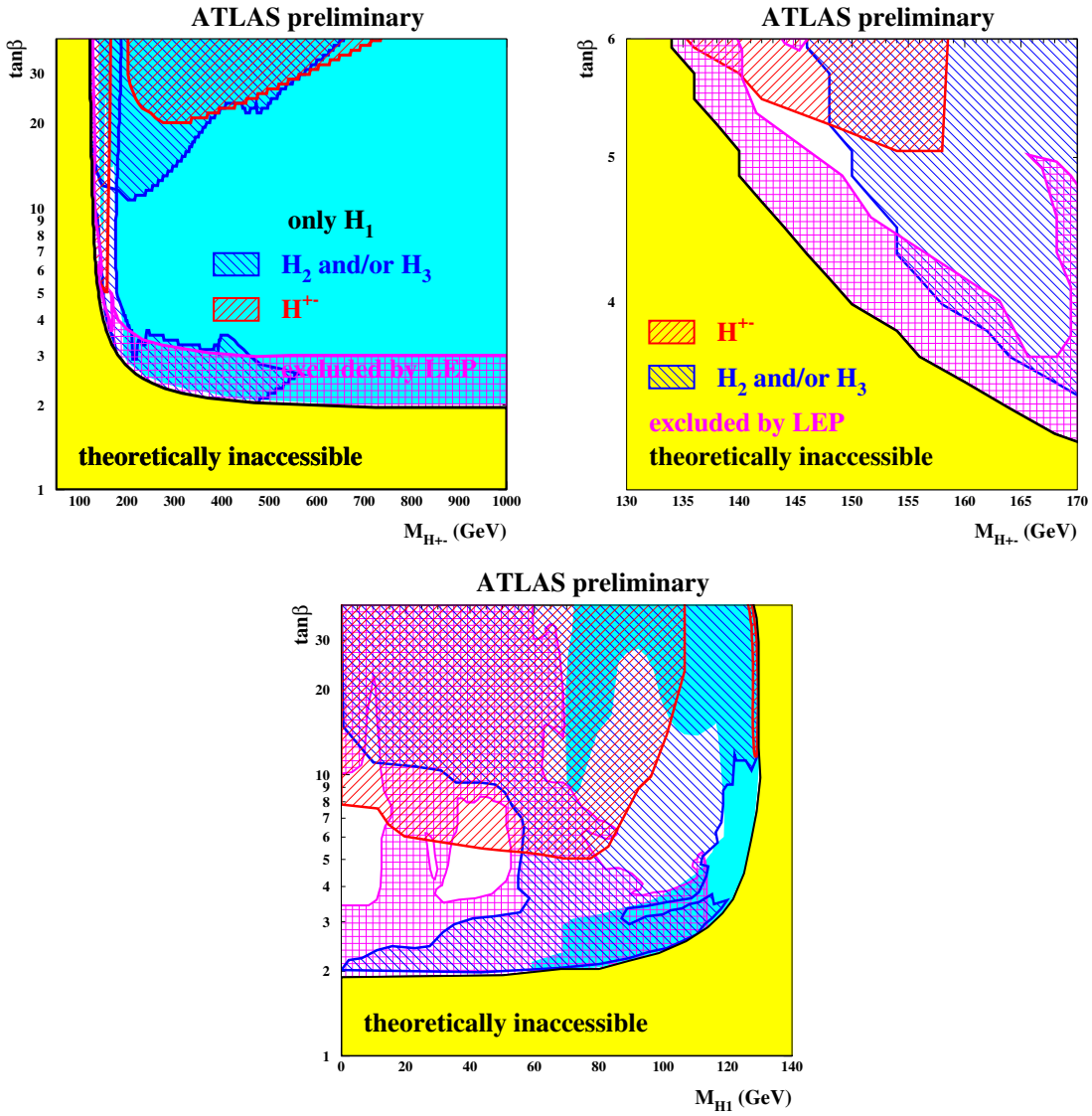

Fig. 3.12: Overall ATLAS discovery potential for Higgs bosons after collecting 300 fb^{-1}. The lightest neutral Higgs boson H_1 is expected to be seen in the solid medium gray (cyan) area. One or both of the heavier neutral Higgs bosons H_2 and H_3 are expected to be observed in in the right top to left bottom hatched (blue) area. The charged Higgs bosons $H^{\pm}$ are expected to be observed in in the right bottom to left top hatched (red) area. The cross hatched (magenta) area is excluded by the LEP experiments [206]. The light grey (yellow) area is theoretically inaccesible.

model parameter space is uncovered by the current MC studies. This area corresponds to small values for the lightest Higgs boson of less than 50 GeV, which is not yet excluded by the LEP searches and the sensitivity of the ATLAS experiment has not yet been studied. The most promising channel for simultaneous observation of the charged and the lightest neutral Higgs boson in this area of parameter space seems to be top quark pair production with the following decay chain: $t \to bW \to bl\nu$, $t \to bH^{\pm} \to bWH_1 \to bqqbb$ [73]. An ATLAS MC study in this channel is in preparation.

3.4 Higgs phenomenology with CPsuperH

John Ellis, Jae Sik Lee and Apostolos Pilaftsis

The Fortran code CPsuperH [131] is a powerful and efficient computational tool for understanding quantitatively phenomenological subjects within the framework of the MSSM with explicit CP violation. It calculates the mass spectrum and decay widths of the neutral and charged Higgs bosons in the most general MSSM including CP-violating phases. In addition, it computes all the couplings of the neutral Higgs bosons $H_{1,2,3}$ and the charged Higgs boson H^+. The program is based on the results obtained in Refs. [141–143] and the most recent renormalization-group-improved effective-potential approach, which includes dominant higher-order logarithmic and threshold corrections, b-quark Yukawa-coupling resummation effects, and Higgs-boson pole-mass shifts [53, 58]. The masses and couplings of the charged and neutral Higgs bosons are computed at a similar high-precision level. Even in the CP-conserving case, CPsuperH is unique in computing the neutral and charged Higgs-boson couplings and masses with equally high levels of precision, and is therefore a useful tool for the study of MSSM Higgs phenomenology at present and future colliders.

3.4.1 Introduction to CPsuperH

The tarred and gzipped program file CPsuperH.tgz can be downloaded from [3]:

http://www.hep.man.ac.uk/u/jslee/CPsuperH.html

Typing tar -xvzf CPsuperH.tgz will create a directory called CPsuperH containing files : OLIST, ARRAY, COMMON, cpsuperh.f, fillpara.f, fillhiggs.f, fillcoupl.f, fillgambr.f, makelib, compit, and run. A library file libcpsuperh.a will be created by ./makelib from the four Fortran files of fillpara.f, fillhiggs.f, fillcoupl.f, and fillgambr.f and the shell-script compit compiles cpsuperh.f linked with the library file. Input values are supplied by the shell-script file run. Straightforwardly, type './makelib' and './compit' followed by './run':

Run CPsuperH: ./makelib → ./compit → ./run

and then one can see some outputs depending on input values. For a full description of the input parameters SMPARA_H(IP), SSPARA_H(IP), IFLAG_H(NFLAG), see Ref. [131].

In CPsuperH, the main numerical output is stored in arrays. The masses of the three neutral Higgs bosons, labelled in order of increasing mass such that $M_{H_1} \leq M_{H_2} \leq M_{H_3}$, are stored in HMASS_H(3). Since the neutral pseudoscalar Higgs bosons mixes with the neautral scalars in the presence of CP violation, the charged Higgs boson mass $M_{H^\pm}$ is used as an input parameter. The array OMIX_H(3,3) yields the 3×3 Higgs mixing matrix, $O_{\alpha i}$: $(\phi_1, \phi_2, a)^T_\alpha = O_{\alpha i}(H_1, H_2, H_3)^T_i$. All the couplings of the neutral and charged Higgs bosons are stored in NHC_H(NC,IH) and CHC_H(NC), respectively. These include Higgs couplings to leptons, quarks, neutralinos, charginos, stops, sbottoms, staus, tau sneutrinos, gluons, photons, and massive vector bosons. The array SHC_H(NC) contains Higgs-boson self-couplings. We note that the masses and mixing matrices of the stops, sbottoms, staus, charginos, and neutralinos are also calculated and stored in corresponding arrays. For the decay widths and branching fractions, the arrays GAMBRN(IM,IWB,IH) and GAMBRC(IM,IWB) are used for the neutral and charged Higgs bosons. For a full description, we refer again to Ref. [131]. The masses and branching fractions of the Higgs bosons and its couplings to a pair of vector bosons obtained by use of CPsuperH are shown in Sec. 3.1.

[3] Some new features appearing in this write-up, for example, the propagator matrix DH(3,3) and some low-energy observables, will be implemented in the forthcoming version of CPsuperH.

3.4.2 Collider signatures

To analyze CP-violating phenomena in the production, mixing and decay of a coupled system of multiple CP-violating MSSM neutral Higgs bosons at colliders, we need a "full" 3×3 propagator matrix $D(s)$, given by [158]

$$D(\hat{s}) = \hat{s} \begin{pmatrix} \hat{s} - M_{H_1}^2 + i\,\mathrm{Im\,m}\widehat{\Pi}_{11}(\hat{s}) & i\,\mathrm{Im\,m}\widehat{\Pi}_{12}(\hat{s}) & i\,\mathrm{Im\,m}\widehat{\Pi}_{13}(\hat{s}) \\ i\,\mathrm{Im\,m}\widehat{\Pi}_{21}(\hat{s}) & \hat{s} - M_{H_2}^2 + i\,\mathrm{Im\,m}\widehat{\Pi}_{22}(\hat{s}) & i\,\mathrm{Im\,m}\widehat{\Pi}_{23}(\hat{s}) \\ i\,\mathrm{Im\,m}\widehat{\Pi}_{31}(\hat{s}) & i\,\mathrm{Im\,m}\widehat{\Pi}_{32}(\hat{s}) & \hat{s} - M_{H_3}^2 + i\,\mathrm{Im\,m}\widehat{\Pi}_{33}(\hat{s}) \end{pmatrix}^{-1}, \tag{3.23}$$

where $\hat{s}$ is the center-of-mass energy squared, $M_{H_{1,2,3}}$ are the one-loop Higgs-boson pole masses, and the absorptive parts of the Higgs self-energies $\mathrm{Im\,m}\widehat{\Pi}_{ij}(\hat{s})$ receive contributions from loops of fermions, vector bosons, associated pairs of Higgs and vector bosons, Higgs-boson pairs, and sfermions. The calculated propagator matrix has been stored in the array `DH(3,3)`.

The so called tri-mixing scenario has been taken for studying the production, mixing and decay of a coupled system of the neutral Higgs bosons at colliders. This scenario is different from the CPX scenario and characterized by large value of $\tan\beta = 50$ and the light charged charged Higgs boson $M_{H^\pm}^{\rm pole} = 155$ GeV. All the three-Higgs states mix significantly in this scenario in the presence of CP-violating mixing. Without CP violation, only two CP-even states mix. For details of the scenario, see Refs. [76, 93, 153, 158].

A. LHC

At the LHC, the matrix element for the process $g(\lambda_1)g(\lambda_2) \to H \to f(\sigma)\bar{f}(\bar{\sigma})$ can conveniently be represented by the helicity amplitude

$$\mathcal{M}^{gg}(\sigma\bar{\sigma};\lambda_1\lambda_2) \;=\; \frac{\alpha_s\, g_f\, \sqrt{\hat{s}}\, \delta^{ab}}{4\pi v} \langle\sigma;\lambda_1\rangle_g \delta_{\sigma\bar{\sigma}} \delta_{\lambda_1\lambda_2}\,, \tag{3.24}$$

where a and b are indices of the SU(3) generators in the adjoint representation and σ, $\bar{\sigma}$, and $\lambda_{1,2}$ denote the helicities of fermion, antifermion, and gluons, respectively. The amplitude $\langle\sigma;\lambda\rangle_g$ is defined as

$$\langle\sigma;\lambda\rangle_g \equiv \sum_{i,j=1,2,3} [S_i^g(\sqrt{\hat{s}}) + i\lambda P_i^g(\sqrt{\hat{s}})]\, D_{ij}(\hat{s})\, (\sigma\beta_f g^S_{H_j\bar{f}f} - i g^P_{H_j\bar{f}f})\,, \tag{3.25}$$

where

$$\begin{aligned} S_i^g(\sqrt{\hat{s}}) &= \sum_{f=b,t} g_f g^S_{H_i\bar{f}f}\, \frac{v}{m_f} F_{sf}(\tau_f) - \sum_{\tilde{f}_j=\tilde{t}_1,\tilde{t}_2,\tilde{b}_1,\tilde{b}_2} g_{H_i\tilde{f}_j^*\tilde{f}_j}\, \frac{v^2}{4m^2_{\tilde{f}_j}} F_0(\tau_{\tilde{f}_j})\,, \\ P_i^g(\sqrt{\hat{s}}) &= \sum_{f=b,t} g_f g^P_{H_i\bar{f}f}\, \frac{v}{m_f} F_{pf}(\tau_f)\,, \end{aligned} \tag{3.26}$$

where $\tau_x = \hat{s}/4m_x^2$ and $\hat{s}$-dependent S_i^g and P_i^g are scalar and pseudoscalar form factors [4], respectively. The Higgs-boson couplings to quarks $g^{S,P}_{H_i\bar{f}f}$ and squarks $g_{H_i\tilde{f}_j^*\tilde{f}_j}$, and the explicit forms of the functions $F_{sf,pf,0}$ are coded in `CPsuperH` [131]. When $f = \tau\,, t\,, \chi^0\,, \chi^\pm$, etc, one can construct CP asymmetries in the longitudinal and/or transverse polarizations of the final fermions which can be observed at the LHC. For other production mechanisms such as b-quark and weak-boson fusions, the CP asymmetries can be defined similarly as in the case of gluon fusion.

When $\tan\beta$ is large and $M_{H^\pm} \sim 150$ GeV, b-quark fusion is a dominant production mechanism and the CP asymmetries in gluon fusion can be diluted. In this case, the most promising channel for probing Higgs-sector CP violation may be the weak-boson fusion process and subsequent decays into

[4] These $\hat{s}$-dependent gluon-gluon-Higgs couplings are stored in arrays `SGLUE(3)` and `PGLUE(3)`.

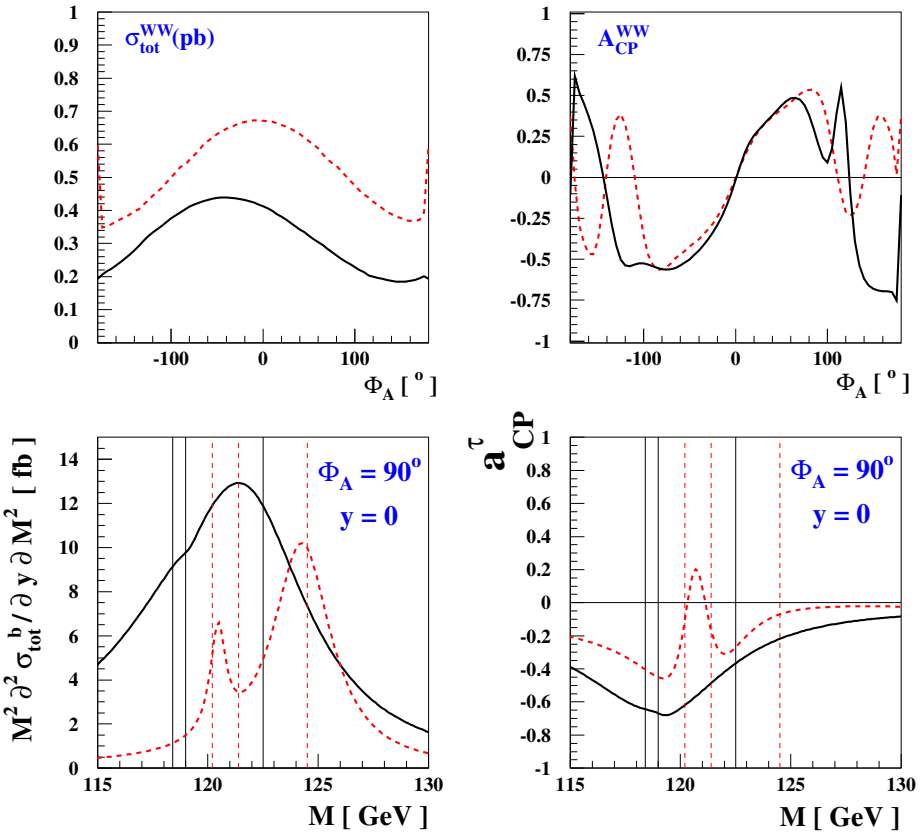

Fig. 3.13: The cross section $\sigma_{\rm tot}^{WW}[pp(WW) \to \tau^+\tau^- X]$ (upper-left panel) at the LHC and its associated total CP asymmetry $\mathcal{A}_{\rm CP}^{WW} \equiv [\sigma_{RR}^{WW} - \sigma_{LL}^{WW}]/[\sigma_{RR}^{WW} + \sigma_{LL}^{WW}]$ (upper-right panel) as functions of $\Phi_A = \Phi_{A_t} = \Phi_{A_b} = \Phi_{A_\tau}$, where $\sigma_{RR(LL)}^{WW} \equiv \sigma(pp\,(WW) \to \tau_{R(L)}^+\tau_{R(L)}^- X)$. We have considered a tri-mixing scenario with $\Phi_3 = -10°$ (dotted lines) and $-90°$ (solid lines). For details of the scenario and the CP asymmetry, see [158]. The lower frames are for Higgs bosons produced in diffractive collisions at the LHC. The lower-left frame shows the hadron-level cross sections when the Higgs bosons decay into b quarks, as functions of the invariant mass M with $\Phi_A = 90°$ and rapidity $y = 0$. The vertical lines indicate the three Higgs-boson pole-mass positions. The lower-right frame shows the CP-violating asymmetry when the Higgs bosons decay into τ leptons. See [76] for details.

tau leptons: $W^+W^- \to H_{1,2,3} \to \tau^+\tau^-$. The cross section $\sigma[pp(W^+W^-) \to H \to \tau^+\tau^- X]$ lies between 0.2 and 0.6 pb and the CP asymmetry is large for a wide range of CP phases, see the two upper frames of Fig. 3.13.

Higgs-boson production in an exclusive diffractive collision $p + p \to p + H_i + p$ offers unique possibilities for exploring Higgs physics in ways that would be difficult or even impossible in inclusive Higgs production [76]. In spite of the low and theoretically uncertain luminosity of the process, what makes diffraction so attractive compared to the inclusive processes are the clean environment due to the large rapidity gap and the good Higgs-mass resolution of the order of 1 GeV which may be achievable by precise measurements of the momenta of the outgoing protons in detectors a long way downstream from the interaction point. It may be possible to disentangle nearly-degenerate Higgs bosons by examining the production lineshape of the coupled system of neutral Higgs bosons, see lower-left frame of Fig. 3.13. Moreover, the CP-odd polarization asymmetry can be measured when the polarization information of Higgs decay products is available, see the lower-right frame of Fig. 3.13. For more studies

of the diffractive production and decay of Higgs bosons in the MSSM scenario with CP violation, see Section 3.8.

B. ILC

A future e^+e^- linear collider, such as the projected ILC, will have the potential to probe the Higgs sector with higher precision than the LHC. At the ILC, the Higgs-boson coupling to a pair of vector bosons, $g_{H_iVV} = c_\beta O_{\phi_1 i} + s_\beta O_{\phi 2i}$, plays a crucial role. There are three main processes for producing the neutral Higgs bosons: Higgs strahlung, WW fusion, and pair production. The cross section of each process is given by

$$\begin{aligned}
\sigma(e^+e^- \to ZH_i) &= g^2_{H_iVV}\, \sigma_{\rm SM}(M_{H_{\rm SM}} \to M_{H_i})\,, \\
\sigma(e^+e^- \to \nu\nu H_i) &= g^2_{H_iVV}\, \sigma^{WW}_{\rm SM}(M_{H_{\rm SM}} \to M_{H_i})\,, \\
\sigma(e^+e^- \to H_iH_j) &= g^2_{H_iH_jV}\, \frac{G_F^2 M_Z^4}{6\pi s}(v_e^2 + a_e^2) \frac{\lambda^{3/2}(1, M^2_{H_i}/s, M^2_{H_j}/s)}{(1 - M_Z^2/s)^2}\,,
\end{aligned} \tag{3.27}$$

where $g_{H_iH_jV} = \mathrm{sign}[\det(O)]\epsilon_{ijk}\, g_{H_kVV}$, $v_e = -1/4 + s^2_W\,, a_e = 1/4$ and $\sigma^{(WW)}_{\rm SM}$ denotes the corresponding production cross section of the SM Higgs boson. As is well known, the WW fusion cross section grows as $\ln(s)$ compared to the Higgs strahlung and becomes dominant for large center-of-mass energy $\sqrt{s}$. In the decoupling limit, $M_{H^\pm} \gtrsim 200$ GeV, the couplings for heavier Higgs bosons $g_{H_{2,3}VV}$ are suppressed, see Fig. 3.1 of Sec. 3.1. In this case, for the production of H_2 and H_3, the pair production mechanism is active since $|g_{H_2H_3V}| = |g_{H_1VV}| \sim 1$. When $M_{H^\pm} \lesssim 200$ GeV, the excellent energy and momentum resolution of electrons and muons coming from measurements of the Z boson in Higgs strahlung may help to resolve a coupled system of neutral Higgs bosons by analyzing the production lineshape, see the two upper panels of Fig. 3.14.

As noted in the previous section, if one observes three Higgs bosons in Higgsstrahlung and WW fusion and/or all three pairs of Higgs bosons in pair production, this can be interpreted as a signal of CP violation in the MSSM framework. However, such an interpretation relies on the hypothesis that there exist no additional singlet or doublet Higgs fields. To confirm the existence of genuine CP violation, one needs to measure other observables such as CP asymmetries. In this light, the final fermion spin-spin correlations in Higgs decays into tau leptons, neutralinos, charginos, and top quarks need to be investigated. See the lower panels of Fig. 3.14 for an example when Higgs bosons are are produced in Higgs strahlung and decay into τ leptons. The two CP asymmetries a_L^τ and a_T^τ are defined in terms of the longitudinal and transverse polarizations of final τ leptons, see [153] for details.

C. γLC

The two-photon collider option of the ILC, the γLC, offers unique capabilities for probing CP violation in the MSSM Higgs sector, because one may vary the initial-state polarizations as well as measure the polarizations of some final states in Higgs decays [93]. The amplitude contributing to $\gamma(\lambda_1)\gamma(\lambda_2) \to H \to f(\sigma)\bar{f}(\bar{\sigma})$ is given by

$$\mathcal{M}_H \;=\; \frac{\alpha\, m_f\, \sqrt{\hat{s}}}{4\pi v^2} \langle \sigma; \lambda_1 \rangle_H \delta_{\sigma\bar{\sigma}} \delta_{\lambda_1\lambda_2}, \tag{3.28}$$

where the reduced amplitude

$$\langle \sigma; \lambda \rangle_H \;=\; \sum_{i,j=1}^{3} [S_i^\gamma(\sqrt{\hat{s}}) + i\lambda P_i^\gamma(\sqrt{\hat{s}})]\; D_{ij}(\hat{s})\; (\sigma\beta_f g^S_{H_j\bar{f}f} - i g^P_{H_j\bar{f}f}), \tag{3.29}$$

is a quantity given by the Higgs-boson propagator matrix Eq. (3.23) combined with the production and decay vertices. The one-loop induced complex couplings of the $\gamma\gamma H_i$ vertex, $S_i^\gamma(\sqrt{\hat{s}})$ and $P_i^\gamma(\sqrt{\hat{s}})$, get dominant contributions from charged particles such as the bottom and top quarks, tau leptons, $W^\pm$

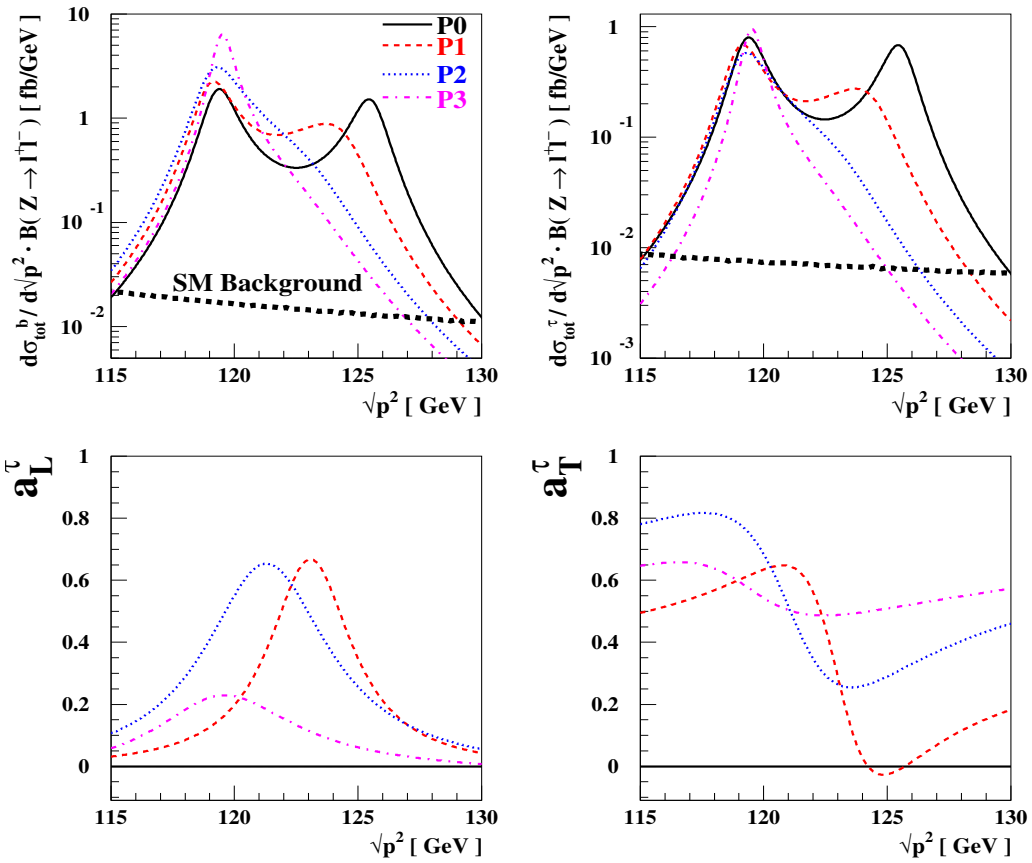

Fig. 3.14: The differential total cross section $d\hat{\sigma}^f_{\rm tot}(e^-e^+ \to ZH_i \to Z\bar{f}f)/d\sqrt{p^2}$ multiplied by $B(Z \to l^+l^-) = B(Z \to e^+e^-) + B(Z \to \mu^+\mu^-)$ as functions of the invariant mass of the Higgs decay products $\sqrt{p^2}$ in units of fb/GeV when $f = b$ (upper-left panel) and $f = \tau$ (upper-right panel). The CP-conserving two-way mixing (**P0**) and three CP-violating tri-mixing (**P1**-**P3**) scenarios have been taken. The lower two frames show the CP-violating asymmetries when Higgs bosons decay into tau leptons. See [153] for details.

bosons, charginos, third-generation sfermions and charged Higgs bosons [5] :

$$
\begin{aligned}
S_i^\gamma(\sqrt{\hat{s}}) &= 2\sum_{f=b,t,\tilde{\chi}^\pm_{1,2}} N_C\, Q_f^2\, g_f g^S_{H_i\bar{f}f}\, \frac{v}{m_f} F_{sf}(\tau_f) - \sum_{\tilde{f}_j=\tilde{t}_{1,2},\tilde{b}_{1,2},\tilde{\tau}_{1,2}} N_C\, Q_f^2 g_{H_i\tilde{f}_j^*\tilde{f}_j} \frac{v^2}{2m^2_{\tilde{f}_j}} F_0(\tau_{\tilde{f}_j}) \\
&\quad - g_{H_iVV} F_1(\tau_W) - g_{H_iH^+H^-} \frac{v^2}{2M^2_{H^\pm}} F_0(\tau_{H^\pm})\,, \\
P_i^\gamma(\sqrt{\hat{s}}) &= 2\sum_{f=b,t,\tilde{\chi}^\pm_{1,2}} N_C\, Q_f^2\, g_f g^P_{H_i\bar{f}f}\, \frac{v}{m_f} F_{pf}(\tau_f)\,,
\end{aligned}
\tag{3.30}
$$

where $\tau_x = \hat{s}/4m_x^2$, $N_C = 3$ for (s)quarks and $N_C = 1$ for staus and charginos, respectively. For the explicit forms of F_1 and couplings, see [131].

One advantage of γLC over the e^+e^- option at the ILC is that one can construct CP asymmetries even when Higgs bosons decay into muons and b quarks, by exploiting the controllable beam polarizations of the colliding photons, see Fig. 3.15.

[5] The arrays `SPHO(3)` and `PPHO(3)` are used for the $\hat{s}$-dependent γ-γ-Higgs couplings.

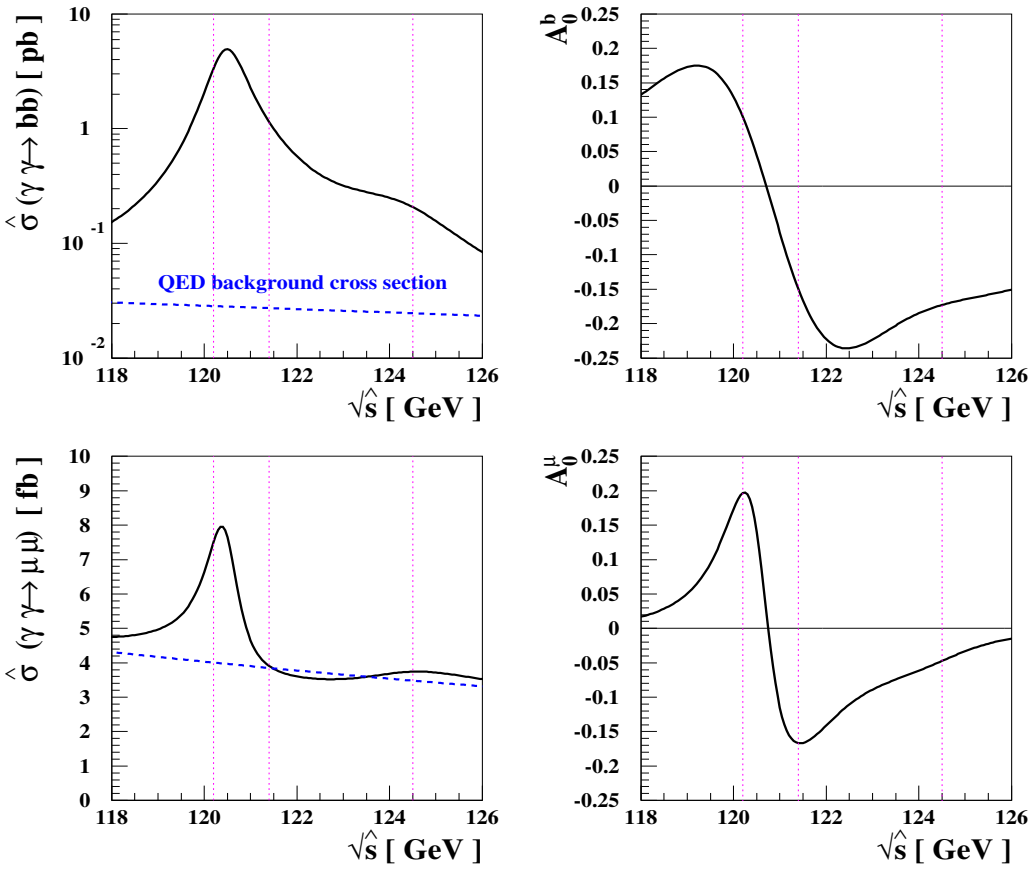

Fig. 3.15: The cross sections (left column) and the CP asymmetries $\mathcal{A}_0^f$ (right column) for the processes $\gamma\gamma \to \bar{b}b$ (upper) and $\gamma\gamma \to \mu^+\mu^-$ (lower). The QED continuum contributions to the cross sections are also shown. The tri-mixing scenario with $\Phi_3 = -10^\circ$ and $\Phi_A = 90^\circ$ has been considered, making the angle cuts $\theta^b_{\rm cut} = 280$ mrad and $\theta^\mu_{\rm cut} = 130$ mrad. The three Higgs masses are indicated by vertical lines. See [93] for details.

One can investigate all possible spin-spin correlations in the final states such as tau leptons, neutralinos, charginos, top quarks, vector bosons, etc., with the goal of complete determination of CP-violating Higgs-boson couplings to them. The cases of tau-lepton and top-quark final states are demonstrated in [93].

For the complete determination of CP-violating Higgs-boson couplings to SM as well as Supersymmetric particles, a muon collider is even better than the γLC. At a muon collider, it is possible to control the energy resolution and polarizations of both the muon and the anti-muon. Compared to the γLC case, the center-of-mass frame is known and it has much better resolving power for a nearly-degenerate system of Higgs bosons [100].

3.4.3 Low-energy observables

Low-energy observables such as EDMs, $(g-2)_\mu$, BR$(b \to s\gamma)$, $\mathcal{A}_{\rm CP}(b \to s\gamma)$, BR$(B \to Kll)$, BR$(B_{s,d} \to l^+l^-)$, etc. provide indirect constraints on the soft SUSY breaking parameters. Specifically, we show in [153] that it is straightforward to obtain the expressions of the coefficient C_S and the Higgs-mediated d_e for the thallium EDM by use of couplings calculated by `CPsuperH`. Fig. 3.16 shows that one can implement the thallium EDM constraint on the CP-violating phases and demonstrate that they leave open the possibility of large CP-violating effects in Higgs production at the ILC.

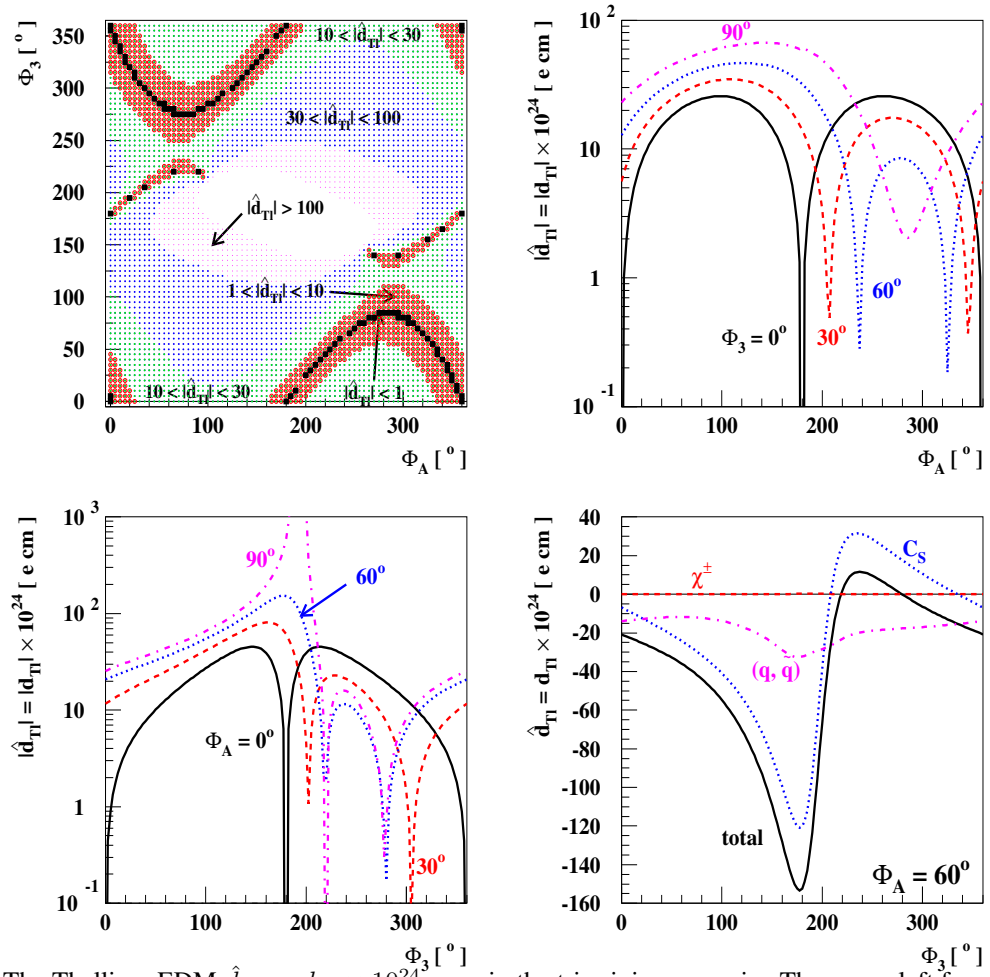

Fig. 3.16: The Thallium EDM $\hat{d}_{\rm Tl} \equiv d_{\rm Tl} \times 10^{24}\, e\, cm$ in the tri-mixing scenario. The upper-left frame displays $|\hat{d}_{\rm Tl}|$ in the (Φ_A, Φ_3) plane. The unshaded region around the point $\Phi_3 = \Phi_A = 180^o$ is not theoretically allowed. The different shaded regions correspond to different ranges of $|\hat{d}_{\rm Tl}|$, as shown: specifically, $|\hat{d}_{\rm Tl}| < 1$ in the narrow region denoted by filled black squares. In the upper-right frame, we show $|\hat{d}_{\rm Tl}|$ as a function of Φ_A for several values of Φ_3. In the lower-left frame, we show $|\hat{d}_{\rm Tl}|$ as a function of Φ_3 for four values of Φ_A. In the lower-right frame, we show the C_S (dotted line) and d_e (dash-dotted line) contributions to $\hat{d}_{\rm Tl}$ separately as functions of Φ_3 when $\Phi_A = 60^o$. As shown by the dashed line, the chargino contribution is negligible. See [153] for details.

The code `CPsuperH` will be extended in near future to include CP-violating effective FCNC Higgs-boson interactions to up- and down-type quarks [207–210]. The determination of these effective interactions may be further improved in the framework of an effective potential approach, where the most significant subleading contributions to the couplings can be consistently incorporated. At large values of $\tan\beta$, Higgs-mediated interactions contribute significantly to the B-meson observables mentioned above and so may offer novel constraints on the parameter space of constrained versions of the MSSM, such as the scenario of minimal flavour violation.

3.5 Higgs phenomenology in the Feynman-diagrammatic approach / FeynHiggs

Thomas Hahn, Sven Heinemeyer, Wolfgang Hollik, Heidi Rzehak, Georg Weiglein and Karina Williams

In this contribution we present recent higher-order corrections to the Higgs boson masses and decay widths involving complex phases that have been obtained in the Feynman diagrammatic (FD) approach. A precise prediction for the masses of the Higgs bosons, their couplings, and their production and decay processes in terms of the relevant SUSY parameters is necessary in order to determine the discovery and exclusion potential of the Tevatron [211–214], and for physics at the LHC [196, 215–219] and the ILC [220–225].

In the following we discuss the two-loop corrections of $\mathcal{O}(\alpha_t\alpha_s)$ to the Higgs boson masses and mixings. We give a short description of the calculation and show numerical examples, comparing the phase dependence at the one-loop and the two-loop level. We furthermore present the vertex corrections to the decay $H_2 \to H_1 H_1$, which plays an important role for the Higgs search in the CP-violating MSSM [162]. We discuss some details of the calculation and present the numerical results, showing the impact of higher-order corrections and the dependence on the complex phase. The new results discussed in this contribution are currently implemented into the Fortran code `FeynHiggs`. We provide a brief description of this code, including a summary of the evaluated observables and instructions for its installation and use.

3.5.1 Higher-order corrections to the Higgs boson masses and mixings

The current status can be summarized as follows: after the first more general investigations [48, 49], one-loop calculations have been performed in the effective potential (EP) approach [51, 52], and leading two-loop contributions have been incorporated with the renormalisation-group (RG) improved one-loop EP method [50, 53]. These results have been restricted to the corrections coming from the (s)fermion sector and some leading logarithmic corrections from the gaugino sector. Within the FD approach the leading one-loop corrections have been calculated in Ref. [59], and the complete one-loop result has been obtained in Refs. [60, 61, 148]. Within the FD approach the two-loop corrections in the $t/\tilde{t}$ sector had so far been restricted to the MSSM with real parameters [113–115, 118]. The FD result in the MSSM with real parameters contains subleading two-loop corrections that go beyond the result obtained in the EP/RG approach, leading to a shift in the lightest Higgs boson mass of about 4 GeV [132]. It is clearly desirable to extend the FD two-loop result to the CP-violating MSSM.

In this section we present the $\mathcal{O}(\alpha_t\alpha_s)$ corrections to Higgs boson masses and mixings including the full phase dependence at the two-loop level.

3.5.1.1 Calculation of two-loop corrections

In order to compute the Higgs boson masses and mixings up to $\mathcal{O}(\alpha_t\alpha_s)$ the determinant of the inverse propagator matrix Γ has to be evaluated,

$$\Gamma(k^2) = k^2 \mathbb{1} - \begin{pmatrix} (M_H^{(0)})^2 - \hat{\Sigma}_{HH}(k^2) & -\hat{\Sigma}_{hH}(k^2) & -\hat{\Sigma}_{AH}(k^2) \\ -\hat{\Sigma}_{hH}(k^2) & (M_h^{(0)})^2 - \hat{\Sigma}_{hh}(k^2) & -\hat{\Sigma}_{Ah}(k^2) \\ -\hat{\Sigma}_{AH}(k^2) & -\hat{\Sigma}_{Ah}(k^2) & (M_A^{(0)})^2 - \hat{\Sigma}_{AA}(k^2) \end{pmatrix} . \tag{3.31}$$

The Higgs masses are given by the roots of det(Γ). The tree-level masses are denoted by $M^{(0)}$. The renormalized self-energies, $\hat{\Sigma}_{\phi\phi}(k^2)$ with $\phi = H, h, A$, contain a one-loop and a two-loop part,

$$\hat{\Sigma}_{\phi\phi} = \hat{\Sigma}^{(1)}_{\phi\phi} + \hat{\Sigma}^{(2)}_{\phi\phi} . \tag{3.32}$$

In our calculation we have evaluated the dominant part of the two-loop self-energies, i.e. the contributions of $\mathcal{O}(\alpha_t\alpha_s)$, taking into account the full complex phase dependence. To extract this dominant part

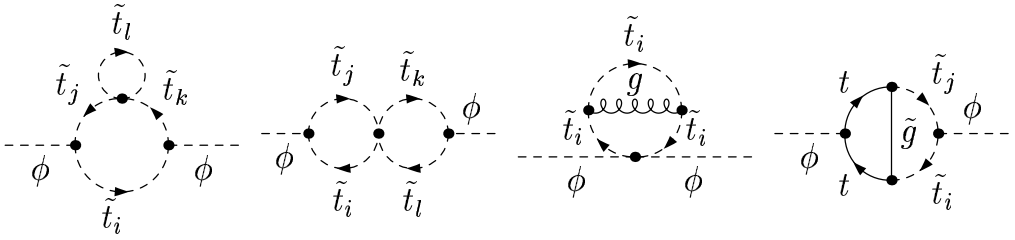

Fig. 3.17: Sample of two-loop diagrams for the Higgs-boson self-energies ($\phi = h, H, A;\ i, j, k, l = 1, 2$).

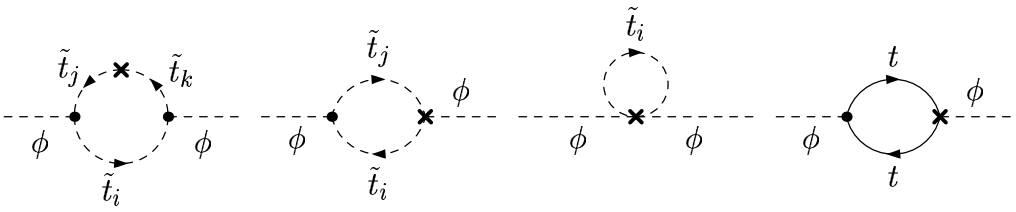

Fig. 3.18: Sample diagrams for the Higgs self-energies with counterterm insertion ($\phi = h, H, A;\ i, j, k = 1, 2$).

the generic self-energy diagrams (see Fig. 3.17) and the corresponding diagrams with counterterm insertions (see Fig. 3.18) have been evaluated applying the approximation of vanishing electroweak gauge couplings and vanishing external momenta. The Feynman diagrams have been generated with the package `FeynArts` [226–229] and the tensor reduction has been performed with the package `TwoCalc` [230].

In the calculation of the renormalised self-energies the input parameter $M_{H^\pm}$ enters and has to be defined at the two-loop level. We use the on-shell renormalisation for the charged Higgs boson,

$$\mathrm{Re}\hat{\Sigma}_{H^+H^-}(M^2_{H^\pm}) = 0\,, \tag{3.33}$$

where as explained above the external momentum is neglected in the two-loop contribution. The on-shell condition ensures that $M_{H^\pm}$ corresponds to the physical (pole) mass. Also the SM gauge bosons are renormalized on-shell. The tadpole coefficients must vanish in order not to shift the vacuum expectation values,

$$T_\phi + \delta T_\phi = 0 \quad (\phi = h, H, A)\,. \tag{3.34}$$

The counterterm expressions enter the the renormalised Higgs self-energies in Eq. (3.31).

The parameters of the $\tilde{t}$ sector have to be defined at the one-loop level. The top quark mass, m_t, as well as the two $\tilde{t}$ masses, $m_{\tilde{t}_1}$ and $m_{\tilde{t}_2}$, are defined as pole masses. The mixing is fixed by (generalizing the condition used in Ref. [231])

$$\widetilde{\mathrm{Re}}\hat{\Sigma}_{\tilde{t}_{12}}(m^2_{\tilde{t}_1}) + \widetilde{\mathrm{Re}}\hat{\Sigma}_{\tilde{t}_{12}}(m^2_{\tilde{t}_2}) = 0\,, \tag{3.35}$$

where $\widetilde{\mathrm{Re}}$ gives the real part of the loop functions and does not act on complex parameters.

3.5.1.2 Numerical results

At the two-loop level the phases of the $\tilde{t}$ sector, Φ_{A_t} and Φ_μ, and of the gluino mass parameter, Φ_3, enter the prediction of the Higgs boson masses and mixings. The phase of the Higgs mixing parameter, Φ_μ, is tightly constrained by the measurements of the electric dipole moments [232] (we use the convention where $\Phi_{M_2} = 0$), and we therefore do not consider non-zero values of this phase.

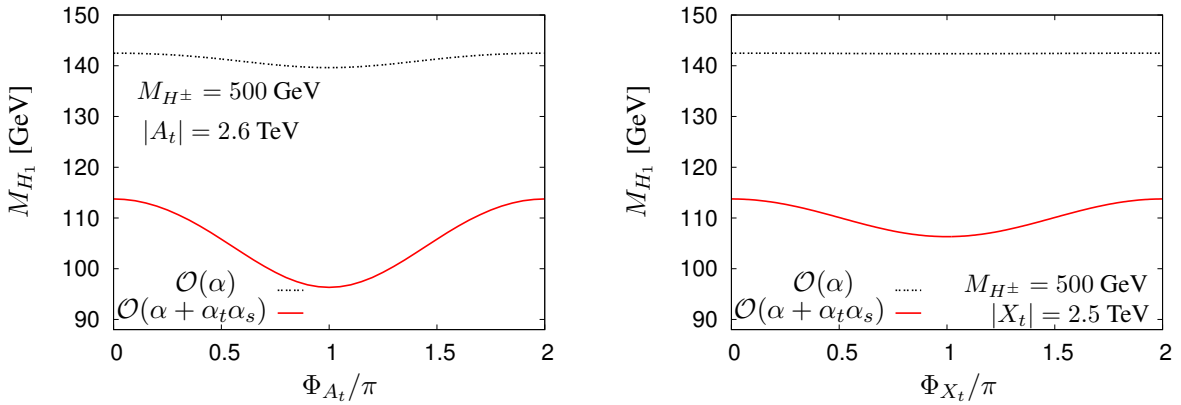

Fig. 3.19: Dependence of the mass of the lightest Higgs boson, M_{H_1}, on the phase Φ_{A_t} (left) and the phase Φ_{X_t} (right). The mass prediction is shown including $\mathcal{O}(\alpha)$ (one-loop) and $\mathcal{O}(\alpha + \alpha_t\alpha_s)$ (two-loop) corrections.

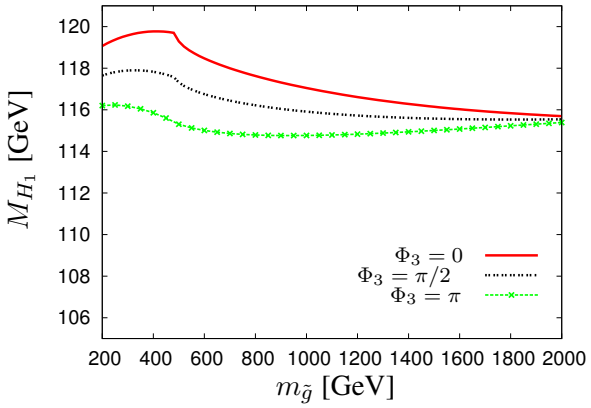

Fig. 3.20: Dependence of M_{H_1} on $m_{\tilde{g}}$ for $\Phi_3 = 0, \pi/2, \pi$ with $M_{\rm SUSY} = 500$ GeV.

The following default values for the parameters have been used unless indicated otherwise: $m_t = 174.3$ GeV, $M_{H^\pm} = 500$ GeV, $\tan\beta = 10$, $\mu = 1000$ GeV, $M_1 = 5/3 \tan^2\theta_W M_2$, $M_2 = 500$ GeV, $M_3 = 1000$ GeV, $M_{\rm SUSY} = 1000$ GeV (the soft SUSY-breaking parameters in the diagonal entries in the sfermion mass matrices), $|A_f| = 1000$ GeV (the trilinear sfermion-Higgs couplings), and $\Phi_{A_f} = 0$.

In Fig. 3.19 two numerical examples are shown. In the left plot the dependence of M_{H_1} on the phase of the trilinear coupling, Φ_{A_t}, is shown, taking into account the one-loop and the one- and two-loop contributions, respectively. The phase dependence is much stronger in the case of the two-loop corrected mass. This is related in particular to the two-loop contributions with gluino exchange, see Fig. 3.17. Varying Φ_{A_t} also changes the amount of $\tilde{t}$ mixing, $X_t := A_t - \mu^* \cot\beta$, and hence also the values of the $\tilde{t}$ masses. In the right plot of Fig. 3.19 the phase of the squark mixing Φ_{X_t} is varied, which keeps the $\tilde{t}$ masses constant. The parameters are chosen such that for vanishing phases the Higgs masses in both plots in Fig. 3.19 are equal. In the right plot the phase dependence is negligible for the one-loop mass but still sizeable in the two-loop case. This behaviour is related to the fact that the one-loop result in the MSSM is symmetric w.r.t. changing the sign of X_t, while the FD two-loop result contains contributions proportional to odd powers of X_t that amount to several GeV in M_{H_1}, see e.g. Ref. [132].

In Fig. 3.20 we show the dependence of M_{H_1} on $m_{\tilde{g}} \equiv |M_3|$ for three different values of the gluino phase, $\Phi_3 = 0, \pi/2, \pi$. The plot shows that both the variation of $m_{\tilde{g}}$ (see also Ref. [115]) and the impact of the complex phase Φ_3 can lead to shifts in the prediction for M_{H_1} of several GeV. The dependence on Φ_3 is most pronounced in the threshold region seen in Fig. 3.20, where $m_{\tilde{g}} \approx m_{\tilde{t}_1} + m_t$.

The numerical examples shown above demonstrate that the effects of complex phases at the two-loop level are relevant for a precise prediction of the Higgs masses and thus for confronting SUSY theories with present and future experimental results from the Higgs searches. The implementation of the new two-loop corrections into the program `FeynHiggs` is in progress.

3.5.2 Higher-order corrections to the decay $H_2 \to H_1 H_1$

Due to the two Higgs-doublet structure of the MSSM, the on-shell decay of a heavier Higgs boson to two lighter Higgs bosons is possible. For real parameters this can be $h \to AA$ in a small parameter region with very light M_A [233] or $H \to hh$ for large values of M_A. The former decay leads to small unexcluded parameter regions in the M_A–$\tan\beta$ plane from LEP Higgs searches [162] (especially in the "no-mixing" scenario [234]).

Within the CP-violating MSSM, where all three neutral Higgs bosons can mix, the decays H_2, H_3 – $H_1 H_1$ can be important. In the parameter region of the CPX scenario [54] probed by the LEP Higgs searches the decay $H_2 \to H_1 H_1$ can be large, leading to unexcluded areas in the $M_{H^\pm}$–$\tan\beta$ parameter plane for $\tan\beta \sim 4$ and M_{H_1} values of ~ 40 GeV [162]. A precise prediction of this decay in the CP-violating MSSM is crucial in order to translate the experimental limits into reliable bounds on the SUSY parameter space.

In the following we present results for the leading vertex corrections to the decay $H_2 \to H_1 H_1$, obtained in the FD approach. The results for the genuine vertex contributions are combined with the propagator corrections for the external Higgs bosons (evaluated with `FeynHiggs` [60, 115, 130, 144, 147, 148, 235], see Section 3.5.3).

3.5.2.1 Calculation

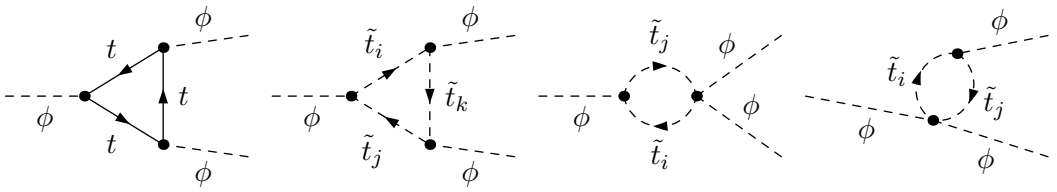

Fig. 3.21: Leading vertex corrections to the decay $H_2 \to H_1 H_1$, involving $t/\tilde{t}$ loops. ($\phi = h, H, A$; $i, j, k = 1, 2$)

The first step in the calculation is the evaluation of the leading one-loop vertex contributions. They consist of the Yukawa-enhanced terms (i.e. those proportional to m_t^4) of the diagrams with $t/\tilde{t}$ loops depicted in Fig. 3.21. In order to extract the leading contributions it is sufficient to neglect the gauge couplings and the external momentum. The contributions obtained in this way form a UV-finite subclass. The diagrams were evaluated using the packages `FeynArts` [226–229] and `FormCalc` [236].

The vertex corrections are supplemented with the external propagator corrections, evaluated up to the two-loop level [59–61, 115, 130, 147, 148]. These contributions are incorporated using the the elements of the matrix U, see Eq. (3.37). The elements of the mixing matrix and the masses M_{H_1}, M_{H_2} of the external particles were obtained from `FeynHiggs` (see Section 3.5.3). Accordingly, the amplitude

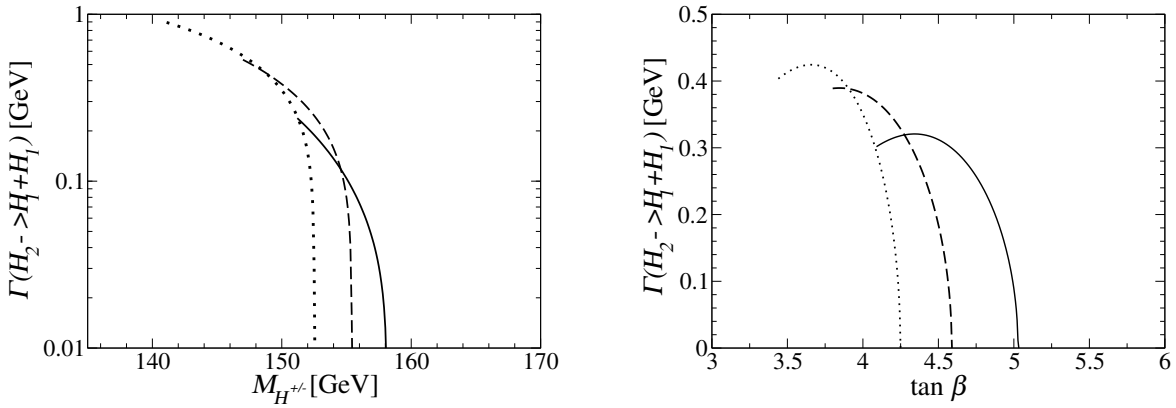

Fig. 3.22: Decay width $\Gamma(H_2 \to H_1 H_1)$ in the CPX scenario (using the CPX values as on-shell parameters) as function of $M_{H^\pm}$ for $\tan\beta = 4$ (left) and as function of $\tan\beta$ for $M_{H^\pm}$ = 150 GeV (right). The genuine vertex contributions are supplemented with the external propagator corrections evaluated with `FeynHiggs` incorporating the one-loop $t, \tilde{t}, b, \tilde{b}$ contributions for vanishing external momentum (dotted lines), the full one-loop result (dashed lines), and the two-loop result (solid lines).

for the decay can be written as:

$$\begin{aligned} A(H_2 \to H_1 H_1) \;=\; & U_{21}U_{11}^2\Gamma_{hhh} + U_{13}^2U_{23}\Gamma_{AAA} + \left(U_{21}U_{13}^2 + 2U_{11}U_{23}U_{13}\right)\Gamma_{hAA} \\ & + \left(U_{22}U_{13}^2 + 2U_{12}U_{23}U_{13}\right)\Gamma_{HAA} + \left(U_{23}U_{11}^2 + 2U_{13}U_{21}U_{11}\right)\Gamma_{hhA} \\ & + (2U_{12}U_{13}U_{21} + 2U_{11}U_{13}U_{22} + 2U_{11}U_{12}U_{23})\Gamma_{hHA} \\ & + \left(U_{23}U_{12}^2 + 2U_{13}U_{22}U_{12}\right)\Gamma_{HHA} + \left(U_{22}U_{11}^2 + 2U_{12}U_{21}U_{11}\right)\Gamma_{hhH} \\ & + \left(U_{21}U_{12}^2 + 2U_{11}U_{22}U_{12}\right)\Gamma_{hHH} + U_{12}^2U_{22}\Gamma_{HHH}, \end{aligned} \tag{3.36}$$

with

$$U = O^T \begin{pmatrix} -s_\alpha & c_\alpha & 0 \\ c_\alpha & s_\alpha & 0 \\ 0 & 0 & 1 \end{pmatrix}, \tag{3.37}$$

where O is defined in Eq. (3.5), and Γ denotes the genuine one-loop vertex contributions. α is the angle diagonalizing the CP-even Higgs-boson mass matrix at tree-level.

3.5.2.2 Numerical results

Results for the decay width $\Gamma(H_2 \to H_1 H_1)$ are shown in Figs. 3.22, 3.23. As described above, our numerical results for $\Gamma(H_2 \to H_1 H_1)$ are obtained by supplementing the genuine one-loop vertex contributions with the external propagator corrections according to Eq. (3.36). These external propagator corrections are evaluated with the program `FeynHiggs` incorporating different sets of higher-order contributions. The dotted lines in Figs. 3.22, 3.23 indicate the result where only the one-loop $t, \tilde{t}, b, \tilde{b}$ contributions for vanishing external momentum are taken into account, the dashed lines correspond to the full one-loop result for the propagator corrections, while the full lines indicate the results incorporating also the two-loop propagator corrections.

Fig. 3.22 shows the prediction for the decay width $\Gamma(H_2 \to H_1 H_1)$ as function of $M_{H^\pm}$ (left plot) and as a function of $\tan\beta$ (right plot). The parameters are those of the CPX scenario as defined in Eq. (3.13), with $M_{\rm SUSY} = 500$ GeV and $\Phi_{A_t} = \pi/2$. Once two-loop corrections are taken into account, the renormalisation scheme for the parameters in the stop sector needs to be specified. For simplicity, we interpret $|A_t|$ and $M_{\rm SUSY}$ as on-shell parameters in Fig. 3.22. The figure illustrates the fact that the

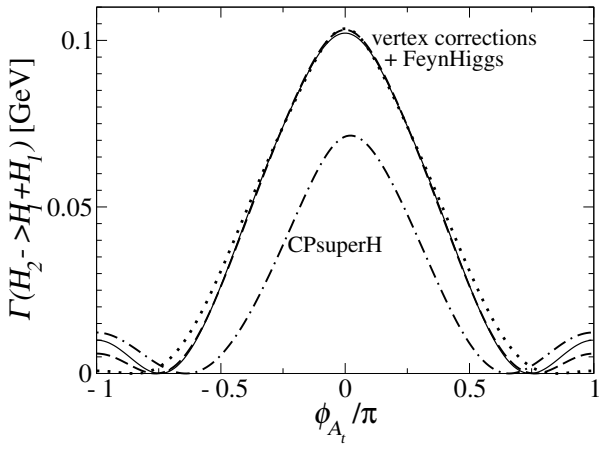

Fig. 3.23: Decay width $\Gamma(H_2 \to H_1 H_1)$ in the CPX scenario as function of the complex phase Φ_{A_t} for $M_{H^\pm} = 500$ GeV, $\tan\beta = 10$ (using the CPX value of $|A_t|$ as $\overline{\rm DR}$ parameter). Our results are shown including the genuine vertex contributions, supplemented with the external propagator corrections evaluated with `FeynHiggs` in different approximations (dotted, dashed and solid line, as in Fig. 3.22). They are compared with the result of the program `CPsuperH` (dot–dashed line).

decay $H_2 \to H_1 H_1$ can be important in the CPX scenario for $\tan\beta \approx 4$ and relatively low $M_{H^\pm}$. The dependence on both $M_{H^\pm}$ and $\tan\beta$ is very pronounced in this region. While the three implementations of the external propagator corrections lead to the same qualitative behaviour of $\Gamma(H_2 \to H_1 H_1)$, they give rise to a sizeable shift in $M_{H^\pm}$ and $\tan\beta$.

In Fig. 3.23 our result for $\Gamma(H_2 \to H_1 H_1)$ is shown as a function of the complex phase Φ_{A_t} in the CPX scenario with $M_{\rm SUSY} = 500$ GeV in comparison with the result of the program `CPsuperH` [131]. While in `FeynHiggs`, based on the FD approach, the on-shell scheme is used (see Section 3.5.3 for details), the input parameters of the program `CPsuperH`, based on the EP/RG approach, correspond to the $\overline{\rm DR}$ scheme. In order to be able to compare the results of the two programs, the relevant input parameters have to be appropriately converted. We have used the CPX value of $|A_t|$ as $\overline{\rm DR}$ parameter at the scale $M_S \equiv (M^2_{\rm SUSY} + m_t^2)^{1/2}$. This value has been taken as input for `CPsuperH`, while for our FD result we have used the corresponding on-shell parameter as obtained from the simple conversion relations given in Ref. [132].

Fig. 3.23 shows that the dependence of the decay width $\Gamma(H_2 \to H_1 H_1)$ on the complex phase Φ_{A_t} is very pronounced. The three implementations of the external propagator corrections evaluated with `FeynHiggs` yield very similar results. The qualitative behaviour of the result obtained from the program `CPsuperH` is similar to our FD result. A sizeable difference occurs, however, in particular in the region of small values of Φ_{A_t}.

The implementation of the genuine vertex corrections for the decays of a Higgs boson into two other Higgses into the program `FeynHiggs` is in progress. While the numerical results shown above are based on the leading Yukawa corrections in the $t/\tilde{t}$ sector, the full one-loop vertex corrections in the CP-violating MSSM are currently being evaluated. Combining these with the most up-to-date propagator corrections should prove valuable in order to arrive at an accurate prediction for these decay processes.

3.5.3 The Code FeynHiggs

FeynHiggs [60, 115, 130, 144, 147, 148, 235][6] is a Fortran code for the evaluation of the masses, decay properties and production processes of Higgs bosons in the MSSM with real or complex parameters. The calculation of the higher-order corrections is based on the FD approach [59]. The renormalisation has been performed in a hybrid $\overline{\rm DR}$/on-shell scheme. For the masses and mixings, the one-loop contributions incorporate the complete set of MSSM corrections, including the full momentum and phase dependence and the full 6×6 non-minimal flavor violation (NMFV) contributions [237, 238]. At the two-loop level all existing corrections from the real MSSM have been included (see Ref. [130] for a review). They are supplemented by the resummation of the leading effects from the (scalar) b sector including the full complex phase dependence.

3.5.3.1 Evaluation of observables

The evaluation of the Higgs-boson masses and mixing angles is supplemented with an estimate of the theory uncertainties from unknown higher-order corrections. The estimate for the total uncertainty is obtained as the sum of deviations from the central value[7], $\Delta X = \sum_{i=1}^{3} |X_i - X|$ with $X = \{M_{h_1,h_2,h_3,H^\pm}, \sin\alpha_{\rm eff}, U_{ij}\}$, where $\alpha_{\rm eff}$ is the loop corrected mixing angle in the CP-even Higgs sector (in the absence of CP-violating phases) and U_{ij} is defined in Eq. (3.37). The X_i are calculated as follows:

- X_1: varying the renormalization scale (entering via the $\overline{\rm DR}$ renormalization) within $1/2 m_t \leq \mu \leq 2m_t$,
- X_2: using $m_t^{\rm pole}$ instead of the running m_t in the two-loop corrections,
- X_3: using instead of a resummation in the (scalar) b sector an unresummed bottom Yukawa coupling, y_b, i.e. an y_b including the leading $\mathcal{O}(\alpha_s \alpha_b)$ corrections, but not resummed to all orders.

Besides predictions for the masses and mixing angles, FeynHiggs2.4 contains the evaluation of all relevant Higgs-boson decay widths and hadron collider production cross sections. These are in particular:

- the total width for the three neutral and the charged Higgs bosons,
- the couplings and branching ratios of the neutral Higgs bosons to
  - SM fermions (see also Ref. [239]), $h_i \to \bar{f} f$,
  - SM gauge bosons (possibly off-shell), $h_i \to \gamma\gamma, ZZ^*, WW^*, gg$,
  - gauge and Higgs bosons, $h_i \to Z h_j$, $h_i \to h_j h_k$,
  - scalar fermions, $h_i \to \tilde{f}^\dagger \tilde{f}$,
  - gauginos, $h_i \to \tilde{\chi}_k^\pm \tilde{\chi}_j^\mp$, $h_i \to \tilde{\chi}_l^0 \tilde{\chi}_m^0$,
- the couplings and branching ratios of the charged Higgs boson to
  - SM fermions, $H^- \to \bar{f} f'$,
  - a gauge and Higgs boson, $H^- \to h_i W^-$,
  - scalar fermions, $H^- \to \tilde{f}^\dagger \tilde{f}'$,
  - gauginos, $H^- \to \tilde{\chi}_k^- \tilde{\chi}_l^0$,
- the neutral Higgs boson production cross sections at the Tevatron and the LHC for all relevant channels (in an effective coupling approximation [240]).

For comparisons with the SM, the following quantities are also evaluated for SM Higgs bosons with the same mass as the three neutral MSSM Higgs bosons:

- the total decay width,
- the couplings and BRs of a SM Higgs boson to SM fermions,
- the couplings and BRs of a SM Higgs boson to SM gauge bosons (possibly off-shell),

[6] Current version: FeynHiggs2.4.0.

[7] Note that in FeynHiggs we use h_i instead of H_i as symbols for the Higgs boson states.

– the production cross sections at the Tevatron and the LHC for all relevant channels [240].

`FeynHiggs2.4` furthermore provides results for electroweak precision observables that give rise to constraints on the SUSY parameter space (see Ref. [47] and references therein)

– the leading corrections to the observables M_W and $\sin^2\theta_{\rm eff}$ entering via the quantity $\Delta\rho$, evaluated up to the two-loop level [241–246],
– an evaluation of M_W and $\sin^2\theta_{\rm eff}$ (via $\Delta\rho$) including at the one-loop level the dependence on complex phases from the scalar top/bottom sector [247] and NMFV effects [237],
– the anomalous magnetic moment of the muon, including a full one-loop calculation [248] as well as leading and subleading two-loop corrections [249–251],
– the evaluation of BR($b \to s\gamma$) including NMFV effects [238].

Some further features of `FeynHiggs2.4` are:

– Transformation of the input parameters from the $\overline{\rm DR}$ to the on-shell scheme (for the scalar top and bottom parameters), including the full $\mathcal{O}(\alpha_s)$ and $\mathcal{O}(\alpha_{t,b})$ corrections.
– Processing of SUSY Les Houches Accord (SLHA 2) data [252–254]. `FeynHiggs2.4` reads the output of a spectrum generator file and evaluates the Higgs boson masses, branching ratios etc. The results are written in the SLHA format to a new output file.
– Predefined input files for the SPS benchmark scenarios [255] and the Les Houches benchmarks for Higgs boson searches at hadron colliders [234] are included.
– Detailed information about all the features of `FeynHiggs2.4` are provided in man pages.

3.5.3.2 New features in `FeynHiggs2.4`

The main new features in `FeynHiggs2.4` as compared to older versions are summarized as follows:

– The imaginary parts of the Higgs-boson self-energies are taken into account in determining the poles of the propagators. The Higgs-boson pole masses are derived as the real parts of the complex poles of the complex propagator matrix.
– The mixing matrix (for internal Higgs bosons) is derived from the real part of the complex propagator matrix. This is also taken into account in the Higgs-boson couplings and decay widths.
– Neutral Higgs boson decays are evaluated with the full rotation to on-shell Higgs bosons. The corresponding rotation matrix for external Higgs bosons, derived from the complex propagator matrix, is provided.
– At the one-loop level the full 6×6 NMFV effects for the Higgs boson masses and mixings are included [237, 238].
– Negative entries are allowed for the squares of the soft SUSY-breaking parameters (for the diagonal entries for the sfermion mass matrices). The input is given as a negative mass, $-m$, that is then internally converted to $-(m^2)$.
– The two-loop corrections to $(g-2)_\mu$ have been extended, see Refs. [250, 251].
– The evaluation of BR($b \to s\gamma$) has been incorporated, including NMFV effects [238].

3.5.3.3 Installation and use

The installation process is straightforward and should take no more than a few minutes:

– Download the latest version from `www.feynhiggs.de` and unpack the tar archive.
– The package is built with `./configure` and `make`. This creates the library `libFH.a` and the command-line frontend `FeynHiggs`.
– To build also the Mathematica frontend `MFeynHiggs`, invoke `make all`.
– `make install` installs the files into a platform-dependent directory tree, for example `i586-linux/{bin,lib,include}`.

– Finally, remove the intermediate files with `make clean`.

`FeynHiggs2.4` has four modes of operation:

1. Library Mode: The core functionality of `FeynHiggs2.4` is implemented in a static Fortran 77 library `libFH.a`. All other interfaces are 'just' frontends to this library.
   The library provides the following functions:
   – `FHSetFlags` sets the flags for the calculation.
   – `FHSetPara` sets the input parameters directly, or
   `FHSetSLHA` sets the input parameters from SLHA data.
   – `FHSetCKM` sets the elements of the CKM matrix.
   – `FHSetNMFV` sets the off-diagonal soft SUSY-breaking parameters that induce NMFV effects.
   – `FHSetDebug` sets the debugging level.
   – `FHGetPara` retrieves (some of) the MSSM parameters calculated from the input parameters, e.g. the sfermion masses.
   – `FHHiggsCorr` computes the corrected Higgs masses and mixings.
   – `FHUncertainties` estimates the uncertainties of the Higgs masses and mixings.
   – `FHCouplings` computes the Higgs couplings and BRs.
   – `FHConstraints` evaluates further electroweak precision observables.
   These functions are described in detail on their respective man pages in the `FeynHiggs` package.
2. Command-line Mode: The `FeynHiggs` executable is a command-line frontend to the `libFH.a` library. It is invoked at the shell prompt as
   ```
   FeynHiggs inputfile [flags] [scalefactor]
   ```
   where
   – `inputfile` is the name of a parameter file (see below).
   – `flags` is an (optional) string of integers giving the flag values, e.g. `40030211`. If `flags` is not specified, `40020211` is used.
   – `scalefactor` is an optional factor multiplying the renormalization scale.
   `FeynHiggs` understands two kinds of parameter files:
   – Files in SUSY Les Houches Accord (SLHA) format [252] (using Ref. [253]). In this case `FeynHiggs` adds the Higgs masses and mixings to the SLHA data structure and writes the latter to a file *inputfile*`.fh`.
   – Files in its native format, for example
   ```
   MT          172.5
   MSusy       500
   MA0         200
   TB          5
   Abs(Xt)     1000
   ...
   ```
   Complex quantities can be given either in terms of absolute value `Abs(X)` and phase `Arg(X)`, or as real part `Re(X)` and imaginary part `Im(X)`. Abbreviations, summarizing several parameters (such as `MSusy`) can be used, or detailed information about the various soft SUSY-breaking parameters can be given. Furthermore, it is possible to define loops over parameters in order to scan parts of parameter space. The output is written in a human-readable form to the screen. The output can also be piped through the `table` filter to yield a machine-readable version appropriate for plotting etc.
3. WWW Mode: The `FeynHiggs` User Control Center (FHUCC) is a WWW interface to the command-line executable `FeynHiggs`. It provides a convenient way to play with parameters, but is of course not suited for large-scale parameter scans or extensive analyses. To use the FHUCC, point your favorite Web browser at `www.feynhiggs.de/fhucc`. adjust the parameters, and submit the form to see the results.

4. Mathematica Mode: The `MFeynHiggs` executable provides access to the `FeynHiggs` functions from Mathematica via the MathLink protocol. This is particularly convenient both because `FeynHig` can be used interactively this way and because Mathematica's sophisticated numerical and graphical tools, e.g. FindMinimum, are available. After starting Mathematica, install the package with

   ```
   In[1]:= Install["MFeynHiggs"]
   ```

   which makes all `FeynHiggs` subroutines available as Mathematica functions.

3.5.4 Conclusions

We have presented new results on higher-order corrections in the MSSM with complex phases obtained in the Feynman diagrammatic approach. The Fortran code `FeynHiggs` provides the evaluation of masses, decay properties and production processes of Higgs bosons in the CP-violating MSSM. We have described the features of the program and its installation and use.

We have analysed the dependence of the two-loop corrections of $\mathcal{O}(\alpha_t\alpha_s)$ to the Higgs boson masses and mixings on the phases Φ_{A_t} and Φ_3, i.e. the complex phase of the trilinear coupling in the stop sector and the gluino phase. The two-loop corrections significantly enhance the impact of Φ_{A_t} compared to the one-loop case. The gluino phase, which enters the Higgs-mass predictions only at the two-loop level, can give rise to a shift of the lightest Higgs-boson mass of several GeV.

A prediction for the decay $H_2 \to H_1H_1$ has been obtained by combining genuine vertex contributions with external propagator corrections evaluated with `FeynHiggs`. The decay width depends sensitively on higher-order corrections. Varying the complex phase Φ_{A_t} has a very large effect on $\Gamma(H_2 \to H_1H_1)$. The comparison with the program `CPsuperH` based on the EP/RG approach shows qualitative agreement in the phase dependence, while a sizeable difference occurs in the maximum value of $\Gamma(H_2 \to H_1H_1)$.

3.6 Self-couplings of Higgs bosons in scenarios with mixing of CP-even/CP-odd states

Elza Akhmetzyanova, Mikhail Dolgopolov and Mikhail Dubinin

The effective two-doublet Higgs potential of the MSSM at the energy scale m_{top} has the form of a general two-Higgs-doublet potential, see Eq. (2.1), with four real parameters λ_1-λ_4 and three complex-valued parameters λ_5, λ_6, λ_7 which explicitly violate CP invariance in the Higgs sector. The parameters λ_1-λ_7 can be calculated [50, 110, 256, 257] and expressed through the parameters of the MSSM in the sector of scalar quarks–Higgs bosons interaction. In this sense the MSSM Higgs sector as an effective field theory at the scale m_{top} can be embedded in a general two-Higgs-doublet model, providing possibilities to interpret some special MSSM features in the language of the THDM parameter space.

In the following we are using the formalism described in [256, 258]. First the THDM mass eigenstates of CP conserving limit $\mathtt{Im}\lambda_{5,6,7} = 0$ which are h, H (CP-even scalars), A (CP-odd scalar) and $H^\pm$ (charged scalar), see Eqs. (2.23), (2.25) and (2.29), are defined using the two mixing angles α and β. There is no CP violation at the scale M_{SUSY}, where λ_i are real-valued, at the scale m_{top} it is radiatively induced. The evaluation of λ_{1-7} parameters is based on the effective field theory approach [257] using the MSSM potential of the Higgs bosons - scalar quarks interaction and including the contributions from the F-terms, leading and nonleading D-terms, the wave-function renormalization terms, and the leading two-loop Yukawa QCD-corrections.

In this section we calculate the trilinear and the quartic couplings of physical Higgs bosons in the CPX scenario [54] of the MSSM. Continious interest to the self-interactions of Higgs bosons both in the case of CP conservation [259–263] and the case of CP violation [131, 256, 258] is motivated by the experimental accessibility of the two and three Higgs bosons production signals [62, 64, 65, 78, 89, 91, 264, 265] providing possibilities to reconstruct experimentally the effective Higgs potential.

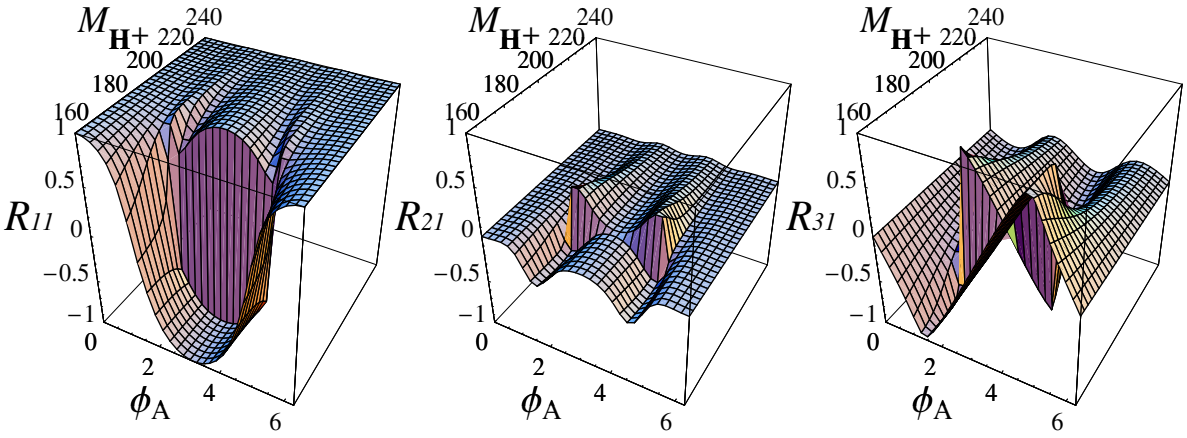

Fig. 3.24: The mixing matrix elements R_{i1} (i =1,2,3) as a two-dimensional functions of the mass $M_{H^\pm}$ (GeV) and the phase Φ_A (rad) calculated at the one-loop approximation for $\lambda_{1,...7}$ parameters of the MSSM two-doublet potential, CPX$_{500}$ scenario. With the discontinuities of R_{i1} at $M_{H^\pm}$ =184 GeV and the discontinuites of R_{i2}, which are also introduced at the same charged scalar mass, the eigenvector basis is left-handed at any $\{\Phi_A, M_{H^\pm}\}$.

The effective trilinear and quartic couplings of physical Higgs bosons H_1, H_2 and H_3, Eq. (2.35) (i.e. their mass term $M^2_{ij}H_iH_j$ in the two-doublet potential is diagonal in the local minimum) can be written in a compact form, see [131]. For example, the trilinear couplings

$$\mathcal{L}_{3H} \;=\; v\sum_{i\geq j\geq k=1}^{3} g_{H_iH_jH_k}\,\frac{1}{N_S^{ijk}}\,H_iH_jH_k \;+\; v\sum_{i=1}^{3} g_{H_iH^+H^-}\,H_iH^+H^- \qquad (3.38)$$

where N_S are the combinatorial factors and

$$g_{H_iH_jH_k} \;=\; \sum_{\alpha\geq\beta\geq\gamma=1}^{3}\{R_{\alpha i}R_{\beta j}R_{\gamma k}\}\;g_{\alpha\beta\gamma}\,, \qquad g_{H_iH^+H^-}=\sum_{\alpha=1}^{3}R_{\alpha i}\,g_{\alpha H^+H^-}\,. \qquad (3.39)$$

where curly brackets denote the symmetrization in the i,j,k indices. Couplings $g_{\alpha\beta\gamma}$ and $g_{\alpha H^+H^-}$ are an intermediate expressions defined in the unphysical basis. Our mixing matrix $R = R_2^T\,R_3^T$ is specified by Eq. (2.35), $(h,H,A)^T = \|R_{ij}\|\,(H_1,H_2,H_3)^T$. The matrix elements R_{ij} are defined in the orthonormal basis for eigenvectors, $R_{ij} = R^{'}_{ij}\,/n_j$:

$$R^{'}_{11}=((M^2_H-M^2_{H_1})(M^2_A-M^2_{H_1})-M^{'4}_{23}),\; R^{'}_{21}=M^{'2}_{13}M^{'2}_{23},\; R^{'}_{31}=-M^{'2}_{13}(M^2_H-M^2_{H_1}), \qquad (3.40)$$

$$R^{'}_{12}=-M^{'2}_{13}M^{'2}_{23},\; R^{'}_{22}=-((M^2_h-M^2_{H_2})(M^2_A-M^2_{H_2})-M^{'4}_{13}),\; R^{'}_{32}=M^{'2}_{23}(M^2_h-M^2_{H_2}), \qquad (3.41)$$

$$R^{'}_{13}=-M^{'2}_{13}(M^2_H-M^2_{H_3}),\; R^{'}_{23}=-M^{'2}_{23}(M^2_h-M^2_{H_3}),\; R^{'}_{33}=(M^2_h-M^2_{H_3})(M^2_H-M^2_{H_3}), \qquad (3.42)$$

where $n_i = k_i\sqrt{(R^{'2}_{1i}+R^{'2}_{2i}+R^{'2}_{3i})}$ and the sign factors k_i are introduced to ensure definitely chosen (left-handed, $\mathtt{det}\|R_{ij}\|$ =1) orientation of the eigenvector basis at any phase $\Phi_A = \mathtt{arg}(\mu A_t) = \mathtt{arg}(\mu A_b)$ and charged scalar mass $M_{H^\pm}$, together with matching to the states h, H and A of the CP conserving limit.

For the two-Higgs doublet potential the off-diagonal mass matrix elements $M^{'2}_{13}$ and $M^{'2}_{23}$, Eq. (2.30), depend on the imaginary parts of λ_5, λ_6 and λ_7, see Eqs. (2.33–2.34) [256]. In the framework of MSSM the λ_i, i=1,...7 are calculated [50,110,256,257] by means of the effective potential method, taking into account the one-loop triangle and box squark insertions to the quartic vertices of the two-doublet potential. If the universal phase of complex parameters $\mathtt{arg}(\mu A_t) = \mathtt{arg}(\mu A_b)$ is introduced, the phases of $\lambda_{5,6,7}$

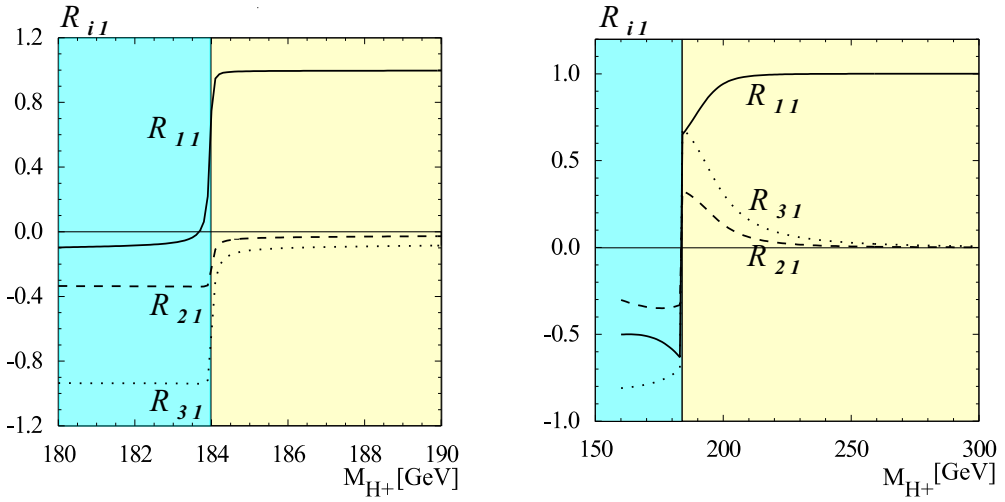

Fig. 3.25: The mixing matrix elements R_{i1} as a function of the charged scalar mass $M_{H^\pm}$ (GeV) at the phases $\Phi_A = \pi/2$ (left plot) and $\Phi_A = 7\pi/12$ (right plot) calculated in the one-loop approximation for $\lambda_{1,...7}$ parameters of the MSSM two-doublet potential, CPX_{500} scenario. Both pictures are the superimposed cross sections of the two-dimensional plots in Fig. 3.24 by a plane orthogonal to the Φ_A axis. The discontinuities of R_{i1} at $M_{H^\pm}$ =184 GeV are introduced at the phase $\pi/2 < \Phi_A < 3\pi/2$. Then the eigenvector basis is left-handed at any $\{\Phi_A, M_{H^\pm}\}$

.

respect the constraint $\texttt{arg}(\lambda_5) = 2\,\texttt{arg}(\lambda_{6,7})$. In this way the off-diagonal mass matrix elements M'^2_{13} and M'^2_{23} can be fixed at a given point of the MSSM parameter space $\{\Phi_A, \texttt{tan}\beta, M_{H^\pm}, \mu, A_{t,b}, M_{SUSY}\}$.

The squared masses of Higgs bosons are ($M^2_{H_1} \le M^2_{H_2} \le M^2_{H_3}$)

$$M^2_{H_1} = p\,\cos\left(\frac{\Theta + 2\pi}{3}\right) - \frac{a_2}{3}\,, M^2_{H_2} = p\,\cos\left(\frac{\Theta - 2\pi}{3}\right) - \frac{a_2}{3}\,, M^2_{H_3} = p\,\cos\left(\frac{\Theta}{3}\right) - \frac{a_2}{3}, \quad (3.43)$$

where $p = 2\sqrt{(-q)}$, $\cos\Theta = r/\sqrt{(-q^3)}$, $r = (9a_1a_2 - 27a_0 - 2a_2^3)/54$, $q = (3a_1 - a_2^2)/9$, $a_1 = M_h^2M_H^2 + M_h^2M_A^2 + M_H^2M_A^2 - M'^4_{13} - M'^4_{23}$, $a_2 = -M_h^2 - M_H^2 - M_A^2$, $a_0 = M'^4_{13}M_H^2 + M'^4_{23}M_h^2 - M_h^2M_H^2M_A^2$. Squared masses of Higgs bosons $M^2_{H_i}$ are the roots of the cubic equation $(M^2_{H_i})^3 + a_2(M^2_{H_i})^2 + a_1M^2_{H_i} + a_0 = 0$ which can be rewritten in the equivalent form

$$(M_h^2 - M^2_{H_i})[(M_H^2 - M^2_{H_i})(M_A^2 - M^2_{H_i}) - M'^4_{23}] - M'^4_{13}(M_H^2 - M^2_{H_i}) = 0. \quad (3.44)$$

If $i = 1$ then Eq. (3.44) takes the form $(M_h^2 - M^2_{H_1})R'_{11} + M'^2_{13}R'_{31} = 0$, so if $M'^2_{13} = 0$ then either $R'_{11} = 0$ or $M_{H_1} = M_h$ precisely. The special case of degenerate masses $M_{H_1} = M_{H_2}$ takes place when Θ =0, see Eq. (3.43). For CPX scenario at M_{SUSY} =500 GeV, $\texttt{tan}\beta$ =5 (denoted by CPX_{500} everywhere in the following) Θ =0 at $M_{H^\pm}$ = 184 GeV. The case M'^2_{13} =0, when the mixing matrix elements R'_{31} and R'_{21} change their sign crossing zero, is distinguished in mixing scenarios. Such property of the off-diagonal mass matrix is inherent to the MSSM. In other nonstandard models it may not take place. In the CPX_{500} scenario of the MSSM $M'^2_{13}(\Phi_A)$ =0 at the phase very close to $\pi/2$. For example, the normalized matrix element $R_{11}(\Phi_A)$, see Fig. 3.24 and Fig. 3.25, decreases with increasing Φ_A, but reaches zero $R_{11}(\Phi_A)$ =0 only if $M_{H_\pm} < 184$ GeV. The cubic equation (3.44) for eigenvalues is respected in this case because $R'_{11} = 0$. The negative sign of $R_{11}(\Phi_A)$ (i.e. k_1 =-1 above) must be taken to keep proper orientation of the eigenvector basis (always left-handed). In the case $M_{H^\pm} > 184$ GeV R'_{11} does not reach zero, remaining always positive. The cubic equation (3.44) for eigenvalues is then respected because $M_h = M_{H_1}$. No change of sign for R_{11} is possible here. Different parametric behaviour of $R_{ij}(\Phi_A)$ at $M_{H^\pm}$ less or greater than 184 GeV leads to discontinuities of matrix elements

R_{i1} and R_{i2} as a functions of $M_{H^\pm}$ in the vicinity of $M_{H^\pm}$=184 GeV (Fig. 3.24,3.25). With the two-loop calculation of λ_i the situation remains qualitatively the same, but discontinuites of R_{i1} and R_{i2} are shifted to lower charged Higgs boson mass $M_{H^\pm}$ =162 GeV. Discontinuites are not a special feature of our approach. They take place in the `CPsuperH` [131] and `FeynHiggs` [60] packages, which are using different sign conventions for the basis, so other pattern of discontinuites exists there. Our convention is implemented in `CompHEP` [266].

The effective trilinear and quartic Higgs boson self-couplings of the general two-Higgs-doublet model can be written down in two equivalent representations. First one uses λ_i parameters and the second representation expresses the effective couplings by means of Higgs boson masses in the CP conserving limit Φ_A =0. The effective charged Higgs boson triple couplings, see Eq. (3.38), in the λ_i representation and the mass representation can be found in [256]. In the MSSM CPX$_{500}$ scenario the coupling $g_{H^+H^-H_1}$ goes through zero at $\Phi_A \sim \pi/2$, see Fig. 3.26, with the overall variation range approximately from -100 GeV to 100 GeV. The Θ parameter (3.43) is close to maximum in the vicinity of weak self-interaction, when $M_{H_1} \sim M_{H_2}$. Representations of quartic self-couplings in the λ_i basis are more complicated. For example (using compact notation $\sin\alpha \equiv s_\alpha$ and so on)

$$g_{H_1H_1H_1H_1} = \sum_{i=1}^{4} l_i\,\lambda_i + \sum_{i=5}^{7} R_i\,\mathtt{Re}\lambda_i + \sum_{i=5}^{7} I_i\,\mathtt{Im}\lambda_i\,, \tag{3.45}$$

$$\begin{aligned}
l_1 &= -3(1+(-R_{11}^2+R_{21}^2)c_{2\alpha} - R_{31}^2c_{2\beta} - 2R_{11}R_{21}s_{2\alpha})^2/4,\\
l_2 &= -3(1+(R_{11}^2-R_{21}^2)c_{2\alpha} + R_{31}^2c_{2\beta} + 2R_{11}R_{21}s_{2\alpha})^2/4,\\
l_3 &= l_4 = 3(-(R_{11}^2+R_{21}^2)^2 - 4(R_{11}^2+R_{21}^2)R_{31}^2 - R_{31}^4 + (R_{11}^4 - 6R_{11}^2R_{21}^2 + R_{21}^4)c_{4\alpha} + R_{31}^4c_{4\beta}\\
&\quad +4R_{31}^2c_{2\beta}((R_{11}^2-R_{21}^2)c_{2\alpha} + 2R_{11}R_{21}s_{2\alpha}) + 4R_{11}(R_{11}^2-R_{21}^2)R_{21}s_{4\alpha})/4,
\end{aligned} \tag{3.46}$$

$$\begin{aligned}
R_5 &= 3(-(R_{11}^2+R_{21}^2)^2 + 4(R_{11}^2+R_{21}^2)R_{31}^2 - R_{31}^4 + (R_{11}^4 - 6R_{11}^2R_{21}^2 + R_{21}^4)c_{4\alpha}\\
&\quad +R_{31}^4c_{4\beta} + 4R_{11}(R_{11}^2-R_{21}^2)R_{21}s_{4\alpha} + 4R_{31}^2c_{2\alpha}((-R_{11}^2+R_{21}^2)c_{2\beta} + 4R_{11}R_{21}s_{2\beta})\\
&\quad -8R_{31}^2s_{2\alpha}(R_{11}R_{21}c_{2\beta} + (R_{11}^2-R_{21}^2)s_{2\beta}))/4,\\
R_6 &= (-6R_{31}^2c_{2\beta}(-2R_{11}R_{21}c_{2\alpha} + (R_{11}^2-R_{21}^2)s_{2\alpha}) - 6(-1+(R_{11}^2-R_{21}^2)c_{2\alpha}\\
&\quad +2R_{11}R_{21}s_{2\alpha})(-2R_{11}R_{21}c_{2\alpha} + (R_{11}^2-R_{21}^2)s_{2\alpha})\\
&\quad +6R_{31}^2(1+(-R_{11}^2+R_{21}^2)c_{2\alpha} - 2R_{11}R_{21}s_{2\alpha})s_{2\beta} - 3R_{31}^4s_{4\beta})/2,\\
R_7 &= (6R_{31}^2c_{2\beta}(-2R_{11}R_{21}c_{2\alpha} + (R_{11}^2-R_{21}^2)s_{2\alpha}) + 6(1+(R_{11}^2-R_{21}^2)c_{2\alpha}\\
&\quad +2R_{11}R_{21}s_{2\alpha})(-2R_{11}R_{21}c_{2\alpha} + (R_{11}^2-R_{21}^2)s_{2\alpha})\\
&\quad +6R_{31}^2(1+(R_{11}^2-R_{21}^2)c_{2\alpha} + 2R_{11}R_{21}s_{2\alpha})s_{2\beta} + 3R_{31}^4s_{4\beta})/2,
\end{aligned} \tag{3.47}$$

$$\begin{aligned}
I_5 &= -6R_{31}(R_{21}c_{\alpha-\beta} - R_{11}s_{\alpha-\beta})(-2R_{11}R_{21}c_{2\alpha} + (R_{11}^2-R_{21}^2)s_{2\alpha} + R_{31}^2s_{2\beta}),\\
I_6 &= 6R_{31}(1+(-R_{11}^2+R_{21}^2)c_{2\alpha} - R_{31}^2c_{2\beta} - 2R_{11}R_{21}s_{2\alpha})(R_{21}c_{\alpha-\beta} - R_{11}s_{\alpha-\beta}),\\
I_7 &= 6R_{31}(1+(R_{11}^2-R_{21}^2)c_{2\alpha} + R_{31}^2c_{2\beta} + 2R_{11}R_{21}s_{2\alpha})(R_{21}c_{\alpha-\beta} - R_{11}s_{\alpha-\beta}).
\end{aligned} \tag{3.48}$$

Various physical self-couplings in the CPX$_{500}$ scenario are shown in Fig. 3.26-3.28. Note that in the CPX$_{500}$ large contributions to them come from the terms with λ_6 $\sim$0.5. The λ_6 parameter has the Yukawa coupling h_{top}^4 in front of the main power term $\mu^3 A_t/M_{SUSY}^4$.

Our calculations demonstrate that the structure of Higgs boson self-interactions for the two-doublet model with complex parameters in the CP violating potential is extremely strongly sensitive to radiative corrections and phases of effective parameters. Some detailed numerical evaluations illustrating this sensitivity were performed in the framework of the CPX scenario at the SUSY scale M_{SUSY} =500

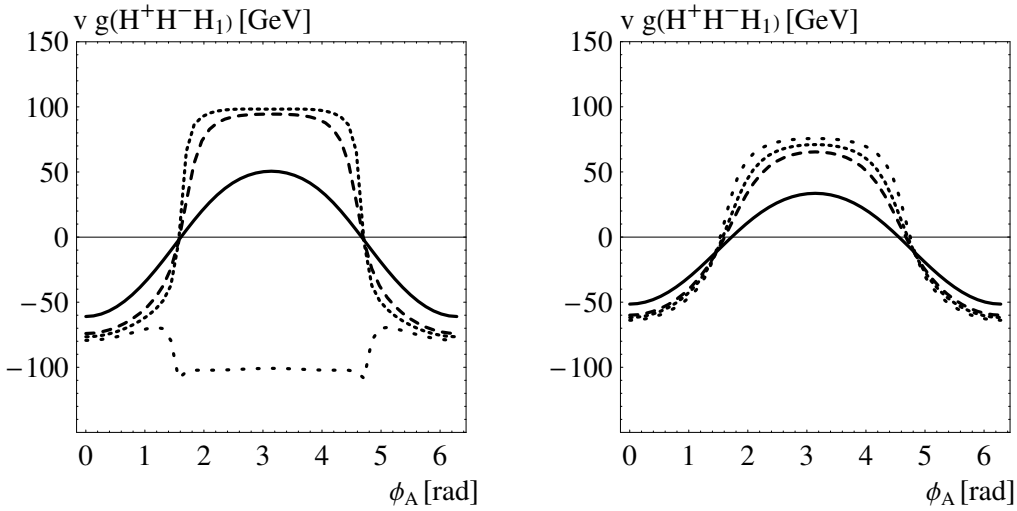

Fig. 3.26: The triple Higgs boson interaction vertex $v \cdot g_{H^+\,H^-\,H_1}$ (GeV) vs the phase $\mathtt{arg}(\mu A_{t,b})$ (left figure for 1-loop approximation and the right figure with additional leading QCD Yukawa corrections to λ_i included) at parameter values $M_{SUSY} = 500$ GeV, $\mathtt{tg}\beta$ =5, $A_{t,b}$ =1000 GeV, $\mu = 2000$ GeV. Solid line – $M_{H^\pm} = 300$ GeV, long dashed line – $M_{H^\pm} = 200$ GeV, short dashed line – $M_{H^\pm} = 190$ GeV, rare dotted line – $M_{H^\pm} = 180$ GeV.

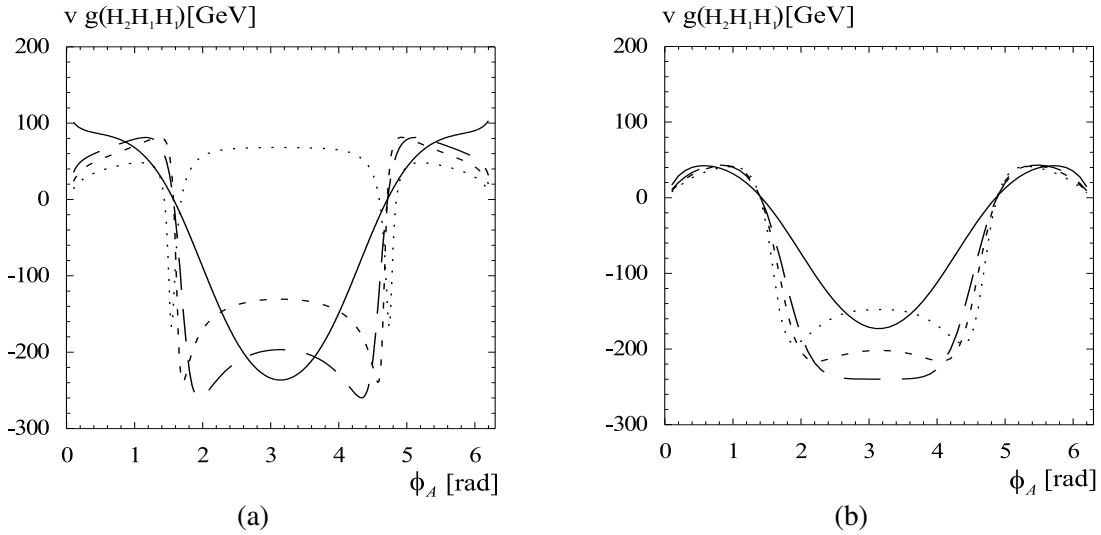

Fig. 3.27: The triple Higgs boson interaction vertex $v \cdot g_{H_1 H_1 H_2}$ (GeV) vs the phase $\mathtt{arg}(\mu A_{t,b})$ at parameter values $M_{SUSY} = 500\,\text{GeV}$, $\mathtt{tg}\beta = 5$, $A_{t,b} = 1000\,\text{GeV}$, $\mu = 2000\,\text{GeV}$. Solid line – $M_{H^\pm} = 300\,\text{GeV}$, long dashed line – $M_{H^\pm} = 200\,\text{GeV}$, short dashed line – $M_{H^\pm} = 190\,\text{GeV}$, dotted line – $M_{H^\pm} = 180\,\text{GeV}$. (a) – the case of effective one-loop potential, (b) – leading two-loop corrections included.

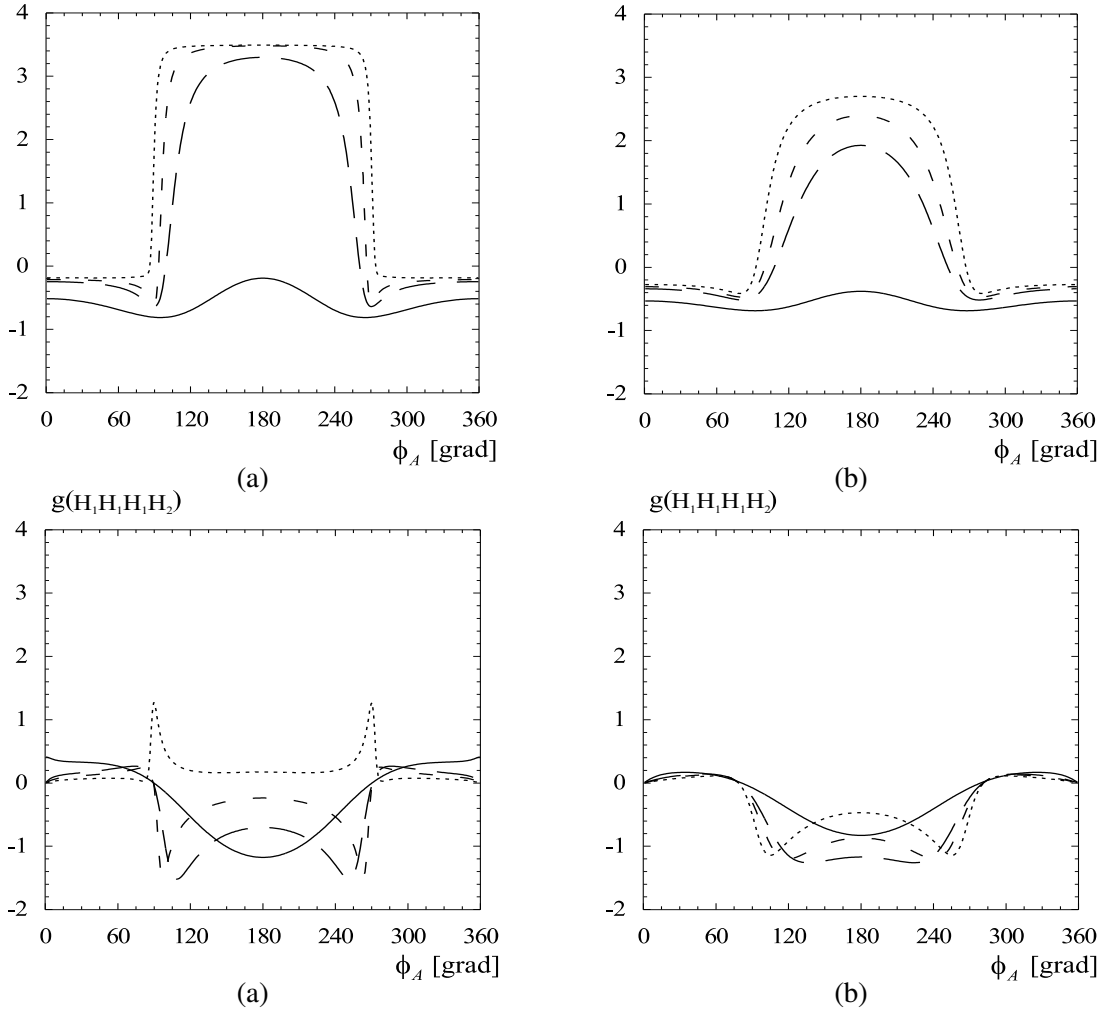

Fig. 3.28: The quartic interaction vertices $g_{H_1H_1H_1H_i}$, i =1,2, *vs* the phase $\mathtt{arg}(\mu A_{t,b})$ at parameter values M_{SUSY} = 500 GeV, $\mathtt{tg}\beta$ = 5, $A_{t,b}$ = 1000 GeV, μ = 2000 GeV. Solid line – $M_{H^\pm}$ = 300 GeV, long dashed line – $M_{H^\pm}$ = 200 GeV, short dashed line – $M_{H^\pm}$ = 190 GeV, dotted line – $M_{H^\pm}$ = 180 GeV. (a) – effective one-loop approximation, (b) – with leading two-loop corrections included.

GeV and $\mathtt{tan}\beta$ =5 (CPX$_{500}$). A lot of self-couplings of physical scalars are very small at the phase $\Phi_A = \mathtt{arg}(\mu A_{t,b}) \sim \pi/2$, which is related to vanishing off-diagonal Higgs boson mass matrix element $M'^2_{13}(\Phi_A)$, and mass degeneracy of the states h,H_1 and H_2, that takes place in the vicinity of Θ =0, see Eq. (3.43). The availability of zero for the mass matrix element $M'^2_{13}(\Phi_A)$ is connected with the relation between phases $\mathtt{arg}(\lambda_5)$ =2 $\mathtt{arg}(\lambda_{6,7})$, inherent to the MSSM. In other representations of the THDM or other MSSM mixing scenarios the situation may be different. Mass degeneracy of the states H_1 and H_2 takes place in the MSSM, CPX$_{500}$ scenario, for the charged scalar mass $M_{H^\pm}$ =184 GeV at the one-loop approximation for λ_i. We point out an interesting property of the CPX$_{500}$ scenario, namely, definite (always left-handed, $\mathtt{det}\|R_{ij}\|$ =1) orientation of the eigenvector basis for scalars $H_{1,2,3}$ is respected in the $(\Phi_A, M_{H^\pm})$ parameter space (together with the mass ordering and matching to the (h,H,A) states in the CP-conserving limit), if the discontinuity of the matrix elements $R_{ij}(\Phi_A, M_{H^\pm})$ at $M_{H^\pm}$ =184 GeV is introduced (see Fig. 3.24 and Fig. 3.25). The two-dimensional functions $R_{ij}(\Phi_A, M_{H^\pm})$, if taken continious, define different orientations of the eigenvector basis for $H_{1,2,3}$ states inside the three intervals of phase variation. A discontinuity of the mixing matrix elements R_{ij} leads to a discontinuity in the couplings, see for example Eq. (3.39), where terms linear in R_{ij} appear. Such property could be relevant for systems that evolve in the phase and charged scalar mass, related to the phase transitions in

cosmological models. Toy model with phase transitions can be found in [267]. Within the perturbation theory the discontinuites do not show up in the amplitudes (with the sign compensation in the product $R_{i1}\,R_{j1}$ for each H_1 propagator), however, this could be not the case for the nonperturbative insertions to diagrams. Specific features of self-interactions in the case of complex $\lambda_{5,6,7}$ in the THDM technically appear as a consequence of the eigenvalue and eigenvector problems for the 3×3 neutral Higgs bosons mixing matrix, dependent on several parameters. In such schemes very small radiative corrections to the input parameters may lead to large changes of a physical observables evaluated.

3.7 Production of neutral Higgs bosons through b-quark fusion in CP-violating SUSY scenarios

Francesca Borzumati and Jae Sik Lee

The $b\bar{b}$ fusion process can be one of the leading production channels of the two heaviest neutral Higgs bosons at the Tevatron and at the LHC for values of $\tan\beta$ ranging from intermediate up to large or very large. In scenarios with large CP-violating mixing among the neutral Higgs states [48–58], this channel can be relevant also for the lightest neutral Higgs boson. Moreover, the vertex and m_b corrections induced by supersymmetric particles [124–128, 169–176] can affect substantially the size of the production cross sections of all three neutral Higgs bosons [77].

To illustrate these effects, we consider the CPX scenario defined in Eq. (3.13) of Section 3.1, that is in general used to highlight CP-violating effects in the Higgs sector. We choose the two free parameters $M_{\rm SUSY}$ and $\tan\beta$ to be: $M_{\rm SUSY} = 0.5\,\text{TeV}$ and $\tan\beta = 10$. (We shall comment later on the rational for this choice of $\tan\beta$.) Moreover, after we fix the phases $\Phi_A \equiv \mathrm{Arg}(A_t\mu) = \mathrm{Arg}(A_b\mu)$ and $\Phi_3 \equiv \mathrm{Arg}(M_3\mu)$, the charged Higgs-boson mass is solved to give $M_{H_1} = 115\,\text{GeV}$. Our numerical analyses make use of the program `CPsuperH` [131].

We show in Fig. 3.29 masses and widths of the three neutral Higgs bosons obtained in such a scenario, as functions of Φ_A for three different values of Φ_3: $0^\circ, 90^\circ, 180^\circ$. We observe that all three neutral Higgs bosons are relatively light and widths reaching few GeV for $\Phi_3 = 180^\circ$.

The effective Lagrangian for the interaction of these neutral Higgs bosons to b quarks can be written as

$$\mathcal{L} \;=\; -\frac{m_b}{v}\,\bar{b}\left(g^S_{H_i\bar{b}b} + i g^P_{H_i\bar{b}b}\gamma_5\right) b\,H_i\,, \tag{3.49}$$

where the couplings $g^{S,P}_{H_i\bar{b}b}$ are $g^{S,P}_{H_i\bar{b}b} = \sum_\alpha O_{\alpha i}\,g^{S,P}_\alpha$ with $\alpha = (\phi_1, \phi_2, a)$ and the 3×3 matrix O describing the CP-violating neutral Higgs-boson mixing. After including vertex and m_b corrections induced by supersymmetric particles, the couplings $g^{S,P}_\alpha$ are given by [152]

$$\begin{aligned}
g^S_{\phi_1} &= \frac{1}{\cos\beta}\,\mathrm{Re\,e}\left(\frac{1}{R_b}\right), & g^P_{\phi_1} &= \frac{\tan\beta}{\cos\beta}\,\mathrm{Im\,m}\left(\frac{\kappa_b}{R_b}\right),\\
g^S_{\phi_2} &= \frac{1}{\cos\beta}\,\mathrm{Re\,e}\left(\frac{\kappa_b}{R_b}\right), & g^P_{\phi_2} &= -\frac{1}{\cos\beta}\,\mathrm{Im\,m}\left(\frac{\kappa_b}{R_b}\right),\\
g^S_a &= (\tan^2\beta + 1)\,\mathrm{Im\,m}\left(\frac{\kappa_b}{R_b}\right), & g^P_a &= -\,\mathrm{Re\,e}\left(\frac{\tan\beta - \kappa_b}{R_b}\right).
\end{aligned} \tag{3.50}$$

Here R_b and κ_b are defined through:

$$h_b = \frac{\sqrt{2}\,m_b}{v\cos\beta}\,\frac{1}{R_b} = \frac{\sqrt{2}\,m_b}{v\cos\beta}\,\frac{1}{1+\kappa_b\tan\beta}\,, \tag{3.51}$$

with $v \simeq 254\,\text{GeV}$. (Corrections not enhanced by $\tan\beta$ are also included in our numerical analysis.) In the above expression, the finite corrections to the b-quark mass are collected in $\kappa_b = \epsilon_g + \epsilon_H$ in which the contributions from the sbottom-gluino exchange diagram and those from the stop-Higgsino diagram,

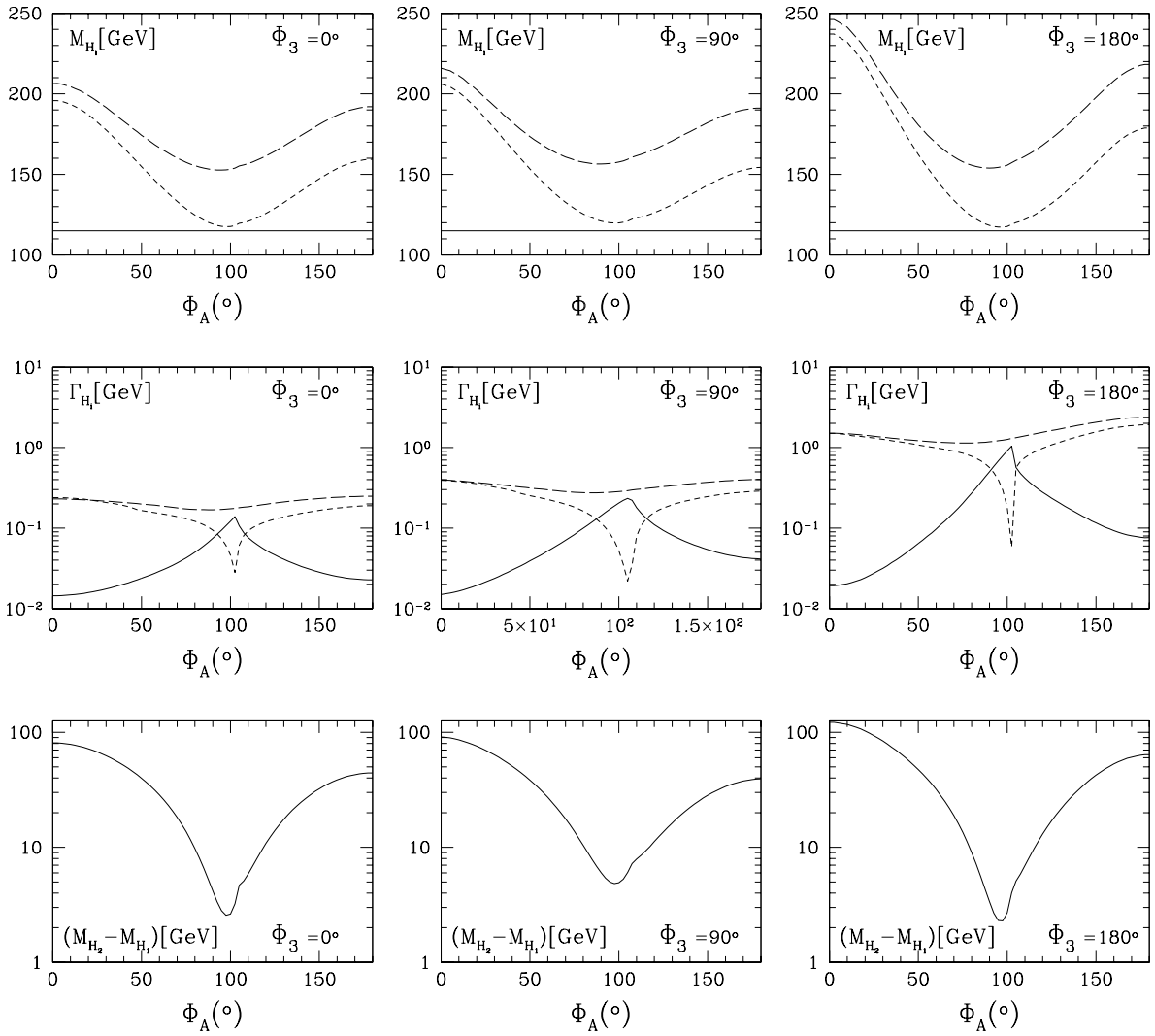

Fig. 3.29: The masses (top) and widths (middle) of the neutral Higgs bosons as functions of Φ_A for the spectrum in Eq. (3.13) with $M_{\rm SUSY} = 0.5\,$TeV and $\tan\beta = 10$, for three different values of Φ_3: 0° (left column), 90° (central column), and 180° (right column). The solid lines are for H_1, the dashed ones for H_2, and the long-dashed ones for H_3. The bottom frames are for the mass difference between H_2 and H_1.

respectively ϵ_g and ϵ_H, are

$$\epsilon_g = \frac{2\alpha_s}{3\pi}\, M_3^* \mu^* I(m^2_{\tilde{b}_1}, m^2_{\tilde{b}_2}, |M_3|^2)\,, \qquad \epsilon_H = \frac{|h_t|^2}{16\pi^2}\, A_t^* \mu^* I(m^2_{\tilde{t}_1}, m^2_{\tilde{t}_2}, |\mu|^2)\,. \tag{3.52}$$

The one-loop function $I(a,b,c)$ is well known and can be found, for example, in Ref. [172].

Note that, in general, κ_b is complex due to the CP phases of the combinations $M_3\mu$ and/or $A_t\mu$. In particular, the value $\Phi_3 \sim 180^\circ$ plays an important role in the CPX scenario. While it does not affect considerably the masses of the three neutral Higgs bosons, and modifies their widths only by a factor 2-3, see Fig. 3.29, it can have consequences for the positivity of the lightest sbottom squark squared mass. Indeed, for $\Phi_3 \sim 180^\circ \pm 30^\circ$, the mass eigenstate $\tilde{b}_1$ is tachyonic at values of $\tan\beta$ ranging from intermediate to large, depending on the value of Φ_A. See Ref. [77] for details. In this study, we choose $\tan\beta = 10$, at which all values of Φ_3 and Φ_A are allowed.

For values of $\tan\beta$ such that $|\kappa_b|\tan\beta \sim 1$, with $\mathrm{Re\,e}(\kappa_b)\tan\beta \sim 1$ and/or $\mathrm{Im\,m}(\kappa_b)\tan\beta \sim 1$

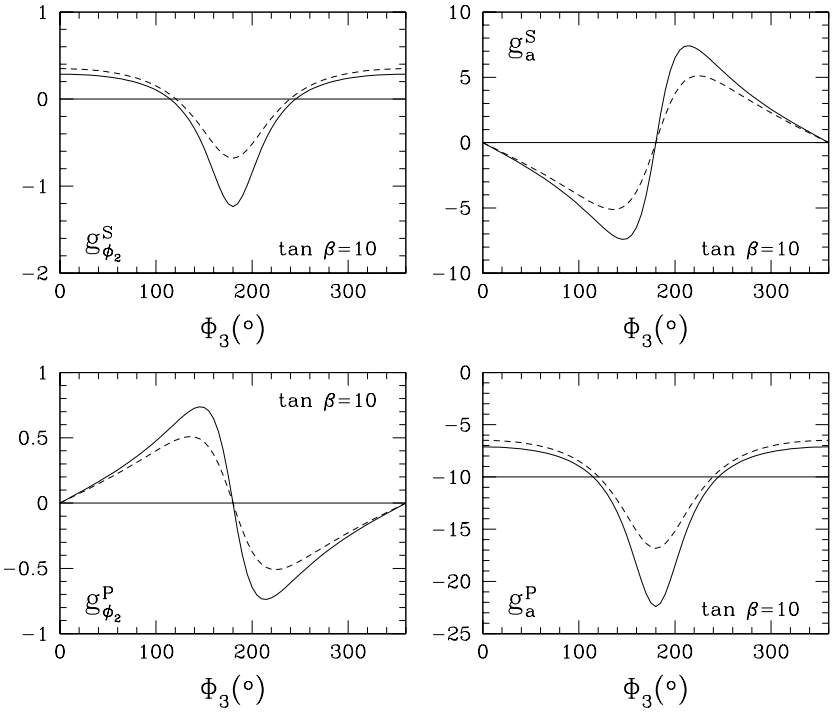

Fig. 3.30: Couplings $g^{S,P}_{\phi_2}$ and $g^{S,P}_a$ vs. Φ_3, for the spectrum in Eq. (3.13) with $M_{\rm SUSY} = 0.5$ TeV and $\tan\beta = 10$. The dashed lines are for $\Phi_A = 0^\circ$, the solid ones for $\Phi_A = 180^\circ$. The horizontal lines indicate the values of the uncorrected couplings.

($\tan\beta = 10$ is one of those), the expressions for the couplings $g^{S,P}_\alpha$ reduce to

$$\begin{aligned}
g^S_{\phi_1} &= \frac{\tan\beta}{|R_b|^2}\left[1 + \mathrm{Re}\,e(\kappa_b)\tan\beta\right], & g^P_{\phi_1} &= \frac{\tan\beta}{|R_b|^2}\left[\mathrm{Im}\,m(\kappa_b)\tan\beta\right], \\
g^S_{\phi_2} &= \frac{1}{|R_b|^2}\left[\mathrm{Re}\,e(\kappa_b)\tan\beta + |\kappa_b|^2\tan^2\beta\right], & g^P_{\phi_2} &= -\frac{1}{|R_b|^2}\left[\mathrm{Im}\,m(\kappa_b)\tan\beta\right], \\
g^S_a &= \frac{\tan\beta}{|R_b|^2}\left[\mathrm{Im}\,m(\kappa_b)\tan\beta\right], & g^P_a &= -\frac{\tan\beta}{|R_b|^2}\left[1 + \mathrm{Re}\,e(\kappa_b)\tan\beta\right]
\end{aligned} \quad (3.53)$$

If no threshold corrections are included, the only nonvanishing couplings are $g^S_{\phi_1} = 1/\cos\beta$ and $g^P_a = -\tan\beta$. The inclusion of these corrections affects these two couplings mainly through the factor $\mathrm{Re}\,e(1/R_b)$, which is a suppression or an enhancement factor, depending on the value of $\mathrm{Arg}(\kappa_b)$, and varies between $1/(1+|\kappa_b|\tan\beta)$ and $1/(1-|\kappa_b|\tan\beta)$. Note that the factor $\mathrm{Re}\,e(1/R_b)$ is larger than 1 for $\cos(\mathrm{Arg}(\kappa_b)) \lesssim -|\kappa_b|\tan\beta$. The other four couplings are loop-induced. Among these, $g^S_{\phi_2}$ is the only one present if there are no CP-violating phases, and the couplings $g^S_a \approx g^P_{\phi_1}$ have an overall $\tan\beta$ enhancement factor compared to the couplings $g^{S,P}_{\phi_2}$. We show explicitly in Fig. 3.30 the couplings $g^{S,P}_{\phi_2}$ and $g^{S,P}_a$. The remaining two, in the same approximation of Eq. (3.53), are $g^S_{\phi_1} = -g^P_a$ and $g^P_{\phi_1} = g^S_a$, respectively. This figure shows clearly that the couplings $g^{S,P}_{\phi_2}$ and $g^{S,P}_a$ have a dependence on the CP phase Φ_A weaker than that on Φ_3. This is because $|\epsilon_g|$ is about one order of magnitude larger than $|\epsilon_H|$ for the scenario under consideration.

We are now in position to discuss the production cross sections of the neutral Higgs bosons H_i via b-quark fusion at hadron colliders. These cross sections can be expressed as:

$$\sigma(\mathrm{had_1 had_2} \to b\bar{b} \to H_i) = \sigma(b\bar{b} \to H_i)\int_{\tau_i}^1 \mathrm{d}x\left[\frac{\tau_i}{x}\, b_{\mathrm{had}_1}(x,Q)\,\bar{b}_{\mathrm{had}_2}\Big(\frac{\tau_i}{x},Q\Big) + (b \leftrightarrow \bar{b})\right], \quad (3.54)$$

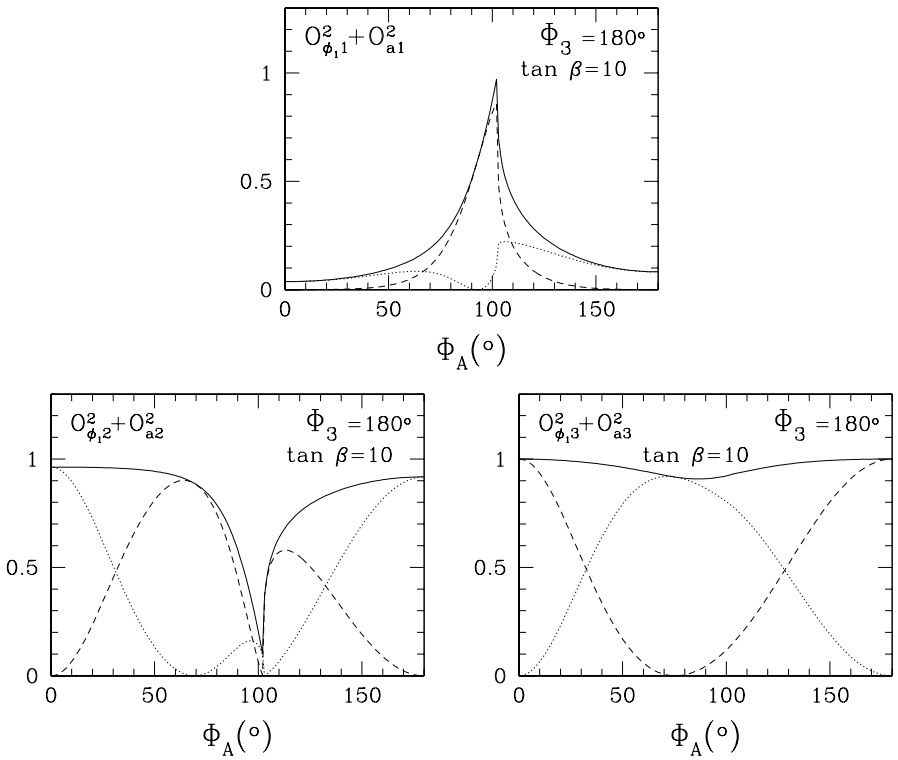

Fig. 3.31: The sums $O^2_{\phi_1 i} + O^2_{ai}$ vs. Φ_A, for the spectrum of Eq. (3.13), with $M_{\rm SUSY} = 0.5\,$TeV, $\tan\beta = 10$ and $\Phi_3 = 180^{\rm o}$. The dashed lines show O^2_{ai}, the dotted ones, $O^2_{\phi_1 i}$.

where $b_{{\rm had}_i}(x,Q)$ and $\bar{b}_{{\rm had}_i}(x,Q)$ are the b- and $\bar{b}$-quark distribution functions in the hadron ${\rm had}_i$, Q is the factorization scale, and τ_i the Drell–Yan variable $\tau_i = M^2_{H_i}/s$, with s the invariant hadron-collider energy squared. The partonic cross section is

$$\sigma(b\bar{b}\to H_i) = \frac{m_b^2}{v^2}\frac{\pi}{6M^2_{H_i}}\left[(g^S_{H_i\bar{b}b})^2 + (g^P_{H_i\bar{b}b})^2\right] \approx \frac{m_b^2}{v^2}\frac{\pi}{6M^2_{H_i}}\left[O^2_{\phi_1 i} + O^2_{ai}\right]\left[(g^S_a)^2 + (g^P_a)^2\right]\,. \tag{3.55}$$

where the last approximation is valid when $g^{S,P}_{\phi_2}$ can be neglected. See discussion in Ref. [77]. The sums $O^2_{\phi_1 i} + O^2_{ai}$ are shown explicitly in Fig. 3.31, for the value $\Phi_3 = 180^\circ$. This is sufficient since the dependence of these sums on Φ_3 is rather weak, coming from the two-loop corrections to the Higgs potential. Notice that, for $\Phi_A \approx 100^{\rm o}$, H_1 is predominantly the CP-odd a boson, whereas H_2 and H_3 are mainly ϕ_2 and ϕ_1, respectively.

The hadronic cross sections for the Tevatron ($\sqrt{s} = 1.96\,$TeV) and the LHC ($\sqrt{s} = 14\,$TeV) are obtained using the leading-order CTEQ6L [268] parton distribution functions, with the factorization scale fixed at $Q = M_{H_i}/4$. This has been suggested in most of the papers in Ref. [269–275] as the scale that minimizes the next-to-leading-order QCD corrections to these cross sections when no threshold corrections to m_b are kept into account. Although this should be explicitly checked, we believe that the inclusion of these corrections should not affect substantially this result. We notice also that these supersymmetric threshold corrections capture the main part of all supersymmetric corrections to the production cross sections of neutral Higgs bosons through b-quark fusion. Other corrections, with a nontrivial dependence on the momenta of the H_i bosons are of decoupling nature, and therefore subleading.

The cross sections are shown in Fig. 3.32 vs. Φ_A, for two values of Φ_3: $0^{\rm o}$ (dashed lines) and $180^{\rm o}$ (solid lines). These two curves delimit all cross sections obtained for all values of Φ_3 between 0° and 180°. We observe that these cross section can deviate substantially from those obtained in CP conserving scenarios, thanks to the nontrivial role played by the threshold corrections to m_b and the CP-

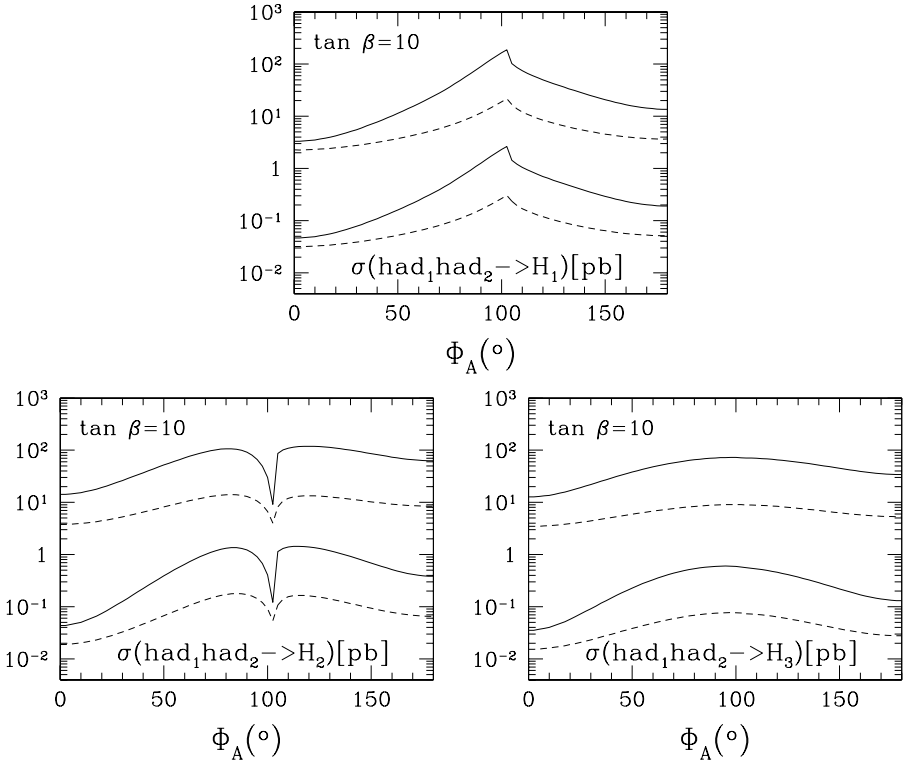

Fig. 3.32: Cross sections for the b-fusion production of H_1, H_2, and H_3 vs. Φ_A, for $\Phi_3 = 180^o$ (solid lines) and 0^o (dashed lines), at the LHC with $\sqrt{s} = 14\,\text{TeV}$ (two upper lines) and at the Tevatron with $\sqrt{s} = 1.96\,\text{TeV}$ (two lower lines). The symbol had_1had_2 indicates pp for the LHC, $p\bar{p}$ for the Tevatron.

violating mixing effects. The largest deviations in the case of H_1 and H_2 are around $\Phi_A = 100°$, with a large enhancement for the production cross section of H_1 and a large suppression for that of H_2. The former is due to the fact that the component of the field a in H_1 around these values of Φ_A is large, where it is depleted by the same large amount in H_2. The cross section for H_3 can also deviate substantially from that in CP conserving scenarios, but this deviation is roughly independent of Φ_A.

The region of maximal enhancement or suppression of the production cross sections, around $\Phi_A = 100°$, is also the region in which H_1 and H_2 are nearly degenerate. Compare with Fig. 3.29. Thus, we should worry about the fact that a further transition $H_1 \leftrightarrow H_2$ may occur during propagation (before decays) due to the off-diagonal absorbitive parts in the 3×3 matrix for the neutral Higgs boson propagator considered in Ref. [158]. In the present case, we observe that $\sqrt{\Gamma_{H_1}\Gamma_{H_2}}$ is much smaller than twice the H_1–H_2 mass difference. This may imply that such a transition does not occur. We have numerically checked that this is the case [276].

The mass difference between H_1 and H_2 is, however, still small enough to question whether it is possible to disentangle the two corresponding peaks in the invariant mass distributions of the H_1- and H_2-decay products. There is no similar problem for the H_3 eigenstate, that has a mass always larger than $\sim 160\,\text{GeV}$, and therefore a splitting from H_2 always larger than $\sim 10\,\text{GeV}$. Having a width smaller than $\sim 2\,\text{GeV}$, H_3 can be easily separated from H_2, and therefore also from H_1. In the case of H_1 and H_2, on the contrary, the mass difference can be as small $2\,\text{GeV}$ around $\Phi_A = 100°$. It will therefore be very challenging to disentangle H_2 from H_1 experimentally. An analysis of the decay modes and their resolution can help in this sense. At the LHC, the best energy and momentum resolution is for the Higgs-boson decays into muon and photon pairs, with $\delta M_{\gamma\gamma} \sim 1\,\text{GeV}$ and $\delta M_{\mu\mu} \sim 3\,\text{GeV}$, respectively [196]. Thus, it is presumably by combining the analyses of these two decay modes that H_2 can be disentagled from H_1 when the mass difference is as small as the resolution for the dimuon invariant mass [276].

3.8 CP-violating Higgs in diffraction at the LHC

Valery A. Khoze, Alan D. Martin and Mikhail G. Ryskin

Recently much attention has focussed on the use of forward proton tagging as a way to discover new physics at the LHC; see, for example, [277–281]. This method promises to provide an exceptionally clean environment to search for, and to identify the nature of, new objects at the LHC. A key motivation behind the recent proposal [282] to add forward proton taggers to the CMS and ATLAS detectors is the study of the central exclusive diffractive (CED) Higgs production process: $pp \to p + H + p$, where the $+$ signs denote the presence of large rapidity gaps.

In some MSSM Higgs scenarios, CED processes provide an opportunity for lineshape analyses [281, 283] and offer a way for direct observation of a CP-violating signal in the Higgs sector [279, 281]. Here, following Ref. [279] we illustrate the phenomenological consequences of CED Higgs production, using a benchmark scenario of maximal CP-violation (called CPX) which was introduced in Ref. [284]. The parameters are fixed according to Eq. (3.13) As shown in [284] the LEP2 data do not exclude the existence of a light Higgs boson with mass $M_H < 60$ GeV (40 GeV) in the model with $\tan\beta \sim$ 3–4 (2–3) and CP phase $\Phi_A = \Phi_3 = 90°(60°)$.

As discussed in [279, 281, 285], CED production (which we show in Fig. 3.33) has unique advantages in hunting for CP-violating Higgses as compared to the traditional non-diffractive processes. For numerical estimates, we use the formalism of [277, 286] to describe CED production, together with the Higgs parameters given by the code `CPsuperH` [287], where we choose $\Phi_A = \Phi_3 = 90°$, $\tan\beta = 4$, $M_{\rm SUSY} = 0.5$ TeV, (that is $|A_f| = 1$ TeV, $|\mu| = 2$ TeV, $|M_3| = 1$ TeV) and $M_{H^\pm} = 135.72$ GeV, so that the mass of the lightest Higgs boson, H_1, is $M_{H_1} = 40$ GeV. The cross section is written [277, 286] as

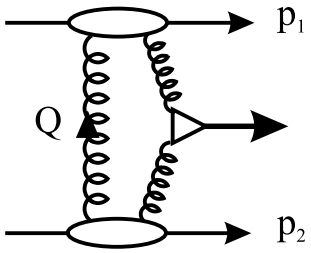

Fig. 3.33: Schematic diagram for the exclusive central diffractive (CED) production of a Higgs boson.

the product of the effective gluon–gluon luminosity $\mathcal{L}$, and the square of the matrix element of the subprocess $gg \to H$. Note that the hard subprocess is mediated by the quark/squark triangles in Fig. 3.33. For a CP-violating Higgs the $gg \to H$ matrix element contains two terms

$$\mathcal{M} = g_S \cdot (e_1^\perp \cdot e_2^\perp) - g_P \cdot \varepsilon^{\mu\nu\alpha\beta} e_{1\mu} e_{2\nu} p_{1\alpha} p_{2\beta} / (p_1 \cdot p_2) \tag{3.56}$$

where $e^\perp$ are the gluon polarisation vectors and $\varepsilon^{\mu\nu\alpha\beta}$ is the antisymmetric tensor. In forward CED production, the gluon polarisations are correlated, in such a way that the effective luminosity satisfies the P-even, $J_z = 0$ selection rule [277, 288] . Therefore only the first term contributes to the strictly forward cross section. However, at non-zero transverse momenta of the recoil protons, $p_{1,2}^\perp \neq 0$, there is an admixture of the P-odd $J_z = 0$ amplitude of order $p_1^\perp p_2^\perp / Q_\perp^2$, on account of the g_P term becoming active. For non-zero recoil proton transverse momenta, the interference between the CP-even (g_S) and CP-odd (g_P) terms leads to left-right asymmetry in the azimuthal distribution of the outgoing protons.

3.8.1 Exclusive diffractive H_1 production followed by $b\bar{b}$ decay

Let us consider the CED process

$$pp \to p + (H \to b\bar{b}) + p\,. \tag{3.57}$$

The signal-to-background ratio is given by the ratio of the cross sections for the hard subprocesses, since the effective gluon–gluon luminosity $\mathcal{L}$ cancels out. The cross section for the $gg \to H$ subprocess[8] [277]

$$\hat{\sigma}(gg \to H) \;=\; \frac{2\pi^2\Gamma(H \to gg)}{M_H^3}\delta\left(1 - \frac{M_{b\bar{b}}^2}{M_H^2}\right) \;\sim\; \text{constant} \times \delta\left(1 - \frac{M_{b\bar{b}}^2}{M_H^2}\right), \tag{3.58}$$

On the other hand, at leading order, the QCD background is given by the $gg \to b\bar{b}$ subprocess

$$\frac{d\hat{\sigma}_{\rm QCD}}{dE_T^2} \sim \frac{m_b^2}{E_T^2}\frac{\alpha_S^2}{M_{b\bar{b}}^2 E_T^2}, \tag{3.59}$$

where E_T is the transverse energy of the b and $\bar{b}$ jets. At leading order (LO), the cross section is suppressed by the $J_z = 0$ selection rule in comparison with the inclusive process. It was shown in [278] that it is possible to achieve a signal-to-background ratio of about 1 for the detection of a SM Higgs with $M_H \sim 120$ GeV, by selecting $b\bar{b}$ exclusive events where the polar angle θ between the outgoing jets lies in the interval $60^\circ < \theta < 120^\circ$ if the mass window $\Delta m_{\rm missing} = 3$ GeV. The situation is much worse for a light Higgs, since the signal-to-background ratio behaves as

$$\frac{\displaystyle\int \frac{d\mathcal{L}}{d\ln M_{b\bar{b}}^2}\,\hat{\sigma}(gg \to H)\,d\ln M_{b\bar{b}}^2}{\displaystyle\int \frac{d\mathcal{L}}{d\ln M_{b\bar{b}}^2}\,\hat{\sigma}_{\rm QCD}\,d\ln M_{b\bar{b}}^2} \;\sim\; M_{b\bar{b}}^5 \tag{3.60}$$

where we have used $\Delta \ln M_{b\bar{b}}^2 = 2\Delta M_{b\bar{b}}/M_{b\bar{b}}$. The M^5 behaviour comes just from dimensional counting. Thus, in going from $M_H \sim 120$ GeV to $M_H \sim 40$ GeV, the expected LO QCD $b\bar{b}$ background increases by a factor of 240 in comparison with that for $M_{b\bar{b}} = 120$ GeV.

Strictly speaking, there are other sources of background [278]. However, for $M_{H_1} \sim 40$ GeV, the LO $b\bar{b}$ contribution dominates. Finally, with the cuts of Ref. [278], we predict that the cross section of the H_1 signal is

$$\sigma^{\rm CED}(pp \to p + (H_1 \to b\bar{b}) + p) \simeq 14 \text{ fb}$$

as compared to the QCD background cross section, with the same cuts, of

$$\sigma^{\rm CED}(pp \to p + (b\bar{b}) + p) \simeq 1.4\frac{\Delta M}{1 \text{ GeV}} \text{ pb}.$$

That is the signal-to-background ratio is only $S/B \sim 1/300$, and so even for an integrated luminosity $\mathcal{L} = 300 \text{ fb}^{-1}$ for $\Delta M = 3$ GeV the significance of the signal is too low. Therefore, to identify a light Higgs, it is desirable to study a decay mode other than $H_1 \to b\bar{b}$. The next largest mode is $H_1 \to \tau\tau$, with a branching fraction of about 0.07.

The dependence of the results on the mass of the H_1 Higgs boson is illustrated in Table 3.2. Clearly the cross section decreases with increasing mass. On the other hand the signal-to-background ratio increases.

3.8.2 The $\tau\tau$ decay mode

At the LHC energy, the expected CED cross section for H_1 production, followed by $\tau\tau$ decay, is

$$\sigma\,(pp \to p + (H \to \tau\tau) + p) \sim 1.1 \text{ fb}, \tag{3.61}$$

[8] In [277] we denoted the initial state by gg^{PP} to indicate that each of the incoming gluons belongs to colour-singlet Pomeron exchange. Here this notation is assumed to be implicit.

Table 3.2: The cross sections (in fb) of CED production of H_i neutral Higgs bosons, together with those of the QCD($b\bar{b}$) and QED($\tau\tau$) backgrounds. The acceptance cuts applied are (a) the polar angle cut $60^\circ < \theta(b \text{ or } \tau) < 120^\circ$ in the Higgs rest frame, (b) $p_i^\perp > 300$ MeV for the forward outgoing protons and (c) the polar angle cut $45^\circ < \theta(b) < 135^\circ$. The azimuthal asymmetries A_i are defined in Eq. (3.63).

$M(H_1)$ GeV	cuts	30	40	50
$\sigma(H_1) \times \mathrm{Br}(b\bar{b})$	a	45	14	6
$\sigma^{\mathrm{QCD}}(b\bar{b})$	a	48000	4200	600
$A_{b\bar{b}}$		0.14	0.07	0.04
$\sigma(H_1) \times \mathrm{Br}(\tau\tau)$	a, b	1.9	0.6	0.3
$\sigma^{\mathrm{QED}}(\tau\tau)$	a, b	0.6	0.3	0.12
$A_{\tau\tau}$	b	0.2	0.1	0.05
$M(H_2)$ GeV		103.4	104.7	106.2
$\sigma \times \mathrm{Br}(H_2 \to 2H_1 \to 4b)$	c	0.5	0.5	0.5
$\sigma \times \mathrm{Br}(H_2 \to 2b)$	a	0.1	0.1	0.2
$M(H_3)$ GeV		141.9	143.6	146.0
$\sigma \times \mathrm{Br}(H_3 \to 2H_1 \to 4b)$	c	0.14	0.2	0.18
$\sigma \times \mathrm{Br}(H_3 \to 2b)$	a	0.04	0.07	0.1

where the $60^\circ < \theta < 120^\circ$ polar angle cut has already been included. Despite the low Higgs mass, we note that the exclusive cross section is rather small. As we already saw in (3.58), the cross section of the hard subprocess $\hat{\sigma}(gg \to H)$ is approximately independent of M_H. Of course, we expect some enhancement from the larger effective gluon–gluon luminosity $\mathcal{L}$ for smaller M_H. This gives an enhancement of about 20 (for $M_H = 40$ GeV in comparison with that for $M_H = 120$ GeV).

On the other hand, in the appropriate region of SUSY parameter space, the CP-even $H \to gg$ vertex, g_S, is almost 2 times smaller [285, 287] than that of a SM Higgs, giving a suppression of 4. Also the ratio $B(H \to \tau\tau)/B(H \to b\bar{b})$ gives a further suppression of about 12. Although the $\tau\tau$ signal has the advantage that there is practically no QCD background, exclusive $\tau^+\tau^-$ events may be produced by $\gamma\gamma$ fusion. To suppress this QED background, one may select events with relatively large transverse momenta of the outgoing protons. For example, if $p_{1,2}^\perp > 300$ MeV, then the cross section for the QED background, for $M_{\tau\tau} = 40$ GeV, is about

$$\sigma_{\mathrm{QED}}(pp \to p + \tau\tau + p) \;\simeq\; 0.1 \frac{\Delta M}{1 \text{ GeV}} \text{ fb}, \tag{3.62}$$

while the signal (3.61) contribution is diminished by the cuts, $p_{1,2}^\perp > 300$ MeV, down to 0.6 fb. Thus, assuming an experimental resolution of $\Delta M \sim 3$ GeV, we obtain a signal-to-background ratio of $S/B \sim 2$ for $M_{H_1} \sim 40$ GeV.

Note that in all the estimates given above, we include the appropriate soft survival factors S^2—that is the probabilities that the rapidity gaps are not populated by the secondaries produced in the soft rescattering [290]. Moreover, here we account for the fact that only events with proton transverse momenta $p_{1,2}^\perp > 300$ MeV were selected.

3.8.3 Azimuthal asymmetry of the outgoing protons

A specific prediction, in the case of a CP-violating Higgs boson, is the asymmetry in the azimuthal φ distribution of the outgoing protons, caused by the interference between the two terms in (3.56). The polarisations of the active gluons are aligned along their respective transverse momenta, $Q_\perp - p_1^\perp$ and

$Q_\perp + p_2^\perp$. Hence the contribution caused by the second term, g_P, is proportional to the vector product

$$\vec{n}_0 \cdot (\vec{p}_1^{\,\perp} \times \vec{p}_2^{\,\perp}) \sim \sin\varphi,$$

where $\vec{n}_0$ is a unit vector in the beam direction, $\vec{p}_1$. The sign of the angle φ is fixed by the four-dimensional structure of the second term in (3.56). Of course, due to the selection rule, this contribution is suppressed in the amplitude by $p_1^\perp p_2^\perp / Q_\perp^2$, in comparison with that of the g_S term. Note that there is a partial compensation of the suppression due to the ratio $g_P/g_S \sim 2$. Also the soft survival factors S^2 are higher for the pseudoscalar and interference terms, than for the scalar term.

An observation of the azimuthal asymmetry may therefore be a direct indication of the existence of CP-violation in the Higgs sector. Neglecting rescattering effects, we find, for example, an asymmetry

$$A = \frac{\sigma(\varphi < \pi) - \sigma(\varphi > \pi)}{\sigma(\varphi < \pi) + \sigma(\varphi > \pi)} = 2\mathrm{Re}(g_S g_P^*) r_{S/P} (2/\pi) / (|g_S|^2 + |r_{S/P} g_P|^2/2). \tag{3.63}$$

Here the parameter $r_{S/P}$ reflects the suppression of the P-odd contribution. At the LHC energy $A \simeq 0.09$ for $M_{H_1} = 40$ GeV. However we find soft rescattering tends to wash out the azimuthal distribution, and to weaken the asymmetry. Besides this the real part of the rescattering amplitude multiplied by the imaginary part of the pseudoscalar vertex g_P (with respect to g_S) gives some negative contribution. So finally we predict[9] $A \simeq 0.07$.

The asymmetries expected at the LHC, with and without the cut $p_{1,2}^\perp > 300$ MeV, are shown for different H_1 masses in Table 1. The asymmetry decreases with increasing Higgs mass, first, due to the decrease of $|g_P|/|g_S|$ ratio in this mass range and, second, due to the extra suppression of the P-odd amplitude arising from the factor $p_1^\perp p_2^\perp / Q_\perp^2$ in which the typical value of $Q_\perp$ in the gluon loop increases with mass.

3.8.4 Heavy H_2 and H_3 Higgs production with H_1H_1 decay

Another possibility to study the Higgs sector in the CPX scenario is to observe CED production of the heavy neutral H_2 and H_3 Higgs bosons, using the $H_2, H_3 \to H_1 + H_1$ decay modes. For the case we considered above ($\tan\beta = 4$, $\phi_{\rm CPX} = 90^\circ$, $M_{H_1} = 40$ GeV), the masses of the heavy bosons bosons are $M_{H_2} = 104.7$ GeV and $M_{H_3} = 143.6$ GeV. At the LHC energy, the CED cross sections of the H_2 and H_3 bosons are not too small – $\sigma^{\rm CED} = 1.5$ and 0.9 fb respectively. When the branching fractions, $\mathrm{Br}(H_2 \to H_1H_1) = 0.84$, $\mathrm{Br}(H_3 \to H_1H_1) = 0.54$ and $\mathrm{Br}(H_1 \to b\bar{b}) = 0.92$, are included, we find

$$\sigma(pp \to p + (H \to b\bar{b}\, b\bar{b}) + p) = 1.1 \text{ and } 0.4 \text{ fb}$$

for H_2 and H_3 respectively. Thus there is a chance to observe, and to identify, the CED production of all three neutral Higgs bosons, H_1, H_2 and H_3, at the LHC. The QCD background for exclusive diffractive production of four b-jets is significantly less than the signal.

3.8.5 Central Higgs production with double diffractive dissociation

To enhance the Higgs signal we study a less exclusive reaction in which we allow both of the incoming protons to dissociate. In Ref. [277] it was called double diffractive *inclusive* production (here denoted CDD), and was written

$$pp \to X + H + Y. \tag{3.64}$$

Typical results, for the LHC energy, are shown in Table 3.3.

Of course, the missing mass method cannot be used to measure the mass of the Higgs for CDD production. Therefore the mass resolution will be not so good as for CED. Moreover, with the absence

[9] We expect a similar asymmetry in the tri-mixing scenario of Ref. [281].

Table 3.3: The cross sections (in fb) for the central production of H_i neutral Higgs bosons by *inclusive* double diffractive dissociation (CDD), together with that of the QED($\tau\tau$) background. A polar angle acceptance cuts of $60^\circ < \theta(b \text{ or } \tau) < 120^\circ$ ($45^\circ < \theta(b) < 145^\circ$) in the Higgs rest frame is applied for the case of H_1 (H_2, H_3) bosons. The numbers in brackets correspond to the imposition of the additional cut of $E_i^\perp > 7$ GeV for the proton dissociated systems.

$M(H_1)$ GeV	30	40	50
$\sigma(H_1) \times \mathrm{Br}(\tau\tau)$	19 (4)	6 (2)	2.6 (0.8)
$\sigma^{\mathrm{QED}}(\tau\tau)$	66 (2.2)	30 (1.5)	15 (0.9)
$M(H_2)$ GeV	103.4	104.7	106.2
$\sigma \times \mathrm{Br}(H_2 \to 2H_1 \to 4b)$	4 (2)	4 (2)	3.5 (2)
$M(H_3)$ GeV	141.9	143.6	146.0
$\sigma \times \mathrm{Br}(H_3 \to 2H_1 \to 4b)$	1.5 (0.8)	2.2 (1.2)	2 (1.1)

of the selection rule, the LO QCD $b\bar{b}$-background is not suppressed. Hence we study only the $\tau\tau$ decay mode for the light boson, H_1, and the four b-jet final state for the heavy H_2 and H_3 bosons.

The background to the $H_1 \to \tau\tau$ signal arises from the $\gamma\gamma \to \tau\tau$ QED process. It is evaluated in the equivalent photon approximation. From Table 2 we see that the H_1 signal for CDD production, (3.64), exceeds the exclusive signal by more than a factor of ten. On the other hand the signal-to-background ratio is worse; S/B_{QED} is about 1/5. Moreover there could be a huge background due the misidentification of a gluon dijet as a $\tau\tau$-system.

For the four b-jet signals of the heavy H_2 and H_3 bosons, the QCD background can be suppressed by requiring each of the four b-jets to have polar angle in the interval $(45^\circ, 135^\circ)$, in the frame where the four b-jet system has zero rapidity. However in the absence of a good mass resolution, that is with only $\Delta M = 10$ GeV, we expect the four b-jet background to be 3-5 times the signal. Nevertheless these signals are still feasible, with cross sections of the order of a few fb. For example, with an integrated luminosity of $\mathcal{L} = 300$ fb^{-1} and an efficiency of $4b$-tagging of $(0.6)^2$ [278], we predict about 400 H_2 events and 200 H_3 events.

The CDD kinematics allow a study of CP-violation, and the separation of the contributions coming from the scalar and pseudoscalar couplings, g_S and g_P of (3.56), respectively. Indeed, the polarizations of the incoming active gluons are aligned along their transverse momenta, $\vec{Q}_\perp - \vec{p}_1^{\,\perp}$ and $\vec{Q}_\perp + \vec{p}_2^{\,\perp}$. Hence the $gg \to H$ fusion vertices take the forms

$$V_S = (\vec{Q}_\perp - \vec{p}_1^{\,\perp}) \cdot (\vec{Q}_\perp + \vec{p}_2^{\,\perp}) g_S \tag{3.65}$$

$$V_P = \vec{n}_0 \cdot [(\vec{Q}_\perp - \vec{p}_1^{\,\perp}) \times (\vec{Q}_\perp + \vec{p}_2^{\,\perp})] g_P, \tag{3.66}$$

where g_S and g_P are defined in (3.56).

For the exclusive (CED) process the momenta $p_{1,2}^\perp$ were limited by the proton form factor, and typically $Q^2 \gg p_{1,2}^2$. Thus

$$V_S = g_S\, Q_\perp^2 \quad \text{while} \quad V_P = g_P\, (\vec{n}_0 \cdot [\vec{p}_2^{\,\perp} \times \vec{p}_1^{\,\perp}]). \tag{3.67}$$

On the contrary, for double diffractive dissociation production (CDD) $Q^2 < p_{1,2}^2$. In this case

$$V_S = g_S\, p_1^\perp p_2^\perp \cos\varphi \quad \text{and} \quad V_P = g_P\, p_1^\perp p_2^\perp \sin\varphi. \tag{3.68}$$

Moreover we can select events with large outgoing transverse momenta of the dissociating systems, say $p_{1,2}^\perp > 7$ GeV, in order to make reasonable measurements of the directions of the vectors $\vec{p}_1^{\,\perp} = \vec{E}_1^{\,\perp}$

Table 3.4: The coefficients in the azimuthal distribution $d\sigma/d\varphi = \sigma_0(1 + a\sin 2\varphi + b\cos 2\varphi)$, where φ is the azimuthal angle between the $E^\perp$ flows of the two proton dissociated systems. If there were no CP-violation, then the coefficients would be $a = 0$ and $|b| = 1$.

$M(H_1)$ GeV	30		40		50	
	a	b	a	b	a	b
H_1	-0.53	-0.73	-0.56	-0.55	-0.53	-0.33
H_2	0.44	0.90	0.41	0.91	0.37	0.92
H_3	-0.38	0.92	-0.40	0.91	-0.42	0.90

and $\vec{p}_2^{\perp} = \vec{E}_2^{\perp}$. Here $E_{1,2}^{\perp}$ are the transverse energy flows of the dissociating systems of the incoming protons. At LO, this transverse energy is carried mainly by the jet with minimal rapidity in the overall centre-of-mass frame. The azimuthal angular distribution has the form

$$\frac{d\sigma}{d\varphi} = \sigma_0(1 + a\,\sin2\varphi + b\,\cos2\varphi), \tag{3.69}$$

where the coefficients are given by

$$a = \frac{2\mathrm{Re}(g_S g_P^*)}{|g_S|^2 + |g_P|^2} \quad \text{and} \quad b = \frac{|g_S|^2 - |g_P|^2}{|g_S|^2 + |g_P|^2}. \tag{3.70}$$

Note that the coefficient a arises from scalar-pseudoscalar interference, and reflects the presence of a T-odd effect. Its observation would signal an explicit CP-violating mixing in the Higgs sector.

The predictions for the coefficients are given in Table 3.4 for different values of the Higgs mass, namely M_{H_1} = 30, 40 and 50 GeV. The coefficients are of appreciable size and, given sufficient luminosity, may be measured at the LHC. Imposing the cuts $E_i^{\perp} > 7$ GeV reduces the cross sections by about a factor of two, but does not alter the signal-to-background ratio, S/B_{QCD}. However the cuts do give increased suppression of the QED $\tau\tau$ background and now, for the light H_1 boson, the ratio S/B_{QED} exceeds one. We emphasize here that, since we have relatively large $E^{\perp}$, the angular dependences are quite insensitive to the soft rescattering corrections.

3.8.6 Conclusions

We have evaluated the cross sections, and the corresponding backgrounds, for the central double-diffractive production of the (three neutral) CP-violating Higgs bosons at the LHC using, for illustration, the CPX scenario of Ref. [284]. We have studied the production of the three states, H_1, H_2, H_3, both with exclusive kinematics, $pp \to p + H + p$ which we denoted CED, and in double-diffractive reactions where both the incoming protons may be destroyed, $pp \to X + H + Y$ which we denoted CDD. Proton taggers are required in the former processes, but not in the latter. Typical results are summarised in Tables 1 and 2, respectively. The cross sections are not large, but should be accessible at the LHC. The azimuthal asymmetries of the outgoing protons, induced by CP-violation, are quite sizeable, of order 10%.

It would be very informative to measure the azimuthal angular dependence of the outgoing proton systems, for both the CED and CDD processes. Such measurements would reveal explicitly any CP-violating effect, via the interference of the scalar and pseudoscalar $gg \to H$ vertices.

3.9 CP violation in supersymmetric charged Higgs production at the LHC

Jennifer Williams

We investigate the possibility of observing CP violation in the production of MSSM charged Higgs bosons at the LHC. The CP violation arises from allowing the trilinear scalar couplings in the soft breaking Lagrangian to be complex, leading to complex phases. We have chosen to investigate the effect of a complex A_t, leaving the other phases zero. Initially, we set the phase of A_t, Φ_{A_t}, to be maximal ($\frac{\pi}{2}$) and vary the magnitudes of A_t and A_b, with $|A_t| = |A_b|$. In a study which is currently in preparation [291] we also consider fixing the magnitudes of the trilinear couplings and vary the phases of A_t and A_b.

The main production modes for charged Higgs bosons at the LHC are through b quark induced processes, due to the large coupling of the Higgs bosons to heavy quarks. The dominant production process is b quark – gluon fusion, in which a charged Higgs boson is produced in association with a t quark, this is shown in Fig. 3.34. The cross section for this process was found using HERWIG [292] to be 135×10^{-3} pb. The cross section for the gluon – gluon fusion was found to be 8.24×10^{-3} pb. For this reason this investigation only considers charged Higgs boson production by b quark – gluon fusion.

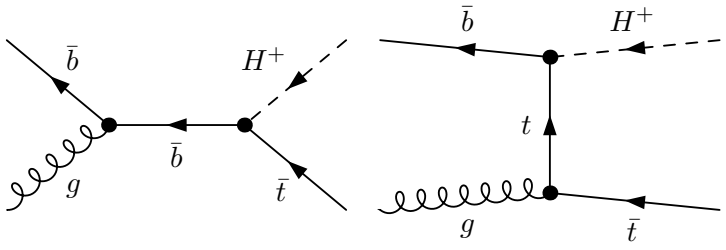

Fig. 3.34: Tree level production of charged Higgs bosons.

In order for the CP violation which is present in the complex phases to be manifest, it is necessary for there to be interference between the tree level and loop level processes. This is because we require the matrix element squared for the two CP conjugate processes (one producing H^+ and the other H^- bosons) to be different. If there is no interference term, then $|\mathcal{M}|^2 = |\text{tree}|^2 + |\text{loop}|^2$ which must be the same for both CP conjugate processes.

Since there is no CP violation in the tree level process (A_t does not enter at tree level), it is also necessary for the loop level matrix element to be complex in order for the tree – loop interference term to be different for the two CP conjugate processes. It is an intermediate result of the Optical Theorem that the matrix element at one loop level will have an imaginary part if the energy of the process is sufficient for the particles in the loop to be produced on mass shell.

At one loop level, the loops which contribute to the asymmetry are those involving stop and sbottom squarks. A selection of these loops is shown in Fig. 3.35. In later figures they are referred to in groups, with TB $\tilde{t}\tilde{b}\tilde{g}$ referring to the triangle and box diagrams containing stop and sbottom squarks and gluinos, SE $\tilde{t}\tilde{b}$ referring to the self energy diagrams containing stop and sbottom squarks and TB $\tilde{t}\tilde{b}\tilde{\chi}^0$ referring to the triangle and box diagrams containing stop and sbottom squarks and neutralinos.

The CP asymmetry in the production of H^+ and H^- bosons at the parton level was calculated using FormCalc [228, 236] as

$$\mathcal{A}_{\text{parton}} = \frac{\sigma(H^+) - \sigma(H^-)}{\sigma(H^+) + \sigma(H^-)}. \tag{3.71}$$

The MSSM parameters which were used as input for FormCalc were chosen to give parameter space points based on SPS 1a [255], similar to that used in a study of the decay of charged Higgs bosons

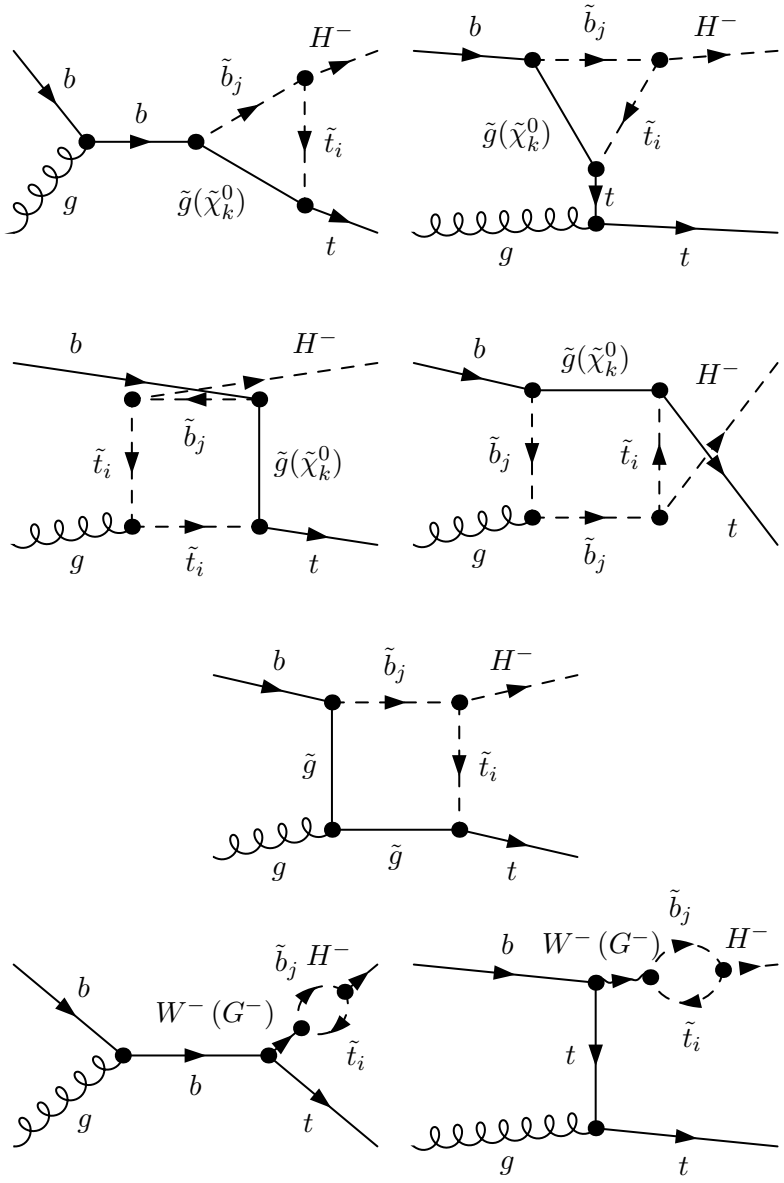

Fig. 3.35: A selection of diagrams contributing to the CP violating asymmetry in charged Higgs boson production at one loop level.

by Christova et al. [68]. The MSSM parameters used are given in Table 3.5. The Standard Model parameters used were the default parameters in `FormCalc`.

The CP asymmetry at parton level is shown in Fig. 3.36, both versus the partonic centre of mass energy, $\sqrt{\hat{s}}$ and versus changing Higgs mass, $M_{H^\pm}$. The very clear thresholds (marked with vertical lines) that can be seen occur at values of the partonic centre of mass energy or charged Higgs boson mass when the loop particles can be produced on mass shell, thus increasing the imaginary part of the loop matrix element. For example the thresholds in $\sqrt{\hat{s}}$ for the loop containing a gluino and stop and sbottom squarks occurs at values of $M_{\tilde{g}} + M_{\tilde{b}_j}$ and the thresholds in $M_{H^\pm}$ for the self energy loop containing stop and sbottom squarks occurs at values of $M_{\tilde{t}_i} + M_{\tilde{b}_j}$.

Up to this point we have considered the b quark and the gluon as free on shell particles. In reality they are constituents of the protons and it is the protons that will be collided at the LHC. We now convolute the parton level results with the parton distribution functions; this effectively integrates over the partonic centre of mass energy. We used the 2004 MRST pdfs at next-to-leading order at a q^2 value of

Table 3.5: Constrained Minimal Supersymmetric Standard Model parameters used for this study.

Parameter	Value	
	SPS 1a	SPS 1b
$\tan\beta$	10	30
$\lvert\mu\rvert$	352.39 GeV	501.08 GeV
M_2	192 GeV	311.38
$\lvert A_t\rvert$	varied $250 \rightarrow 1000$ GeV usually 500 or 1000 GeV	
Φ_{A_t}	$\frac{\pi}{2}$	
$\lvert A_b\rvert$	$= \lvert A_t\rvert$	
Φ_{A_b}	0	
M_{SUSY}	490 GeV	707.06 GeV
$M_{\tilde{Q}_3}$	535 GeV	767 GeV
$M_{\tilde{U}_3}$	340 GeV	672 GeV
$M_{\tilde{D}_3}$	490 GeV	788 GeV

$(M_{H^\pm} + M_t)^2$ [293]. The CP violating asymmetry for the hadronic production of charged Higgs bosons is given by

$$\mathcal{A}_{\text{hadron}} = \frac{\sigma(pp \rightarrow \bar{b}g \rightarrow H^+\bar{t} + X) - \sigma(pp \rightarrow bg \rightarrow H^-t + X)}{\sigma(pp \rightarrow \bar{b}g \rightarrow H^+\bar{t} + X) + \sigma(pp \rightarrow bg \rightarrow H^-t + X)}. \tag{3.72}$$

The results for the CP asymmetry at hadron level are shown in Fig. 3.37. The thresholds marked in Fig. 3.37a are thresholds in the charged Higgs boson mass at values of $M_{\tilde{t}_i} + M_{\tilde{b}_j}$.

We combined our results for the CP asymmetry in the production of charged Higgs bosons with those of Christova et al [68] for the decay after correcting a conjugation error in their decay results. The combined asymmetry for the production and the decay is given by

$$\mathcal{A}_{\text{total}} = \frac{\sigma\left(pp \rightarrow \bar{b}g \rightarrow H^+\bar{t} + X\right)\Gamma\left(H^+ \rightarrow t\bar{b}\right) - \sigma\left(pp \rightarrow bg \rightarrow H^-t + X\right)\Gamma\left(H^- \rightarrow \bar{t}b\right)}{\sigma\left(pp \rightarrow \bar{b}g \rightarrow H^+\bar{t} + X\right)\Gamma\left(H^+ \rightarrow t\bar{b}\right) + \sigma\left(pp \rightarrow bg \rightarrow H^-t + X\right)\Gamma\left(H^- \rightarrow \bar{t}b\right)}. \tag{3.73}$$

Because the loop contributions are small compared to the tree level this can be approximated as

$$\mathcal{A}_{\text{total}} = \mathcal{A}_{\text{hadron}} + \mathcal{A}_{\text{decay}}. \tag{3.74}$$

The results for combining the production and decay asymmetries are shown in Fig. 3.38.

Finally, we consider the possibility of observing this asymmetry at the LHC. The number of charged Higgs events which will be seen in the detector is given by

$$N = \sigma\left(pp \rightarrow bg \rightarrow H^\pm t\right) \text{BR}\left(H^\pm \rightarrow tb\right) \times \text{acceptance} \times \text{luminosity}. \tag{3.75}$$

We consider an optimistic acceptance of 0.05 and an integrated luminosity of 300 fb^{-1}. The acceptance is based on the acceptance given in the ATLAS TDR for b quarks [196]. The significance of the signal over the background, measured in standard deviations is then, $f = \sqrt{N}\mathcal{A}$. This significance is shown in Fig. 3.39. The significance is reduced by the poor acceptance to an insignificant level, meaning that it will not be possible to observe this asymmetry at the LHC.

It should be born in mind however, that we have only considered one production method and one decay in this study. The inclusion of other processes could increase the CP asymmetry. It is also possible to investigate the variation of other phases in the soft supersymmetry breaking Lagrangian. This has been done in [291]. It would also be worthwhile to investigate the possibility of observing a CP violating asymmetry in a similar process at an e^+e^- collider which is a cleaner environment.

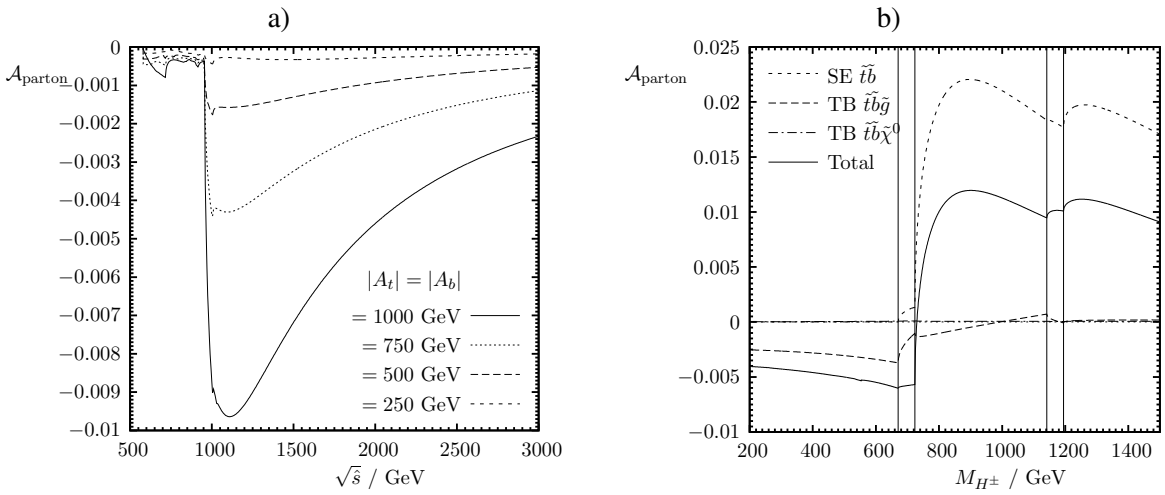

Fig. 3.36: CP asymmetry at parton level, for $\Phi_{A_t} = \frac{\pi}{2}$ and $\Phi_{A_b} = 0$. a) Plotted vs $\sqrt{\hat{s}}$, for $M_{H^\pm} = 402$ GeV and several values of $|A_t| = |A_b|$. b) Plotted vs $M_{H^\pm}$, for $\sqrt{\hat{s}} = 2000$ GeV, showing the contribution from different loops with $|A_t| = |A_b| = 1000$.

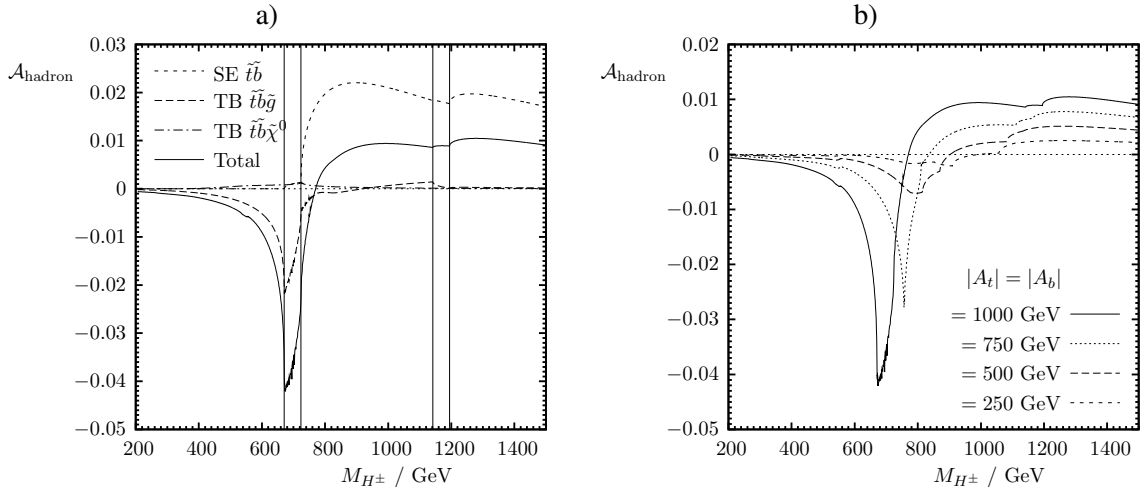

Fig. 3.37: The CP violating asymmetry at hadron level, plotted versus $M_{H^\pm}$, for $\Phi_{A_t} = \frac{\pi}{2}$ and $\Phi_{A_b} = 0$. a) contributions from different loops, with $|A_t| = |A_b| = 1000$. b) asymmetry for a range of trilinear couplings, $|A_t| = |A_b|$.

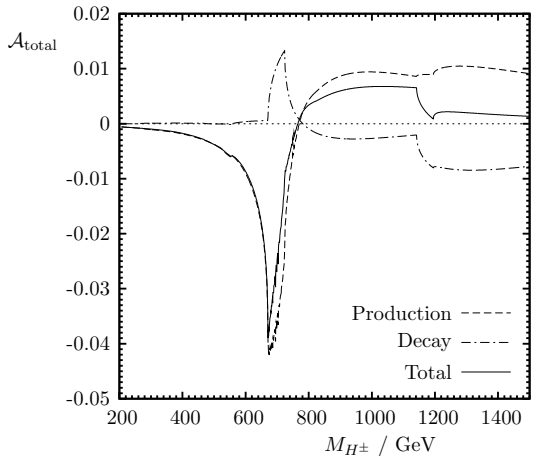

Fig. 3.38: Combined asymmetry for the production and decay, for $\Phi_{A_t} = \frac{\pi}{2}$ and $\Phi_{A_b} = 0$ and $|A_t| = |A_b| = 1000$.

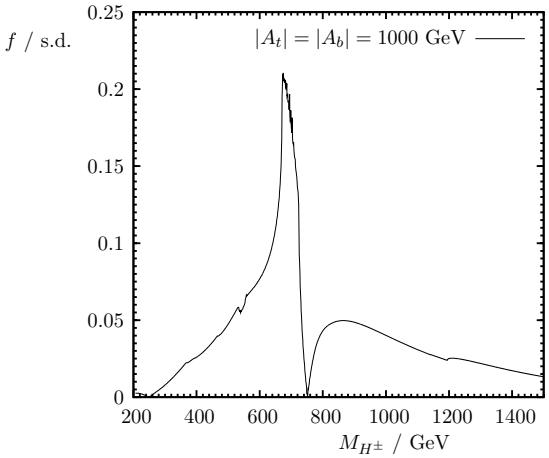

Fig. 3.39: The significance of the CP violating asymmetry expected to be seen in the ATLAS detector, for $\Phi_{A_t} = \frac{\pi}{2}$ and $\Phi_{A_b} = 0$ and $|A_t| = |A_b| = 1000$.

3.10 Exploring CP phases of the MSSM at future colliders

Sven Heinemeyer and Mayda Velasco

Measuring the phases of the CP-violating MSSM will be one of the important tasks of future high-energy colliders. We discuss the impact of complex phases within the MSSM on various Higgs boson production and decay channels (entering via loop corrections [48–53, 55, 56, 59–61]). Results are compared for the LHC, the ILC, and a $\gamma\gamma$ collider (γC). While the precision of the branching ratio measurement at the LHC is not accurate enough, both the ILC and the γC could in principle be sensitive to the effects of complex phases (depending on the scenario). The precisions for the various Higgs boson decay channels at the three colliders are summarized in Table 3.6. The Higgs boson mass is set to "typical" values below the upper bound of $M_h \lesssim 135$ GeV [115, 130], which is valid in the real as well as in the complex MSSM.

3.10.1 Comparison of different colliders

We compare the sensitivity of a future γC with that of the LHC and the ILC. The comparison is based on two different physics scenarios:

The CPX scenario:
This scenario has been designed to give maximum effects of CP-violating phases [54]. The definition is given in Eq. (3.13). For the sake of comparison with the BGX scenario, the parameters are

$$\begin{aligned} &M_{\rm SUSY} = 500 \text{ GeV}, |A_t| = 1000 \text{ GeV}, A_t = A_b = A_\tau \\ &M_2 = 500 \text{ GeV}, |M_3| = 1000 \text{ GeV}, \mu = 2000 \text{ GeV} \\ &\Phi = \Phi_{A_{t,b,\tau}} = \Phi_3 \,. \end{aligned} \tag{3.76}$$

$M_{\rm SUSY}$ denotes a common soft SUSY-breaking mass in the sfermion mass matrices. A_f is the trilinear Higgs-Sfermion coupling with the phase Φ_{A_f}. M_2 is a gaugino mass parameter, M_3 denotes the gluino mass parameter, and μ is the Higgs mixing parameter.

The BGX scenario:
This scenario is motivated by baryogenesis. It has been shown in [154] that in this scenario (depending on the Higgs sector parameters) baryogenesis in the early universe could be possible. It is thus a physics motivated scenario, not emphazising possible effects of complex phases. The parameters are

$$\begin{aligned} &M_{\tilde{Q}_3} = 1.5 \text{ TeV}, M_{\tilde{U}_3} = 0, M_{\tilde{Q}_{1,2}} = 1.2 \text{ TeV}, M_{\tilde{L}_{1,2}} = 1.0 \text{ TeV} \\ &|X_t| = 0.7 \text{ TeV}, A_t = A_b = A_\tau \\ &M_2 = 220 \text{ GeV}, M_3 = 1 \text{ TeV}, \mu = 200 \text{ GeV} \\ &\Phi = \Phi_{A_{t,b,\tau}} = \Phi_3 \end{aligned} \tag{3.77}$$

Here $M_{\tilde{Q}_3,\tilde{U}_3}$ are the soft SUSY-breaking parameters in the scalar top mass matrix. $M_{\tilde{Q}_{1,2}}$ are the corresponding parameters for the squarks of the first two generations, while $M_{\tilde{L}_{1,2}}$ refer to the sleptons of the first two generations. $m_t X_t$ is the off-diagonal entry in the scalar top mass matrix with $X_t = A_t - \mu^* / \tan\beta$.

The results presented here have been obtained with the code `FeynHiggs2.2` [59,115,130,144,148, 235]. It should be noted that the higher-order uncertainties in these evaluations are somewhat less under control as compared to the real case, see e.g. Ref. [61]. The same applies to the parametric uncertainties due to the experimental errors of the input parameters [47, 61, 294, 295]. Results for branching ratios obtained with an alternative code, `CPsuperH` [131], can differ quantitatively to some extent from the results shown here. A main difference between the two codes is the more complete inclusion of real two-loop

Table 3.6: Expected experimental precision of the branching ratio measurement of $h \to X$ at the LHC, the ILC operating at $\sqrt{s} = 500, 1000$ GeV, and the γC (based on the CLICHE design [297]). "—" means that no analysis exists or that the channel is not accessible.

Study	M_h	$b\bar{b}$	WW^*	$\tau^+\tau^-$	$c\bar{c}$	gg	$\gamma\gamma$
LHC [216,217]	120 GeV	$\sim 20\%$	$\sim 10\%$	$\sim 15\%$	—	—	—
ILC ($\sqrt{s} = 500$ GeV) [220,298]	120 GeV	1.5%	3%	4.5%	6%	4%	19%
ILC ($\sqrt{s} = 1000$ GeV) [220,299]	120 GeV	1.5%	2%	—	—	2.3%	5.4%
γC [297,300]	115 GeV	2%	5%	—	—	—	22%

corrections in `FeynHiggs2.2`, resulting in somewhat higher values for the lightest Higgs boson mass. While the complex phase dependence at the one-loop level is included completely in `FeynHiggs2.2`, at the two-loop level it is more complete in `CPsuperH`, which makes it difficult to disentangle the source of possible deviations. A more complete discussion can be found in [296].

3.10.1.1 The CPX scenario

We start our analysis by the investigation of the CPX scenario, see Eq. (3.76). We first show the results for the γC in Fig. 3.40 for the decay channel $h \to b\bar{b}$, which has the best sensitivity at this collider. The variation of $\Gamma_{\gamma\gamma} \times \text{BR}(h \to b\bar{b})$ is shown in the $\Phi_{A_{t,b}}$–$\tan\beta$ plane. The strips correspond to constant values of the lightest Higgs mass, while the color code shows the deviation from the corresponding SM value. It should be kept in mind that the Higgs boson mass will be measured to very high accuracy so that one will be confined to one of the strips. We are neglecting the parametric errors from the imperfect knowledge of the input parameters. In reality these parametric errors would widen the strips. The future intrinsic error of ~ 0.5 GeV [47], however, is included in the width of the strips. One can see that this channel can be strongly enhanced as compared to the SM. The variation along each strip is much larger than the anticipated precision of $\sim 2\%$ for this channel. This would allow to constrain the values of the complex phases. The picture becomes of course more complicated if the complex phases are varied independently. Various channels will have to be combined to disentangle the different effects.

Results for the LHC are shown in Fig. 3.41. The left plots gives the results for the channel $gg \to h \to \gamma\gamma$, while the right plots depicts $WW \to h \to \tau^+\tau^-$. The latter channel (like $h \to b\bar{b}$) is usually somewhat enhanced in the MSSM, the BR$(h \to WW^*)$ (not shown) and BR$(h \to \gamma\gamma)$ (see the left plot of Fig. 3.41) are normally suppressed in this scenario. The precision of the LHC will not be good enough to obtain information about complex phases in this way.

Finally in Fig. 3.42 shows the ILC results in the CPX scenario. The left plot shows the BR$(h \to b\bar{b})$, while the right plot depicts BR$(h \to \tau^+\tau^-)$. Both channels are enhances as compared to the SM in this scenario. The high precision of the ILC (see Table 3.6) shows that this collider has a good potential to disentangle the complex phases.

Since in the examples shown here for the γC and the ILC the largest deviations occur for different regions of the parameter space, the results from both colliders could be combined in order to extract the maximum information on $\Phi_{A_{t,b}}$.

3.10.1.2 The BGX scenario

Now we turn to the investigation of the baryogenesis motivated BGX scenario, see Eq. (3.77). The effects in this scenario are expected to be smaller than in the CPX scenario that had been designed to give maximum effects of the complex phases.

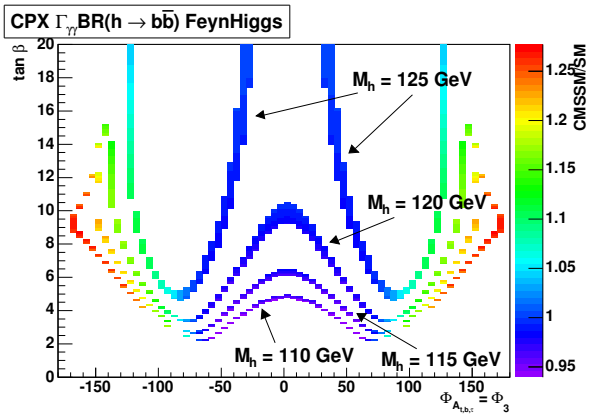

Fig. 3.40: The deviations of $\Gamma_{\gamma\gamma} \times \mathrm{BR}(h \to b\bar{b})$ within the CPX scenario from the SM value is shown in the $\Phi_{A_{t,b}}$–$\tan\beta$ plane. The corresponding precision obtainable at a γC is $\sim 2\%$.

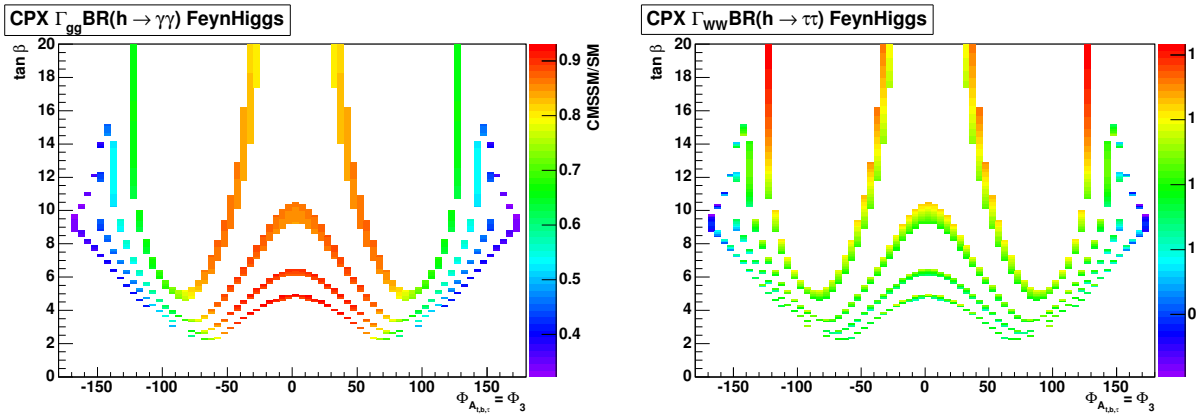

Fig. 3.41: The deviations of $\Gamma_{gg} \times \mathrm{BR}(h \to \gamma\gamma)$ (left) and of $\Gamma_{WW} \times \mathrm{BR}(h \to \tau^+\tau^-)$ (right) within the CPX scenario from the SM value is shown in the $\Phi_{A_{t,b}}$–$\tan\beta$ plane. The corresponding experimental precision can be found in Table 3.6.

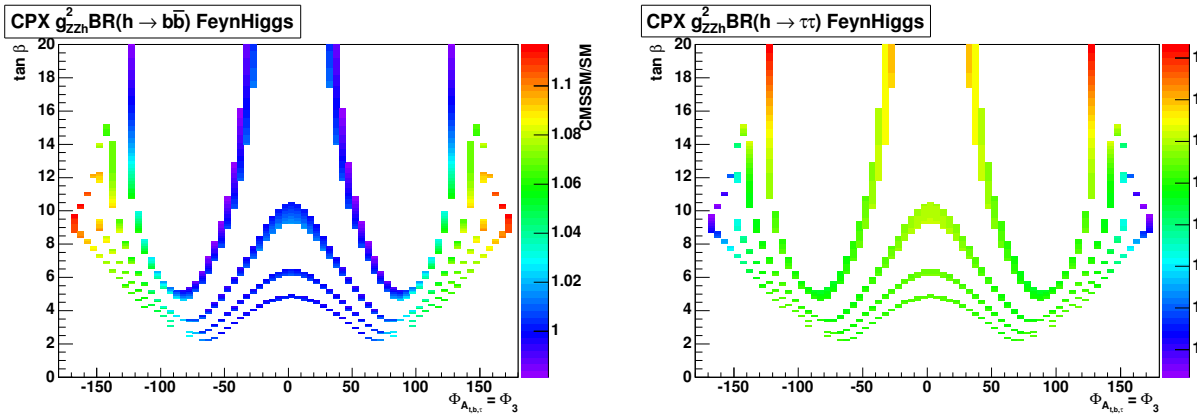

Fig. 3.42: The deviations of $g^2_{ZZh} \times \mathrm{BR}(h \to b\bar{b})$ (left) and of $g^2_{ZZh} \times \mathrm{BR}(h \to \tau^+\tau^-)$ (right) within the CPX scenario from the SM value is shown in the $\Phi_{A_{t,b}}$–$\tan\beta$ plane. The corresponding experimental precision can be found in Table 3.6.

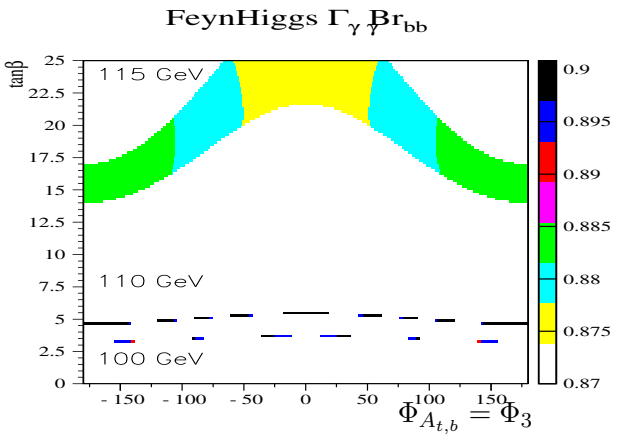

Fig. 3.43: The deviations of $\Gamma_{\gamma\gamma} \times \mathrm{BR}(h \to b\bar{b})$ within the BGX scenario from the SM value is shown in the $\Phi_{A_{t,b}}$–$\tan\beta$ plane. The corresponding precision obtainable at a γC is $\sim 2\%$.

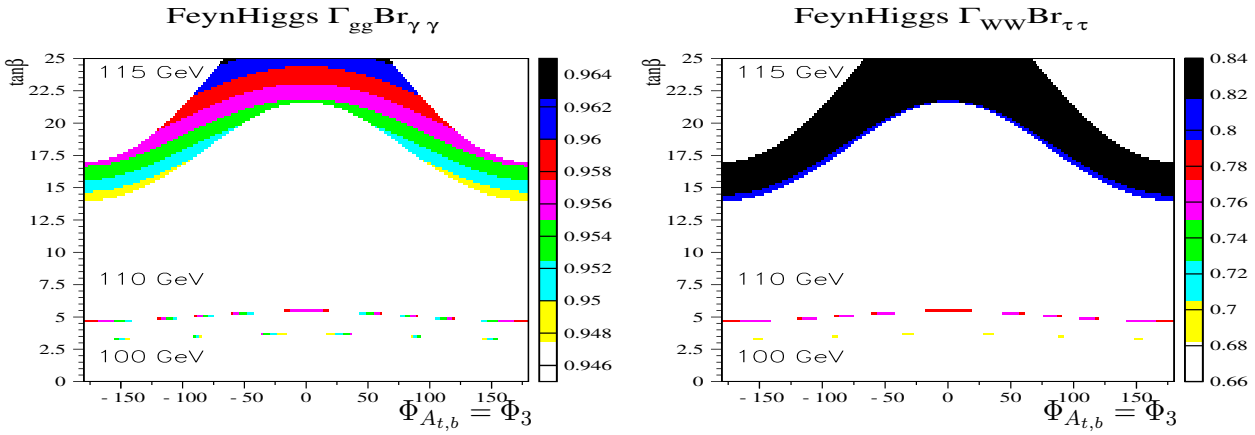

Fig. 3.44: The deviations of $\Gamma_{gg} \times \mathrm{BR}(h \to \gamma\gamma)$ (left) and of $\Gamma_{WW} \times \mathrm{BR}(h \to \tau^+\tau^-)$ (right) within the BGX scenario from the SM value is shown in the $\Phi_{A_{t,b}}$–$\tan\beta$ plane. The corresponding experimental precision can be found in Table 3.6.

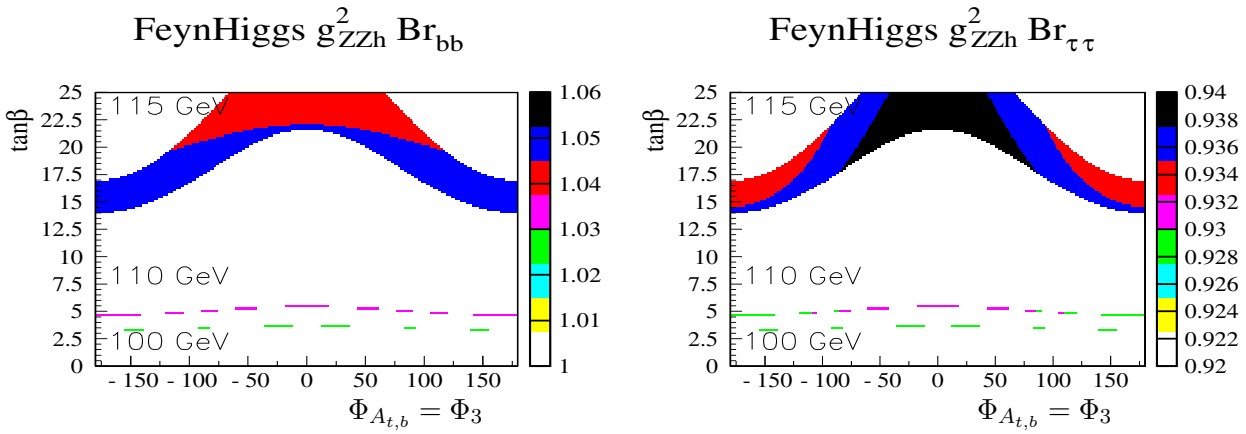

Fig. 3.45: The deviations of $g^2_{ZZh} \times \mathrm{BR}(h \to b\bar{b})$ (left) and of $g^2_{ZZh} \times \mathrm{BR}(h \to \tau^+\tau^-)$ (right) within the BGX scenario from the SM value is shown in the $\Phi_{A_{t,b}}$–$\tan\beta$ plane. The corresponding experimental precision can be found in Table 3.6.

In Fig. 3.43 we show the $h \to b\bar{b}$ channel at the γC. A substantial suppression with respect to the SM can be observed. However, the variation of $\Gamma_{\gamma\gamma} \times \mathrm{BR}(h \to b\bar{b})$ for fixed Higgs boson mass (which will be known with high precision) with the complex phase $\Phi_{A_{t,b}}$ is very small. Thus a precise measurement of this channel at the γC will not reveal any information about the complex phases entering the MSSM Higgs sector.

The two LHC channels in the BGX scenario are shown in Fig. 3.44, while the two ILC channels are given in Fig. 3.45. As for the CPX scenario no phase determination can be expected from he LHC measurements. The situation at the ILC in the BGX scenario is similar to the γC. A deviation from the SM value can be measured, but the variation of $g^2_{ZZh} \times \mathrm{BR}(h \to b\bar{b}, \tau^+\tau^-)$ is too small to reveal any information on $\Phi_{A_{t,b}}$.

3.10.2 Conclusions

We have compared the LHC, the ILC and the γC in view of their power to determine the complex phases of the CP-violating MSSM. We have focused on the Higgs sector, where the complex phases enter via radiative corrections. Especially we have investigated the most promising combinations of Higgs production and decay ($\sigma \times$ BR) for each collider.

The analysis has been performed in two scenarios: The CPX scenario designed to maximize the effect of complex phases in the MSSM Higgs sector. The other scenario (BGX) is based on a part of the CP-violating MSSM that is motivated by baryogenesis.

The CPX scenario may offer good prospects for the γC and the ILC to determine $\Phi_{A_{t,b}}$ via Higgs branching ratio measurements. On the other hand, the BGX scenario will only show a deviation from the SM. The variation of the analyzed channels is too small to give information on the complex phases.

It should be kept in mind that we have neglected the future parametric errors on the SUSY parameters (see e.g. Ref. [224] and references therein). These uncertainties will further widen the bands shown in Figs. 3.40–3.45.

3.11 Probing CP-violating Higgs contributions in $\gamma\gamma \to f\bar{f}$

Rohini M. Godbole, Sabine Kraml, Saurabh D. Rindani and Ritesh K. Singh

At a photon collider, fermion-pair production proceeds through the QED diagrams of Figs. 3.46(a,b) as well as through s-channel Higgs mediation, Fig. 3.46(c). Here ϕ denotes a generic Higgs boson which may or may not be a CP eigenstate; in the MSSM with CP phases we have of course $\phi = H_{1,2,3}$. The QED vertex $\gamma f \bar{f}$ conserves chirality, whereas the $\phi f \bar{f}$ coupling mixes different chiralities. In the absence of the Higgs contribution, the fermion mass m_f is the only source of chirality-mixing. With unpolarized photons in the initial state, the QED contribution leads to unpolarized fermions in the final state. The same is true for the Higgs exchange should the Higgs boson(s) be a CP eigenstate; CP violation (CPV) in the Higgs sector leads to a net, though very small, polarization of the fermions. With polarized initial-state photons, the QED contribution alone gives rise to a finite polarization. The additional chirality-mixing contribution from the Higgs boson exchange diagram causes a change in this polarization in both the CP-conserving and the CP-violating case. It is thus possible to construct observables involving the polarizations of the initial-state photons and those of the final-state fermions (τ/t), which can probe the Higgs boson couplings, including possible CP violation in the Higgs sector.

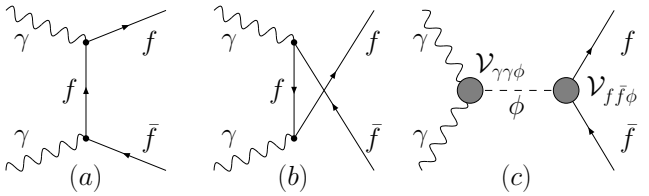

Fig. 3.46: Feynman diagrams contributing to $\gamma\gamma \to f\bar{f}$ production.

Table 3.7: Combinations of form factors that occur in the helicity amplitudes of Eqs. (3.78) and (3.79).

Combination	Alias	CP	Combination	Alias	CP
$s_f \,\mathrm{Re}\, e(S_\gamma)$	x_1	even	$s_f \,\mathrm{Im}\, m(S_\gamma)$	x_2	even
$s_f \,\mathrm{Re}\, e(P_\gamma)$	y_1	odd	$s_f \,\mathrm{Im}\, m(P_\gamma)$	y_2	odd
$p_f \,\mathrm{Re}\, e(S_\gamma)$	y_3	odd	$p_f \,\mathrm{Im}\, m(S_\gamma)$	y_4	odd
$p_f \,\mathrm{Re}\, e(P_\gamma)$	x_3	even	$p_f \,\mathrm{Im}\, m(P_\gamma)$	x_4	even

3.11.1 Helicity amplitudes

The helicity amplitudes for the fermion-pair production in the t/u- and s-channels are [90, 91]

$$M_{QED}(\lambda_1,\lambda_2;\lambda_f,\lambda_{\bar{f}}) = \frac{-i4\pi\alpha Q^2}{1-\beta^2\cos^2\theta_f}\left[\frac{4m_f}{\sqrt{s}}\,(\lambda_1+\lambda_f\beta)\,\delta_{\lambda_1,\lambda_2}\delta_{\lambda_f,\lambda_{\bar{f}}}\right.$$
$$\left. -\,\frac{4m_f}{\sqrt{s}}\,\lambda_f\beta\sin^2\theta_f\,\delta_{\lambda_1,-\lambda_2}\delta_{\lambda_f,\lambda_{\bar{f}}} - 2\beta\,(\cos\theta_f+\lambda_1\lambda_f)\sin\theta_f\,\delta_{\lambda_1,-\lambda_2}\delta_{\lambda_f,-\lambda_{\bar{f}}}\right], \quad (3.78)$$

$$M_\phi(\lambda_1,\lambda_2;\lambda_f,\lambda_{\bar{f}}) = \frac{-ie\alpha m_f}{4\pi M_W}\,\frac{s}{s-m_\phi^2+iM_\phi\Gamma_\phi}$$
$$\times\,[S_\gamma(s)+i\lambda_1 P_\gamma(s)]\;[\lambda_f\beta s_f - ip_f]\;\delta_{\lambda_1,\lambda_2}\delta_{\lambda_f,\lambda_{\bar{f}}}\,, \quad (3.79)$$

respectively. Here, $\lambda_{1,2}$ are the helicities of the incoming photons and $\lambda_{f,\bar{f}}$ those of the produced fermions; $\beta = \sqrt{1-4m_f^2/s}$ and θ_f is the scattering angle. The form factors S_γ and P_γ are complex, whereas s_f and p_f may be taken to be real without loss of generality. In fact, only some specific combinations of these form factors occur as listed in Table 3.7. Only five of these eight combinations are independent, the other three can be obtained by inter-relations such as $x_1x_3 = y_1y_3$, etc. Simultaneous existence of s_f and p_f, or S_γ and P_γ, signifies CP violation and leads to non-vanishing values of y_i $(i = 1, ..., 4)$. Even if no CPV is present, so that only the x_i's are nonzero, the Higgs-boson contribution still alters the polarization of the fermions f from that predicted by pure QED. CP violation, giving rise to nonzero y_i's, gives an additional contribution to this fermion polarization.

3.11.2 Fermion polarization

The fermion polarization is defined as the fractional surplus of positive helicity fermions over negative helicity ones,

$$P_f^{ij} = \frac{N_+^{ij} - N_-^{ij}}{N_+^{ij} + N_-^{ij}}\,, \quad (3.80)$$

where the superscript ij stands for the polarizations of the parent e^+e^- beams $(P_e,\ P_{\bar{e}})$ of the ILC. N_+ and N_- stand for the number of fermions with positive and negative helicities, respectively. The

Table 3.8: Polarization observables, interactions and the form-factor combinations that they can probe.

Observable	Type of interaction	Combinations probed
P_f^U	P/CP violating	y_i's
$\delta P_f^+ = P_f^{++} - (P_f^{++})^{QED}$	chirality mixing	x_i's, y_i's
$\delta P_f^- = P_f^{--} - (P_f^{--})^{QED}$	chirality mixing	x_i's, y_i's
$\delta P_f^{CP} = P_f^{++} + P_f^{--}$	P/CP violating	y_i's

polarization of anti-fermions, $\bar{P}_f^{ij}$, is defined analogously; conservation of linear and angular momenta implies $P_f^{ij} = \bar{P}_f^{ij}$.

From Eqs. (3.79) and (3.78) we see that the chirality mixing amplitudes, containing $\delta_{\lambda_f,\lambda_{\bar{f}}}$, are proportional to the fermion mass m_f. Hence these are small for light fermions. Further, the Higgs-exchange diagram contributes only when the helicities of the colliding photons are equal; at the same time the QED contribution can be suppressed by choosing $\lambda_1 = \lambda_2$. For the case of the polarized, peaked photon spectrum [83] this amounts to choosing $(P_e,\ P_{\bar{e}}) = (\pm, \pm)$ for the parent e^+/e^- beams.

The final state fermion polarization with unpolarized initial state, P_f^U, is zero should the Higgs boson have a definite CP quantum number. Nonzero values of P_f^U only arise for $y_i \neq 0$, thus being a signal of CP violation in the Higgs sector. For polarized initial states, the final-state fermion polarization is always nonzero. Regardless whether CP is violated or not, any deviation of P_f^{++} and P_f^{--} from their QED predictions probes the Higgs boson contribution. Moreover, since P-invariance implies $P_f^{++} = -P_f^{--}$ for the QED contribution, $P_f^{++} + P_f^{--} \neq 0$ is a signal of CP violation. The polarization observables are summarized in Table 3.8. Here note that $\delta P_f^{CP} = \delta P_f^+ + \delta P_f^-$. In the following, we choose δP_f^- and δP_f^{CP} as the independent observables.

In order to test the relevance of our polarization observables, we perform a numerical analysis for $\gamma\gamma \to \tau^+\tau^-$ and $\gamma\gamma \to t\bar{t}$ in the CPX scenario, Eq. (3.13). We vary $M_{H^\pm} = 150$–500 GeV and $\tan\beta = 3$–40 and consider different phases Φ_A, keeping $\Phi_3 = 90^\circ$ fixed. The Higgs boson masses, couplings and widths are computed with both `CPsuperH` [131] and `FeynHiggs` [59]. For the polarized photon beams, we use the ideal Compton-backscattered photon spectrum of [83]. The beam energy E_b for the parent e^+e^- collider is chosen such that the peak in the spectrum of the $\gamma\gamma$ invariant mass corresponds to the relevant Higgs boson mass(es). This choice explores the ultimate potential of the polarization observables; we call it the "peak E_B" choice. In general, $P_f^U \neq 0$ would be a clear signal of CPV. However, P_f^U is found to be very small, well below experimental sensitivity. So we have to work with polarized beams and consider δP_f^- and δP_f^{CP}.

Let us start with $f = \tau$. Due to the small τ mass, the contribution to the τ polarization from the Higgs boson exchange diagram is very small unless one puts a cut on the $\tau^+\tau^-$ invariant mass. We use a cut $|m_{\tau\tau} - M_{H_1}| \leq \max(dE_m,\ 5\ \Gamma_{H_1})$ with $dE_m = 1$ GeV. In Fig. 3.47 we show δP_τ^- for both `CPsuperH` and `FeynHiggs` for zero and maximal phase Φ_A. The $e^\pm$ beam energy is chosen such that $\sqrt{s}_{\gamma\gamma}$ at the peak of the photon spectrum is equal to the mass of the lightest Higgs boson H_1. The deviation in the polarization due to the H_1 exchange is large for both $\Phi_A = 0$ and 90°. δP_τ^- increases with $\tan\beta$ because the τ Yukawa coupling increases. However, it turns out that $\delta P_\tau^+ \simeq -\delta P_\tau^-$, so that $\delta P_\tau^{CP} \simeq 0$ over all the $\tan\beta$–$M_{H^\pm}$ plane. The difference between `CPsuperH` and `FeynHiggs` in Fig. 3.47 can be traced to somewhat different predictions of the masses, couplings and decay widths as a result of the different approximations used in the two programs.

In the case of $t\bar{t}$ production, it is the heavier Higgs bosons $H_{2,3}$ which contribute. Since the masses of $H_{2,3}$ are in general close to each other, we choose the beam energy such that the mean value $(M_{H_2} + M_{H_3})/2$ matches with $\sqrt{s}_{\gamma\gamma}$ at the peak of the photon spectrum. We find that the top polarization

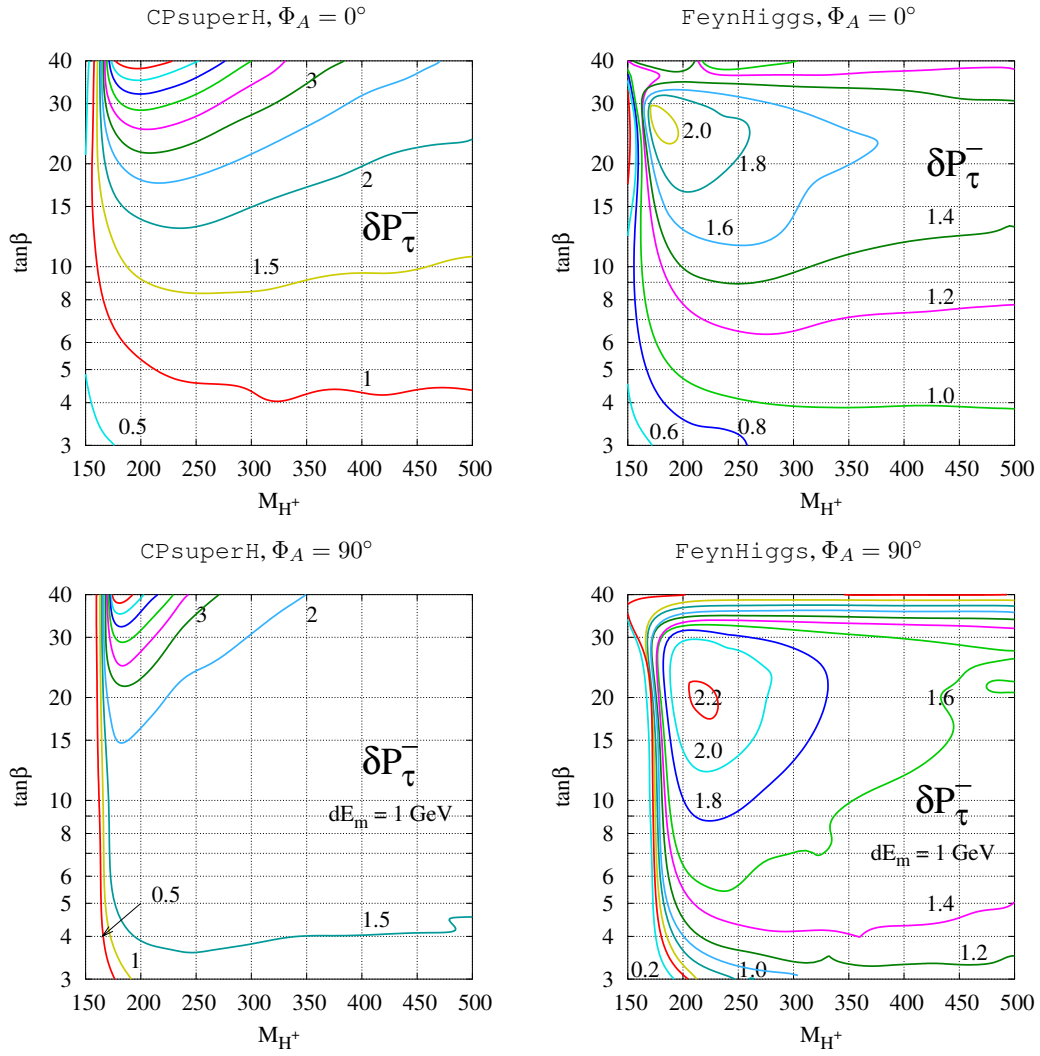

Fig. 3.47: Contours of constant δP_τ^- in units of 10^{-2} in the $(\tan\beta$–$M_{H^\pm})$ plane for the CPX scenario with $\Phi_A = 0°$ (top panel) and $\Phi_A = 90°$ (bottom panel) with $dE_m = 1$ GeV. The left panels show the results obtained with CPsuperH, the rights panels those obtained with FeynHiggs.

is sensitive not only to the Higgs contribution in general ($\delta P_t^\pm$) but also to CP violation (δP_t^{CP}). In Fig. 3.48 we show contours of constant δP_t^{CP} in the $\tan\beta$–$M_{H^\pm}$ plane for $\Phi_A = 90°$. Of course one needs $M_{H^\pm} \geq 2m_t$. Since the top Yukawa coupling decreases with $\tan\beta$, δP_t^{CP} is only sizable for small values of $\tan\beta$. Note that due to the large top-quark mass, no cut on the $t\bar{t}$ invariant mass is needed to increase the sensitivity. The difference in the sign of δP_t^{CP} in the two panels in Fig. 3.48 is due to different conventions in CPsuperH and FeynHiggs leading to the opposite signs of y_i, $i = 1...4$, for the same input MSSM parameters.

3.11.3 Leptonic asymmetries

The polarization of τ leptons can be measured using the energy distribution of the decay pions [301–305]. The polarization of top quarks can be measured using energy distribution of b quarks [306] or the angular distribution of decay leptons [307–309]. This kind of analysis requires the full reconstruction of the top momentum. Such a reconstruction may not always be possible for the semi-leptonic decay of the t (or $\bar{t}$) quark. On the other hand, it is possible to construct simple asymmetries involving the polarization of

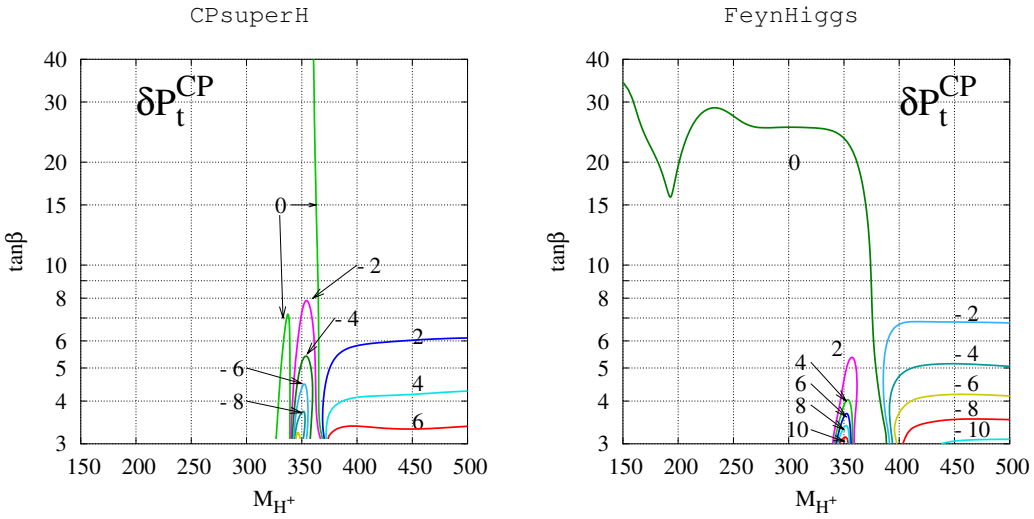

Fig. 3.48: Contours of constant δP_t^{CP} in units of 10^{-2} in the $(\tan\beta$–$M_{H^\pm})$ plane for the CPX scenario with $\Phi_A = 90°$. The left panel shows the results obtained with `CPsuperH`, the right panel obtained with `FeynHiggs`.

the initial-state $e^\pm$ (and hence of the photons) and the charge of the final-state lepton, which are sensitive to CP violation. We denote the integrated cross-section for the process $\gamma\gamma \to t\bar{t} \to l^+\nu b\bar{t}$ $(tl^-\bar{\nu}\bar{b})$ by $\sigma(\lambda_{e^-}, Q_l)$, where λ_{e^-} is the polarization of the electron beam in the parent collider and Q_l the charge of the secondary lepton coming from the $t/(\bar{t})$ decay. The polarizations of all the other beams are adjusted to get a peaked spectrum and equal helicities for the incident photons. With this setup, we can define the following asymmetries [91]:

$$\mathcal{A}_1 = \frac{\sigma(+,+) - \sigma(-,-)}{\sigma(+,+) + \sigma(-,-)}\,, \qquad \mathcal{A}_2 = \frac{\sigma(+,-) - \sigma(-,+)}{\sigma(+,-) + \sigma(-,+)}\,,$$
$$\mathcal{A}_3 = \frac{\sigma(+,+) - \sigma(-,+)}{\sigma(+,+) + \sigma(-,+)}\,, \qquad \mathcal{A}_4 = \frac{\sigma(+,-) - \sigma(-,-)}{\sigma(+,-) + \sigma(-,-)}\,. \tag{3.81}$$

Only one of the above asymmetries is independent [91] if no cut is put on the lepton's polar angle in the laboratory frame. Even with a finite cut on the polar angle, the $\mathcal{A}_{1\ldots4}$ have almost identical sensitivities to the Higgs couplings. We use a 20° beam-pipe cut on the lepton. Figure 3.49 shows contours of constant $\mathcal{A}_3$ for $\Phi_A = 30°$ and 90°, as obtained with `CPsuperH`. The asymmetry is large for large values of Φ_A and decreases rapidly as Φ_A decreases. Hence $\mathcal{A}_i$ can probe large regions in the $\tan\beta - M_{H^+}$ plane should Φ_A be large.

Last but not least we note that, as shown in [91], the lepton asymmetries of Eq. (3.81) are sensitive only to the CP-odd combinations of the form factors, i.e. to the y_i's. This should be contrasted with the polarization observables $\delta P_f^\pm$, which are sensitive to both the CP-odd and CP-even combinations.

3.11.4 Summary

In summary, the polarization of heavy fermions is a good probe of the coupling of the Higgs boson including CP-violation. We have analyzed this in the MSSM with CPV in the CPX scenario . We find that the polarization of τ-leptons may be used to probe the couplings of the lightest Higgs boson, especially in the large $\tan\beta$ region. The t-quark polarization, which is sensitive to the contribution of the two heavier Higgs bosons, can be used in the low $\tan\beta$ and large $M_{H^\pm}$ region of the MSSM parameter space. The leptonic asymmetries constructed using the secondary $t/\bar{t}$ decay leptons, which involve only a simple number counting experiment, can probe CPV contributions in $\gamma\gamma \to t\bar{t}$.

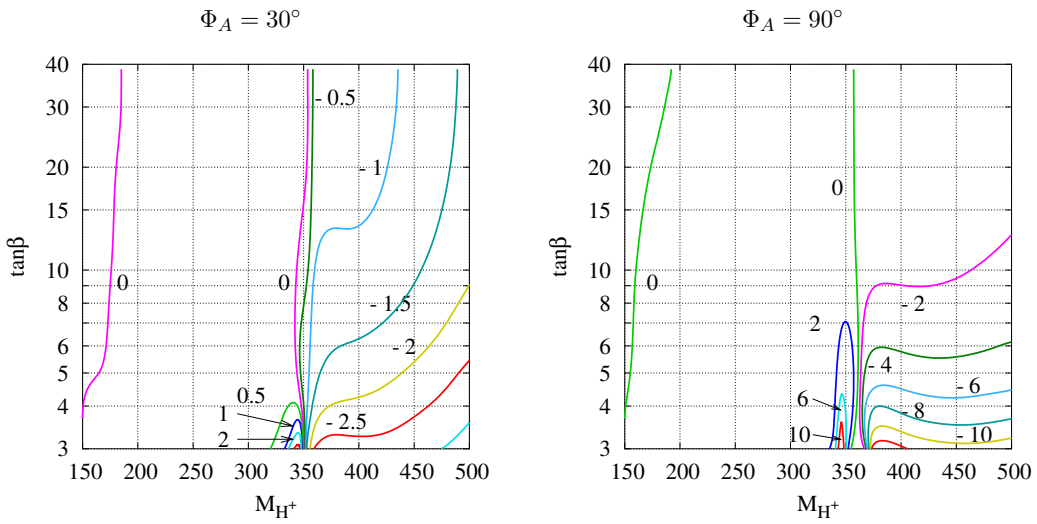

Fig. 3.49: Contours of constant $\mathcal{A}_3$ for $\Phi_A = 30°$ and $90°$; computed with `CPsuperH`.

3.12 Resonant H and A mixing in the CP-noninvariant MSSM

Seong Youl Choi, Jan Kalinowski, Yi Liao and Peter M. Zerwas

In CP-noninvariant extensions of the MSSM the three neutral Higgs boson states mix to form a triplet with both even and odd components in the wave–functions under CP transformations [48–53,78,159,181, 310]. The mixing can become very large if the states are nearly mass–degenerate [159]. This situation is naturally realized for supersymmetric theories in the decoupling limit [107] in which two of the neutral states are heavy.

In the present section we describe a simple quantum mechanical (QM) formalism for the CP-violating resonant H/A mixing in the decoupling limit. Subsequently we discuss some experimental signatures of CP-violating mixing in Higgs production and decay processes at a photon collider with polarized photon beams [178].

3.12.1 Mixing formalism

The self–interaction of two Higgs doublets in a CP-noninvariant theory is described by the potential given in Eq. (2.1), where the coefficients are in general all non–zero and $m_{12}^2, \lambda_{5,6,7}$ can be complex. The complex $Y = 1$, SU(2)$_L$ iso–doublet fields can be rotated by an angle β [where $\tan\beta = v_2/v_1$ is the ratio of the vev's of the original neutral fields] to a new basis in which only one doublet field acquires a non–zero vev. The real matrix $\mathcal{M}_0^2$ of the three neutral physical Higgs fields in this basis, H_a, H_b and A, can be written in the form

$$\mathcal{M}_0^2 = v^2 \begin{pmatrix} \lambda & -\hat{\lambda} & -\hat{\lambda}_p \\ -\hat{\lambda} & \lambda - \lambda_A + M_A^2/v^2 & -\lambda_p \\ -\hat{\lambda}_p & -\lambda_p & M_A^2/v^2 \end{pmatrix} \tag{3.82}$$

The mass matrix is hermitian and symmetric by CPT invariance. The parameters λ, $\hat{\lambda}$ and λ_A are combinations of the real parts of the coefficients of bilinear and quartic terms in the Higgs potential, while λ_p and $\hat{\lambda}_p$ are given by the imaginary parts of the coefficients; their explicit form can be found in Ref. [159]. The *auxiliary* parameter M_A^2 is also a derivative of the real parts of bilinear and quartic coefficients in the Higgs potential; it plays a crucial rôle in characterizing the mass scale of the Higgs system.

In a CP-invariant theory all quartic couplings in the Higgs potential are real and the off–diagonal elements $\lambda_p, \hat{\lambda}_p$ vanish. Thus the neutral mass matrix breaks into the CP-even 2×2 part, and the [stand–alone] CP-odd part. The 2×2 part gives rise to two CP-even neutral mass eigenstates h and H, while M_A is identified as the mass of the CP-odd Higgs boson A. In the CP-violating case, however, all three states mix leading to $H_{1,2,3}$ mass eigenstates with no definite CP parities.

For small mass differences, the mixing of the states is strongly affected by their widths. This is a well–known phenomenon for resonant mixing [311] and has also been recognized for the Higgs sector [96, 157, 312–314]. The hermitian mass matrix (3.82) has therefore to be supplemented by the anti–hermitian part $-iM\Gamma$ incorporating the decay matrix [315]

$$\mathcal{M}^2 = \mathcal{M}_0^2 - iM\Gamma \tag{3.83}$$

This matrix includes the widths of the Higgs states in the diagonal elements as well as the transition elements within any combination of pairs. Following from the uncertainty principle, they are particularly important in the case of nearly mass–degenerate states. All these elements $M\Gamma$ are built by loops of virtual particles in the self–energy matrix of the Higgs fields.

In general, the light Higgs boson, the fermions and electroweak gauge bosons, and in supersymmetric theories, gauginos, higgsinos and scalar states may contribute to the loops in the propagator matrix. In the physically interesting case of decoupling, the mixing structure simplifies considerably, allowing a simple and transparent analysis [159]. Alternatively a full coupled–channel analysis may be applied [76, 93, 153, 158].

3.12.1.1 Decoupling limit

The decoupling limit [107] is defined by the inequality $M_A^2 \gg |\lambda_i|\, v^2$ with the quartic couplings in the Higgs potential $|\lambda_i| \lesssim O(1)$. In this limit the H_a state becomes the CP-even light Higgs boson h and decouples from $H = H_b$ and A. The heavy states H and A are nearly mass degenerate, which turns out to be crucial for large mixing effects between H and A. It is therefore sufficient to consider the lower–right 2×2 submatrix of the matrix (3.82) for the heavy H/A states which we write as follows

$$\mathcal{M}_{HA}^2 = \begin{pmatrix} M_H^2 - iM_H\Gamma_H & \Delta_{HA}^2 \\ \Delta_{HA}^2 & M_A^2 - iM_A\Gamma_A \end{pmatrix} \tag{3.84}$$

The mixing element Δ_{HA}^2 includes a real dissipative part and an imaginary absorptive part. The couplings of the heavy Higgs bosons to gauge bosons and their supersymmetric partners are suppressed. In the case in which all supersymmetric particle contributions are suppressed either by couplings or by phase space in $M\Gamma$, it is sufficient to consider only loops built by the light Higgs boson and the top quark; the explicit form of the light Higgs and top contributions to the matrix $M\Gamma$ is presented in Ref. [159]. The loops also contribute to the real part of the mass matrix, either renormalizing the λ parameters of the Higgs potential or generating such parameters if not present yet at the tree level.

3.12.1.2 Physical masses and states

The symmetric complex mass–squared matrix $\mathcal{M}_{HA}^2$ in Eq. (3.84) can be diagonalized [10] through a *complex rotation*

$$\mathcal{M}_{H_iH_j}^2 = \begin{pmatrix} M_{H_2}^2 - iM_{H_2}\Gamma_{H_2} & 0 \\ 0 & M_{H_3}^2 - iM_{H_3}\Gamma_{H_3} \end{pmatrix} = C\mathcal{M}_{HA}^2 C^{-1} \tag{3.85}$$

[10] The states H_2 and H_3 are in general not ordered in ascending mass values. Thus, if $M_{H_2} > M_{H_3}$ the indices may be interchanged *ad hoc* to comply with the convention in the Introduction.

where the mixing matrix and the mixing angle are given by

$$C = \begin{pmatrix} \cos\theta & \sin\theta \\ -\sin\theta & \cos\theta \end{pmatrix}, \qquad X = \frac{1}{2}\tan 2\theta = \frac{\Delta^2_{HA}}{M^2_H - M^2_A - i\,[M_H\Gamma_H - M_A\Gamma_A]} \tag{3.86}$$

A non–vanishing (complex) mixing parameter $X \neq 0$ requires CP-violating transitions between H and A either in the real mass matrix, $\lambda_p \neq 0$, or in the decay mass matrix, $(M\Gamma)_{HA} \neq 0$, [or both]. However, even for nearly degenerate masses, the mixing could be suppressed if the widths are significantly different. As a result, the mixing phenomena are strongly affected by the form of the decay matrix $M\Gamma$. Since the difference of the widths enters through the denominator in X, the modulus $|X|$ becomes large for small mass differences and small widths.[11]

The mixing shifts the Higgs masses and widths in a characteristic pattern [311]. The two complex mass values after and before diagonalization are related by the complex mixing angle θ:

$$M^2_{H_3} - M^2_{H_2} - i\,(M_{H_3}\Gamma_{H_3} - M_{H_2}\Gamma_{H_2}) = \left[M^2_A - M^2_H - i(M_A\Gamma_A - M_H\Gamma_H)\right] \times \sqrt{1+4X^2} \tag{3.87}$$

Since the eigenstates of the complex, non–hermitian matrix $\mathcal{M}^2_{HA}$ are no longer orthogonal, the ket and bra mass eigenstates have to be defined separately: $|H_i\rangle = C_{i\alpha}|H_\alpha\rangle$ and $\langle\widetilde{H}_i| = C_{i\alpha}\langle H_\alpha|$ ($i = 2,3$ and $H_\alpha = H, A$). The final state F in heavy Higgs formation from the initial state I is described by the amplitude

$$\langle F|H|I\rangle = \sum_{i=2,3} \langle F|H_i\rangle \frac{1}{s - M^2_{H_i} + iM_{H_i}\Gamma_{H_i}} \langle\widetilde{H}_i|I\rangle \tag{3.88}$$

where the sum runs only over diagonal transitions in the mass–eigenstate basis.

3.12.2 Experimental signatures

To illustrate the general QM results in a realistic example, we adopt a specific MSSM scenario with the source of CP-violation localized in the complex trilinear coupling A_t of the soft supersymmetry breaking part involving the stop.[12] All other interactions are assumed to be CP-conserving. For complex A_t the stop–loop corrections induce CP-violation in the effective Higgs potential. The effective λ_i parameters have been calculated in Ref. [50] to two–loop accuracy; to illustrate the crucial points we focus on the dominant one–loop $t/\tilde{t}$ contributions.

More specifically, we take a typical set of parameters from Ref. [131],

$$M_{\rm SUSY} = 0.5\ {\rm TeV}, \quad |A_t| = 1.0\ {\rm TeV}, \quad \mu = 1.0\ {\rm TeV}; \quad \tan\beta = 5 \tag{3.89}$$

and change the phase Φ_A of the trilinear parameter A_t. With $\Phi_A = 0$ we find the following values of the light and heavy Higgs masses and decay widths, and the stop masses:

$$M_h = 129.6\,{\rm GeV},\ M_H = 500.3\,{\rm GeV},\ M_A = 500.0\,{\rm GeV}$$
$$\Gamma_H = 1.2\,{\rm GeV},\ \Gamma_A = 1.5\,{\rm GeV};\ m_{\tilde{t}_{1/2}} = 372/647\,{\rm GeV}$$

Clearly, with the mass splitting of 0.3 GeV, the heavy Higgs states are not distinguishable. When the phase Φ_A is turned on,[13] the CP composition, the masses and the decay widths of heavy states are

[11] Though H, A masses and widths are very close in the decoupling regime of supersymmetric models, they are not expected to be exactly identical if artificially large fine–tuning of unrelated parameters is disregarded; for comments see Ref. [157].

[12] This assignment is compatible with the bounds on CP-violating SUSY phases from experiments on electric dipole moments [232, 316–321].

[13] With one phase Φ_A, the complex mixing parameter X obeys the relation $X(2\pi - \Phi_A) = X^*(\Phi_A)$, implying all CP-even quantities to be symmetric and all CP-odd quantities to be anti–symmetric about π.

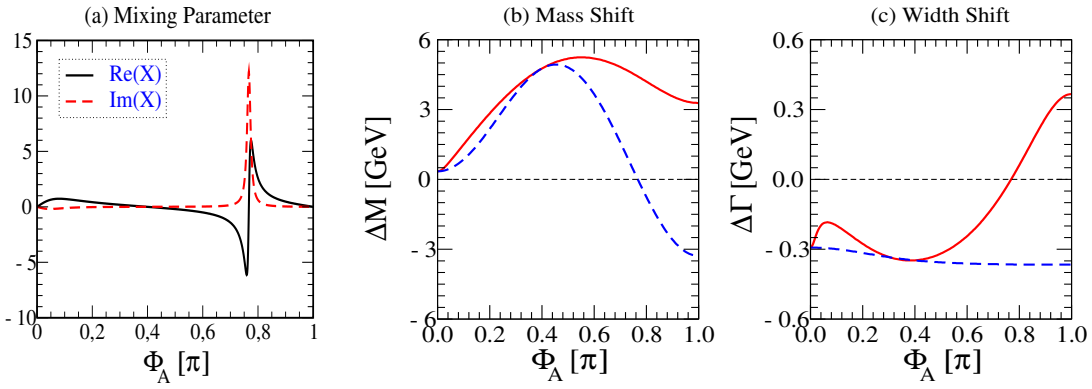

Fig. 3.50: The Φ_A dependence of (a) the mixing parameter X and of the shifts of (b) masses and (c) widths with the phase Φ_A evolving from 0 to π for $\tan\beta = 5$, $M_A = 0.5$ TeV and couplings as specified in the text; in (b,c) the mass and width differences without mixing are shown by the broken lines. $\mathrm{Re\,e}/\,\mathrm{Im\,m}X(2\pi - \Phi_A) = +\,\mathrm{Re\,e}/-\,\mathrm{Im\,m}X(\Phi_A)$ for angles above π.

strongly affected, as shown in Figs. 3.50(a), (b) and (c), while the mass of the light Higgs boson h is not. The heavy two–state system shows a very sharp resonant CP-violating mixing, purely imaginary a little above $\Phi_A = 3\pi/4$, Fig. 3.50(a). The mass shift $\Delta M = M_{H_2} - M_{H_3}$ is enhanced by more than an order of magnitude if the CP-violating phase rises to non–zero values[14], reaching a maximal value of ~ 5.3 GeV; the shift of the width $\Delta\Gamma = \Gamma_2 - \Gamma_3$ changes from -0.3 GeV to a range extending up to $+0.4$ GeV. As a result, the two mass–eigenstates should become clearly distinguishable at future colliders, in particular at a photon collider [179]. Moreover, both states have significant admixtures of CP-even and CP-odd components in the wave–functions. Since $\gamma\gamma$ colliders offer unique conditions for probing the CP-mixing [85, 90–92, 95, 159, 322–328], we discuss two experimental examples: (a) Higgs formation in polarized $\gamma\gamma$ collisions and (b) polarization of top quarks in Higgs decays, where spectacular signatures of resonant mixing can be expected.

(a) The amplitude of the reaction $\gamma\gamma \to H_i \to F$ is a superposition of H_2 and H_3 Higgs exchanges. For equal helicities $\lambda = \pm 1$ of the two photons, the amplitude reads

$$\mathcal{M}^F_\lambda = \sum_{i=2,3} \langle F|H_i\rangle \frac{1}{s - M^2_{H_i} + iM_{H_i}\Gamma_{H_i}} [S^\gamma_i(s) + i\lambda P^\gamma_i(s)] \tag{3.90}$$

where $\sqrt{s}$ is the $\gamma\gamma$ energy. The loop–induced $\gamma\gamma H_i$ scalar and pseudoscalar form factors, $S^\gamma_i(s)$ and $P^\gamma_i(s)$, are related to the well–known conventional $\gamma\gamma H/A$ form factors, $S^\gamma_{H,A}$ and $P^\gamma_{H,A}$ (explicit form in Refs. [159] and [131]). In our scenario the Higgs–tt couplings are assumed to be CP-conserving, implying negligible top–loop contributions to P^γ_H and S^γ_A since the gluino mass is sufficiently heavy compared with the stop masses, while the $\tilde{t}_1$ loop generates a non–negligible CP-violating amplitude S^γ_A. In the region of strong mixing on which we focus, the CP-violating vertex corrections have only a small effect however on the experimental asymmetries compared with the large impact of CP-violating Higgs–boson mixing.

Polarized photons provide a very powerful tool to investigate the CP properties of Higgs bosons. With linearly polarized photons one can project out the CP-even and CP-odd components of the H_i wave–functions by arranging the photon polarization vectors to be parallel or perpendicular. On the other hand, circular polarization provides us with direct insight into the CP-violating nature of Higgs

[14]Note that in this illustrative example H_2 is heavier than H_3 across the entire Φ_A range. To avoid confusion with the elaborate paper Ref. [159], we have chosen not to relabel the states in this report.

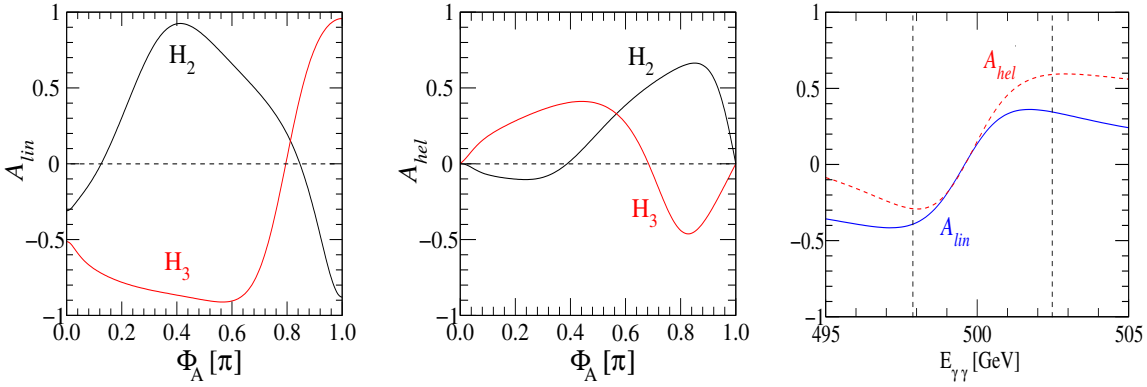

Fig. 3.51: The Φ_A dependence of the CP-even and CP-odd correlators, $\mathcal{A}_{lin}$ (leftmost panel) and $\mathcal{A}_{hel}$ (center panel), at the poles of the heavy Higgs bosons H_2 and H_3, respectively; and the $\gamma\gamma$ energy dependence (rightmost panel) of the correlators, $\mathcal{A}_{lin,hel}$, for $\Phi_A = 3\pi/4$ in the production process $\gamma\gamma \to H_i$ in the limit in which H/A mixing is the dominant CP-violating effect. The same parameter set as in Fig. 3.50 is employed. The vertical lines on the right panel mark positions of the two mass eigenvalues, M_{H_3} and M_{H_2}.

bosons. Two asymmetries are of interest

$$\mathcal{A}_{lin} = \frac{\sigma_{\parallel} - \sigma_{\perp}}{\sigma_{\parallel} + \sigma_{\perp}}, \qquad \mathcal{A}_{hel} = \frac{\sigma_{++} - \sigma_{--}}{\sigma_{++} + \sigma_{--}} \tag{3.91}$$

where $\sigma_{\parallel}$, $\sigma_{\perp}$ and σ_{++}, σ_{--} are the corresponding total $\gamma\gamma$ fusion cross sections for linear and circular polarizations, respectively. Though CP-even, the asymmetry $\mathcal{A}_{lin}$ can serve as a powerful tool nevertheless to probe CP-violating admixtures to the Higgs states since $|\mathcal{A}_{lin}| < 1$ requires both S_i^{γ} and P_i^{γ} couplings to be non–zero. A more direct probe of CP-violation due to H/A mixing is provided by the CP-odd asymmetry $\mathcal{A}_{hel}$.

In Fig. 3.51 the Φ_A dependence of the asymmetries $\mathcal{A}_{lin}$ and $\mathcal{A}_{hel}$ is shown at the poles of the heavy Higgs bosons H_2 and H_3 for the same parameter set as in Fig. 3.50 and with the common SUSY scale $M_{\tilde{Q}_3} = M_{\tilde{U}_3} = M_{\rm SUSY} = 0.5$ TeV for the soft SUSY breaking stop mass parameters. By varying the $\gamma\gamma$ energy from below M_{H_3} to above M_{H_2}, the asymmetries, $\mathcal{A}_{lin}$ (blue solid line) and $\mathcal{A}_{hel}$ (red dashed line), move from -0.39 to 0.34 and from -0.29 to 0.59, respectively, as shown in the rightmost panel of Fig. 3.51 with $\Phi_A = 3\pi/4$, a phase value close to resonant CP-mixing.

(b) A second observable of interest is the polarization of the top quarks in $H_{2,3} \to t\bar{t}$ decays produced by $\gamma\gamma$ fusion or elsewhere in various production processes at an e^+e^- linear collider and LHC. Even if the H/Att couplings are [approximately] CP-conserving, the complex rotation matrix C may mix the CP-even H and the CP-odd A states, leading to CP-violation. In the production–decay process $\gamma\gamma \to H_i \to t\bar{t}$, two CP-even and CP-odd correlators between the transverse t and $\bar{t}$ polarization vectors $s_{\perp}$ and $\bar{s}_{\perp}$,

$$\mathcal{C}_{\parallel} = \langle s_{\perp} \cdot \bar{s}_{\perp} \rangle \qquad \text{and,} \qquad \mathcal{C}_{\perp} = \langle \hat{p}_t \cdot (s_{\perp} \times \bar{s}_{\perp}) \rangle \tag{3.92}$$

can be extracted from the azimuthal–angle correlation between the two decay planes $t \to bW^+$ and $\bar{t} \to \bar{b}W^-$ [322, 323].

Fig. 3.52 shows the Φ_A dependence of the CP-even and CP-odd asymmetries, $\mathcal{C}_{\parallel}$ and $\mathcal{C}_{\perp}$, at the poles of H_2 and of H_3 (leftmost and center panels, respectively). If the invariant $t\bar{t}$ energy is varied throughout the resonance region, the correlators $\mathcal{C}_{\parallel}$ (blue solid line) and $\mathcal{C}_{\perp}$ (red dashed line) vary characteristically from -0.43 to -0.27 and from 0.84 to -0.94, respectively, as shown in the rightmost panel of Fig. 3.52.

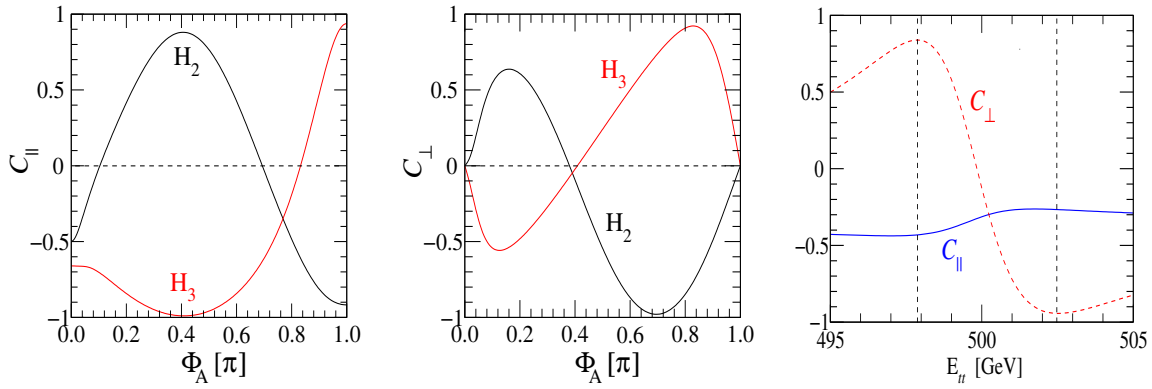

Fig. 3.52: The Φ_A dependence of the CP-even and CP-odd correlators, $\mathcal{C}_\parallel$ (leftmost panel) and $\mathcal{C}_\perp$ (center panel), at the pole of H_2 and H_3, and the invariant $t\bar{t}$ energy dependence (rightmost panel) of the correlators $\mathcal{C}_{\parallel,\perp}$ for $\Phi_A = 3\pi/4$ in the production–decay chain $\gamma\gamma \to H_i \to t\bar{t}$. [Same SUSY parameter set as in Fig.3.51.]

3.12.3 Conclusions

Exciting mixing effects can occur in the supersymmetric Higgs sector if CP-noninvariant interactions are realized. In the decoupling regime these effects can become very large, leading to interesting experimental consequences. Higgs formation in $\gamma\gamma$ collisions with polarized beams proves particularly exciting for observing such effects. However, valuable experimental effects are also predicted in such scenarios for $t\bar{t}$ final–state analyses in decays of the heavy Higgs bosons at LHC and in the e^+e^- mode of linear colliders.

Detailed experimental simulations would be needed to estimate the accuracy with which the asymmetries presented here can be measured. Though not easy to measure, the large magnitude and the rapid and significant variation of the CP-even and CP-odd asymmetries through the resonance region with respect to both the phase Φ_A and the $\gamma\gamma$ energy would be a very exciting effect to observe in any case.

3.13 Higgs boson interferences in chargino and neutralino production at a muon collider

Hans Fraas, Olaf Kittel and Federico von der Pahlen

A muon collider is an excellent tool to study the masses, widths and couplings of the heavy neutral MSSM Higgs bosons, since they are resonantly produced in s-channels [100,102,329–335]. In particular, interference effects of two nearly degenerate Higgs bosons can give valuable information on their CP properties [101, 336]. For the production of neutralinos [337] and charginos [338] with longitudinally polarized beams, it has been shown recently that energy distributions of their decay products can be used to analyze the CP-even and CP-odd Higgs boson couplings in the CP-conserving MSSM. We extend these studies [337,338] to the CP-violating MSSM with a nonvanishing physical phase Φ_A of the trilinear scalar coupling $A = A_t = A_b = A_\tau$, which induces CP violation in the Higgs sector at loop level. In the decoupling limit the heavier neutral Higgs bosons are nearly degenerate and CP-violating effects may be resonantly enhanced [93, 96, 157–159, 311–314]. In this report we define CP-sensitive polarization and charge asymmetries, which we analyze in CP-violating MSSM scenarios.

For chargino $\tilde{\chi}_i = \tilde{\chi}_i^\pm$ or neutralino $\tilde{\chi}_i = \tilde{\chi}_i^0$ production

$$\mu^+ + \mu^- \to \tilde{\chi}_i + \tilde{\chi}_j \tag{3.93}$$

via Higgs exchange H_k with $k = 1, 2, 3$, the effective CP-violating MSSM interaction Lagrangians are

$$\mathcal{L}_{\mu^+\mu^- H} = \bar{\mu}\,[g^S_{H_k\mu\mu} + i\gamma^5 g^P_{H_k\mu\mu}]\,\mu\,H_k, \tag{3.94}$$

$$\mathcal{L}_{\tilde{\chi}\tilde{\chi}H} = \kappa_{\tilde{\chi}}\bar{\tilde{\chi}}_i[g^S_{H_k\chi_i\chi_j} + i\gamma^5 g^P_{H_k\chi_i\chi_j}]\tilde{\chi}_j\,H_k, \tag{3.95}$$

with $\kappa_{\tilde{\chi}^\pm} = 1$ and $\kappa_{\tilde{\chi}^0} = 1/2$. The effective Higgs couplings to the initial muons and the final charginos/neutralinos are obtained from their tree level couplings $g^{S,P}_{\phi_\alpha\mu\mu}$ and $g^{S,P}_{\phi_\alpha\chi_i\chi_j}$, respectively [6],

$$g^{S,P}_{H_k\mu\mu} = C_{k\alpha}g^{S,P}_{\phi_\alpha\mu\mu}, \tag{3.96}$$

$$g^{S,P}_{H_k\chi_i\chi_j} = C_{k\alpha}g^{S,P}_{\phi_\alpha\chi_i\chi_j}, \quad \phi_\alpha = h, H, A, \tag{3.97}$$

where C is a complex orthogonal matrix which diagonalizes the complex Weisskopf-Wigner mass matrix $\mathcal{M}^2$ in the h, H, A basis, in analogy to Eq. (3.85) in Section 3.12. The leading radiative corrections are thus included into the Higgs couplings, as well as their masses and widths. In particular, observables can be defined which are sensitive to the off-diagonal absorptive parts of the Higgs-boson self energies [158], see Eq. (3.23) in Section 3.4. These CP$\tilde{\rm T}$-odd observables, where $\tilde{\rm T}$ denotes naive time reversal, depend strongly on the mass difference and widths of the overlapping Higgs bosons.

To analyze the longitudinal polarizations of the produced charginos or neutralinos, we consider their subsequent CP-conserving but P-violating leptonic two-body decays [337, 338]

$$\tilde{\chi}^\pm_j \to \ell^\pm + \tilde{\nu}^{(*)}_\ell, \qquad \tilde{\chi}^0_j \to \ell^\pm + \tilde{\ell}^\mp_a, \quad a = 1, 2. \tag{3.98}$$

In the center-of-mass system the differential cross section in the energy E_ℓ of the decay lepton $\ell^\pm$ is

$$\frac{d\sigma_{\ell^\pm}}{dE_\ell} = \frac{\sigma(\mu^+\mu^- \to \tilde{\chi}_i\tilde{\chi}_j){\rm BR}(\tilde{\chi}_j \to \ell^\pm \ldots)}{E^{\rm max}_\ell - E^{\rm min}_\ell}\left[1 + \eta_{\ell^\pm}\frac{\bar{\Sigma}^3}{\bar{P}}\frac{2(E_\ell - \hat{E}_\ell)}{E^{\rm max}_\ell - E^{\rm min}_\ell}\right], \tag{3.99}$$

with the mean lepton energy $\hat{E}_\ell = (E^{\rm max}_\ell + E^{\rm min}_\ell)/2$ and the kinematical end-points $E^{\rm max}_\ell$ and $E^{\rm min}_\ell$ [337, 338]. The coefficient $|\eta_{\ell^\pm}| \le 1$ is a measure of parity violation in the chargino/neutralino decay [337, 338]. The coefficients $\bar{P}$ and $\bar{\Sigma}^3$ of the production spin-density matrix are averaged over the chargino/neutralino production solid angle, indicated by a bar in our notation. The cross section $\sigma(\mu^+\mu^- \to \tilde{\chi}_i\tilde{\chi}_j)$ is proportional to $\bar{P}$, whereas the longitudinal chargino/neutralino polarization is proportional to $\bar{\Sigma}^3$. Both coefficients have resonant (res) contributions from Higgs $H_{1,2,3}$ exchange, and continuum (cont) contributions from gauge boson and slepton exchange

$$\bar{P} = P_{\rm res} + \bar{P}_{\rm cont}, \qquad \bar{\Sigma}^3 = \Sigma^3_{\rm res} + \bar{\Sigma}^3_{\rm cont}. \tag{3.100}$$

The dependence of the isotropic resonant contributions $P_{\rm res}$ and $\Sigma^3_{\rm res}$ on the longitudinal μ^+ and μ^- beam polarizations $\mathcal{P}_+$ and $\mathcal{P}_-$, respectively, is given by

$$P_{\rm res} = (1 + \mathcal{P}_+\mathcal{P}_-)a_0 + (\mathcal{P}_+ + \mathcal{P}_-)a_1, \tag{3.101}$$

$$\Sigma^3_{\rm res} = (1 + \mathcal{P}_+\mathcal{P}_-)b_0 + (\mathcal{P}_+ + \mathcal{P}_-)b_1, \tag{3.102}$$

with

$$a_n = \sum_{H_k, H_l (k \le l)} (2 - \delta_{kl})a^{kl}_n, \quad b_n = \sum_{H_k, H_l (k \le l)} (2 - \delta_{kl})b^{kl}_n; \quad n = 0, 1; \quad k, l = 1, 2, 3 \tag{3.103}$$

and, suppressing the chargino/neutralino indices i and j of the couplings,

$$a^{kl}_0 = \frac{s}{2}|\Delta_{(kl)}|\Big[|c^+_\mu||c^+_\chi|f_{ij}\cos(\delta^+_\mu + \delta^+_\chi + \delta_\Delta) - |c^+_\mu||c^{RL}_\chi|m_i m_j \cos(\delta^+_\mu + \delta^{RL}_\chi + \delta_\Delta)\Big]_{(kl)} \tag{3.104}$$

$$a^{kl}_1 = \frac{s}{2}|\Delta_{(kl)}|\Big[|c^-_\mu||c^+_\chi|f_{ij}\cos(\delta^-_\mu + \delta^+_\chi + \delta_\Delta) - |c^-_\mu||c^{RL}_\chi|m_i m_j \cos(\delta^-_\mu + \delta^{RL}_\chi + \delta_\Delta)\Big]_{(kl)} \tag{3.105}$$

$$b^{kl}_0 = -\frac{s}{2}|\Delta_{(kl)}|\Big[|c^+_\mu||c^-_\chi|g_{ij}\cos(\delta^+_\mu + \delta^-_\chi + \delta_\Delta)\Big]_{(kl)} \tag{3.106}$$

$$b^{kl}_1 = -\frac{s}{2}|\Delta_{(kl)}|\Big[|c^-_\mu||c^-_\chi|g_{ij}\cos(\delta^-_\mu + \delta^-_\chi + \delta_\Delta)\Big]_{(kl)} \tag{3.107}$$

We have defined the products of couplings,

$$c^+_{\lambda(kl)} = g^S_{H_k\lambda\lambda} g^{S*}_{H_l\lambda\lambda} + g^P_{H_k\lambda\lambda} g^{P*}_{H_l\lambda\lambda} = \Big[|c^+_\lambda| \exp(i\delta^+_\lambda)\Big]_{(kl)}, \quad \lambda = \mu, \chi, \tag{3.108}$$

$$c^-_{\lambda(kl)} = -i(g^S_{H_k\lambda\lambda} g^{P*}_{H_l\lambda\lambda} - g^P_{H_k\lambda\lambda} g^{S*}_{H_l\lambda\lambda}) = \Big[|c^-_\lambda| \exp(i\delta^-_\lambda)\Big]_{(kl)}, \quad \lambda = \mu, \chi, \tag{3.109}$$

$$c^{RL}_{\chi(kl)} = g^S_{H_k\chi\chi} g^{S*}_{H_l\chi\chi} - g^P_{H_k\chi\chi} g^{P*}_{H_l\chi\chi} = \Big[|c^{RL}_\chi| \exp(i\delta^{RL}_\chi)\Big]_{(kl)}, \tag{3.110}$$

the product of the Higgs boson propagators,

$$\Delta_{(kl)} = \Delta(H_k)\Delta(H_l)^* = \Big[|\Delta| \exp(i\delta_\Delta)\Big]_{(kl)}, \tag{3.111}$$

and the kinematical functions $f_{ij} = (s - m_i^2 - m_j^2)/2$ and $g_{ij} = \sqrt{\lambda(s, m_i^2, m_j^2)}/2$ of the chargino/neutralino masses m_i, m_j, and the center of mass energy s. For longitudinally polarized muon beams, the two combinations a_1, Eq. (3.101), and b_1, Eq. (3.102), of products of Higgs boson couplings to the muons and charginos/neutralinos can be determined, e.g., by polarization asymmetries. A muon collider provides a good beam energy resolution and thus will be the ideal tool to analyze the strong $\sqrt{s}$ dependence of these observables.

3.13.1 Asymmetries of the chargino and neutralino production cross section

For the cross section σ_{ij} of chargino $\sigma(\mu^+\mu^- \to \tilde\chi_i^+\tilde\chi_j^-)$ or neutralino $\sigma(\mu^+\mu^- \to \tilde\chi_i^0\tilde\chi_j^0)$ pair production, Eq. (3.93), we define for equal beam polarizations $\mathcal{P}_+ = \mathcal{P}_- \equiv \mathcal{P}$ the asymmetries

$$\mathcal{A}^{\mathrm{pol}\pm}_{\mathrm{prod}} = \frac{[\sigma_{ij}(\mathcal{P}) - \sigma_{ij}(-\mathcal{P})] \pm [i \leftrightarrow j]}{[\sigma_{ij}(\mathcal{P}) + \sigma_{ij}(-\mathcal{P})] + [i \leftrightarrow j]}. \tag{3.112}$$

The asymmetry $\mathcal{A}^{\mathrm{pol}+}_{\mathrm{prod}}$ is CP-odd and CP$\tilde{\mathrm{T}}$-odd, with $\tilde{\mathrm{T}}$ naive time reversal $t \to -t$, and is thus non-zero only for complex transition amplitudes with absorptive phases. It is therefore sensitive to the CP phases of the Higgs boson couplings to the charginos/neutralinos and to the muons, and is largest if the mass difference of the two heavy Higgs bosons is of the order of their widths. In Fig. 3.53 we show, for $\tilde\chi_1^+\tilde\chi_1^-$ production, $\mathcal{A}^{\mathrm{pol}+}_{\mathrm{prod}}$ and σ_{11} for $\mathcal{P} = 0.3$, $\mathcal{P} = -0.3$ and $\Phi_A = 0.2\pi$. We obtain an asymmetry of 30% which can be measured at a muon collider with longitudinally polarized beams. For neutralino production $\mu^+\mu^- \to \tilde\chi_1^0\tilde\chi_2^0$, the asymmetry $\mathcal{A}^{\mathrm{pol}+}_{\mathrm{prod}}$ reaches 16%, for the parameters as given in the caption of Fig. 3.53, and the neutralino production cross section σ_{12} is of the order of 400 fb. The asymmetries are proportional to a_1/a_0, Eq. (3.101), if the continuum contributions $\bar{P}_{\mathrm{cont}}$ are subtracted, e.g., through extrapolation of the cross section around the resonances [339], or by chargino/neutralino cross section measurements at the ILC [220]. The CP-even asymmetry $\mathcal{A}^{\mathrm{pol}-}_{\mathrm{prod}}$ vanishes for the production of neutralinos, due to their Majorana character, as well as for the production of equal charginos. For the production of unequal charginos $\tilde\chi_i^+\tilde\chi_j^-$, with $i \neq j$, measurements of $\mathcal{A}^{\mathrm{pol}\pm}_{\mathrm{prod}}$ allow to separate the CP-even and CP-odd parts of the coefficient a_1.

Similarly, for $\tilde\chi_i^+\tilde\chi_j^-$ production with $i \neq j$, the coefficients a_0, b_0 and b_1 can be separated into their symmetric and antisymmetric parts under exchange of i and j, to obtain CP-even and CP-odd observables. We define the charge asymmetry

$$\mathcal{A}^C_{\mathrm{prod}} = \frac{\sigma_{12}(\mathcal{P}) - \sigma_{21}(\mathcal{P}) + \sigma_{12}(-\mathcal{P}) - \sigma_{21}(-\mathcal{P})}{\sigma_{12}(\mathcal{P}) + \sigma_{21}(\mathcal{P}) + \sigma_{12}(-\mathcal{P}) + \sigma_{21}(-\mathcal{P})} \tag{3.113}$$

of the chargino production cross sections σ_{ij}. This asymmetry is CP-odd and CP$\tilde{\mathrm{T}}$-even. In Fig. 3.54 we show $\mathcal{A}^C_{\mathrm{prod}}$ for two scenarios with different scalar mass parameters M_{SUSY} and trilinear coupling parameters $|A|$ for unpolarized beams $\mathcal{P} = 0$. The production of $\tilde t_1$ pair production strongly suppresses one chargino production amplitude of the Higgs boson, enhancing $\mathcal{A}^C_{\mathrm{prod}}$.

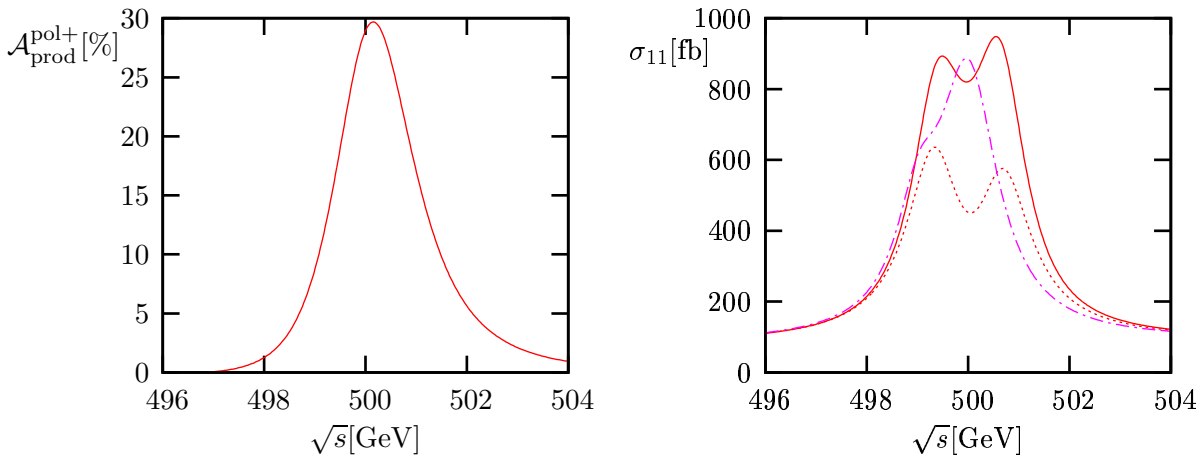

Fig. 3.53: Chargino production asymmetry $\mathcal{A}_{\rm prod}^{\rm pol+}$, Eq. (3.112), and cross section $\sigma_{11} = \sigma(\mu^+\mu^- \to \tilde{\chi}_1^+\tilde{\chi}_1^-)$ for $\Phi_A = 0.2\pi$, $\mathcal{P}_+ = \mathcal{P}_- = \mathcal{P} = 0.3$ (solid), $\mathcal{P} = -0.3$ (dotted), and for $\Phi_A = 0$, $\mathcal{P} = \pm 0.3$ (dash-dotted), with $M_A = 500$ GeV ($M_{H^\pm} = 506.9$ GeV), $\tan\beta = 10$, $\mu = 500$ GeV, $M_2 = 220$ GeV, $|A| = 2\,M_{\rm SUSY} = 1$ TeV, evaluated using `FeynHiggs2.3` [144]. The Higgs masses and widths for $\Phi_A = 0.2\pi$ are $M_{H_{2,3}} = 499.4$ GeV, 500.7 GeV and $\Gamma_{H_{2,3}} = 1.3$ GeV, respectively, and $m_{\chi_1^\pm} = 210$ GeV.

3.13.2 Asymmetries of the energy distributions for the chargino and neutralino decay products

For the cross section $\sigma_{\ell^\pm}$ of chargino/neutralino production, Eq. (3.93), followed by their subsequent decay into a lepton $\ell^\pm$, Eq. (3.98), we define the asymmetry of the leptonic energy distribution, Eq. (3.99),

$$\mathcal{A}_{\ell^\pm} \;=\; \frac{\Delta\sigma_{\ell^\pm}}{\sigma_{\ell^\pm}} = \frac{1}{2}\eta_{\ell^\pm}\frac{\bar{\Sigma}^3}{\bar{P}}, \tag{3.114}$$

with $\Delta\sigma_{\ell^\pm} = \sigma_{\ell^\pm}(E_\ell > \hat{E}_\ell) - \sigma_{\ell^\pm}(E_\ell < \hat{E}_\ell)$. Since $\mathcal{A}_{\ell^\pm}$ is proportional to the averaged longitudinal chargino/neutralino polarization $\bar{\Sigma}^3/\bar{P}$ it allows to determine the coefficients b_1 and b_0, Eq. (3.102), with, respectively, the polarization asymmetries

$$\mathcal{A}_{\ell^\pm}^{\rm pol} \;=\; \frac{\Delta\sigma_{\ell^\pm}(\mathcal{P}) - \Delta\sigma_{\ell^\pm}(-\mathcal{P})}{\sigma_{\ell^\pm}(\mathcal{P}) + \sigma_{\ell^\pm}(-\mathcal{P})} = \eta_{\ell^\pm}\frac{\mathcal{P}b_1}{(1+\mathcal{P}^2)a_0 + \bar{P}_{\rm cont}}, \tag{3.115}$$

$$\mathcal{A}_{\ell^\pm}^{\prime\rm pol} \;=\; \frac{\Delta\sigma_{\ell^\pm}(\mathcal{P}) + \Delta\sigma_{\ell^\pm}(-\mathcal{P})}{\sigma_{\ell^\pm}(\mathcal{P}) + \sigma_{\ell^\pm}(-\mathcal{P})} = \frac{1}{2}\eta_{\ell^\pm}\frac{(1+\mathcal{P}^2)b_0 + \bar{\Sigma}^3_{\rm cont}}{(1+\mathcal{P}^2)a_0 + \bar{P}_{\rm cont}}, \tag{3.116}$$

for equal muon beam polarizations $\mathcal{P}_+ = \mathcal{P}_- \equiv \mathcal{P}$. The asymmetry $\mathcal{A}_{\ell^\pm}^{\rm pol}$ measures the correlation between initial and final longitudinal polarizations, and is CP-even for the production of neutralinos or equal charginos. Large values of $\mathcal{A}_{\ell^\pm}^{\rm pol}$ are obtained if both resonances are degenerate and their amplitudes are of the same magnitude. As in the CP-conserving MSSM [337, 338], the relative phase of the interfering resonances is approximately $\pi/2$ in the Higgs decoupling limit. However, resonantly enhanced CP violation tends to widen the mass difference of the heavy Higgs bosons [159] and thus suppress this asymmetry, as can be observed on the left hand side of Fig. 3.55, where we show the asymmetry $\mathcal{A}_{\ell^+}^{\rm pol}$ for light chargino pair production, both for $\Phi_A = 0.2\pi$ and for $\Phi_A = 0$. The corresponding asymmetry $\mathcal{A}_{\ell^+}^{\prime\rm pol}$, Eq. (3.116), depends on the continuum contributions of the chargino polarization $\bar{\Sigma}^3_{\rm cont}$, which can be eliminated in the charge asymmetry

$$\mathcal{A}_{\ell^+}^{\prime\rm C} \;=\; \frac{1}{2}(\mathcal{A}_{\ell^+}^{\prime\rm pol} - \mathcal{A}_{\ell^-}^{\prime\rm pol}) = \frac{1}{2}\eta_{\ell^\pm}\frac{(1+\mathcal{P}^2)b_0}{(1+\mathcal{P}^2)a_0 + \bar{P}_{\rm cont}}, \tag{3.117}$$

shown on the r.h.s. of Fig. 3.55. For neutralino production the continuum $\bar{\Sigma}^3_{\rm cont} = 0$ vanishes naturally due to their Majorana character [340], thus $\mathcal{A}_{\ell^+}^{\prime C} = \mathcal{A}_{\ell^+}^{\prime\rm pol}$. For the production of neutralinos, $\mu^+\mu^- \to$

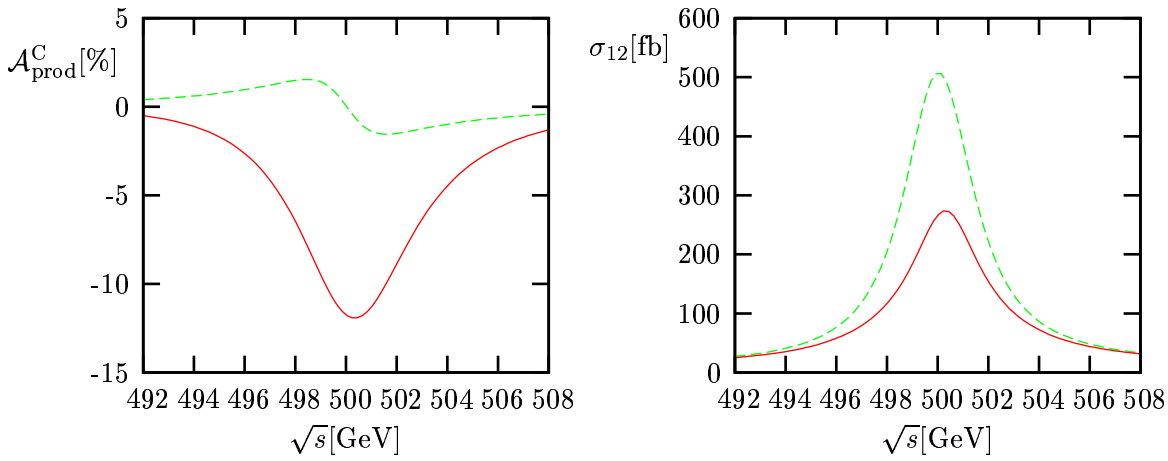

Fig. 3.54: Chargino production asymmetry $\mathcal{A}^{C}_{\rm prod}$, Eq. (3.113), and cross section $\sigma_{12} = \sigma(\mu^+\mu^- \to \tilde{\chi}^+_1\tilde{\chi}^-_2)$ for $|A| = 500$ GeV, $M_{\rm SUSY} = 300$ GeV (solid), and for $|A| = 2\,M_{\rm SUSY} = 1$ TeV (dashed), with $\mathcal{P}_+ = \mathcal{P}_- = 0$, $\Phi_A = 0.2\pi$, $M_A = 500$ GeV ($M_{H^\pm} = 505.7$ GeV), $\tan\beta = 10$, $\mu = 320$ GeV, $M_2 = 120$ GeV, evaluated using `FeynHiggs2.3` [144]. The Higgs masses and widths are $M_{H_{2,3}} = 500$ GeV, 500.3 GeV, $\Gamma_{H_{2,3}} = 7.5$ GeV, 3.2 GeV (solid), and $M_{H_{2,3}} = 499.8$ GeV, 500.3 GeV, $\Gamma_{H_{2,3}} = 3.2$ GeV (dashed), and $m_{\chi^\pm_1} = 108$ GeV, $m_{\chi^\pm_2} = 344$ GeV.

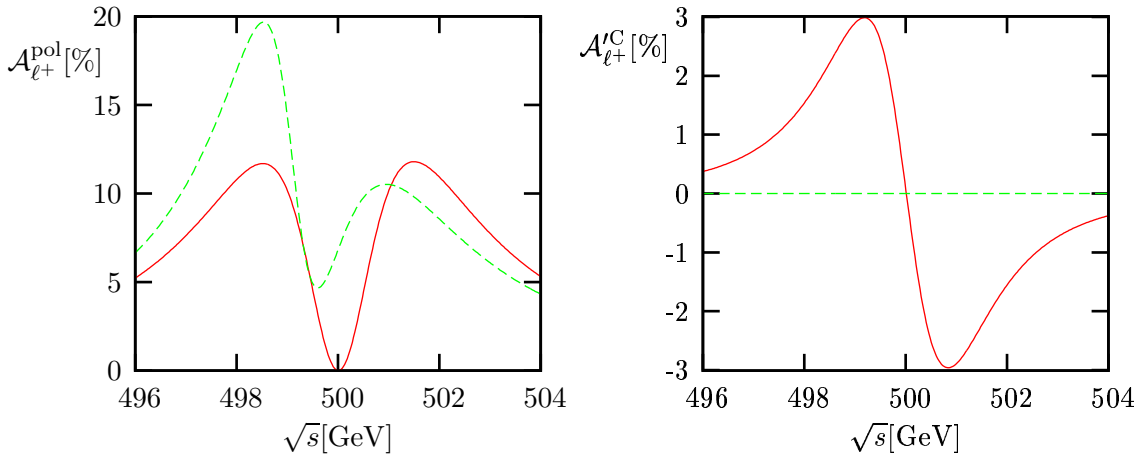

Fig. 3.55: Polarization asymmetry $\mathcal{A}^{\rm pol}_{\ell^+}$, Eq. (3.115), and $\mathcal{A}'^{\rm C}_{\ell^+}$, Eq. (3.117), for $\mu^+\mu^- \to \tilde{\chi}^+_1\tilde{\chi}^-_1$ with subsequent leptonic chargino decay, for $\Phi_A = 0.2\pi$ (solid), $\Phi_A = 0$ (dashed), with $\mathcal{P}_+ = \mathcal{P}_- = \mathcal{P} = -0.3$, evaluated using `FeynHiggs2.3` [144]. For cross sections and other parameters, see Fig. 3.53. The Higgs masses and widths for $\Phi_A = 0$ are $M_{H_{2,3}} = 499.0$ GeV, 500.0 GeV and $\Gamma_{H_{2,3}} = 1.1$ GeV, 1.4 GeV.

$\tilde{\chi}^0_1\tilde{\chi}^0_2$, with subsequent leptonic decay, Eq. (3.98), the asymmetry $\mathcal{A}'^{\rm pol}_{\ell^+}$ reaches 8%, for the scenario as given in the caption of Fig. 3.55. The asymmetry $\mathcal{A}^{\rm pol}_{\ell^+}$, Eq. (3.115), is similar in size and shape as the corresponding asymmetry for chargino production, see Fig. 3.55.

3.13.3 Summary and conclusions

We have studied chargino and neutralino production and their leptonic decays at the muon collider with longitudinally polarized beams. We have defined polarization and charge asymmetries to study the interference of the heavy neutral CP-violating MSSM Higgs bosons with CP violation, radiatively induced by the common phase Φ_A of the trilinear scalar couplings. For nearly degenerate neutral Higgs bosons, with mass differences comparable to their decay widths, the asymmetries for chargino production can be

as large as 30% with cross sections of the order of several hundred fb. In addition, we have defined and analyzed asymmetries of the energy distributions of the chargino and neutralino decay products which probe the longitudinal chargino/neutralino polarizations. Their dependence on the Higgs interference and mixing effects can be used, in addition to the polarization and charge asymmetries of the production cross sections, to study the CP-violating effects in the MSSM Higgs sector at the muon collider.

3.14 Impact of Higgs CP mixing on the neutralino relic density

Geneviève Bélanger, Fawzi Boudjema, Sabine Kraml, Alexander Pukhov and Alexander Semenov

In supersymmetric models with R-parity conservation the lightest supersymmetric particle (LSP), typically the lightest neutralino $\tilde{\chi}_1^0$, is an excellent cold dark matter candidate [30, 31] (see e.g. [341] for a recent review). With the precision measurements by WMAP [342, 343] the relic density of cold dark matter can be constrained to $0.0945 < \Omega h^2 < 0.1287$ at 2σ. This in turn puts strong constraints on the neutralino LSP as a thermal relic from the Big Bang. In particular, some efficient mechanism for $\tilde{\chi}_1^0$ annihilation has to be at work to ensure $\Omega h^2 \sim 0.1$. One such mechanism is annihilation through s-channel Higgs exchange near resonance. In this contribution, we investigate this case in the context of the MSSM with CP violation. This topic has been studied recently in [344, 345], and we here discuss it in more detail. An extensive analysis of the neutralino relic density in the presence of CP phases for various scenarios of neutralino (co)annihilation is given in [346].

We consider the general MSSM with parameters defined at the weak scale. In general, one can have complex parameters in the neutralino/chargino sector with $M_i = |M_i|e^{i\Phi_i}$, $\mu = |\mu|e^{i\Phi_\mu}$ as well as for the trilinear couplings, $A_f = |A_f|e^{i\Phi_{A_f}}$. The phase of M_2 can be rotated away. Among the trilinear couplings, A_t has the largest effect on the Higgs sector, with the loop-induced CP mixing proportional to $\mathrm{Im}\, m(A_t\mu)/(m^2_{\tilde{t}_2} - m^2_{\tilde{t}_1})$. Since the phase of μ is the most severely constrained by electric dipole moment (EDM) measurements, we set it to zero, hence being left with only two relevant phases, Φ_1 and $\Phi_t \equiv \Phi_{A_t}$.

Owing to Fermi statistics, the s-wave state of two identical Majorana fermions has $\mathrm{CP} = -1$. The p-wave state has $\mathrm{CP} = +1$. In the CP-conserving MSSM, the annihilation of two LSP's through the scalar h or H is hence p-wave suppressed at small velocities, while annihilation through the pseudoscalar A is preferred. For mass-degenerate H and A, the scalar exchange therefore only amounts to $\mathcal{O}(10\%)$ of the pseudoscalar exchange at $2m_{\tilde{\chi}_1^0} \sim M_{A,H}$.

In the presence of CP-violating phases, the interaction of the lightest neutralino with a Higgs H_i, $i = 1...3$, which now does not have definite CP properties any more, is given by

$$\mathcal{L}_{H_i\tilde{\chi}_1^0\tilde{\chi}_1^0} = \frac{g}{2}\sum_{i=1}^{3}\overline{\tilde{\chi}_1^0}(g^S_{H_i\tilde{\chi}_1^0\tilde{\chi}_1^0} + i\gamma_5 g^P_{H_i\tilde{\chi}_1^0\tilde{\chi}_1^0})\tilde{\chi}_1^0 H_i \tag{3.118}$$

with the scalar part of the coupling

$$g^S_{H_i\tilde{\chi}_1^0\tilde{\chi}_1^0} = \mathrm{Re}\, e\left[(N_{12}^* - t_W N_{11}^*)\,(O_{1i}N_{13}^* - O_{2i}N_{14}^* - iO_{3i}(s_\beta N_{13}^* - c_\beta N_{14}^*))\right], \tag{3.119}$$

where N is the neutralino mixing matrix in the SLHA notation [252] and O is the Higgs mixing matrix defined in Eq. (3.5). The pseudoscalar coupling $g^P_{H_i\tilde{\chi}_1^0\tilde{\chi}_1^0}$ corresponds to the imaginary part of the same expression. From Eqs. (3.118) and (3.119) it is clear that the neutralino relic density, being inversely proportional to the thermally averaged annihilation cross section, $\Omega_\chi \sim 1/\langle\sigma v\rangle$, will be affected both by Φ_t, which induces scalar-pseudoscalar mixing in the Higgs sector, as well as by Φ_1, which modifies the neutralino mixing. Here note that not only the couplings but also the masses depend on the phases. In what follows it will therefore be important to disentangle effects due to CP violation in the couplings from purely kinematic effects. Note also that there is a kind of sum rule relating the couplings squared of

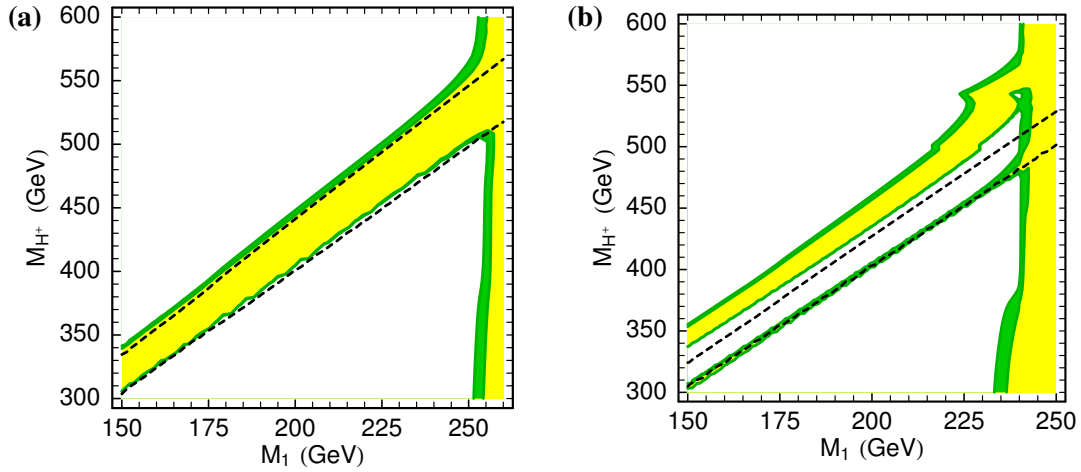

Fig. 3.56: WMAP-allowed bands in the M_{H^+}–M_1 plane for (a) $\mu = 1$ TeV and (b) $\mu = 2$ TeV with $\Phi_t = 90°$, $M_{\rm SUSY} = 0.5$ TeV, $|A_t| = 1.2$ TeV and $\tan\beta = 5$. In the narrow green (dark grey) bands $0.0945 < \Omega h^2 < 0.1287$, while in the yellow (light grey) regions $\Omega h^2 < 0.0945$. The positions of the WMAP-allowed bands for $\Phi_t = 0$ are shown as dashed lines.

the Higgses to neutralinos. Therefore, for the two heavy eigenstates which are in general close in mass, we do not expect a huge effect on the resulting relic density from Higgs mixing alone. A noteworthy exception occurs when, for kinematical reasons, one of the resonances completly dominates the neutralino annihilation. That is for instance the case for $M_{H_2} < 2m_{\tilde{\chi}^0_1} \simeq M_{H_3}$, or when the mass splitting between the heavy Higgs bosons becomes very large.

For the numerical analysis, we are using an extension [347] of `micrOMEGAs` [348,349] that allows for complex parameters in the MSSM. Using `LanHEP` [350], a new MSSM model file with complex parameters was rebuilt in the `CalcHEP` [351] notation, thus specifying all relevant Feynman rules. For the Higgs sector, an effective potential is written in order to include in a consistent way higher-order effects. To compute masses, mixing matrices and parameters of the effective potential the program is interfaced to `CPsuperH` [131]. All cross sections for annihilation and coannihilation processes are computed automatically with `CalcHEP`, and the standard `micrOMEGAs` routines are used to calculate the effective annihilation cross section and the relic density of dark matter. This CPV-MSSM version of `micrOMEGAs` has first been presented in [344].

Let us now turn to the numerical results. In order not to vary too many parameters, we choose $\tan\beta = 5$, $M_{\rm SUSY} \equiv M_{\tilde{Q}_3,\tilde{U}_3,\tilde{D}_3} = 0.5$ TeV and $|A_t| = 1.2$ TeV throughout this study. Moreover, we assume GUT relations for the gaugino masses, hence $M_2 \simeq 2M_1$. EDM constraints are avoided by setting $\Phi_\mu = 0$ and pushing the masses of the 1st and 2nd generation sfermions to 10 TeV. Last but not least in this contribution we are interested in the influence of CP violation in the Higgs sector. Therefore we also choose $\Phi_1 = 0$ and concentrate on the effect of Φ_t. The effect of $\Phi_1 \neq 0$ is discussed in [344, 346].

Figure 3.56 shows the WMAP-allowed regions in the M_{H^+}–M_1 plane for this choice, maximal phase of A_t ($\Phi_t = 90°$) and two values of μ: $\mu = 1$ TeV and $\mu = 2$ TeV. The regions for which $0.094 < \Omega h^2 < 0.129$ are shown in green, and those for which $\Omega h^2 < 0.094$ in yellow. In addition, the positions of the WMAP-allowed strips for $\Phi_t = 0$ are shown as dashed lines. In the CP-conserving case, H_3 is a pure pseudoscalar and H_2 a pure scalar, while for $\Phi_t = 90°$ it is just the opposite and H_2 is dominantly pseudoscalar. The crossovers of 50% scalar-pseudoscalar mixing of $H_{2,3}$ occur at $\Phi_t \sim 15°$ and $145°$. For $\mu = 1$ TeV, Fig. 3.56a, the mass splitting between $H_{2,3}$ is about 10 GeV for $\Phi_t = 90°$, as compared to about 2 GeV for $\Phi_t = 0$. Masses and the pseudoscalar content of $H_{2,3}$ are depicted in Fig. 3.57 as functions of Φ_t. Here note that it is H_2, i.e. the state which changes from scalar

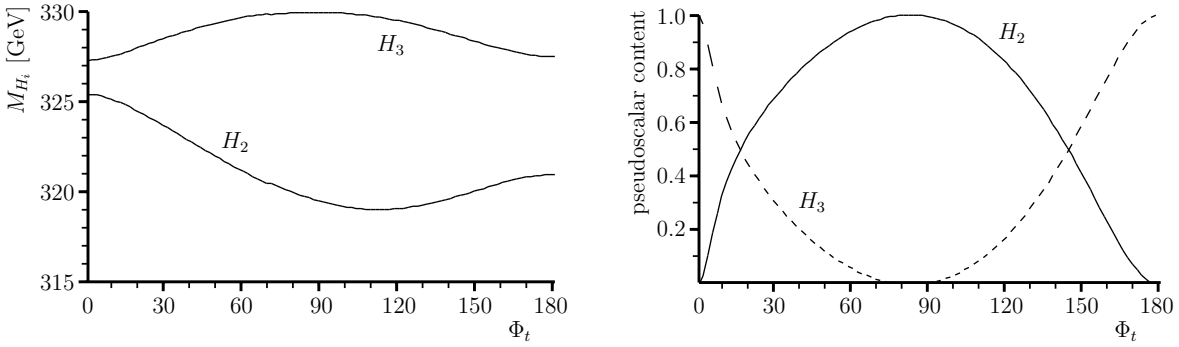

Fig. 3.57: Masses and pseudoscalar content of H_2 and H_3 as function of Φ_t for $M_{H^+} = 335$ GeV, $\mu = 1$ TeV, $|A_t| = 1.2$ TeV, $M_{\rm SUSY} = 0.5$ TeV and $\tan\beta = 5$. The light Higgs H_1 has a mass of $M_{H_1} \simeq 117$ GeV and a pseudoscalar content of $\leq 10^{-4}$.

to pseudoscalar with increasing Φ_t, which shows the more pronounced change in mass. For M_1 values up to 250 GeV, we therefore find in both the CP-conserving and the CP-violating case two narrow bands where $0.094 < \Omega h^2 < 0.129$. For $\Phi_t = 0$ (and also for $\Phi_t = 180^\circ$) both these bands are mainly due to pseudoscalar H_3 exchange, with one band just below and the other one above the pseudoscalar resonance. For $\Phi_t = 90^\circ$ the situation is different: in the lower WMAP-allowed band the LSP annihilates through the scalar H_3, with the pseudoscalar H_2 not accessible because $M_{H_2} < 2m_{\tilde{\chi}^0_1} \simeq M_{H_3}$, while in the upper band both H_2 and H_3 contribute (with H_2 exchange of course dominating). In between the two WMAP-allowed green bands one is too close to the pseudoscalar resonance and Ωh^2 falls below the WMAP bound; this holds for both $\Phi_t = 0$ and $\Phi_t = 90^\circ$. The positions of the WMAP-allowed bands for $\Phi_t = 0$ and $\Phi_t = 90^\circ$ are not very different from each other. Still the difference in the relic density between $\Phi_t = 0$ and $\Phi_t = 90^\circ$ is typically a factor of a few in the WMAP-bands, and can reach orders of magnitudes at a pole. For $M_1 \gtrsim 250$ GeV and $\Phi_t = 90^\circ$, one enters the region of coannihilation with stops, leading to a vertical WMAP-allowed band. For $\Phi_t = 0$, the $\tilde{t}_1$ is 55 GeV heavier, so the stop coannihilation occurs only at $M_1 \sim 305$ GeV (for $\Phi_t = 180^\circ$ on the other hand, $m_{\tilde{t}_1} \simeq 230$ GeV and coannihilation already sets in at $M_1 \sim 200$ GeV).

For $\mu = 2$ TeV, Fig. 3.56b, there is an even stronger CP-mixing of $H_{2,3}$ and the mass splitting between the two states becomes ~ 45 GeV for $\Phi_t = 90^\circ$. The pseudoscalar contents are similar to those in Fig. 3.57 with the 50% cross-over at $\Phi_t \sim 20^\circ$. Moreover, because the LSP has less higgsino admixture, one has to be closer to resonance to obtain the right relic density. As a result, the scalar and pseudoscalar funnels become separated by a region where Ωh^2 is too large. In fact both the H_2 and H_3 exchange each lead to two WMAP-allowed bands, one above and one below the respective resonance. For the H_3 (scalar) exchange, however, these two regions are so close to each other that they appear as one line in Fig. 3.56b. This is in sharp contrast to the CP-conserving case, $\Phi_t = 0$, where the scalar and pseudoscalar states are close in mass, hence leading to only two WMAP-allowed bands. These are again shown as dashed lines in Fig. 3.56b and origin dominantly from the pseudoscalar resonance, the scalar resonance being 'hidden' within.

We next study the explicit dependence on Φ_t, disentangling the effects due to scalar-pseudoscalar mixing from those due to changes in the Higgs masses. For this aim we fix $M_1 = 150$ GeV and $\mu = 1$ TeV. This gives $m_{\tilde{\chi}^0_1} = 149$ GeV with the LSP being 99.8% bino. Figure 3.58 shows the corresponding WMAP-allowed bands in the M_{H^+}–Φ_t plane. We observe a strong dependence on the phase of A_t, leading to huge shifts of up to two orders of magnitude in the relic density for constant M_{H^+}. To understand these huge effects, let us first discuss the upper WMAP-allowed band at $M_{H^+} \sim 335$ GeV, shown in Fig. 3.58a, in more detail. As has been pointed out in [352, 353], the relic density is very sensitive to mass difference $\Delta M_{\tilde{\chi}^0_1 H_i} = M_{H_i} - 2m_{\tilde{\chi}^0_1}$, i.e. to the distance from the Higgs poles.

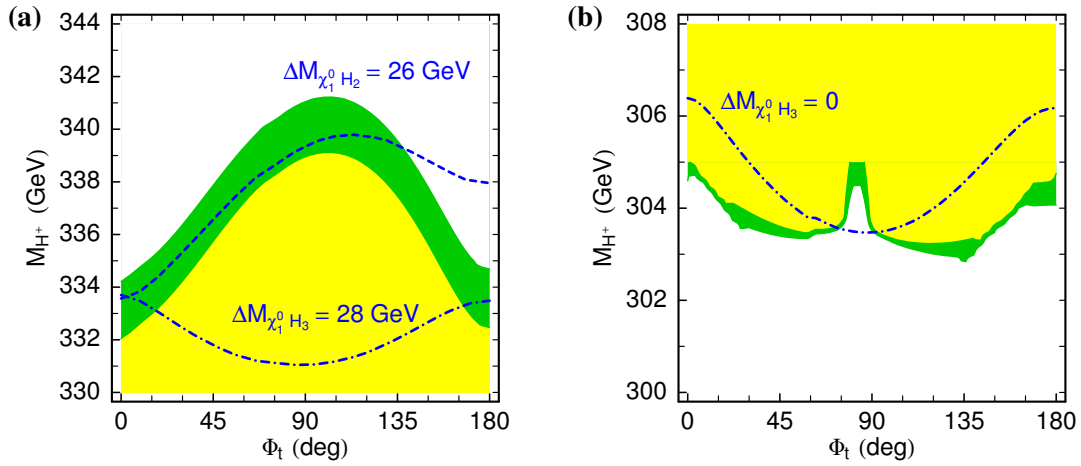

Fig. 3.58: The WMAP-allowed bands (green/dark grey) in the M_{H^+}–Φ_t plane for $M_1 = 150$ GeV, $\mu = 1$ TeV, $|A_t| = 1.2$ TeV, $M_{\rm SUSY} = 0.5$ TeV and $\tan\beta = 5$. Contours of constant mass differences $\Delta M_{\tilde{\chi}_1^0 H_i} \equiv M_{H_i} - 2m_{\tilde{\chi}_1^0}$ are also displayed. In the yellow (light grey) regions, Ωh^2 is below the WMAP range.

At $M_{H^+} = 335$ GeV, the neutral Higgs masses range between $M_{H_2} \simeq 325$–319 GeV and $M_{H_3} \simeq 327$–330 GeV for $\Phi_t = 0$–90°. The LSP annihilates more efficiently through the Higgs which has the larger pseudoscalar content. For $\Phi_t \lesssim 15^\circ$ ($\Phi_t \gtrsim 145^\circ$) this is H_3, while for maximal phase it is H_2. Consequently in Fig. 3.58a agreement with WMAP is reached for $\Delta M_{\tilde{\chi}_1^0 H_i} \sim 26$–$28$ GeV with $H_i = H_3$ at $\Phi_t = 0$ and 180°, and $H_i = H_2$ at $\Phi_t = 90^\circ$. When considering the Higgs–LSP couplings, we find $(g^S, g^P)_{H_2\tilde{\chi}_1^0\tilde{\chi}_1^0} \simeq (0.02, -10^{-5})$ and $(g^S, g^P)_{H_3\tilde{\chi}_1^0\tilde{\chi}_1^0} \simeq (-10^{-5}, -0.02)$ at $M_{H^+} = 335$ GeV and $\Phi_t = 0$, while at $\Phi_t = 90^\circ$ $(g^S, g^P)_{H_2\tilde{\chi}_1^0\tilde{\chi}_1^0} \simeq (10^{-4}, 0.02)$ and $(g^S, g^P)_{H_3\tilde{\chi}_1^0\tilde{\chi}_1^0} \simeq (0.02, -10^{-4})$. We see that in the case where both H_2 and H_3 are accessible, the phase dependence of Ωh^2 is directly linked to the position of the (dominantly) pseudoscalar resonance. For $\Phi_t = 0 - 90^\circ$ and $\Phi_t \simeq 180^\circ$, in the WMAP-allowed green band the dominant annihilation channels are about 75–80% into $b\bar{b}$ and about 10% into $\tau^+\tau^-$, corresponding to the pseudoscalar branching ratios. For $\Phi_t > 90^\circ$, where the WMAP-allowed band deviates from the contour of constant $\Delta M_{\tilde{\chi}_1^0 H_i}$, there is also a sizeable, up to $\sim 25\%$, contribution from $\tilde{\chi}_1^0\tilde{\chi}_1^0 \to H_1 H_1$ with a constructive interference between s-channel H_3 and t-channel neutralino exchange. This is acompanied by roughly 10% annihilation into WW and ZZ. For constant $\Delta M_{\tilde{\chi}_1^0 H_i}$, the variation in Ωh^2 due to changes in the Higgs couplings alone can be $\mathcal{O}(100\%)$.

When the LSP mass is very near the heaviest Higgs resonance one finds another region where the relic density falls within the WMAP range. This is shown in Fig. 3.58b (corresponding to the phase dependence of the lower WMAP-allowed band in Fig. 3.56a). In the real case one needs $M_{H^+} = 305$ GeV, giving a mass difference $\Delta M_{\tilde{\chi}_1^0 H_3} = -1.5$ GeV. Note that annihilation is efficient enough even though one catches only the tail of the pseudoscalar resonance. For the same charged Higgs mass, the mass of H_3 increases when one increases Φ_t, so that neutralino annihilation becomes more efficient despite the fact that H_3 becomes scalar-like and $g^P_{H_3\tilde{\chi}_1^0\tilde{\chi}_1^0}$ decreases. When $\Phi_t \sim 75^\circ$–90°, the coupling $g^P_{H_3\tilde{\chi}_1^0\tilde{\chi}_1^0}$ becomes very small and one needs $\Delta M_{\tilde{\chi}_1^0 H_3} = 0$–$1.5$ GeV to achieve agreement with WMAP. Here we are in the special case where $M_{H_2} < 2m_{\tilde{\chi}_1^0} \simeq M_{H_3}$, so that only H_3 contributes significantly to the relic density. Figure 3.59 shows the $\tilde{\chi}_1^0\tilde{\chi}_1^0 \to b\bar{b}$ annihilation cross section as a function of M_{H^+} and various values of Φ_t. As can be seen, not only the position but also the hight of the peak changes with Φ_t, corresponding to the change in the pseudoscalar content of H_3. In fact, at $M_{H^+} = 305$ GeV and $\Phi_t = 0$, the LSP annihilates to about 80% into $b\bar{b}$, 10% into $\tau\tau$ and 10% into ZH_1, while at $\Phi_t = 90^\circ$, it annihilates to about 50% into $b\bar{b}$, 30% into H_1H_1 and 10% into WW/ZZ. At $\Phi_t = 180^\circ$, the rates are about 70% $b\bar{b}$, 10% $\tau\tau$ and 20% ZH_1,

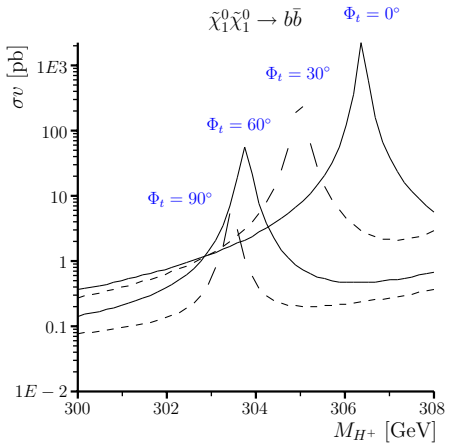

Fig. 3.59: $\sigma v(\tilde{\chi}_1^0\tilde{\chi}_1^0 \to b\bar{b})$ as a function of M_{H^+} and various values of Φ_t; other parameters as in Fig. 3.58.

In conclusion, CP-violating phases can lead to huge variations in the neutralino relic density. For fixed M_{H^+}, we find shifts in Ωh^2 of up to two orders of magnitude, which agrees with the observations in [35] (although in that paper only σv and not Ωh^2 was computed). From the discussion above it is clear that a large part of this can be attributed to changes in the Higgs masses. When disentangling the kinematic effects, we still find a significant dependence of Ωh^2 on the CP-mixing in the Higgs sector. For example, for $\Delta M_{\tilde{\chi}_1^0 H_3} = -1.5$ GeV in Fig. 3.58b, we get an increase in Ωh^2 relative to the $\Phi_t = 0$ case by almost an order of magnitude. Also the relative importance of different final states depends on the CP phases. To infer the relic density of the LSP it is therefore important to pin down the Higgs sector with good precision. This includes not only precise measurements of the Higgs masses and decay widths but also of a possible CP mixing. Last but not least note that loop corrections to neutralino annihilation processes will also be important for a precise prediction of Ωh^2. For more details and other scenarios of neutralino annihilation and coannihilation, see [346].

3.15 Decays of third generation sfermions into Higgs bosons

Alfred Bartl, Stefan Hesselbach, Keisyo Hidaka, Thomas Kernreiter and Werner Porod

A precise knowledge of third generation sfermion parameters is important for Higgs physics as the dominant loop corrections to the masses of the MSSM Higgs bosons are due to stops and sbottoms [354]. Moreover, if the parameters μ, A_τ, A_t, A_b are complex, they induce a mixing between neutral scalar Higgs bosons and the pseudoscalar Higgs boson which within the MSSM is impossible at tree-level. Furthermore, these parameters enter in the mixing matrices of the sfermions as well as in the couplings of sfermions to Higgs bosons. This leads to strong effects on sfermion decay widths and branching ratios which have been analyzed in [355, 356] for the stau sector and in [357–359] for the stop/sbottom sector. Thus sfermion production and subsequent decays into Higgs bosons are an additional source of Higgs bosons at future colliders with a potentially strong dependence on the SUSY CP phases.

3.15.1 SUSY CP phases in sfermion mixing and Higgs-sfermion couplings

The left-right mixing of the stops and sbottoms is described by a hermitian 2×2 mass matrix which in the basis $(\tilde{q}_L, \tilde{q}_R)$ reads

$$\mathcal{L}_M^{\tilde{q}} = -(\tilde{q}_L^\dagger, \tilde{q}_R^\dagger) \begin{pmatrix} M^2_{\tilde{q}_{LL}} & M^2_{\tilde{q}_{LR}} \\ M^2_{\tilde{q}_{RL}} & M^2_{\tilde{q}_{RR}} \end{pmatrix} \begin{pmatrix} \tilde{q}_L \\ \tilde{q}_R \end{pmatrix}, \tag{3.120}$$

with

$$M^2_{\tilde{q}_{LL}} = M^2_{\tilde{Q}_3} + (I^q_{3L} - e_q \sin^2\theta_W)\cos 2\beta\, m_Z^2 + m_q^2, \tag{3.121}$$

$$M^2_{\tilde{q}_{RR}} = M^2_{\tilde{Q}'_3} + e_q \sin^2\theta_W \cos 2\beta\, m_Z^2 + m_q^2, \tag{3.122}$$

$$M^2_{\tilde{q}_{RL}} = (M^2_{\tilde{q}_{LR}})^* = m_q \left(|A_q| e^{i\Phi_{A_q}} - |\mu| e^{-i\Phi_\mu} (\tan\beta)^{-2I^q_{3L}} \right), \tag{3.123}$$

where m_q, e_q and I^q_{3L} are the mass, electric charge and weak isospin of the quark $q = b, t$. θ_W denotes the weak mixing angle, $\tan\beta = v_2/v_1$ with v_1 (v_2) being the vacuum expectation value of the Higgs field H^0_1 (H^0_2) and $M_{\tilde{Q}'_3} = M_{\tilde{D}_3}$ ($M_{\tilde{U}_3}$) for $q = b$ (t). $M_{\tilde{Q}_3}$, $M_{\tilde{D}_3}$, $M_{\tilde{U}_3}$, A_b and A_t are the soft SUSY-breaking parameters of the top squark and bottom squark system. In the case of complex parameters μ and A_q the off-diagonal elements $M^2_{\tilde{q}_{RL}} = (M^2_{\tilde{q}_{LR}})^*$ are also complex with the phase

$$\Phi_{\tilde{q}} = \arg\left[M^2_{\tilde{q}_{RL}}\right] = \arg\left[|A_q| e^{i\Phi_{A_q}} - |\mu| e^{-i\Phi_\mu} (\tan\beta)^{-2I^q_{3L}} \right]. \tag{3.124}$$

The mass eigenstates are

$$\begin{pmatrix} \tilde{q}_1 \\ \tilde{q}_2 \end{pmatrix} = \mathcal{R}^{\tilde{q}} \begin{pmatrix} \tilde{q}_L \\ \tilde{q}_R \end{pmatrix} \tag{3.125}$$

with the $\tilde{q}$-mixing matrix

$$\mathcal{R}^{\tilde{q}} = \begin{pmatrix} e^{i\Phi_{\tilde{q}}} \cos\theta_{\tilde{q}} & \sin\theta_{\tilde{q}} \\ -\sin\theta_{\tilde{q}} & e^{-i\Phi_{\tilde{q}}} \cos\theta_{\tilde{q}} \end{pmatrix}, \tag{3.126}$$

$$\cos\theta_{\tilde{q}} = \frac{-|M^2_{\tilde{q}_{LR}}|}{\sqrt{|M^2_{\tilde{q}_{LR}}|^2 + (m^2_{\tilde{q}_1} - M^2_{\tilde{q}_{LL}})^2}}, \quad \sin\theta_{\tilde{q}} = \frac{M^2_{\tilde{q}_{LL}} - m^2_{\tilde{q}_1}}{\sqrt{|M^2_{\tilde{q}_{LR}}|^2 + (m^2_{\tilde{q}_1} - M^2_{\tilde{q}_{LL}})^2}} \tag{3.127}$$

and the mass eigenvalues

$$m^2_{\tilde{q}_{1,2}} = \frac{1}{2}\left(M^2_{\tilde{q}_{LL}} + M^2_{\tilde{q}_{RR}} \mp \sqrt{(M^2_{\tilde{q}_{LL}} - M^2_{\tilde{q}_{RR}})^2 + 4|M^2_{\tilde{q}_{LR}}|^2} \right), \qquad m_{\tilde{q}_1} < m_{\tilde{q}_2}\,. \tag{3.128}$$

The respective mass and mixing matrices in the stau sector are obtained from those of the sbottoms by the replacement of the soft SUSY-breaking parameters $(M_{\tilde{Q}_3}, M_{\tilde{D}_3}, A_b) \to (M_{\tilde{L}_3}, M_{\tilde{E}_3}, A_\tau)$.

The $\tilde{q}_i - \tilde{q}'_j - H^\pm$ couplings are defined by

$$\mathcal{L}_{\tilde{q}\tilde{q}H^\pm} = g\left(C^H_{\tilde{t}_j\tilde{b}_i} H^+ \tilde{t}^\dagger_j\, \tilde{b}_i + C^H_{\tilde{b}_j\tilde{t}_i} H^- \tilde{b}^\dagger_j\, \tilde{t}_i \right) \tag{3.129}$$

with

$$C^H_{\tilde{t}_i\tilde{b}_j} = (C^H_{\tilde{b}_j\tilde{t}_i})^* = \frac{1}{\sqrt{2}\, m_W} (\mathcal{R}^{\tilde{t}} G \mathcal{R}^{\tilde{b}^\dagger})_{ij} \tag{3.130}$$

and

$$G = \begin{pmatrix} m_b^2 \tan\beta + m_t^2 \cot\beta - m_W^2 \sin 2\beta & m_b\,(|A_b| e^{-i\Phi_{A_b}} \tan\beta + |\mu| e^{i\Phi_\mu}) \\ m_t\,(|A_t| e^{i\Phi_{A_t}} \cot\beta + |\mu| e^{-i\Phi_\mu}) & \dfrac{2 m_t m_b}{\sin 2\beta} \end{pmatrix}. \tag{3.131}$$

For the couplings of squarks to neutral Higgs bosons we have the Lagrangian

$$\mathcal{L}_{\tilde{q}\tilde{q}H} = -g\, C(\tilde{q}^\dagger_k H_i \tilde{q}_j)\, \tilde{q}^\dagger_k H_i \tilde{q}_j \quad (k, j = 1, 2) \tag{3.132}$$

with

$$C(\tilde{q}^\dagger_k H_i \tilde{q}_j) = \mathcal{R}_{\tilde{q}} \cdot \begin{pmatrix} C(\tilde{q}^\dagger_L H_i \tilde{q}_L) & C(\tilde{q}^\dagger_L H_i \tilde{q}_R) \\ C(\tilde{q}^\dagger_R H_i \tilde{q}_L) & C(\tilde{q}^\dagger_R H_i \tilde{q}_R) \end{pmatrix} \cdot \mathcal{R}_{\tilde{q}}{}^\dagger, \tag{3.133}$$

where for $\tilde{q} = \tilde{t}$

$$C(\tilde{t}_L^\dagger H_i \tilde{t}_L) = \frac{m_t^2}{m_W \sin\beta} O_{2i} + \frac{m_Z}{\cos\theta_W}\left(\frac{1}{2} - e_t \sin^2\theta_W\right)(\cos\beta O_{1i} - \sin\beta O_{2i}), \quad (3.134)$$

$$C(\tilde{t}_R^\dagger H_i \tilde{t}_R) = \frac{m_t^2}{m_W \sin\beta} O_{2i} + \frac{e_t m_Z}{\cos\theta_W} \sin^2\theta_W (\cos\beta O_{1i} - \sin\beta O_{2i}), \quad (3.135)$$

$$C(\tilde{t}_L^\dagger H_i \tilde{t}_R) = [C(\tilde{t}_R^\dagger H_i \tilde{t}_L)]^* = \frac{m_t}{2 m_W \sin\beta}\{-i\left(\cos\beta |A_t| e^{-i\Phi_{A_t}} + \sin\beta |\mu| e^{i\Phi_\mu}\right) O_{3i}$$
$$- \left(|\mu| e^{i\Phi_\mu} O_{1i} - |A_t| e^{-i\Phi_{A_t}} O_{2i}\right)\}, \quad (3.136)$$

while for $\tilde{q} = \tilde{b}$

$$C(\tilde{b}_L^\dagger H_i \tilde{b}_L) = \frac{m_b^2}{m_W \cos\beta} O_{1i} + \frac{m_Z}{\cos\theta_W}\left(-\frac{1}{2} - e_b \sin^2\theta_W\right)(\cos\beta O_{1i} - \sin\beta O_{2i}), \quad (3.137)$$

$$C(\tilde{b}_R^\dagger H_i \tilde{b}_R) = \frac{m_b^2}{m_W \cos\beta} O_{1i} + \frac{e_b m_Z}{\cos\theta_W} \sin^2\theta_W (\cos\beta O_{1i} - \sin\beta O_{2i}), \quad (3.138)$$

$$C(\tilde{b}_L^\dagger H_i \tilde{b}_R) = [C(\tilde{b}_R^\dagger H_i \tilde{b}_L)]^* = \frac{m_b}{2 m_W \cos\beta}\{-i\left(\sin\beta |A_b| e^{-i\Phi_{A_b}} + \cos\beta |\mu| e^{i\Phi_\mu}\right) O_{3i}$$
$$- \left(|\mu| e^{i\Phi_\mu} O_{2i} - |A_b| e^{-i\Phi_{A_b}} O_{1i}\right)\}. \quad (3.139)$$

The 3×3 matrix O denotes the mixing matrix of the neutral Higgs bosons as defined in Eq. (3.5). The couplings of the staus to neutral Higgs bosons can be obtained from Eqs. (3.137)–(3.139) by replacing b by τ.

3.15.2 Numerical results

In [357–359] the effects of the phases of the parameters A_t, A_b, μ and M_1 on the phenomenology of the third generation squarks, the stops $\tilde{t}_{1,2}$ and the sbottoms $\tilde{b}_{1,2}$ in the complex MSSM have been studied. The third generation squark sector is particularly interesting because of the effects of the large Yukawa couplings. The phases of A_f and μ enter directly the squark mass matrices and the squark-Higgs couplings, which can cause a strong phase dependence of observables. The off-diagonal mass matrix element $M^2_{\tilde{q}RL}$, which describes the mixing between the left and right squark states, is given in Eq. (3.123). In the case of stops the μ term is suppressed by $1/\tan\beta$, hence the phase $\Phi_{\tilde{t}}$ of $M^2_{\tilde{t}RL}$ is dominated by Φ_{A_t}. Therefore, the phase in the mixing matrix is in practice given by Φ_{A_t} and appears in several couplings due to the strong mixing in the stop sector. In the case of sbottoms the mixing is smaller because of the small bottom mass. It is mainly important for large $\tan\beta$, when the μ term is dominant in $M^2_{\tilde{b}RL}$. Hence the phase of A_b has only minor impact on the sbottom mixing in a large part of the SUSY parameter space. However, in the squark-Higgs couplings, for example in the $H^\pm \tilde{t}_L \tilde{b}_R$ couplings, Eq. (3.131), the phase Φ_{A_b} appears independent of the sbottom mixing. This can lead to a strong Φ_{A_b} dependence of sbottom *and* stop partial decay widths into Higgs bosons. The stau sector behaves similar to the sbottom sector.

In the following we give examples where a strong dependence on phases occurs. We want to stress, that this is a general feature provided the decays into Higgs bosons are kinematically allowed. The masses and mixing matrix O of the neutral Higgs bosons have been calculated with the program `FeynHiggs2.0.2` [59,60]. In Fig. 3.60 we show branching ratios of $\tilde{t}_2$ decays. As can be seen, the sum of the branching ratios into Higgs bosons is about 30% implying that stop decays serve as an additional source for Higgs bosons. As discussed in detail in [359], the partial widths for decays into fermions and the Z-boson have a $1 \pm \cos\Phi_{A_t}$ dependence. In the case of the Higgs bosons the dependence on the phases is much more involved as the parameters A_f and μ appear directly in the couplings, see

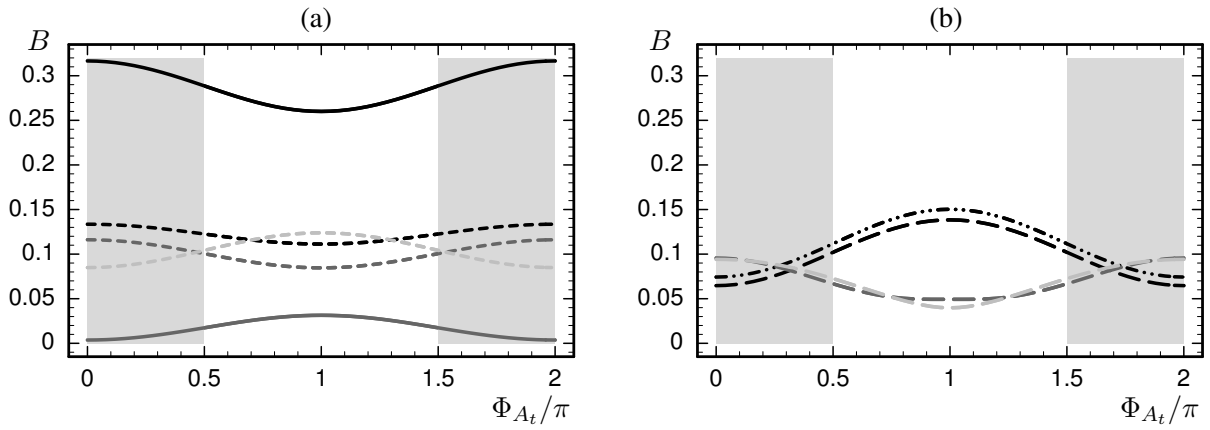

Fig. 3.60: Φ_{A_t} dependence of branching ratios of the decays (a) $\tilde{t}_2 \to \tilde{\chi}^+_{1/2} b$ (solid, black/gray), $\tilde{t}_2 \to \tilde{\chi}^0_{2/3/4} t$ (dashed, black/gray/light gray) and (b) $\tilde{t}_2 \to Z\tilde{t}_1$ (dashdotdotted), $\tilde{t}_2 \to H_{1/2/3}\tilde{t}_1$ (long dashed, black/gray/light gray) for $\tan\beta = 6$, $M_2 = 300$ GeV, $|\mu| = 500$ GeV, $|A_b| = |A_t| = 500$ GeV, $\Phi_\mu = \Phi_1 = \Phi_{A_b} = 0$, $m_{\tilde{t}_1} = 350$ GeV, $m_{\tilde{t}_2} = 800$ GeV, $m_{\tilde{b}_1} = 170$ GeV and $m_{H^\pm} = 350$ GeV, assuming $M_{\tilde{Q}_3} > M_{\tilde{U}_3}$. Only the decay modes with $B \gtrsim 1\,\%$ are shown. The shaded areas mark the region excluded by the experimental limit $B(b \to s\gamma) < 4.5 \times 10^{-4}$. From [359].

Eqs. (3.131), (3.136) and (3.139). Part of the phase dependence is due to the change of the Higgs masses as they depend on the phases. However, this effect is very small. As a test we have kept the Higgs masses constant and the lines in the plots are only shifted in the order of the line-thickness. In Figs. 3.61 and 3.62 it is demonstrated that (i) also the sbottom and stau decay branching ratios show a pronounced dependence on the phases and (ii) the branching ratios into Higgs bosons can be sizable and, thus, serve as an additional source for Higgs bosons. In contrast to the stop sector this dependence is mainly caused by the variations of the partial widths into Higgs bosons. For this reason it is also important if $\tan\beta$ is larger than ~ 20.

3.15.3 Parameter determination via global fit

In order to estimate the precision, which can be expected in the determination of the underlying SUSY parameters, a global fit of many observables in the stop/sbottom sector has been made in [359]. In order to achieve this the following assumptions have been made: (i) At the ILC the masses of the charginos, neutralinos and the lightest Higgs boson can be measured with high precision. If the masses of the squarks and heavier Higgs bosons are below 500 GeV, they can be measured with an error of $1\,\%$ and 1.5 GeV, respectively. (ii) The masses of the squarks and heavier Higgs bosons, which are heavier than 500 GeV, can be measured at a 2 TeV e^+e^- collider like CLIC with an error of $3\,\%$ and $1\,\%$, respectively. (iii) The gluino mass can be measured at the LHC with an error of $3\,\%$. (iv) For the production cross sections $\sigma(e^+e^- \to \tilde{t}_i\bar{\tilde{t}}_j)$ and $\sigma(e^+e^- \to \tilde{b}_i\bar{\tilde{b}}_j)$ and the branching ratios of the $\tilde{t}_i$ and $\tilde{b}_i$ decays we have taken the statistical errors, which we have doubled to be on the conservative side. We have analyzed two scenarios, one with small $\tan\beta = 6$ and one with large $\tan\beta = 30$. In both scenarios we have found that $\mathrm{Re}(A_t)$ and $|\mathrm{Im}(A_t)|$ can be determined with relative errors of 2–3%. For A_b the situation is considerably worse because of the weaker dependence of the observables on this parameter. Here the corresponding errors are of the order of 50–100%. For the squark mass parameters $M_{\tilde{Q}_3}$, $M_{\tilde{U}_3}$, $M_{\tilde{D}_3}$ the relative errors are of order of 1%, for $\tan\beta$ of order of 3 % and for μ and the other fundamental SUSY parameters of order of 1–2%. In a similar analysis in the stau sector [356] it has been found that for $\tan\beta = 3$ (30) the relative errors of $\mathrm{Re}(A_\tau)$ and $|\mathrm{Im}(A_\tau)|$ are 22% and 7% (7% and 3%), respectively, whereas the errors of $M_{\tilde{L}_3}$, $M_{\tilde{E}_3}$ are of the order of 1%. In particular the expected precision in the stop sector will be necessary for the comparison of the theoretical calculations in the Higgs sector and

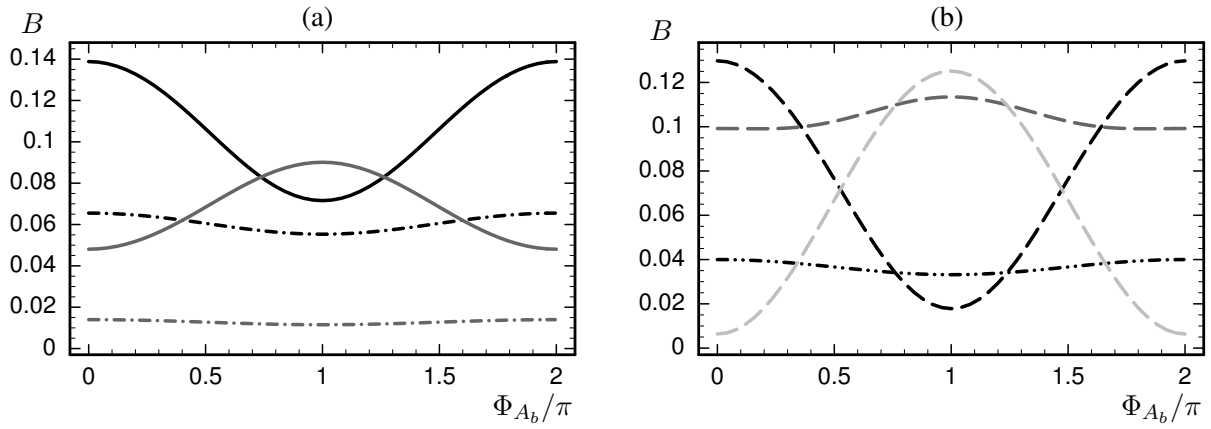

Fig. 3.61: Φ_{A_b} dependences of the branching ratios of the bosonic decays (a) $\tilde{b}_2 \to W^- \tilde{t}_{1/2}$ (dashdotted, black/gray), $\tilde{b}_2 \to H^- \tilde{t}_{1/2}$ (solid, black/gray) and (b) $\tilde{b}_2 \to Z\tilde{b}_1$ (dashdotdotted), $\tilde{b}_2 \to H_{1/2/3}\tilde{b}_1$ (long dashed, black/gray/light gray) for $\tan\beta = 30$, $M_2 = 200$ GeV, $|\mu| = 350$ GeV, $|A_b| = |A_t| = 600$ GeV, $\Phi_\mu = \Phi_{A_t} = \pi$, $\Phi_1 = 0$, $m_{\tilde{b}_1} = 350$ GeV, $m_{\tilde{b}_2} = 700$ GeV, $m_{\tilde{t}_1} = 170$ GeV and $m_{H^\pm} = 150$ GeV, assuming $M_{\tilde{Q}_3} < M_{\tilde{D}_3}$. From [359].

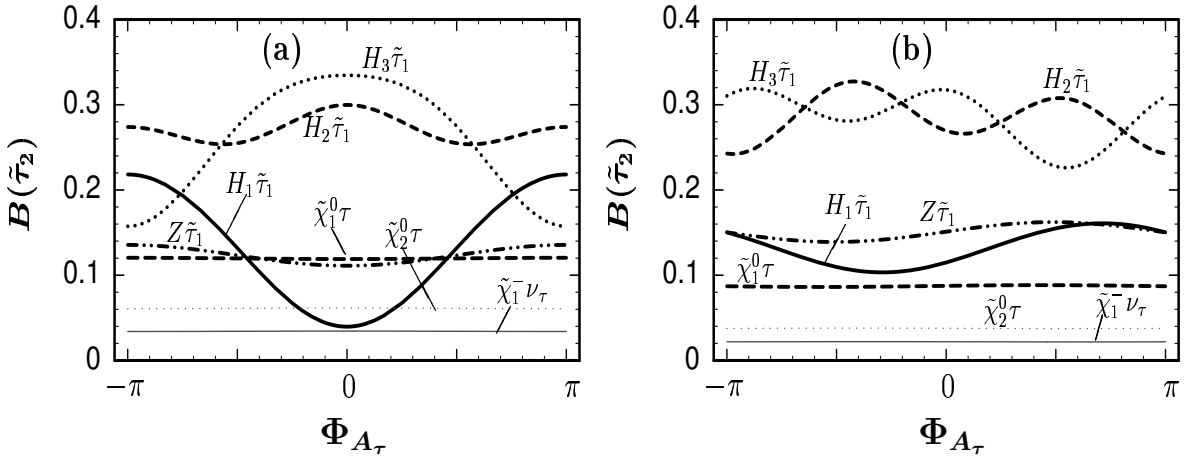

Fig. 3.62: Branching ratios of $\tilde{\tau}_2 \to H_{1,2,3}\tilde{\tau}_1$, $\tilde{\tau}_2 \to Z\tilde{\tau}_1$, $\tilde{\tau}_2 \to \tilde{\chi}^0_{1,2}\tau$ and $\tilde{\tau}_2 \to \tilde{\chi}_1^-\nu_\tau$ as a function of Φ_{A_τ} for a) $\Phi_\mu = 0$ and b) $\Phi_\mu = \pi/2$, with the other parameters $m_{\tilde{\tau}_1} = 240$ GeV, $m_{\tilde{\tau}_2} = 500$ GeV, $m_{H^\pm} = 160$ GeV, $|\mu| = 600$ GeV, $M_2 = 450$ GeV, $\Phi_1 = 0$, $\tan\beta = 30$, and $|A_\tau| = 900$ GeV, assuming $M_{\tilde{L}_3} > M_{\tilde{E}_3}$. From [356].

experimental data.

REFERENCES

[1] L. Maiani, *in* Proceedings of the 1979 Gif-sur-Yvette Summer School on Particle Physics (Editions Frontières, Gif-sur-Yvette, 1971), p. 1.

[2] G. 't Hooft *et al.* (Eds.), NATO Advanced Study Institute - Recent Developments in Gauge Theories (New York, Plenum, l980), (Nato Advanced Study Institutes Series: Series B, Physics, 59).

[3] E. Witten, Phys. Lett. **B105**, 267 (1981).

[4] H. P. Nilles, Phys. Rep. **110**, 1 (1984).

[5] H. E. Haber and G. L. Kane, Phys. Rep. **117**, 75 (1985).

[6] J. F. Gunion, H. E. Haber, G. L. Kane and S. Dawson, SCIPP-89/13.

[7] S. Dimopoulos and H. Georgi, Nucl. Phys. **B193**, 150 (1981).

[8] S. Dimopoulos, S. Raby and F. Wilczek, Phys. Rev. **D24**, 1681 (1981).

[9] L. E. Ibanez and G. G. Ross, Phys. Lett. **B105**, 439 (1981).

[10] J. R. Ellis, S. Kelley and D. V. Nanopoulos, Phys. Lett. **B260**, 131 (1991).

[11] U. Amaldi, W. de Boer and H. Furstenau, Phys. Lett. **B260**, 447 (1991).

[12] P. Langacker and M.-x. Luo, Phys. Rev. **D44**, 817 (1991).

[13] C. Giunti, C. W. Kim and U. W. Lee, Mod. Phys. Lett. **A6**, 1745 (1991).

[14] M. Carena, S. Pokorski and C. E. M. Wagner, Nucl. Phys. **B406**, 59 (1993), [hep-ph/9303202].

[15] V. A. Kuzmin, V. A. Rubakov and M. E. Shaposhnikov, Phys. Lett. **B155**, 36 (1985).

[16] M. Carena, M. Quiros and C. E. M. Wagner, Nucl. Phys. **B524**, 3 (1998), [hep-ph/9710401].

[17] M. Laine and K. Rummukainen, Phys. Rev. Lett. **80**, 5259 (1998), [hep-ph/9804255].

[18] M. Laine and K. Rummukainen, Nucl. Phys. **B535**, 423 (1998), [hep-lat/9804019].

[19] K. Funakubo, Prog. Theor. Phys. **101**, 415 (1999), [hep-ph/9809517].

[20] K. Funakubo, S. Otsuki and F. Toyoda, Prog. Theor. Phys. **102**, 389 (1999), [hep-ph/9903276].

[21] J. Grant and M. Hindmarsh, Phys. Rev. **D59**, 116014 (1999), [hep-ph/9811289].

[22] M. Losada, Nucl. Phys. **B569**, 125 (2000), [hep-ph/9905441].

[23] S. Davidson, M. Losada and A. Riotto, Phys. Rev. Lett. **84**, 4284 (2000), [hep-ph/0001301].

[24] A. B. Lahanas, V. C. Spanos and V. Zarikas, Phys. Lett. **B472**, 119 (2000), [hep-ph/9812535].

[25] J. M. Cline, M. Joyce and K. Kainulainen, JHEP **07**, 018 (2000), [hep-ph/0006119].

[26] M. Carena, J. M. Moreno, M. Quiros, M. Seco and C. E. M. Wagner, Nucl. Phys. **B599**, 158 (2001), [hep-ph/0011055].

[27] M. Laine and K. Rummukainen, Nucl. Phys. **B597**, 23 (2001), [hep-lat/0009025].

[28] S. J. Huber, P. John and M. G. Schmidt, Eur. Phys. J. **C20**, 695 (2001), [hep-ph/0101249].

[29] K. Kainulainen, T. Prokopec, M. G. Schmidt and S. Weinstock, JHEP **06**, 031 (2001), [hep-ph/0105295].

[30] H. Goldberg, Phys. Rev. Lett. **50**, 1419 (1983).

[31] J. R. Ellis, J. S. Hagelin, D. V. Nanopoulos, K. A. Olive and M. Srednicki, Nucl. Phys. **B238**, 453 (1984).

[32] M. Drees and M. M. Nojiri, Phys. Rev. **D47**, 376 (1993), [hep-ph/9207234].

[33] M. E. Gomez, G. Lazarides and C. Pallis, Phys. Lett. **B487**, 313 (2000), [hep-ph/0004028].

[34] J. R. Ellis, T. Falk, G. Ganis, K. A. Olive and M. Srednicki, Phys. Lett. **B510**, 236 (2001), [hep-ph/0102098].

[35] P. Gondolo and K. Freese, JHEP **07**, 052 (2002), [hep-ph/9908390].

[36] T. Falk, A. Ferstl and K. A. Olive, Astropart. Phys. **13**, 301 (2000), [hep-ph/9908311].

[37] S. Y. Choi, S.-C. Park, J. H. Jang and H. S. Song, Phys. Rev. **D64**, 015006 (2001), [hep-

ph/0012370].
[38] J. R. Ellis, G. Ridolfi and F. Zwirner, Phys. Lett. **B257**, 83 (1991).
[39] Y. Okada, M. Yamaguchi and T. Yanagida, Prog. Theor. Phys. **85**, 1 (1991).
[40] Y. Okada, M. Yamaguchi and T. Yanagida, Phys. Lett. **B262**, 54 (1991).
[41] H. E. Haber and R. Hempfling, Phys. Rev. Lett. **66**, 1815 (1991).
[42] A. Brignole, Phys. Lett. **B281**, 284 (1992).
[43] P. H. Chankowski, S. Pokorski and J. Rosiek, Phys. Lett. **B286**, 307 (1992).
[44] P. Chankowski, S. Pokorski and J. Rosiek, Nucl. Phys. **B423**, 437 (1994), [hep-ph/9303309].
[45] The LEP Collaborations ALEPH, DELPHI, L3, OPAL, and The LEP Electroweak Working Group, LEPEWWG/2005-01, available from `http://lepewwg.web.cern.ch/LEPEWWG/stanmod/`.
[46] G.-C. Cho and K. Hagiwara, Nucl. Phys. **B574**, 623 (2000), [hep-ph/9912260].
[47] S. Heinemeyer, W. Hollik and G. Weiglein, Phys. Rep. **425**, 265 (2006), [hep-ph/0412214].
[48] A. Pilaftsis, Phys. Rev. **D58**, 096010 (1998), [hep-ph/9803297].
[49] A. Pilaftsis, Phys. Lett. **B435**, 88 (1998), [hep-ph/9805373].
[50] A. Pilaftsis and C. E. M. Wagner, Nucl. Phys. **B553**, 3 (1999), [hep-ph/9902371].
[51] D. A. Demir, Phys. Rev. **D60**, 055006 (1999), [hep-ph/9901389].
[52] S. Y. Choi, M. Drees and J. S. Lee, Phys. Lett. **B481**, 57 (2000), [hep-ph/0002287].
[53] M. Carena, J. R. Ellis, A. Pilaftsis and C. E. M. Wagner, Nucl. Phys. **B586**, 92 (2000), [hep-ph/0003180].
[54] M. Carena, J. R. Ellis, A. Pilaftsis and C. E. M. Wagner, Phys. Lett. **B495**, 155 (2000), [hep-ph/0009212].
[55] T. Ibrahim and P. Nath, Phys. Rev. **D63**, 035009 (2001), [hep-ph/0008237].
[56] T. Ibrahim and P. Nath, Phys. Rev. **D66**, 015005 (2002), [hep-ph/0204092].
[57] S. W. Ham, S. K. Oh, E. J. Yoo, C. M. Kim and D. Son, Phys. Rev. **D68**, 055003 (2003), [hep-ph/0205244].
[58] M. Carena, J. R. Ellis, A. Pilaftsis and C. E. M. Wagner, Nucl. Phys. **B625**, 345 (2002), [hep-ph/0111245].
[59] S. Heinemeyer, Eur. Phys. J. **C22**, 521 (2001), [hep-ph/0108059].
[60] M. Frank, S. Heinemeyer, W. Hollik and G. Weiglein, hep-ph/0212037.
[61] S. Heinemeyer, hep-ph/0407244.
[62] M. Carena, J. R. Ellis, S. Mrenna, A. Pilaftsis and C. E. M. Wagner, Nucl. Phys. **B659**, 145 (2003), [hep-ph/0211467].
[63] A. Dedes and S. Moretti, Phys. Rev. Lett. **84**, 22 (2000), [hep-ph/9908516].
[64] A. Dedes and S. Moretti, Nucl. Phys. **B576**, 29 (2000), [hep-ph/9909418].
[65] S. Y. Choi and J. S. Lee, Phys. Rev. **D61**, 115002 (2000), [hep-ph/9910557].
[66] S. Y. Choi, K. Hagiwara and J. S. Lee, Phys. Lett. **B529**, 212 (2002), [hep-ph/0110138].
[67] A. Arhrib, D. K. Ghosh and O. C. W. Kong, Phys. Lett. **B537**, 217 (2002), [hep-ph/0112039].
[68] E. Christova, H. Eberl, W. Majerotto and S. Kraml, Nucl. Phys. **B639**, 263 (2002), [hep-ph/0205227].
[69] E. Christova, H. Eberl, W. Majerotto and S. Kraml, JHEP **12**, 021 (2002), [hep-ph/0211063].
[70] W. Khater and P. Osland, Nucl. Phys. **B661**, 209 (2003), [hep-ph/0302004].
[71] B. E. Cox, J. R. Forshaw, J. S. Lee, J. Monk and A. Pilaftsis, Phys. Rev. **D68**, 075004 (2003), [hep-ph/0303206].
[72] A. G. Akeroyd, Phys. Rev. **D68**, 077701 (2003), [hep-ph/0306045].

[73] D. K. Ghosh, R. M. Godbole and D. P. Roy, Phys. Lett. **B628**, 131 (2005), [hep-ph/0412193].

[74] D. K. Ghosh and S. Moretti, Eur. Phys. J. **C42**, 341 (2005), [hep-ph/0412365].

[75] V. A. Khoze, A. D. Martin and M. G. Ryskin, Eur. Phys. J. **C34**, 327 (2004), [hep-ph/0401078].

[76] J. R. Ellis, J. S. Lee and A. Pilaftsis, Phys. Rev. **D71**, 075007 (2005), [hep-ph/0502251].

[77] F. Borzumati, J. S. Lee and W. Y. Song, Phys. Lett. **B595**, 347 (2004), [hep-ph/0401024].

[78] B. Grzadkowski, J. F. Gunion and J. Kalinowski, Phys. Rev. **D60**, 075011 (1999), [hep-ph/9902308].

[79] A. G. Akeroyd and A. Arhrib, Phys. Rev. **D64**, 095018 (2001), [hep-ph/0107040].

[80] P. Garcia-Abia, W. Lohmann and A. Raspereza, hep-ex/0505096.

[81] P. Garcia-Abia and W. Lohmann, 4th International Workshop on Linear Colliders, Sitges, Spain, 1999, Eur. Phys. J. direct **C2**, 2 (2000), [hep-ex/9908065].

[82] E. Boos, V. Bunichev, A. Djouadi and H. J. Schreiber, Phys. Lett. **B622**, 311 (2005), [hep-ph/0412194].

[83] I. F. Ginzburg, G. L. Kotkin, S. L. Panfil, V. G. Serbo and V. I. Telnov, Nucl. Instrum. Methods **A219**, 5 (1984).

[84] ECFA/DESY Photon Collider Working Group, B. Badelek *et al.*, Int. J. Mod. Phys. **A19**, 5097 (2004), [hep-ex/0108012].

[85] S. Y. Choi and J. S. Lee, Phys. Rev. **D62**, 036005 (2000), [hep-ph/9912330].

[86] J. S. Lee, hep-ph/0106327.

[87] S. Y. Choi, B.-c. Chung, P. Ko and J. S. Lee, Phys. Rev. **D66**, 016009 (2002), [hep-ph/0206025].

[88] S. Y. Choi *et al.*, Phys. Lett. **B606**, 164 (2005), [hep-ph/0404119].

[89] S. Heinemeyer and M. Velasco, hep-ph/0506267.

[90] E. Asakawa, S. Y. Choi, K. Hagiwara and J. S. Lee, Phys. Rev. **D62**, 115005 (2000), [hep-ph/0005313].

[91] R. M. Godbole, S. D. Rindani and R. K. Singh, Phys. Rev. **D67**, 095009 (2003), [hep-ph/0211136].

[92] E. Asakawa and K. Hagiwara, Eur. Phys. J. **C31**, 351 (2003), [hep-ph/0305323].

[93] J. R. Ellis, J. S. Lee and A. Pilaftsis, Nucl. Phys. **B718**, 247 (2005), [hep-ph/0411379].

[94] D. Atwood and A. Soni, Phys. Rev. **D52**, 6271 (1995), [hep-ph/9505233].

[95] B. Grzadkowski and J. F. Gunion, Phys. Lett. **B350**, 218 (1995), [hep-ph/9501339].

[96] A. Pilaftsis, Phys. Rev. Lett. **77**, 4996 (1996), [hep-ph/9603328].

[97] S.-Y. Choi and M. Drees, Phys. Rev. Lett. **81**, 5509 (1998), [hep-ph/9808377].

[98] S. Y. Choi and J. S. Lee, Phys. Rev. **D61**, 111702 (2000), [hep-ph/9909315].

[99] M. S. Berger, Phys. Rev. Lett. **87**, 131801 (2001), [hep-ph/0105128].

[100] C. Blochinger *et al.*, hep-ph/0202199.

[101] E. Asakawa, S. Y. Choi and J. S. Lee, Phys. Rev. **D63**, 015012 (2001), [hep-ph/0005118].

[102] S. Y. Choi, M. Drees, B. Gaissmaier and J. S. Lee, Phys. Rev. **D64**, 095009 (2001), [hep-ph/0103284].

[103] M. Dugan, B. Grinstein and L. J. Hall, Nucl. Phys. **B255**, 413 (1985).

[104] S. Dimopoulos and S. D. Thomas, Nucl. Phys. **B465**, 23 (1996), [hep-ph/9510220].

[105] M. Carena, M. Quiros, A. Riotto, I. Vilja and C. E. M. Wagner, Nucl. Phys. **B503**, 387 (1997), [hep-ph/9702409].

[106] M. Carena, M. Quiros, M. Seco and C. E. M. Wagner, Nucl. Phys. **B650**, 24 (2003), [hep-ph/0208043].

[107] J. F. Gunion and H. E. Haber, Phys. Rev. **D67**, 075019 (2003), [hep-ph/0207010].

[108] R. Hempfling and A. H. Hoang, Phys. Lett. **B331**, 99 (1994), [hep-ph/9401219].

[109] J. A. Casas, J. R. Espinosa, M. Quiros and A. Riotto, Nucl. Phys. **B436**, 3 (1995), [hep-ph/9407389].

[110] M. Carena, J. R. Espinosa, M. Quiros and C. E. M. Wagner, Phys. Lett. **B355**, 209 (1995), [hep-ph/9504316].

[111] M. Carena, M. Quiros and C. E. M. Wagner, Nucl. Phys. **B461**, 407 (1996), [hep-ph/9508343].

[112] H. E. Haber, R. Hempfling and A. H. Hoang, Z. Phys. **C75**, 539 (1997), [hep-ph/9609331].

[113] S. Heinemeyer, W. Hollik and G. Weiglein, Phys. Lett. **B440**, 296 (1998), [hep-ph/9807423].

[114] S. Heinemeyer, W. Hollik and G. Weiglein, Phys. Rev. **D58**, 091701 (1998), [hep-ph/9803277].

[115] S. Heinemeyer, W. Hollik and G. Weiglein, Eur. Phys. J. **C9**, 343 (1999), [hep-ph/9812472].

[116] R.-J. Zhang, Phys. Lett. **B447**, 89 (1999), [hep-ph/9808299].

[117] J. R. Espinosa and R.-J. Zhang, JHEP **03**, 026 (2000), [hep-ph/9912236].

[118] G. Degrassi, P. Slavich and F. Zwirner, Nucl. Phys. **B611**, 403 (2001), [hep-ph/0105096].

[119] J. R. Espinosa and R.-J. Zhang, Nucl. Phys. **B586**, 3 (2000), [hep-ph/0003246].

[120] A. Brignole, G. Degrassi, P. Slavich and F. Zwirner, Nucl. Phys. **B631**, 195 (2002), [hep-ph/0112177].

[121] A. Brignole, G. Degrassi, P. Slavich and F. Zwirner, Nucl. Phys. **B643**, 79 (2002), [hep-ph/0206101].

[122] S. Heinemeyer, W. Hollik, H. Rzehak and G. Weiglein, Eur. Phys. J. **C39**, 465 (2005), [hep-ph/0411114].

[123] S. Heinemeyer, W. Hollik, H. Rzehak and G. Weiglein, hep-ph/0506254.

[124] R. Hempfling, Phys. Rev. **D49**, 6168 (1994).

[125] L. J. Hall, R. Rattazzi and U. Sarid, Phys. Rev. **D50**, 7048 (1994), [hep-ph/9306309].

[126] M. Carena, M. Olechowski, S. Pokorski and C. E. M. Wagner, Nucl. Phys. **B426**, 269 (1994), [hep-ph/9402253].

[127] M. Carena, D. Garcia, U. Nierste and C. E. M. Wagner, Nucl. Phys. **B577**, 88 (2000), [hep-ph/9912516].

[128] H. Eberl, K. Hidaka, S. Kraml, W. Majerotto and Y. Yamada, Phys. Rev. **D62**, 055006 (2000), [hep-ph/9912463].

[129] A. Dedes, G. Degrassi and P. Slavich, Nucl. Phys. **B672**, 144 (2003), [hep-ph/0305127].

[130] G. Degrassi, S. Heinemeyer, W. Hollik, P. Slavich and G. Weiglein, Eur. Phys. J. **C28**, 133 (2003), [hep-ph/0212020].

[131] J. S. Lee *et al.*, Comput. Phys. Commun. **156**, 283 (2004), [hep-ph/0307377].

[132] M. Carena *et al.*, Nucl. Phys. **B580**, 29 (2000), [hep-ph/0001002].

[133] S. P. Martin, Phys. Rev. **D65**, 116003 (2002), [hep-ph/0111209].

[134] S. P. Martin, Phys. Rev. **D66**, 096001 (2002), [hep-ph/0206136].

[135] S. P. Martin, Phys. Rev. **D67**, 095012 (2003), [hep-ph/0211366].

[136] S. P. Martin, Phys. Rev. **D68**, 075002 (2003), [hep-ph/0307101].

[137] S. P. Martin, Phys. Rev. **D70**, 016005 (2004), [hep-ph/0312092].

[138] S. P. Martin, Phys. Rev. **D71**, 016012 (2005), [hep-ph/0405022].

[139] S. P. Martin, Phys. Rev. **D71**, 116004 (2005), [hep-ph/0502168].

[140] S. P. Martin and D. G. Robertson, Comput. Phys. Commun. **174**, 133 (2006), [hep-ph/0501132].

[141] S. Y. Choi and J. S. Lee, Phys. Rev. **D61**, 015003 (2000), [hep-ph/9907496].

[142] S. Y. Choi, K. Hagiwara and J. S. Lee, Phys. Rev. **D64**, 032004 (2001), [hep-ph/0103294].

[143] S. Y. Choi, M. Drees, J. S. Lee and J. Song, Eur. Phys. J. **C25**, 307 (2002), [hep-ph/0204200].

[144] S. Heinemeyer, W. Hollik and G. Weiglein, Comput. Phys. Commun. **124**, 76 (2000), [hep-

ph/9812320].

[145] S. Heinemeyer, W. Hollik and G. Weiglein, hep-ph/0002213, see: `www.feynhiggs.de`.

[146] M. Frank, S. Heinemeyer, W. Hollik and G. Weiglein, hep-ph/0202166.

[147] T. Hahn, W. Hollik, S. Heinemeyer and G. Weiglein, hep-ph/0507009.

[148] M. Frank *et al.*, *in preparation*.

[149] G. Abbiendi *et al.* (OPAL Collaboration), Eur. Phys. J. **C37**, 49 (2004), [hep-ex/0406057].

[150] ALEPH, DELPHI, L3 and OPAL Collaborations, and The LEP Working Group for Higgs Boson Searches, Phys. Lett. **B565**, 61 (2003), [hep-ex/0306033].

[151] D. Chang, W.-Y. Keung and A. Pilaftsis, Phys. Rev. Lett. **82**, 900 (1999), [hep-ph/9811202].

[152] A. Pilaftsis, Nucl. Phys. **B644**, 263 (2002), [hep-ph/0207277].

[153] J. R. Ellis, J. S. Lee and A. Pilaftsis, Phys. Rev. **D72**, 095006 (2005), [hep-ph/0507046].

[154] C. Balazs, M. Carena, A. Menon, D. E. Morrissey and C. E. M. Wagner, Phys. Rev. **D71**, 075002 (2005), [hep-ph/0412264].

[155] T. Konstandin, T. Prokopec, M. G. Schmidt and M. Seco, Nucl. Phys. **B738**, 1 (2006), [hep-ph/0505103].

[156] V. Cirigliano, S. Profumo and M. J. Ramsey-Musolf, hep-ph/0603246.

[157] A. Pilaftsis, Nucl. Phys. **B504**, 61 (1997), [hep-ph/9702393].

[158] J. R. Ellis, J. S. Lee and A. Pilaftsis, Phys. Rev. **D70**, 075010 (2004), [hep-ph/0404167].

[159] S. Y. Choi, J. Kalinowski, Y. Liao and P. M. Zerwas, Eur. Phys. J. **C40**, 555 (2005), [hep-ph/0407347].

[160] J. S. Lee, hep-ph/0409020.

[161] J. Abdallah *et al.* (DELPHI Collaboration), in preparation.

[162] ALEPH, DELPHI, L3 and OPAL Collaborations, Search for neutral MSSM Higgs bosons at LEP, hep-ex/0602042.

[163] J. Abdallah *et al.* (DELPHI Collaboration), Eur. Phys. J **C38**, 1 (2004), [hep-ph/0410017].

[164] J. Abdallah *et al.* (DELPHI Collaboration), Eur. Phys. J **C44**, 147 (2005), [hep-ph/0510022].

[165] P. Achard *et al.* (L3 Collaboration), Phys. Lett. **B583**, 14 (2004), [hep-ph/0402003].

[166] G. Abbiendi *et al.* (OPAL Collaboration), Eur. Phys. J. **C40**, 317 (2005), [hep-ph/0408097].

[167] J. Abdallah *et al.* (DELPHI Collaboration), Eur. Phys. J. **C35**, 313 (2004), [hep-ph/0406012].

[168] P. Achard *et al.* (L3 Collaboration), Phys. Lett. **B589**, 89 (2004), [hep-ph/0403037].

[169] T. Banks, Nucl. Phys. **B303**, 172 (1988).

[170] T. Blazek, S. Raby and S. Pokorski, Phys. Rev. **D52**, 4151 (1995), [hep-ph/9504364].

[171] D. M. Pierce, J. A. Bagger, K. T. Matchev and R.-j. Zhang, Nucl. Phys. **B491**, 3 (1997), [hep-ph/9606211].

[172] F. Borzumati, G. R. Farrar, N. Polonsky and S. D. Thomas, Nucl. Phys. **B555**, 53 (1999), [hep-ph/9902443].

[173] K. S. Babu and C. F. Kolda, Phys. Lett. **B451**, 77 (1999), [hep-ph/9811308].

[174] H. E. Haber *et al.*, Phys. Rev. **D63**, 055004 (2001), [hep-ph/0007006].

[175] F. Borzumati, C. Greub and Y. Yamada, hep-ph/0305063 (2003), [hep-ph/0305063].

[176] F. Borzumati, C. Greub and Y. Yamada, Phys. Rev. **D69**, 055005 (2004), [hep-ph/0311151].

[177] E. Boos *et al.*, Nucl. Instrum. Methods **A472**, 100 (2001), [hep-ph/0103090].

[178] M. M. Muhlleitner and P. M. Zerwas, hep-ph/0511339.

[179] M. M. Muhlleitner, M. Kramer, M. Spira and P. M. Zerwas, Phys. Lett. **B508**, 311 (2001), [hep-ph/0101083].

[180] P. Niezurawski, A. F. Zarnecki and M. Krawczyk, hep-ph/0507006.

[181] J. Bernabeu, D. Binosi and J. Papavassiliou, hep-ph/0604046.
[182] A. Heister *et al.* (ALEPH Collaboration), Phys. Lett. **B526**, 191 (2002), [hep-ex/0201014].
[183] J. Abdallah *et al.* (DELPHI Collaboration), Eur. Phys. J. **C32**, 145 (2004), [hep-ex/0303013].
[184] P. Achard *et al.* (L3 Collaboration), Phys. Lett. **B545**, 30 (2002), [hep-ex/0208042].
[185] T. Junk, Nucl. Instrum. Methods **A434**, 435 (1999), [hep-ex/9902006].
[186] P. Bock, hep-ex/0405072.
[187] CDF Collaboration, D0 Collaboration, and the Tevatron Electroweak Working Group, hep-ex/0507091.
[188] H. L. Lai *et al.*, Eur. Phys. J. **C12**, 375 (2000), [hep-ph/9903282].
[189] M. Spira, Fortschr. Phys. **46**, 203 (1998), [hep-ph/9705337].
[190] E. L. Berger, T. Han, J. Jiang and T. Plehn, Phys. Rev. **D71**, 115012 (2005), [hep-ph/0312286].
[191] K. A. Assamagan *et al.*, Higgs Working Group: summary report 2003, hep-ph/0406152.
[192] K. A. Assamagan and Y. Coadou, Acta Phys. Polon. **B33**, 707 (2002).
[193] T. Plehn, Phys. Rev. **D67**, 014018 (2003), [hep-ph/0206121].
[194] T. Sjostrand, Comput. Phys. Commun. **82**, 74 (1994).
[195] T. Sjostrand *et al.*, Comput. Phys. Commun. **135**, 238 (2001), [hep-ph/0010017].
[196] ATLAS Collaboration, ATLAS detector and physics performance, Technical Design Report, Volume 2, CERN-LHCC-99-15 (1999).
[197] S. Asai *et al.*, Eur. Phys. J. **C32S2**, 19 (2004), [hep-ph/0402254].
[198] J. Cammin and M. Schumacher, ATL-PHYS-2003-024.
[199] E. R. S. Gonzales and M. Vos, ATL-PHYS-2002-021.
[200] D. Cavalli and P. Bosatelli, ATL-PHYS-2000-001.
[201] D. Cavalli and S. Resconi, ATL-PHYS-2000-005.
[202] D. Cavalli and G. Negri, ATL-PHYS-2003-009.
[203] J. Thomas, ATL-PHYS-2003-003.
[204] C. Biscarat and M. Dosil, ATL-PHYS-2003-038.
[205] H. Hu and J. Nielsen, Analytic confidence level calculations using the likelihood ratio and Fourier transform, Workshop on Confidence Limits, CERN, Geneva, 2000, CERN 2000–005 (2000), p.109.
[206] The LEP Collaborations and LEP Working Group for Higgs Boson Searches, hep-ex/0602042.
[207] A. Dedes and A. Pilaftsis, Phys. Rev. **D67**, 015012 (2003), [hep-ph/0209306].
[208] T.-F. Feng, X.-Q. Li and J. Maalampi, Phys. Rev. **D73**, 035011 (2006), [hep-ph/0602056].
[209] M. E. Gomez, T. Ibrahim, P. Nath and S. Skadhauge, hep-ph/0601163.
[210] M. Carena, A. Menon, R. Noriega-Papaqui, A. Szynkman and C. E. M. Wagner, hep-ph/0603106.
[211] V. M. Abazov *et al.* (D0 Collaboration), Phys. Rev. Lett. **95**, 151801 (2005), [hep-ex/0504018].
[212] A. Abulencia *et al.* (CDF Collaboration), Phys. Rev. Lett. **96**, 011802 (2006), [hep-ex/0508051].
[213] R. Eusebi, Ph.D. thesis, Search for charged Higgs in $t\bar{t}$ decay products from proton-antiproton collisions at $\sqrt{s} = 1.96\,\mathrm{TeV}$, University of Rochester.
[214] A. Abulencia *et al.* (CDF Collaboration), Phys. Rev. Lett. **96**, 042003 (2006), [hep-ex/0510065].
[215] S. Abdullin *et al.*, Eur. Phys. J. **C39S2**, 41 (2005).
[216] M. Duhrssen *et al.*, Phys. Rev. **D70**, 113009 (2004), [hep-ph/0406323].
[217] M. Duhrssen *et al.*, hep-ph/0407190.
[218] M. Schumacher, Czech. J. Phys. **54**, A103 (2004).
[219] M. Schumacher, hep-ph/0410112.

[220] J. A. Aguilar-Saavedra *et al.* (ECFA/DESY LC Physics Working Group), hep-ph/0106315.
[221] T. Abe *et al.* (American Linear Collider Working Group), hep-ex/0106055.
[222] T. Abe *et al.* (American Linear Collider Working Group), hep-ex/0106056.
[223] K. Abe *et al.* (ACFA Linear Collider Working Group), hep-ph/0109166.
[224] G. Weiglein *et al.* (LHC/LC Study Group), hep-ph/0410364.
[225] S. Heinemeyer *et al.*, hep-ph/0511332.
[226] J. Kublbeck, M. Bohm and A. Denner, Comput. Phys. Commun. **60**, 165 (1990).
[227] T. Hahn, Comput. Phys. Commun. **140**, 418 (2001), [hep-ph/0012260].
[228] T. Hahn and C. Schappacher, Comput. Phys. Commun. **143**, 54 (2002), [hep-ph/0105349].
[229] The program and the user's guide are available via `www.feynarts.de`.
[230] G. Weiglein, R. Scharf and M. Bohm, Nucl. Phys. **B416**, 606 (1994), [hep-ph/9310358].
[231] W. Hollik and H. Rzehak, Eur. Phys. J. **C32**, 127 (2003), [hep-ph/0305328].
[232] V. D. Barger *et al.*, Phys. Rev. **D64**, 056007 (2001), [hep-ph/0101106].
[233] S. Heinemeyer and W. Hollik, Nucl. Phys. **B474**, 32 (1996), [hep-ph/9602318].
[234] M. Carena, S. Heinemeyer, C. E. M. Wagner and G. Weiglein, Eur. Phys. J. **C26**, 601 (2003), [hep-ph/0202167].
[235] The code can be obtained from `www.feynhiggs.de`.
[236] T. Hahn and M. Perez-Victoria, Comput. Phys. Commun. **118**, 153 (1999), [hep-ph/9807565].
[237] S. Heinemeyer, W. Hollik, F. Merz and S. Penaranda, Eur. Phys. J. **C37**, 481 (2004), [hep-ph/0403228].
[238] T. Hahn, W. Hollik, J. I. Illana and S. Penaranda, hep-ph/0512315.
[239] S. Heinemeyer, W. Hollik and G. Weiglein, Eur. Phys. J. **C16**, 139 (2000), [hep-ph/0003022].
[240] T. Hahn, S. Heinemeyer, F. Maltoni, G. Weiglein and S. Willenbrock, to appear in the proceedings of the Tev4LHC Workshop, see: `maltoni.home.cern.ch/maltoni/TeV4LHC/`.
[241] A. Djouadi *et al.*, Phys. Rev. Lett. **78**, 3626 (1997), [hep-ph/9612363].
[242] A. Djouadi *et al.*, Phys. Rev. **D57**, 4179 (1998), [hep-ph/9710438].
[243] S. Heinemeyer and G. Weiglein, JHEP **10**, 072 (2002), [hep-ph/0209305].
[244] S. Heinemeyer and G. Weiglein, hep-ph/0301062.
[245] J. Haestier, S. Heinemeyer, D. Stockinger and G. Weiglein, JHEP **12**, 027 (2005), [hep-ph/0508139].
[246] J. Haestier, D. Stockinger, G. Weiglein and S. Heinemeyer, hep-ph/0506259.
[247] S. Heinemeyer, W. Hollik, D. Stockinger, A. M. Weber and G. Weiglein, hep-ph/0604147.
[248] T. Moroi, Phys. Rev. **D53**, 6565 (1996), [hep-ph/9512396].
[249] G. Degrassi and G. F. Giudice, Phys. Rev. **D58**, 053007 (1998), [hep-ph/9803384].
[250] S. Heinemeyer, D. Stockinger and G. Weiglein, Nucl. Phys. **B690**, 62 (2004), [hep-ph/0312264].
[251] S. Heinemeyer, D. Stockinger and G. Weiglein, Nucl. Phys. **B699**, 103 (2004), [hep-ph/0405255].
[252] P. Skands *et al.*, JHEP **07**, 036 (2004), [hep-ph/0311123].
[253] T. Hahn, hep-ph/0408283.
[254] T. Hahn, hep-ph/0605049.
[255] B. C. Allanach *et al.*, Eur. Phys. J. **C25**, 113 (2002), [hep-ph/0202233];
see also `www.ippp.dur.ac.uk/~georg/sps/`.
[256] E. Akhmetzyanova, M. Dolgopolov and M. Dubinin, Phys. Rev. **D71**, 075008 (2005), [hep-ph/0405264].
[257] H. E. Haber and R. Hempfling, Phys. Rev. **D48**, 4280 (1993), [hep-ph/9307201].

[258] M. N. Dubinin and A. V. Semenov, Eur. Phys. J. **C28**, 223 (2003), [hep-ph/0206205].

[259] M. Moretti, S. Moretti, F. Piccinini, R. Pittau and A. D. Polosa, JHEP **02**, 024 (2005), [hep-ph/0410334].

[260] S. Kanemura, Y. Okada, E. Senaha and C. P. Yuan, Phys. Rev. **D70**, 115002 (2004), [hep-ph/0408364].

[261] F. Boudjema and A. Semenov, Phys. Rev. **D66**, 095007 (2002), [hep-ph/0201219].

[262] S. Kanemura, S. Kiyoura, Y. Okada, E. Senaha and C. P. Yuan, Phys. Lett. **B558**, 157 (2003), [hep-ph/0211308].

[263] M. N. Dubinin and A. V. Semenov, hep-ph/9812246.

[264] A. Djouadi, W. Kilian, M. Muhlleitner and P. M. Zerwas, Eur. Phys. J. **C10**, 27 (1999), [hep-ph/9903229].

[265] A. Djouadi, H. E. Haber and P. M. Zerwas, Phys. Lett. **B375**, 203 (1996), [hep-ph/9602234].

[266] E. Boos *et al.*, Nucl. Instrum. Methods **A534**, 250 (2004), [hep-ph/0403113].

[267] A. Barducci, R. Casalbuoni, G. Pettini and R. Gatto, Phys. Lett. **B301**, 95 (1993), [hep-ph/9212276].

[268] J. Pumplin *et al.*, JHEP **07**, 012 (2002), [hep-ph/0201195].

[269] D. A. Dicus and S. Willenbrock, Phys. Rev. **D39**, 751 (1989).

[270] D. Dicus, T. Stelzer, Z. Sullivan and S. Willenbrock, Phys. Rev. **D59**, 094016 (1999), [hep-ph/9811492].

[271] C. Balazs, H.-J. He and C. P. Yuan, Phys. Rev. **D60**, 114001 (1999), [hep-ph/9812263].

[272] F. Maltoni, Z. Sullivan and S. Willenbrock, Phys. Rev. **D67**, 093005 (2003), [hep-ph/0301033].

[273] E. Boos and T. Plehn, Phys. Rev. **D69**, 094005 (2004), [hep-ph/0304034].

[274] R. V. Harlander and W. B. Kilgore, Phys. Rev. **D68**, 013001 (2003), [hep-ph/0304035].

[275] S. Dittmaier, M. Kramer and M. Spira, Phys. Rev. **D70**, 074010 (2004), [hep-ph/0309204].

[276] F. Borzumati and J. S. Lee, hep-ph/0605273.

[277] V. A. Khoze, A. D. Martin and M. G. Ryskin, Eur. Phys. J. **C23**, 311 (2002).

[278] A. De Roeck, V. A. Khoze, A. D. Martin, R. Orava and M. G. Ryskin, Eur. Phys. J. **C25**, 391 (2002).

[279] V. A. Khoze, A. D. Martin and M. G. Ryskin, Eur. Phys. J. **C34**, 327 (2004).

[280] B. E. Cox, AIP Conf. Proc. **753**, 103 (2005), [hep-ph/0409144].

[281] J. Ellis, J. S. Lee and A. Pilaftsis, Phys. Rev. **D71**, 075007 (2005).

[282] B. Cox *et al.,* CERN-LHCC-2005-025 (2005).

[283] A. Kaidalov, V. A. Khoze, A. D. Martin and M. G. Ryskin, Eur. Phys. J. **C33**, 261 (2004).

[284] M. Carena, J. Ellis, A. Pilaftsis and C. E. M. Wagner, Phys. Lett. **B495**, 155 (2000).

[285] B. Cox, J. Forshaw, J. Lee, J. Monk and A. Pilaftsis, Phys. Rev. **D68**, 075004 (2003).

[286] V. A. Khoze, A. D. Martin and M. G. Ryskin, Eur. Phys. J. **C14**, 525 (2002).

[287] J. Lee *et al.*, Comput. Phys. Commun. **156**, 283 (2004).

[288] V. A. Khoze, A. D. Martin and M. G. Ryskin, Eur. Phys. J. **C19**, 477 (2001), erratum, see reference [289].

[289] V. A. Khoze, A. D. Martin and M. G. Ryskin, Eur. Phys. J. **C20**, 599 (2001).

[290] V. A. Khoze, A. D. Martin and M. G. Ryskin, Eur. Phys. J. **C18**, 167 (2000).

[291] J. A. Williams, *Phenomenology of CP violation in Supersymmetric Charged Higgs Processes*, Ph.D. thesis, Cambridge University, 2006, in preparation.

[292] G. Corcella *et al.*, JHEP **01**, 010 (2001), [hep-ph/0011363].

[293] A. D. Martin, R. G. Roberts, W. J. Stirling and R. S. Thorne, Phys. Lett. **B604**, 61 (2004), [hep-

ph/0410230].

[294] S. Heinemeyer, W. Hollik and G. Weiglein, JHEP **06**, 009 (2000), [hep-ph/9909540].

[295] B. C. Allanach, A. Djouadi, J. L. Kneur, W. Porod and P. Slavich, JHEP **09**, 044 (2004), [hep-ph/0406166].

[296] S. Heinemeyer, W. Hollik, H. Rzehak and G. Weiglein, in preparation.

[297] D. Asner *et al.*, Eur. Phys. J. **C28**, 27 (2003), [hep-ex/0111056].

[298] J. Brient, talk at the Linear Collider Workshop, Cracow, Poland, September 2001, http://webnt.physics.ox.ac.uk/lc/ecfadesy.

[299] T. L. Barklow, hep-ph/0312268.

[300] D. Asner *et al.*, hep-ph/0308103.

[301] B. K. Bullock, K. Hagiwara and A. D. Martin, Phys. Rev. Lett. **67**, 3055 (1991).

[302] D. P. Roy, Phys. Lett. **B277**, 183 (1992).

[303] B. K. Bullock, K. Hagiwara and A. D. Martin, Nucl. Phys. **B395**, 499 (1993).

[304] S. Raychaudhuri and D. P. Roy, Phys. Rev. **D52**, 1556 (1995), [hep-ph/9503251].

[305] S. Raychaudhuri and D. P. Roy, Phys. Rev. **D53**, 4902 (1996), [hep-ph/9507388].

[306] E. Christova and D. Draganov, Phys. Lett. **B434**, 373 (1998), [hep-ph/9710225].

[307] R. H. Dalitz and G. R. Goldstein, Phys. Rev. **D45**, 1531 (1992).

[308] T. Arens and L. M. Sehgal, Nucl. Phys. **B393**, 46 (1993).

[309] D. Espriu and J. Manzano, Phys. Rev. **D66**, 114009 (2002), [hep-ph/0209030].

[310] J. F. Gunion, B. Grzadkowski, H. E. Haber and J. Kalinowski, Phys. Rev. Lett. **79**, 982 (1997), [hep-ph/9704410].

[311] S. Gusken, J. H. Kuhn and P. M. Zerwas, Nucl. Phys. **B262**, 393 (1985).

[312] A. Pilaftsis, Z. Phys. **C47**, 95 (1990).

[313] M. Nowakowski and A. Pilaftsis, Mod. Phys. Lett. **A4**, 821 (1989).

[314] A. Pilaftsis and M. Nowakowski, Phys. Lett. **B245**, 185 (1990).

[315] V. Weisskopf and E. P. Wigner, Z. Phys. **63**, 54 (1930).

[316] Y. Kizukuri and N. Oshimo, Phys. Lett. **B249**, 449 (1990).

[317] T. Ibrahim and P. Nath, Phys. Rev. **D58**, 111301 (1998), [hep-ph/9807501].

[318] T. Ibrahim and P. Nath, Phys. Rev. **D61**, 093004 (2000), [hep-ph/9910553].

[319] M. Brhlik, G. J. Good and G. L. Kane, Phys. Rev. **D59**, 115004 (1999), [hep-ph/9810457].

[320] R. Arnowitt, B. Dutta and Y. Santoso, Phys. Rev. **D64**, 113010 (2001), [hep-ph/0106089].

[321] S. Y. Choi, M. Drees and B. Gaissmaier, Phys. Rev. **D70**, 014010 (2004), [hep-ph/0403054].

[322] M. Kramer, J. H. Kuhn, M. L. Stong and P. M. Zerwas, Z. Phys. **C64**, 21 (1994), [hep-ph/9404280].

[323] J. I. Illana, hep-ph/9912467.

[324] B. Grzadkowski and J. F. Gunion, Phys. Lett. **B294**, 361 (1992), [hep-ph/9206262].

[325] E. Asakawa, J.-i. Kamoshita, A. Sugamoto and I. Watanabe, Eur. Phys. J. **C14**, 335 (2000), [hep-ph/9912373].

[326] P. Niezurawski, A. F. Zarnecki and M. Krawczyk, JHEP **02**, 041 (2005), [hep-ph/0403138].

[327] P. Niezurawski, A. F. Zarnecki and M. Krawczyk, Acta Phys. Polon. **B36**, 833 (2005), [hep-ph/0410291].

[328] J. F. Gunion, B. Grzadkowski and X.-G. He, Phys. Rev. Lett. **77**, 5172 (1996), [hep-ph/9605326].

[329] A. Djouadi, hep-ph/0503173.

[330] B. Autin, A. Blondel and J. R. Ellis, editors, *Prospective Study of Muon Storage Rings at CERN*,

CERN-99-02.

[331] A. Blondel *et al.*, *ECFA/CERN Studies of a European Neutrino Factory Complex*, CERN-2004-002.

[332] V. D. Barger, M. S. Berger, J. F. Gunion and T. Han, Nucl. Phys. Proc. Suppl. **51A**, 13 (1996), [hep-ph/9604334].

[333] R. Casalbuoni *et al.*, JHEP **08**, 011 (1999), [hep-ph/9904268].

[334] V. D. Barger, M. Berger, J. F. Gunion and T. Han, Proc. Snowmass 2001, Snowmass Village, CO, 2001, eConf **C010630**, E110 (2001), [hep-ph/0110340].

[335] V. D. Barger, M. S. Berger, J. F. Gunion and T. Han, Phys. Rep. **286**, 1 (1997), [hep-ph/9602415].

[336] E. Asakawa, A. Sugamoto and I. Watanabe, hep-ph/0004005.

[337] H. Fraas, F. von der Pahlen and C. Sachse, Eur. Phys. J. **C37**, 495 (2004), [hep-ph/0407057].

[338] O. Kittel and F. von der Pahlen, Phys. Rev. **D72**, 095004 (2005), [hep-ph/0508267].

[339] H. Fraas, F. Franke, G. Moortgat-Pick, F. von der Pahlen and A. Wagner, Eur. Phys. J. **C29**, 587 (2003), [hep-ph/0303044].

[340] G. Moortgat-Pick and H. Fraas, Eur. Phys. J. **C25**, 189 (2002), [hep-ph/0204333].

[341] G. Bertone, D. Hooper and J. Silk, Phys. Rep. **405**, 279 (2005), [hep-ph/0404175].

[342] C. L. Bennett *et al.*, Astrophys. J. Suppl. **148**, 1 (2003), [astro-ph/0302207].

[343] D. N. Spergel *et al.* (WMAP Collaboration), Astrophys. J. Suppl. **148**, 175 (2003), [astro-ph/0302209].

[344] G. Belanger, F. Boudjema, S. Kraml, A. Pukhov and A. Semenov, Relic density of dark matter in the MSSM with CP violation, in *Les Houches Physics at TeV colliders 2005, Beyond the Standard Model Working Group, summary report*, [hep-ph/0602198].

[345] S. Y. Choi and Y. G. Kim, hep-ph/0602109.

[346] G. Belanger, F. Boudjema, S. Kraml, A. Pukhov and A. Semenov, Phys. Rev. D **73**, 115007 (2006), [hep-ph/0604150].

[347] G. Belanger, F. Boudjema, A. Pukhov and A. Semenov, micrOMEGAs2.0 and the relic density of dark matter in a generic model, in *Les Houches Physics at TeV colliders 2005, Beyond the Standard Model Working Group, summary report*, [hep-ph/0602198].

[348] G. Belanger, F. Boudjema, A. Pukhov and A. Semenov, hep-ph/0405253.

[349] G. Belanger, F. Boudjema, A. Pukhov and A. Semenov, Comput. Phys. Commun. **149**, 103 (2002), [hep-ph/0112278].

[350] A. V. Semenov, hep-ph/0208011.

[351] A. Pukhov, hep-ph/0412191.

[352] B. C. Allanach, G. Belanger, F. Boudjema and A. Pukhov, JHEP **12**, 020 (2004), [hep-ph/0410091].

[353] G. Belanger, S. Kraml and A. Pukhov, Phys. Rev. **D72**, 015003 (2005), [hep-ph/0502079].

[354] A. Brignole, J. R. Ellis, G. Ridolfi and F. Zwirner, Phys. Lett. **B271**, 123 (1991).

[355] A. Bartl, K. Hidaka, T. Kernreiter and W. Porod, Phys. Lett. **B538**, 137 (2002), [hep-ph/0204071].

[356] A. Bartl, K. Hidaka, T. Kernreiter and W. Porod, Phys. Rev. **D66**, 115009 (2002), [hep-ph/0207186].

[357] A. Bartl, S. Hesselbach, K. Hidaka, T. Kernreiter and W. Porod, hep-ph/0306281.

[358] A. Bartl, S. Hesselbach, K. Hidaka, T. Kernreiter and W. Porod, Phys. Lett. **B573**, 153 (2003), [hep-ph/0307317].

[359] A. Bartl, S. Hesselbach, K. Hidaka, T. Kernreiter and W. Porod, Phys. Rev. **D70**, 035003 (2004), [hep-ph/0311338].